Superconductivity and Mean Field Distribution Theory on a Hubbard Model with Local Symmetries

by

Manjinder Kainth

A thesis submitted to the
University of Birmingham
for the degree of
DOCTOR OF PHILOSOPHY

School of Physics and Astronomy
College of Engineering and Physical Sciences
University of Birmingham
June 16, 2020

ABSTRACT

At the core of thesis is the following particular Hubbard model

$$H = -t_1 \sum_{\langle ij \rangle \sigma} (t^\dagger_{i\sigma} + b^\dagger_{i\sigma})(t_{j\sigma} + b_{j\sigma}) - t_0 \sum_{i\sigma} (t^\dagger_{i\sigma} b_{i\sigma} + b^\dagger_{i\sigma} t_{i\sigma}) + U \sum_i (t^\dagger_{i\uparrow} t_{i\uparrow} t^\dagger_{i\downarrow} t_{i\downarrow} + b^\dagger_{i\uparrow} b_{i\uparrow} b^\dagger_{i\downarrow} b_{i\downarrow}),$$

for which there are two large investigations. In both of these a particular symmetry plays a central role: explicitly the set of local transformations $t^\dagger_{i\sigma} \leftrightarrow b^\dagger_{i\sigma}$, one for each site i in the system. As is with any local symmetry of a Hamiltonian, the basis Hilbert space must be divided into symmetry sectors $\mathbb{Z}_2$ i.e. symmetric or anti-symmetric under the transformation. We exclusively examine systems for which all basis states are either symmetric or anti-symmetric and only consider mixed systems as an afterthought.

The first investigation concerns an effectively exact examination of superconductivity in the limit $U = \infty$. Pairing is shown with binding energy and correlation length calculated exactly. We find that phase diagram of many unconventional superconductors is qualitatively recreated, and in particularly we find a ferromagnetic phase coexisting with a superconducting phase. The limit of $U = \infty$ is lifted perturbatively which gives rise to an anti-ferromagnetic phase at the Mott point.

The second investigation is a new approach for dealing with strongly correlated problems: we create a non-orthogonal basis which is self consistently solved for. With this we can calculate particle dispersions, hole dispersions, and the occupation factor. All three are compared to exact diagonalisation and show great agreement.

DEDICATION

To caffeine and sugar, my companions through many days of writing.

ACKNOWLEDGEMENTS

I would like to acknowledge my supervisor Dr Martin W Long, without whom this work could not be completed. Special thanks also goes to the theoretical physics department; every member of which added to the most enjoyable, supportive environment a PhD student could ask for.

CONTENTS

LIST OF FIGURES

LIST OF TABLES

Part I

Setting The Stage

CHAPTER 1

INTRODUCTION

1.1 How to Read This Thesis

A thesis is a strange document to write. We're expected to write at the level of a recent graduate in physics but the only people who will ever probably read it are us, our examiners, and maybe our supervisor. All of whom are expected to be experts in the field. The result is therefore a document that is written at a level too low for anyone reading it.

With this in mind I've written this thesis in a peculiar manner. I've kept the level low but not laboured the introductory details for which an expert is experienced. I hope that this has resulted in a more readable thesis for the three, maybe four, people who will actually read this document.

Additionally the style of writing is very relaxed when compared to a 'standard scientific document'. The language is often conversational and humour is sometimes attempted but often failed. I hope that this makes reading the 300 page tome easier.

The introductory details are important; especially in the rare case a student does pick this up from the library. For them I've written a hefty, detailed appendix. In this, I go over all the 'standard' tools used in this thesis with a fine tooth comb. I detail how to go from first to second quantisation, modelling materials with physical chemistry,

the Lanczos algorithm, Hartree-Fock mean field theory, resolvent formalism, perturbation theory, and Maxwell constructions. The appendices are around one hundred pages of detailed introduction in topics which are 'standard'. The result should be a thesis which is much lighter and easier to parse for the veterans, and detailed enough for the beginners.

So, how do you read this thesis? If you're a beginner, I recommend reading appendices A and B before reading the first part. This will give a detailed overview on both conventional and unconventional superconductivity. From this point on you can read the thesis in order, and dip into the appropriately referenced appendices when standard techniques are used. If you're a veteran, I recommend reading this thesis in order forgoing the appendices.

1.2 Actual Introduction

The story of superconductivity is filled with twists & turns, and is still being written. Much can be said about these macroscopic quantum materials (which will be presented in the following chapters) but for now know that these materials are perfect diamagnetic conductors [1]. In the broadest form we can say there are two types of superconductors, conventional and unconventional [2]. Only the former are well understood, and we are in a situation where there is a wealth of experimental knowledge but little theoretical understanding of the latter.

Conventional superconductors are well described by the formation of phonon mediated Cooper pairs [3]. As described by the BCS solution [4] these condense and for these materials superconductivity is a solved problem.

This would have been an open and shut case if it wasn't for scientist's drive to increase the superconducting transition temperature. This led to the discovery of a new type of superconductor [5], unable to be described by the conventional BCS theory, and so the field of *unconventional* superconductivity was born. Interestingly the original unconventional superconductors (heavy fermion superconductors) actually had lower absolute transition

temperatures but high when compared to the bandwidth within these materials [6]. The later cuprate superconductors (discovered by Bednorz and Muller [7]) had much higher transition temperatures. To this date, a microscopic theory of unconventional superconductivity does not exist. We will present work to hopefully shed some light on this field.

This thesis is formed of four parts. In the first part we set the stage. Here, we give a history of superconductivity then model both conventional and unconventional superconductors. We will find that unconventional superconductors can be modelled by an ordinary Hubbard model, yet examinations on this model struggle to find superconductivity [8]. This directly leads us to the second part of this thesis. Here we present a particular Hubbard model that exhibits superconductivity, even in the limit of divergent Coulomb repulsion. More interestingly, at finite Coulomb repulsion, this model manifests the phase diagram of unconventional superconductors. In the third part of this thesis we develop a new formalism to deal with finite Coulomb repulsion, with remarkable accuracy. We do this by defining non-orthogonal operators, and self-consistently solving for them. In the final part we conclude and present appendices.

Let's move on to the relevant history in the field.

CHAPTER 2

A HISTORY OF SUPERCONDUCTIVITY

Superconductivity is a rich field with a lot of history. One could write entire books on the subject, and people have. We're left with the difficult job of condensing down 100 years of history down to tens of pages. As a result, we can not cover *everything*, but we can cover the essentials. In this chapter we will review the history of superconductivity, starting with conventional and moving to unconventional. We will focus on the physics in this chapter, and the theory in the next.

2.1 Conventional Superconductivity

In 1911 Kammerlingh-Onnes found that the resistivity of mercury dropped to zero very sharply at about 4K [9]. A resistivity of zero corresponds to a divergent conductivity, and superconductivity was born. Later experiments showed that the resistivity of the superconducting state was less than 10^{-14} of that in the normal state.

Superconductivity is not limited to mercury: many elements and compounds are superconductors. 30 elements superconduct at ambient pressure, and a further 24 at high pressure [10]. It seems like superconductivity is abundant and at a wide range of temperatures. Rhodium superconducts at 35μK [11] and Niobium at 9.26K [12]. The interesting

Figure 2.1: Resistance vs Temperature: Normal State vs Superconductor

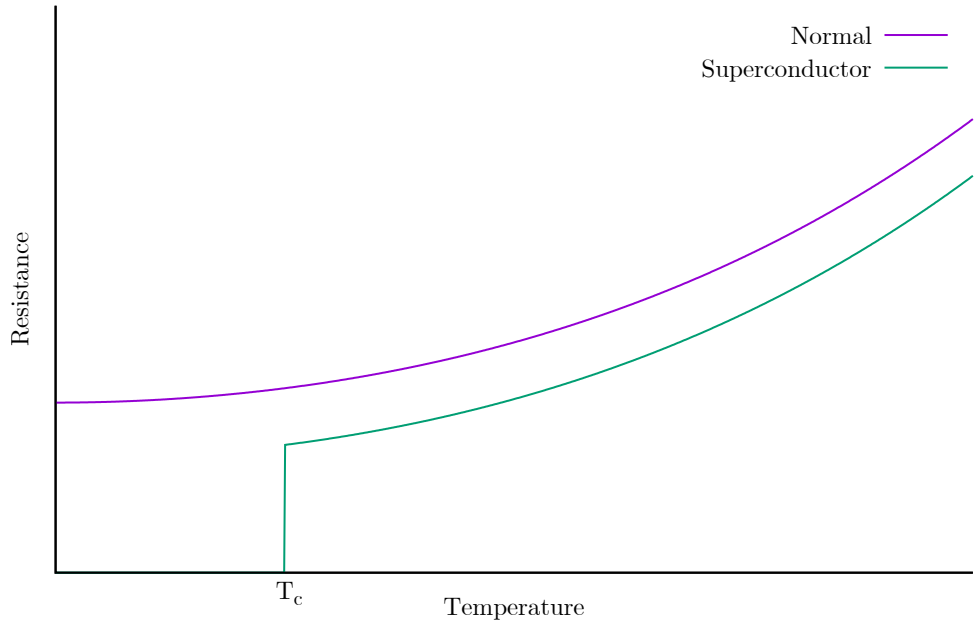

Schematic resistance vs temperature curves for a normal and superconducting state. For a normal metal resistance decreases to a finite value at zero temperature, whilst for a superconductor at a finite temperature T_C the resistance sharply drops to zero.

thing is that copper, silver, and gold do not exhibit superconductivity. Indeed there is a trend that 'good conductors make bad superconductors' [13]. This will turn out to be indicative of the source of superconductivity.

Superconductivity is clearly the phenomenon of perfect conductivity, but is this enough? No. Theoretically it can be shown that perfect conductors would show history dependent behaviour. A perfect conductor would expel a magnetic field applied on it. However, if a magnetic field is applied to a perfect conductor above its transition temperature and subsequently cooled, we would expect the field to be locked [14]. This is not what we see. In superconductors the field is always expelled, regardless of cooling before or after application of the field. This is called the Meissner effect [1], named after the discoverer of the phenomenon. Superconductors aren't just perfect conductors, they're also perfect diamagnets.

In reality things are more complicated. The magnetic field actually penetrates the

Figure 2.2: Field Locking vs Expulsion From a Perfect Conductor

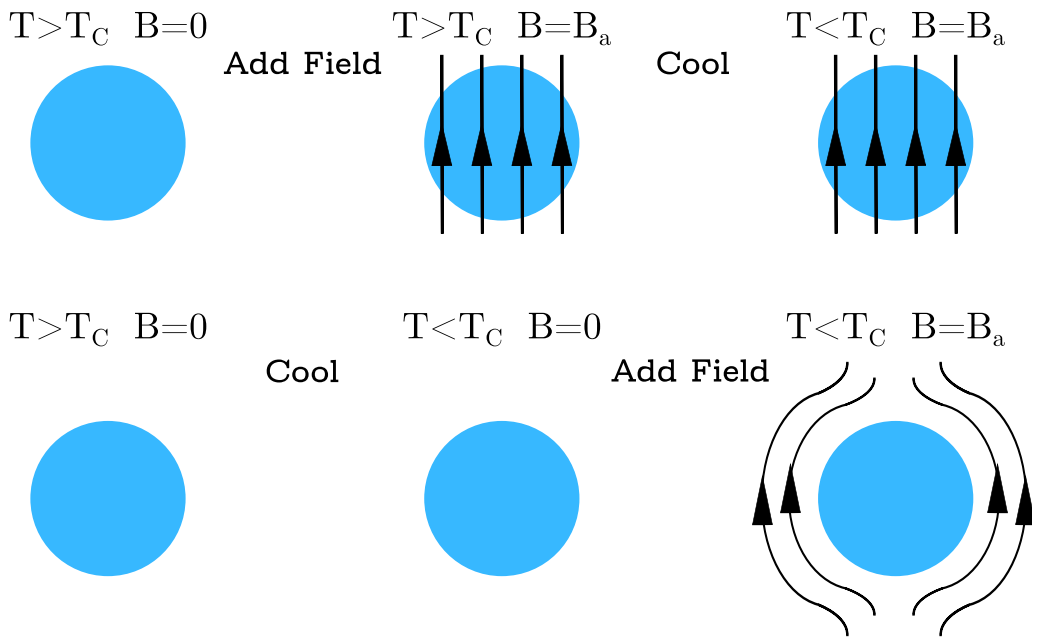

In a perfect conductor we expect different behaviour when applying a field before or after cooling past the transition temperature.

material and exponentially dies at length scale called the 'penetration depth' [15]. Upon increasing the strength of the field superconductivity either vanishes or permits quantised flux to pass through the material in 'vortices' [16]. In the former case we talk about 'Type I' superconductors and in the latter case they are called 'Type II' superconductors. A plethora of work has been carried out on these, is a field of study in and of itself, and is a detail of no relevance for the work in this thesis.

In the mean time theorists are working around the clock to explain this phenomenon, and people do quite well. Honourable mentions go to Fritz and Heinz London [17] who generated phenomenological equations to explain the Meissner effect. This was surpassed by a Ginzburg-Landau theory [18], in which a complex order parameter uniformly changes from zero in the normal state, to non-zero in the superconducting state. Both of these theories were surpassed by the microscopic BCS theory [4] which will be detailed in the next chapter.

The following is a *very brief* physical overview of BCS theory. Phonons couple opposite

spin and momentum particles to form Cooper pairs. These condense, opening up a gap in the spectrum. This gap forces a finite energy cost of creating an excitation, which is the basic explanation for superconductivity.

The race for room temperature superconductivity is now on. Scientists from around the world are trying to create compounds with higher and higher transition temperatures, and they succeed. They get up to 23.2K with Nb_3Ge [19]. Then Bednorz and Muller discover a superconductor with transition temperature 38K [7]; except with this one there is more than meets the eye.

2.2 Unconventional Superconductivity

Unconventional superconductors are simply materials where the source of superconductivity is not phonon mediated [20]. Bednorz and Muller were not the first people to find unconventional superconductivity, but they were the first to find one with such a high transition temperature. This was the first of many high temperature superconductors, and the one with the highest transition temperature (at ambient pressure) to date being in one such material, HBCCO ($HgBa_2Ca_2Cu_3O_x$) [21].

This set of materials are called the cuprates, named after the superconducting copper oxide layers that reside within them. All the cuprates share a few common traits. Each one is associated with a non-doped 'parent compound' that is always an anti-ferromagnetic Mott insulator [22]. Close to zero temperature, when this compound is doped (with particles or holes), this anti-ferromagnetism dies and gives rise to superconductivity. Upon further doping this superconductivity dies and gives rise to a normal metal [23].

Again things are more complicated than they first seem. The phase diagram is not particle hole symmetric [24]. Anti-ferromagnetism extends to higher doping on the particle side, and the superconducting range is smaller. Moreover, two strange phases exist on the hole doped side, the pseudogap and strange metal, and not on the particle doped side. This is depicted in figure 2.3 on page 9. This entry level knowledge of the phase diagram

Figure 2.3: Phase Diagram of Cuprate Superconductors

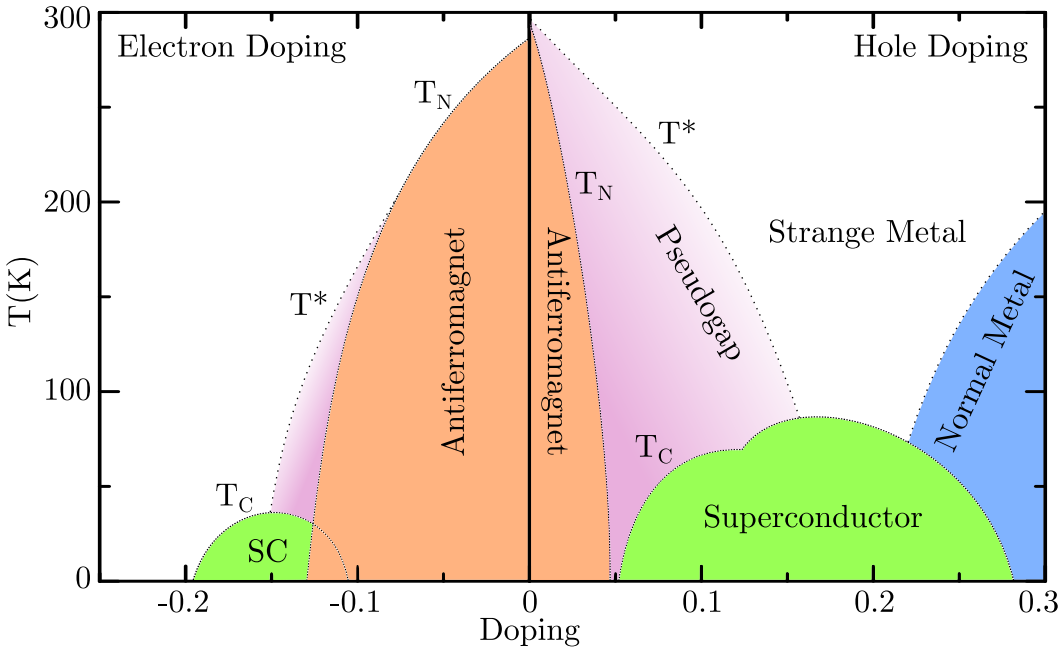

The cuprate phase diagram taken from [25]. All parent compounds are anti-ferromagnetic Mott insulators. The phase diagram is almost particle hole symmetric except for the extent of the anti-ferromagnetism and pseudogap.

is all that is required for this thesis.

Another set of unconventional superconductors are the heavy fermion superconductors [6]. They were discovered before the cuprates and had low transition temperatures. For example $CeCu_2Si_2$, the first heavy fermion superconductor, has a transition temperature of 0.7K [26]. These materials are usually formed of rare earths or actinides which have very localised f-electrons, which hybridise with the normal conduction electrons, giving rise to high quasiparticle mass.

All unconventional superconductors have the following in common: a strongly correlated electron system and small correlation lengths [20]. Compare this to conventional superconductors where they are weakly correlated and the correlation length is large [27].

At this point I would like to highlight targets that our work would like to achieve:

1. A zero temperature phase diagram for cuprates that includes anti-ferromagnetism, superconductivity, and metal in that order

2. Coexistence of superconductivity and ferromagnetism (in some unconventional superconductors)

3. A short correlation length

4. High transition temperature

These are physically motivated targets that theoretical attempts to describe unconventional superconductivity should aim to achieve.

2.3 Ladder Compounds

As the central work in this thesis is done on a model which can be represented as a one dimensional ladder (see figure 7.2 on page 49), we will do a brief review of the key background in the field. Most of the work, both theoretical and experimental, has focused on magnetism in ladder compounds [28]. This is particularly interesting in our case, as the short range anti-ferromagnetic correlations that exist in the cuprates also exist in these ladder compounds. For example, vanadyl pyrophosphate is a two rung ladder with confirmed Heisenberg antiferromagnetic correlations [29]. A more relevant material is $SrCu_2O_3$, which is a quasi-one dimensional spin ladder system. It is a cuprate system, much like the superconducting systems mentioned earlier, and has anti-ferromagnetic correlations [30], but is not superconducting even under pressure [31].

The most relevant ladder compound for this work is the so called "telephone number compound" $Sr_3Ca_{11}Cu_{24}O_{41}$, named due to the large amount of numbers in its structure. This family of compounds (in particular $Sr_{0.4}Ca_{13.6}Cu_{24}O_{41}$) was first shown to exhibit superconductivity under pressures of between 3GPa and 4.5GPa [32]. It has a similar phase diagram to the layered cuprates, but the structure contains ladders of copper oxide chains, similar to that of our model.

This material also exhibits an increase in the superconducting transition temperature when uniaxial pressure is applied [33]. The action of pressure on a solid state condensed

matter system [34] is to bring atoms closer together. Of course, electrostatic pressure is many orders of magnitude higher than what can be applied in the lab, therefore the action of pressure is a perturbation on the original structure. This perturbation changes the hopping parameters slightly. When the pressure is applied uniaxially, some parameters can be controlled while others are changed. This is of particular interest, as we will be tuning parameters and seeing their effects in the results (chapter 11), and in particular find that superconductivity can be strengthened.

In this chapter we gave a historical physical overview of both conventional and unconventional superconductivity, stated the key differences between the two, and gave an overview of ladder compounds in condensed matter physics. In the following chapter we will dive into the mathematics, and model conventional superconductivity.

CHAPTER 3

MODELLING CONVENTIONAL SUPERCONDUCTORS

Modelling conventional superconductivity is a rather simple process. If physical chemistry is unknown to you, please see appendix B.8. In this chapter we will model conventional superconductors, solve the Cooper problem, and then the BCS model. In essence we will show that pairs of particles bind, and these pairs condense manifesting superconductivity.

We're going to start with a tight binding model for the electrons as these materials are metallic, even if they are bad metals. The Coulomb repulsion has been set to zero, thanks to screening due to the background positive lattice.

Even if there is no repulsion between electrons, the tight binding model does not exhibit superconductivity. We need something more. The electrons need an attraction mechanism. In 1950 Frolich proposed an effective interaction mediated by the lattice [35]. As an electron passes through the lattice, the background positive lattice is attracted to it. This forms a local density of increased positive charge. Due to the mass difference between the ions and electrons, the ions do not relax as fast as the electrons. Therefore, the positive charge density remains long after the electron has left. This positive charge forms a site for attraction for a nearby electron. This process is depicted in figure 3.1 on page 14

Figure 3.1: Cartoon of Lattice Distortion Mediating Effective Electron Attraction

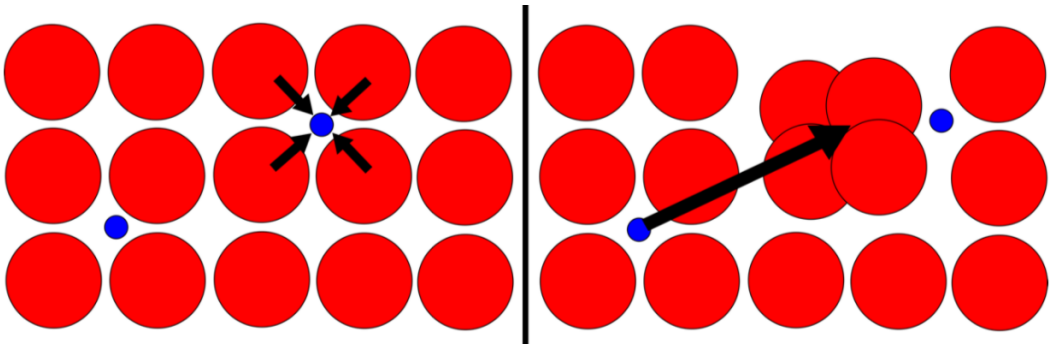

Cartoon of the lattice distortion that attracts two electrons together. As electrons are negative they distort the positive lattice creating a higher density of positive charge. The relaxation time of the lattice is larger than that of the electrons causing an effective attractive field for nearby electrons.

The deformation and relaxation of the ionic lattice is described by the mediation of phonons. These phonons couple electrons together. This explains the 'good conductors make bad superconductors' phenomenon, as at room temperature strong electron phonon coupling is a resistance inducing phenomenon [13].

This picture produces two predictions: a large correlation length [36] and the isotope effect [37]. Since the typical electron speed is of the order of the Fermi velocity $v_F \approx 10^6$, whilst the lattice relaxation time is $\tau \approx \frac{2\pi}{w_D} \approx 10^{-13}s$ where w_D is the Debye frequency. From this we can find a characteristic length called the correlation length $\xi \approx v_F\tau \approx 10^{-7}m$ representing the size of the pair. The characteristic size of this pair is around 1000 atom spacing and is experimentally verified [38]. Moreover, from this picture we expect the superconducting transition temperature to depend on the ionic mass via w_D, and indeed this is what we see

$$T_C \propto \frac{1}{w_D} \approx \frac{1}{\sqrt{M}}, \tag{3.1}$$

this is called the isotope effect.

This physical modelling is boasting a lot of success. In the next section we will examine this picture mathematically and find the Fermi surface is unstable to pair formation.

3.1 Cooper Pairs — Instability at the Fermi Surface

We have already seen why electrons may be attracted to one another, in this section we will show that the Fermi surface is unstable to pair formation with the presence of an attraction [39].

This model assumes a constant uniform attraction $-V$ in a 'skin' of w_D width around a spherical Fermi surface depicted in figure 3.2 on page 16. The Schrodinger equation for this pair is

$$-\frac{\hbar^2}{2m}\nabla_1^2\Psi - \frac{\hbar^2}{2m}\nabla_2^2\Psi + V(\mathbf{r}_1 - \mathbf{r}_2)\Psi = E\Psi, \tag{3.2}$$

where E is the energy of the pair. We use a pair wavefunction that is symmetric in real space and anti-symmetric in spin space given by

$$\Psi(\mathbf{r}_1, \mathbf{r}_2) = \left[\sum_{k>k_F} g_k \cos(\mathbf{k}\cdot(\mathbf{r}_1 - \mathbf{r}_2))\right] \left[|\uparrow\rangle_1 |\downarrow\rangle_2 - |\downarrow\rangle_1 |\uparrow\rangle_2\right], \tag{3.3}$$

where g_k is the momentum space electron-phonon coupling. Substituting in for the wavefunction gives

$$2\epsilon_k g_k + \sum_{k'>k_F} V_{kk'} g_{k'} = E g_k, \tag{3.4}$$

where

$$\epsilon_k = \frac{\hbar^2 k^2}{2m}, \qquad V_{kk'} = \int V(\mathbf{r}) e^{-i(\mathbf{k}-\mathbf{k}')\cdot\mathbf{r}}. \tag{3.5}$$

Assuming $V_{kk'} = -V$ for energies $\epsilon_F - \hbar w_D \leq \epsilon_k$, and $\epsilon_{k'} \leq \epsilon_F + \hbar w_D$ gives

$$(E - 2\epsilon_k) g_k = -V \sum_{k'>k_F} g_{k'} = -VC, \tag{3.6}$$

that can be rearranged to give

$$g_k = \frac{VC}{2\epsilon_k - E}, \tag{3.7}$$

$$C = \sum_{k>k_F} g_k = C \sum_{k>k_F} \frac{V}{2\epsilon_k - E}. \tag{3.8}$$

Figure 3.2: Fermi Surface with DeBye 'Skin' Attracting Phonons

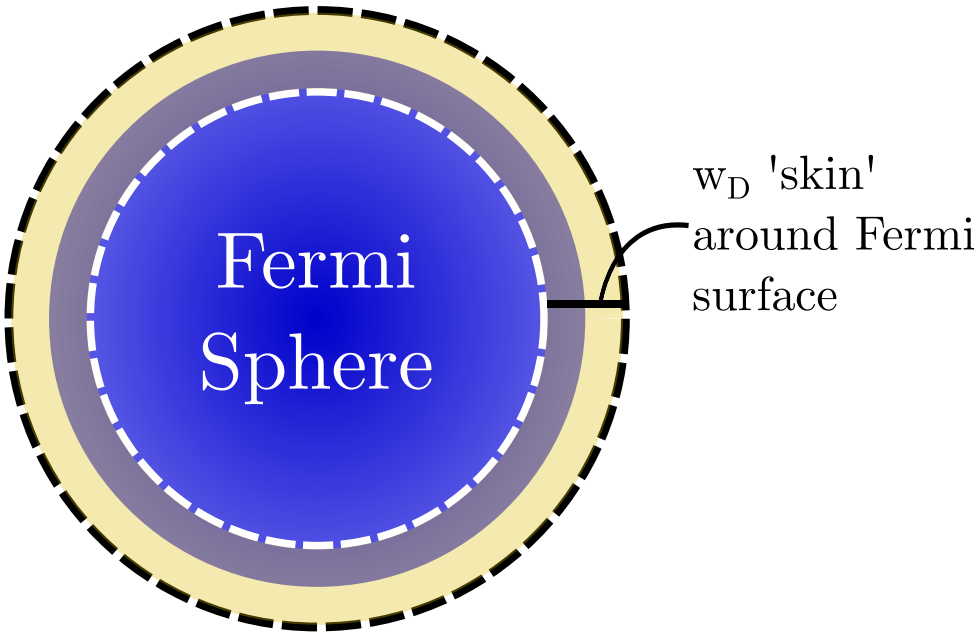

The Fermi surface along with a small window for which electrons are attracted to one another.

Dividing this by C and replacing the momentum sum with an energy integral gives

$$1 = N(\epsilon_F)V \int_{\epsilon_F}^{\epsilon_F+\hbar w_D} \frac{\mathrm{d}\epsilon}{2\epsilon - E} \tag{3.9}$$

$$= \frac{1}{2}N(\epsilon_F)V \log\left[\frac{2\epsilon_F + 2\hbar w_D - E}{2\epsilon_F - E}\right], \tag{3.10}$$

where $N(\epsilon_F)$ is the density of states at the Fermi energy. We can write $E - 2\epsilon_F = -\Delta$, where Δ is the binding energy of the pair. Which gives

$$\Delta = 2\hbar w_D \exp\left[-\frac{2}{N(\epsilon_F)V}\right]. \tag{3.11}$$

The pair of particles is bound! Interestingly this factor of 2 in the exponent is missing in the full BCS calculation. This is due to electron-hole symmetry not being considered correctly in the Cooper calculation.

In this section we showed Cooper's result of pairs binding due to a featureless attraction. In following section we will show the full BCS solution of conventional supercon-

ductivity.

3.2 BCS — Theory of Superconductivity

The BCS solution is remarkably effective in the predictions it makes. In this section we will solve the BCS Hamiltonian but in our own way, closer to the work of Valatin [40]. We will use this opportunity to replicate results that will occur in part II of the thesis. We will look at the total energy, occupation factor, and the superconducting gap. If Hartree-Fock mean field theory is unknown to you please see appendix D. The BCS Hamiltonian is

$$H = \sum_{k\sigma} \epsilon_k c^\dagger_{k\sigma} c_{k\sigma} - V \sum_{kk'q} c^\dagger_{k'\uparrow} c^\dagger_{q-k'\downarrow} c_{q-k\downarrow} c_{k\uparrow}, \tag{3.12}$$

where we are assuming a featureless interaction V, and the sum over q allows for a current to be included in the calculation. Allowing the correlations $n_k = \langle c^\dagger_{k\sigma} c_{k\sigma} \rangle$, $\Delta_k = \langle c^\dagger_{k'\uparrow} c^\dagger_{-k'\downarrow} \rangle$, and $\Delta^*_k = \langle c_{-k\downarrow} c_{k\uparrow} \rangle$ gives an average energy per site of

$$\bar{E} = \sum_{k\sigma} \epsilon_k n_k - V(n_k^2 + |\Delta_k|^2), \tag{3.13}$$

which gives an effective Hamiltonian (using Wick's theorem) of

$$H^{eff} = \sum_{k\sigma} \left[(\epsilon_k - V n_k) c^\dagger_{k\sigma} c_{k\sigma} - V(\Delta^*_k c^\dagger_{-k\uparrow} c^\dagger_{k\downarrow} + \Delta_k c_{-k\downarrow} c_{k\uparrow}) \right], \tag{3.14}$$

which can be rewritten as a matrix equation

$$H^{eff} = \sum_{\mathbf{k}} \begin{bmatrix} c^\dagger_{\mathbf{k}\uparrow} & c_{-\mathbf{k}\downarrow} \end{bmatrix} \begin{bmatrix} (\epsilon_k - V n_k) & V\Delta^*_k \\ V\Delta_k & -(\epsilon_k - V n_k) \end{bmatrix} \begin{bmatrix} c_{\mathbf{k}\uparrow} \\ c^\dagger_{-\mathbf{k}\downarrow} \end{bmatrix} + (\epsilon_k - V n_k). \tag{3.15}$$

Diagonalising this matrix gives the gapped BCS dispersion

$$E^\pm_k = \pm\sqrt{(\epsilon_k - V n_k)^2 + V^2 |\Delta_k|^2}. \tag{3.16}$$

Figure 3.3: BCS Energy as a Function of Occupation

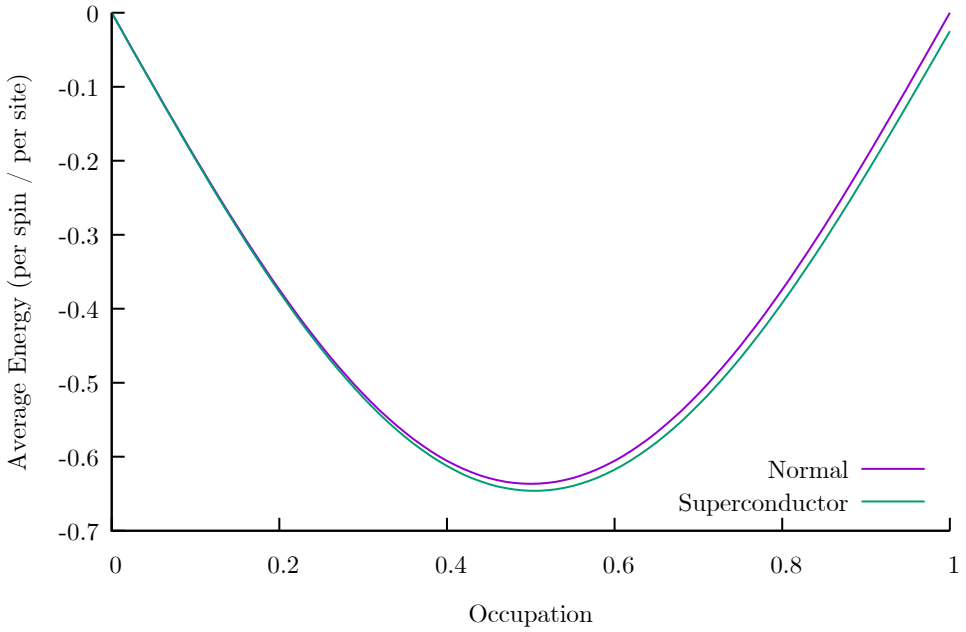

BCS Superconducting and normal energy as a function of occupation, with $V = 0.1$ on the 1D chain. The energies are close but the superconducting solution is energetically favourable for all occupation.

Using the resolvent we can generate the self consistent parameters

$$n_k = \frac{1}{2}\left(1 - \frac{A_k}{E_k^+}\right), \tag{3.17}$$

$$\Delta_k = \left(\frac{-B_k}{2E_k^+}\right), \tag{3.18}$$

where $A_k = \epsilon_k - Vn_k - \mu$, and $B_k = V\Delta_k$.

One can solve these equations in the limit Δ_k is small but we've elected to solve them numerically self consistently for a more accurate result. Figure 3.3 on page 18 depicts the total average energy as a function of occupation for a one dimensional chain. This result will be repeated for our particular system in Part II, and hence provides context with respect to conventional superconductivity. The energies are close but the superconducting solution is energetically favourable for all occupation.

In this chapter we modelled conventional superconductors, ran through the Cooper

demonstration of pairing, and used these pairs as a basis for the BCS mean field solution. These calculations will be repeated for our model in part II. In the following chapter we will model unconventional superconductors and find that we will be able to say very little conclusively.

CHAPTER 4

MODELLING UNCONVENTIONAL SUPERCONDUCTORS

Unconventional superconductors have rich physics. In this chapter we will model $La_{2-x}Sr_xCuO_4$, the simplest cuprate, and $CeCu_2Si_2$ the first heavy fermion superconductor. In the first section we will develop the most accurate model for the cuprates, but it is rather unwieldy. This will be followed up by a dramatic simplification in the next section. Here we will follow the argument made by Zhang & Rice [41] and generate a single band Hubbard model. This will be extended to the $t - J$ model, which is the Hubbard model in the limit of strong Coulomb repulsion. In the next section we look at resonance valence bond theory [42] developed by Anderson to explain unconventional superconductivity. This is an interesting theory but has boasted little quantitative success due to its immense complexity. Finally we look at the Anderson lattice model [43], the simplest model for heavy fermion superconductors. We will be modelling these materials using physical chemistry. If this is unfamiliar see appendix B.8.

4.1 The Three Band Model — Arguments From Physical Chemistry

In this section we will develop an accurate yet complex model for the cuprates, focusing our attention on $La_{2-x}Sr_xCuO_4$ (LSCO). Modelling begins on the parent compound La_2CuO_4, which is an anti-ferromagnetic Mott insulator [44]. Doping will change little to the core modelling and the result will be a three band model on the hole doped side and a single band Hubbard model on the particle doped side.

We begin with the electron configuration of the compound: La is [Xe] $5d^1$ $6s^2$, Cu is [Ar] $3d^{10}$ $4s^1$, and O is [He] $2s^2$ $2p^4$. Oxygen is incredibly electronegative and will occur as O^{2-}, lanthanum is the opposite and will occur as La^{3+}. Basic arithmetic then gives the charge on the copper as $-(2 \times 3 - 4 \times 2) = 2$. Therefore, there are 9 electrons on the copper sites. This is one less electron than a fully occupied 3d shell, therefore it makes sense to use a hole description. The parent compound has one hole on each copper in the 3d shell. Now let's take a look at the structure of the compound and the effect from the crystal field.

The structure of the material is perovskite and is depicted in figure 4.1 on page 23. There are layered copper oxide planes stacked on lanthanum oxide planes, with each copper site being surrounded by an oxygen octahedron. This is depicted in figure 4.2 on page 24. The crystal field lifts angular degeneracy. The positive e_g orbitals have strong overlap with the neighbouring negative oxygen atoms, hence they gain Coulomb energy and are favoured over the t_{2g} orbitals. If the octahedral environment was perfect the two e_g orbitals would be degenerate. The environment is not perfect however, and distortions elongate the octahedra along the z-axis. This lifts the degeneracy and the $d_{x^2-y^2}$ is favoured. The degeneracy lifting is depicted in figure 4.3 on page 24.

The final thing required to model the parent compound is super-exchange [46]. Hybridisation with intermediate oxygen atoms allows for energy gain. This comes in the form of virtual hopping. The two magnetic configurations are ferromagnetism and anti-

Figure 4.1: Structure of Lanthanum Copper Oxide

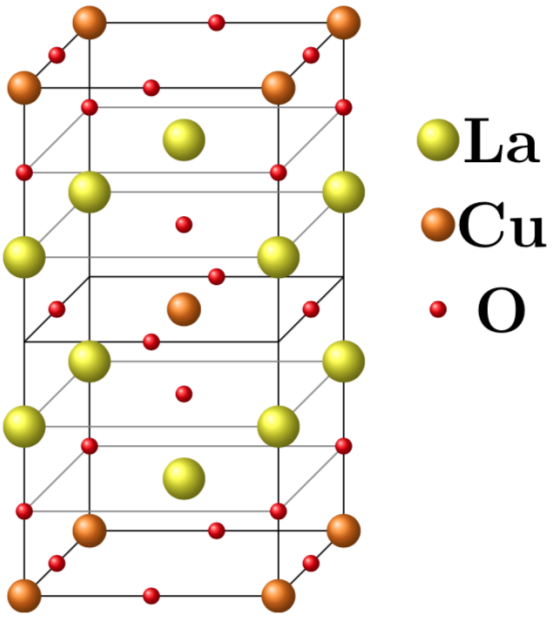

Structure of the parent compound of LSCO [45] Here yellow sites are lanthanum atoms, orange sites are copper atoms, and red sites are oxygen atoms. There is a layered structure with copper oxide layers, followed by two lanthanum oxide layers.

ferromagnetism, with the latter gaining more energy than the former. This process is depicted in figure 4.4 on page 25.

The parent compound is an anti-ferromagnetic Mott insulator formed by $d_{x^2-y^2}$ orbitals on each copper site. Now we examine the effects of doping. For LSCO this comes in the form of strontium doping which takes the place of lanthanum in the compound. The primary effect of the strontium is to act as a hole donator as its electron configuration is [Kr] $5s^2$ which is one fewer valence electron than lanthanum. As a result we are modelling hole doping in the system.

The first question is where do the holes go? To answer this we require knowledge of the energy states of the potential occupation sites. This is depicted in figure 4.5 on page 25. From this we can see that the holes will reside on the oxygen atoms [47].

The next question is which orbitals will they occupy? There are three options p_x, p_y, and p_z. Figure 4.6 on page 26 depicts the relevant configurations from which we can see

Figure 4.2: Octahedral Oxygen Environment Around a Copper Atom

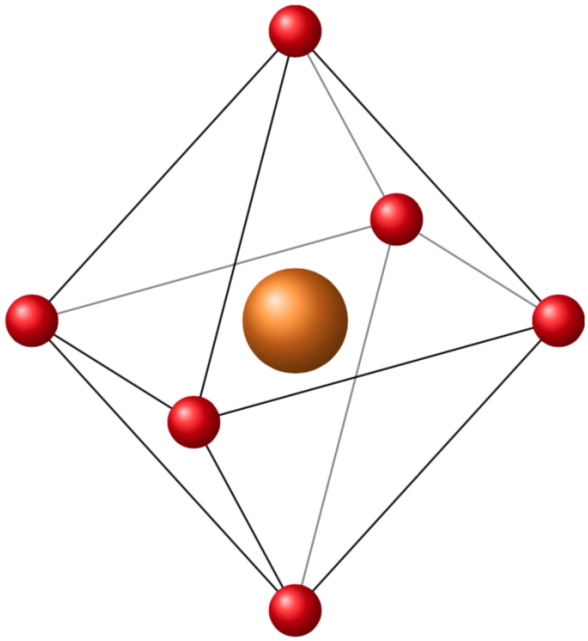

The local oxygen (red sites) environment for every copper (orange sites) atoms. There is an oxygen octahedron surrounding the copper atom creating a crystal field which lifts angular degeneracy.

Figure 4.3: Copper Crystal Field Splitting

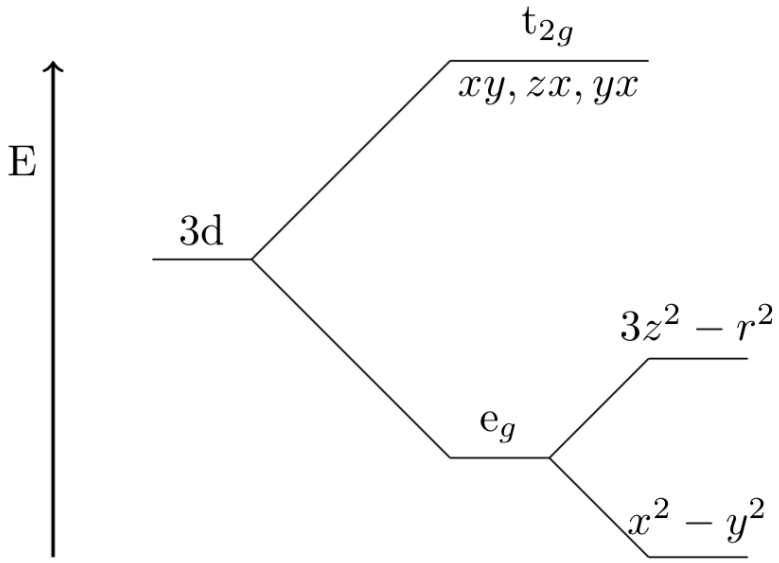

The energy levels of each orbital splitting. The first split is due to the octahedral crystal field, whilst the second is due to the distortion of this octahedral environment.

Figure 4.4: Anti-Ferromagnetic Superexchange

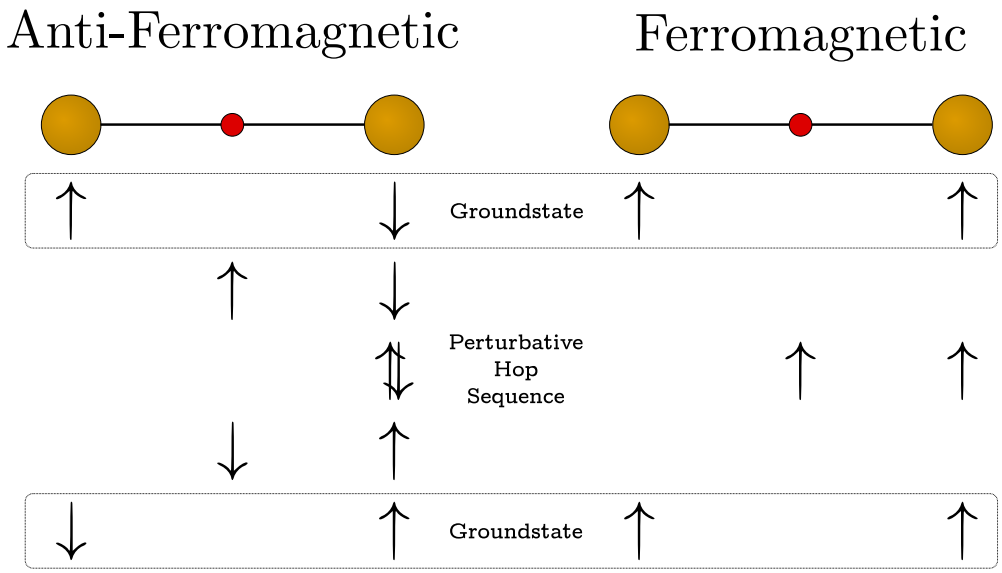

Visual representation explaining the source of anti-ferromagnetism. The large orange sites are Copper and small red sites are oxygen. Antiferromagnetic order allows for virtual hopping onto neighbouring states, ferromagnetism does not.

Figure 4.5: Energy Levels Of Placing Holes on Different Atoms

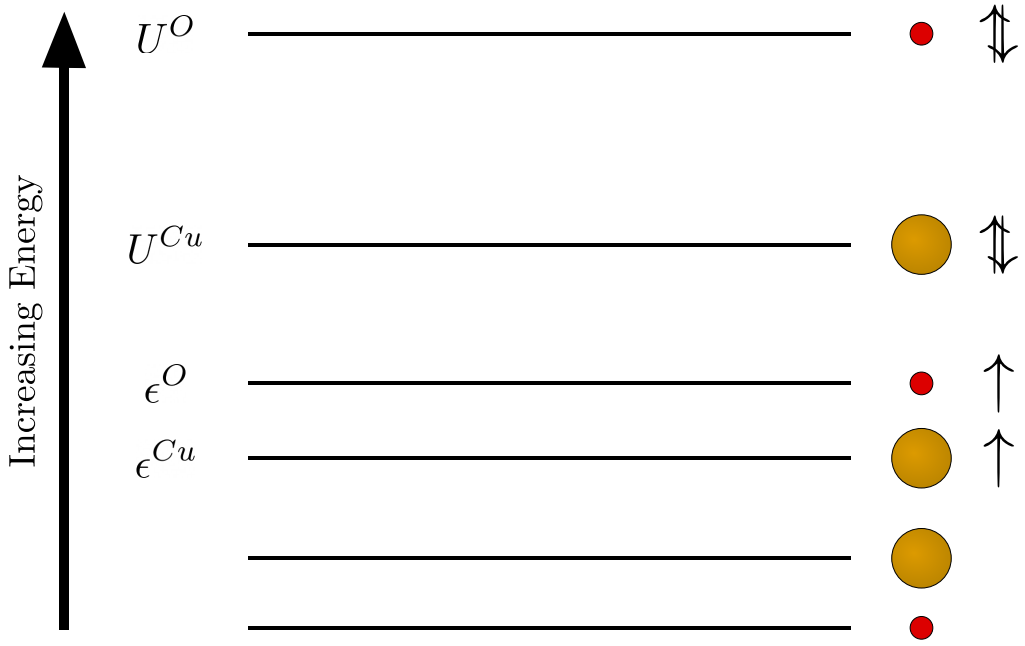

Energy cost for adding holes on different atoms, with example states on the right [48].

Figure 4.6: Different Orbital Configurations to Hybridise with the Copper Hole

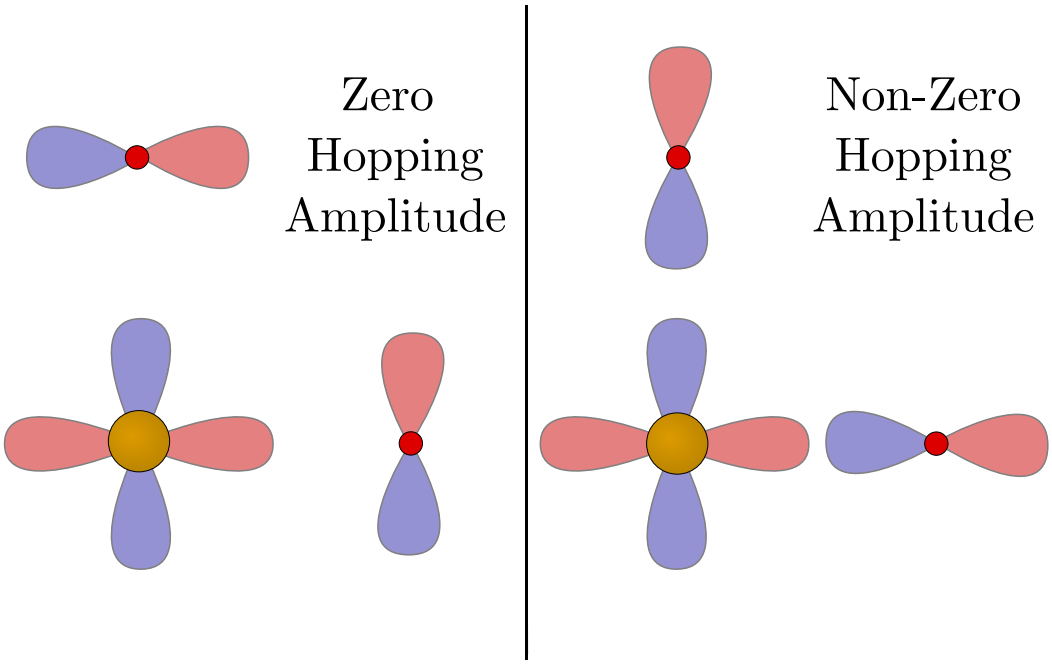

Copper atom (large, orange) with possible hybridisation on the oxygen atom (small, red). The hole on the copper atom occupies the $d_{x^2-y^2}$ state. The hole on the oxygen atom can occupy one of three states: $2p_z$ (not depicted as zero by symmetry), $2p_y$, and $2p_x$. The left depicts hybridisation which are zero by symmetry, and the right are permitted configurations.

that one wins out: the one with the most overlap. The orbitals are p_x when hopping in the $\hat{x}$ direction and p_y when hopping in the $\hat{y}$ direction This is because hybridisation allows for energy gain from hopping. The lack of hybridisation between planes (due to no p_z) means all the physics is contained within the two dimensional copper oxide planes, which are depicted in figure 4.7 on page 27.

We can therefore model this system with a three band Hubbard model for the copper-oxide layers. Therefore, the nearest neighbour Hamiltonian [49] is

$$H_{Holes} = \sum_{ij\sigma}\left[\epsilon^{Cu} d^{\dagger}_{i\sigma} d_{i\sigma} + \epsilon^{O} p_{x_{j\sigma}}^{\dagger} p_{x_{j\sigma}} + \epsilon^{O} p_{y_{j\sigma}}^{\dagger} p_{y_{j\sigma}}\right] + \sum_{ij}\Big[U^{Cu} d^{\dagger}_{i\uparrow} d_{i\uparrow} d^{\dagger}_{i\downarrow} d_{i\downarrow} + U^{O} p_{x_{j\uparrow}}^{\dagger} p_{x_{j\uparrow}} p_{x_{j\downarrow}}^{\dagger} p_{x_{j\downarrow}} + U^{O} p_{y_{j\uparrow}}^{\dagger} p_{y_{j\uparrow}} p_{y_{j\downarrow}}^{\dagger} p_{y_{j\downarrow}}\Big] - V_{d,p} \sum_{\langle ij\rangle\sigma}\left[d^{\dagger}_{i\sigma} p_{x_{j\sigma}} + p_{x_{j\sigma}}^{\dagger} d_{i\sigma} + d^{\dagger}_{i\sigma} p_{y_{j\sigma}} + p_{y_{j\sigma}}^{\dagger} d_{i\sigma}\right], \quad (4.1)$$

where ϵ^{Cu} is the occupation energy for a copper $d_{x^2-y^2}$ hole, ϵ^{O} is the occupation energy for

Figure 4.7: Copper Oxide Layer

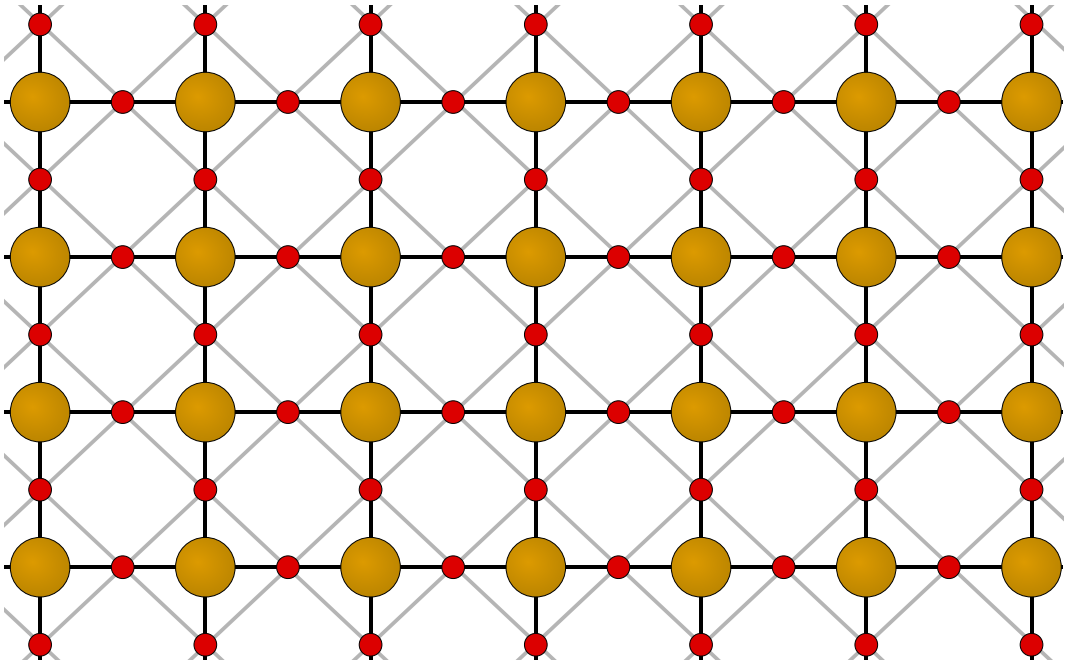

All of the physics of the cuprates are within the copper oxide layers depicted above. Here the orange sites are copper atoms and red sites are oxygen atoms. There is an underlying square lattice made of the copper sites, with oxygen atoms between each copper.

an oxygen p_x or p_y hole, U^{Cu} is the Coulomb penality for doubly occupying a copper site, U^O is the Coulomb penality for doubly occupying an oxygen site, V_{ij} is the hybridisation between copper and oxygen sites, $d^\dagger_{i\sigma}$ creates a $d_{x^2-y^2}$ hole with spin σ on copper site i, ${p_x}^\dagger_{j\sigma}$ creates a p_x hole with spin σ on oxygen site $i + \hat{\mathbf{x}}$, and ${p_y}^\dagger_{j\sigma}$ creates a p_y hole with spin σ on oxygen site $i + \hat{\mathbf{y}}$. This is depicted in figure 4.8 on page 28.

This model contains all the hole physics but is incredibly complicated. Interestingly the particle doped Hamiltonian is quite simple in comparison. From figure 4.5 on page 25 we can see that upon particle doping electrons will reside on the copper sites filling the 3d shell, which is a vacuum in the hole picture. The remaining holes are able to move but only via hybridisation through the intermediate oxygen sites, for example $\langle ij\rangle\langle ji'\rangle$. What remains is an ordinary Hubbard model on the 2D square lattice

$$H_{Particles} = \epsilon^{Cu} \sum_{i\sigma} d^\dagger_{i\sigma} d_{i\sigma} + U^{Cu} \sum_i d^\dagger_{i\uparrow} d_{i\uparrow} d^\dagger_{i\downarrow} d_{i\downarrow} - t \sum_{\langle ii'\rangle\sigma} d^\dagger_{i\sigma} d_{i'\sigma}, \tag{4.2}$$

Figure 4.8: Orbital Configuration of the Copper Oxide Layers

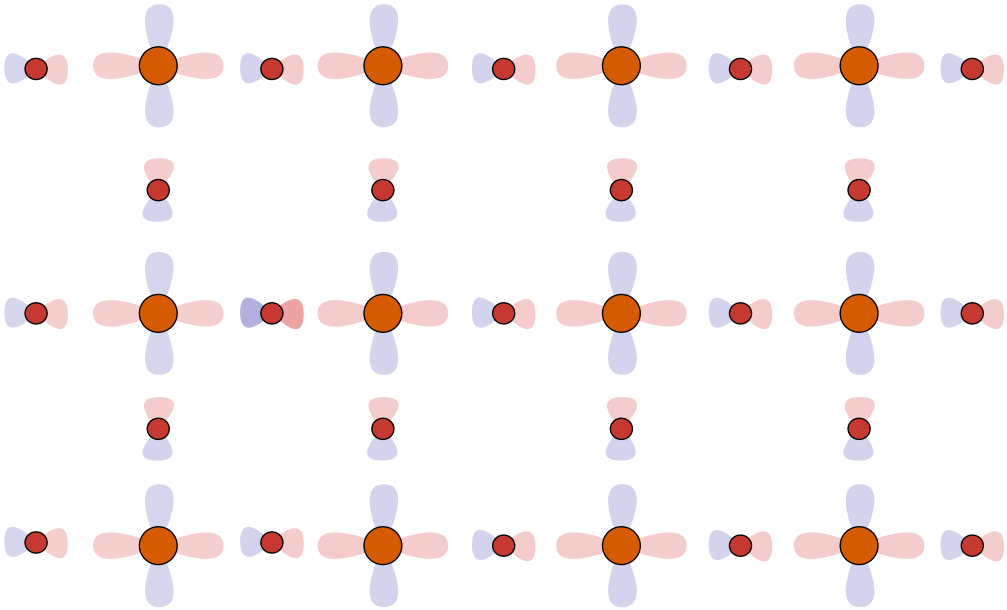

All copper sites are occupied by a $d_{x^2-y^2}$ hole. The oxygen sites (when occupied) are in either the $2p_x$ or $2p_y$ state if they are on the $i+\hat{\mathbf{x}}$ orbital or $i+\hat{\mathbf{y}}$ respectively.

where the hopping can be perturbatively shown to be

$$t = \frac{V^2}{\epsilon^{Cu} - \epsilon^{O}}. \tag{4.3}$$

In this section we modelled the copper oxide layers of the cuprates. In the hole doped side we got a complicated three band Hubbard model, whilst on the particle doped side we derived an ordinary Hubbard model. In the next section we will dramatically simplify the hole doped model by replicating Zhang & Rice's calculation.

4.2 The Single Band Hubbard Model — Zhang & Rice's Calculation

In this section we will go over the work done by Zhang and Rice [41], where they mapped the three band Hubbard model from the previous section to a single band Hubbard model.

Strong hybridisation between the copper and oxygen atoms bind a hole on each square of oxygen atoms around a central copper. This singlet moves through the lattice like a hole in the original model.

In this calculation we set $\epsilon^{Cu} = 0$, $\epsilon^{O} > 0$, and consider the case $V << U^{Cu}$, ϵ^{O}, $U^{Cu} - \epsilon^{O}$. As $\epsilon^{O} < U^{O}$ extra holes reside on the oxygen sites but as $V > 0$ there is energy to be gained from hybridisation.

We will consider the symmetric and anti-symmetric plaquette operator

$$P_{i\sigma}^{(S,A)} = \frac{1}{2}\sum_{l\in i}(\mp 1)p_{l\sigma}, \tag{4.4}$$

which creates a symmetric $(S,-)$, or anti-symmetric $(A,+)$ superposition over the 4 oxygen sites around a copper atom on site i. The creation of p_x or p_y is implicit for the appropriate sites. Both $P_{i\sigma}^{S}$ and $P_{i\sigma}^{A}$ can hybridise with a copper $d_{x^2-y^2}$ hole to form singlet or triplet states. Using second order perturbation theory it can be shown that the hybridisation energy of $P_{i\sigma}^{S}$ singlet is $-8(t_1+t_2)$, of the $P_{i\sigma}^{S}$ triplet is 0, and of the $P_{i\sigma}^{A}$ is $-4t_1$. Here $t_1 = \frac{V^2}{\epsilon^O}$, and $t_2 = \frac{V^2}{U^{Cu}-\epsilon^O}$. The largest energy gain is that of the $P_{i\sigma}^{S}$ singlet state, due to phase coherence. This is the Zhang-Rice singlet and is depicted in figure 4.9 on page 30.

This needs to be compared with the energy of a hole at a fixed site l to see what is preferred. Using the same second order perturbation theory, the binding energy of a singlet combination of an oxygen hole and its neighbouring copper site is $-2(t_1+t_2)$, which is only a quarter of the binding energy of the Zhang-Rice singlet. The effective hopping energy from one oxygen site to another is either t_1 or t_2, as it requires hopping through an intermediary copper site. Both of these are much smaller than the separation between these states so we can safely project out the anti-symmetric oxygen hole states and work in subspace of $P_{i\sigma}^{S}$ states.

Now let's look at the motion of the Zhang-Rice singlets. The energy of two singlets on the same square i.e. $P_{i\uparrow}^{S}P_{i\downarrow}^{S}d_{i\sigma}$ is $-(6t_1+4t_2)$, much higher than two separated singlets.

Figure 4.9: Zhang-Rice Singlet

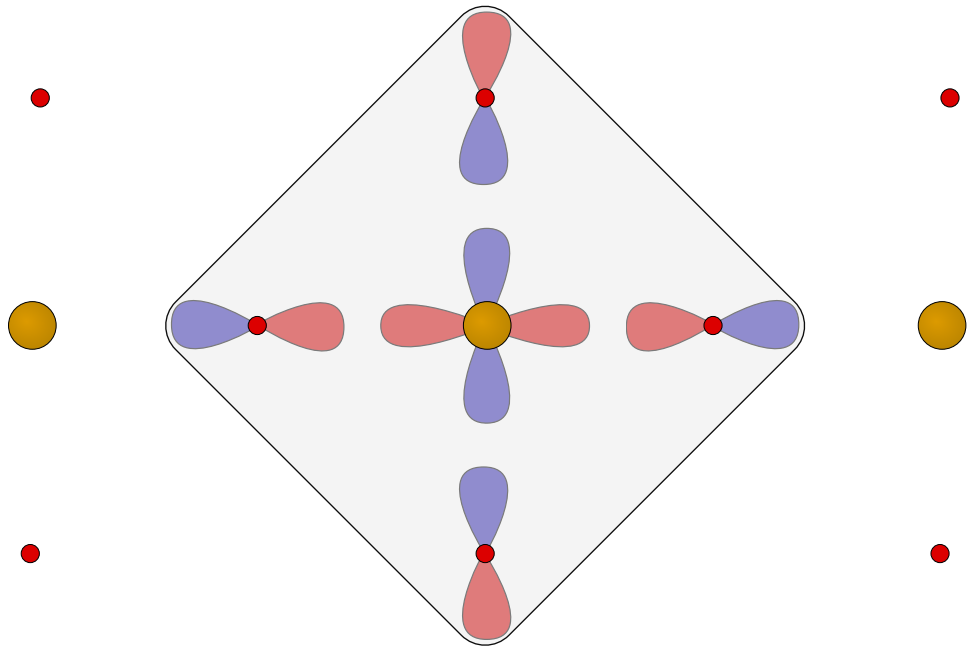

Visual representation of the Zhang-Rice singlet (grey box). A singlet hybridisation of $P^S_{i\sigma}$ operator with a central copper site.

Zhang-Rice singlets feel a strong repulsion on the same site. The singlets are not orthogonal as neighbouring ones share a common oxygen site. To examine the motion we are required to construct a Wannier basis. Here, Zhang and Rice decided to set $t_1 = t_2 = t$ and showed using second order perturbation theory that nearest neighbour hopping was of strength $\approx -1.5t$ and next nearest neighbour hopping was of strength $\approx -0.16t$. They showed that when a singlet moves from site i to j a copper hole moves simultaneously from j to i. This means that the singlet, for all intents and purposes, acts like a hole in the original copper operator picture, and what we are left with is an ordinary Hubbard model. This is given by

$$H^{ZR}_{Holes} = \epsilon^{Cu} \sum_{i\sigma} d^\dagger_{i\sigma} d_{i\sigma} + U^{Cu} \sum_i d^\dagger_{i\uparrow} d_{i\uparrow} d^\dagger_{i\downarrow} d_{i\downarrow} - 1.5t \sum_{\langle ij\rangle\sigma} d^\dagger_{i\sigma} d_{j\sigma}, \tag{4.5}$$

which is nearly identical to the Hubbard model for particles.

In this section we followed Zhang and Rice's argument that the Hamiltonian for the

hole doped cuprates is the nearest neighbour single band Hubbard model. In the following section we will look at a natural representation of this model in the large U limit, along with its limitations.

4.3 The $t - J$ Model

Unfortunately, reducing the three band Hubbard model to the single band Hubbard model does little in tackling superconductivity. This is because the Hubbard model is notoriously difficult to tackle highlighted by the fact a solution only exists for the 1D chain. However, theorists have been motivated by the physics of unconventional superconductors; namely the large on-site Coulomb repulsion to chemical bonding ratio [48]. For example, in the cuprates $U \approx 8t$. In this section we will look at one such limiting model, the $t - J$ model.

Let's take the ordinary Hubbard model

$$H = -t \sum_{\langle ij \rangle \sigma} c^\dagger_{i\sigma} c_{j\sigma} + U \sum_i c^\dagger_{i\uparrow} c_{i\uparrow} c^\dagger_{i\downarrow} c_{i\downarrow}. \tag{4.6}$$

In the limit $U = \infty$ double occupation is prohibited on a site, as this state costs infinite energy. To deal with this we can simply project this state out when dealing with hopping. The operator

$$T^\dagger_{i\sigma} = (1 - c^\dagger_{i\bar{\sigma}} c_{i\bar{\sigma}}) c^\dagger_{i\sigma}, \tag{4.7}$$

creates a particle on site i with spin σ provided there is not already a particle with spin $\bar{\sigma}$ there. Therefore we can enforce the limit $U = \infty$ using $c_{i\sigma} \to T_{i\sigma}$, which gives

$$H = -t \sum_{\langle ij \rangle \sigma} (1 - c^\dagger_{i\bar{\sigma}} c_{i\bar{\sigma}}) c^\dagger_{i\sigma} c_{j\sigma} (1 - c^\dagger_{j\bar{\sigma}} c_{j\bar{\sigma}}). \tag{4.8}$$

This is the t model.

In reality though U is not infinite, it is finite. To deal with this we can perturbatively lift this limit using Heisenberg corrections. This process is standard and, if unfamiliar,

has been detailed in appendix F. Combining the t model with the Heisenberg model gives the $t-J$ model (where $J=\frac{t^2}{U}$)

$$H=-t\sum_{\langle ij\rangle\sigma}(1-c^{\dagger}_{i\bar{\sigma}}c_{i\bar{\sigma}})c^{\dagger}_{i\sigma}c_{j\sigma}(1-c^{\dagger}_{j\bar{\sigma}}c_{j\bar{\sigma}})+J\sum_{\langle ij\rangle}\mathbf{S}_i\cdot\mathbf{S}_j. \tag{4.9}$$

In principle this accurately deals with the large U limit of the Hubbard model and is therefore the model of the cuprate superconductors; however, there are limitations to this model.

4.3.1 Limitation of This Model

The biggest limitation of this model is that it is arguably more difficult to deal with than the original Hamiltonian. As exact techniques are not sophisticated enough we are required to use approximate techniques. All approximate techniques cannot exactly constrain the projection; they only keep the constraint on *average*. This is because approximation schemes are designed to convert many body problems into single particle ones, but the operators that restrict the subspace are many body by construction. Therefore there are fluctuations on to previously prohibited states! The only way to to mitigate this issue is to use a basis which completely covers the accessible states.

There are also inconsistencies with this model and experiment. Firstly the phase diagram is *not* symmetric with respect to doping. This model would predict that it is. There is a reduced pseudogap or strange metal phase in the particle doped side of the phase diagram [50]. Add to that the fact experiments see a square Fermi surface [51], and the nearest neighbour model would produce a diamond. The next nearest neighbour hopping would have to be approximately half the size of nearest neighbour hopping to create this. This is *not* predicted by Zhang and Rice.

The last, most interesting, limitation of this model is that of the local structure a hole creates. In the $t-J$ model the biggest scale is t so we examine the effects from just the hopping. A hole, at the Mott point, in the t model drives the local environment

Figure 4.10: Local Copper Oxygen Environment with a Hole

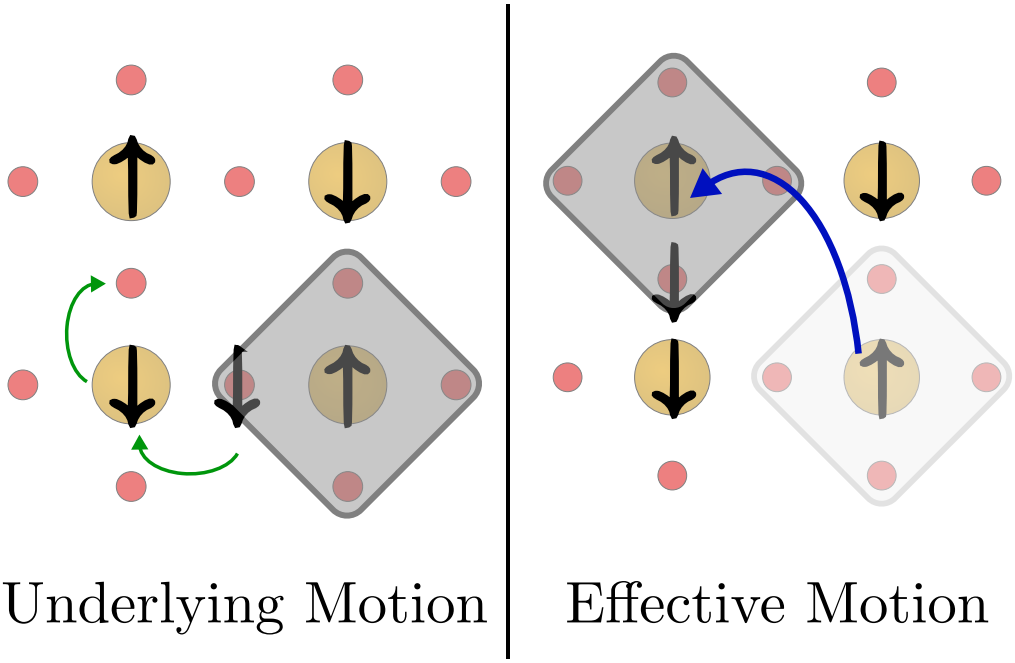

Oxygen and copper atoms are (small) red and (large) orange sites respectively. The diamonds are Zhang-Rice singlets. The spin configuration plays a more important role than the energetics. At the same strength of an ordinary Zhang-Rice singlet hop we can make a next nearest neighbour hop if the spin configuration permits it.

ferromagnetic. This is Nagaoka's theorem [52]. However, in the original three band model a hole drives the local environment to a low spin environment. Zhang and Rice's model only looks at the energetics but not the spin configuration. This is depicted in figure 4.10 on page 33.

In this section we derived the $t - J$ model by taking the physically motivated limit U is large from the Hubbard model. We found that there are many limitations to this approach. In the next section we look at Anderson's resonating valence bond theory.

4.4 Resonance Valence Bonds — An Idea by Anderson

The last section on the cuprates is on Anderson resonating valence bond theory [42]. This theory is interesting but has boasted little quantitative success. The theory is rather simple

1. The cuprates are dominated by Mott physics and therefore the $t - J$ model is the minimal model.

2. The ground state is a superposition (resonance) of all possible configurations of singlets (valence bonds). This ensures no Coulomb penalty and maximal gain from hybridisation.

3. This Mott localisation remains when doping occurs, and hence these singlets propagate in the metallic state mediating the superconductivity. These singlets are the Cooper pairs which cause superconductivity.

Unfortunately there has been little analytical work on this model and, as many use these ideas on the $t - J$ model, suffer from the limitations previously mentioned.

So why mention this model at all? Well, the work presented in part II of this thesis will have remnants of this theory spontaneously appear, but the work will be rather rigorous. Now let's take a look at the model for heavy Fermion superconductors.

4.5 Anderson Lattice Model

In this section we will model $CeCu_2Si_2$, the first heavy fermion superconductor [26]. This model will apply to most heavy fermion superconductors and the Anderson lattice model will be the result.

We begin with the electron configuration of the compound: Ce is [Xe] $4f^1$ $5d^1$ $6s^2$, Cu is [Ar] $3d^{10}$ $4s^1$, and Si is [Ne] $3s^2$ $3p^2$. Cerium is a lanthanide and will form a Ce^{3+} core

leaving a 4f electron, and silicon bonds covalently as expected (being underneath carbon). This system is metallic and these electrons are described by a tight binding model.

The structure is largely irrelevant for this modelling. Instead we focus on the remaining f electron on the cerium sites. These are in the Hill limit, meaning they do not directly hybridise with one another. Instead they hybridise with the copper electrons. This is naturally described by the Anderson lattice model [43]

$$H = \sum_{j\sigma} \epsilon_f f^\dagger_{j\sigma} f_{j\sigma} + \sum_{\langle j,j'\rangle\sigma} t_{jj'} c^\dagger_{j\sigma} c_{j'\sigma} + \sum_{j,\sigma} \left(V_j f^\dagger_{j\sigma} c_{j\sigma} + V_j^* c^\dagger_{j\sigma} f_{j\sigma} \right) + U \sum_j f^\dagger_{j\uparrow} f_{j\uparrow} f^\dagger_{j\downarrow} f_{j\downarrow}, \quad (4.10)$$

where $f^\dagger_{i\sigma}$ creates a 4f electron on a cerium site i with spin σ, and $c^\dagger_{i\sigma}$ creates a 3d electron on a copper site i with spin σ.

Similar to the Hubbard model that is generated for the cuprates, this model is simple but tough to tackle. The key difference in this case is that V is small in heavy fermion systems whilst for the cuprates it is the dominant interaction. Heavy fermion systems are dominated by the background metal with the flat band physics from the f-electrons only acting to increase the effective mass of the system [53]. Whereas the cuprates are not dominated by the metal, instead they are dominated by the Hubbard interaction.

In this chapter we modelled unconventional superconductors. For the cuprates we found they were described by a three or one band Hubbard model for hole and particle doping respectively. The three band model can be represented as a one band model if the arguments of Zhang and Rice are followed, but the resulting $t - J$ model has limitations. Finally, we modelled heavy fermion superconductors and found a similarly difficult Hamiltonian to tackle. When it comes to unconventional superconductivity we have just about got the model, and even then there are issues.

CHAPTER 5

SUMMARY

In this first part we set the stage for the rest of this thesis. As the work is on unconventional superconductivity we began with a history of superconductivity. Here we learnt the essentials. Superconductivity is the phenomena of zero resistivity and perfect diamagnetism. In conventional superconductors electrons are attracted to one another with phonons. Unconventional superconductors are simply ones where this is not what drives superconductivity. They have rich phase diagrams which include magnetism, and are strongly correlated electron systems with small correlation lengths.

The next chapter had us adding mathematical flesh onto the bones of the previous chapter. Here we discussed the source of attraction: lattice distortions mediated by phonons. This made the prediction of temperature dependence on ionic mass and a large correlation length which were experimentally verified. We then showed that the Fermi surface is unstable to pairing under a featureless attractive interaction whose source is phonons (the Cooper calculation). Next we took this further and showed the BCS solution.

Following that, we modelled unconventional superconductors. Here we generated an unwieldy three band Hubbard model for the hole doped cuprates and a single band model for the particle doped cuprates. We then followed the work of Zhang and Rice to show that the three band model could be mapped to a single band model. The resulting model has limitations such as lacking corroboration with experiments. Finally we introduced An-

derson's resonance valance bond theory, and we modelled heavy fermion superconductors using the Anderson lattice model.

There is a wealth of work done within the field of superconductivity. As a result we only gave a sliver of what is out there. This included all the background to understand the work that is to come in this thesis.

In the next part of this thesis, we are going to present a rigorous demonstration of superconductivity in a repulsive Hubbard model. This is relevant as we have shown the cuprates can be modelled by a Hubbard model. This work will follow the BCS story, beginning with a *proof* of pairing and subsequent mean field solution. The results presented will mirror the BCS results presented in this first part.

The third part of this thesis will look at a new technique we've created to deal with strongly interacting problems non-perturbatively with remarkable accuracy. This directly addresses the issues raised in this part about the difficulty in dealing with the Hubbard model.

Part II

Superconductivity in a Particular $U = \infty$ Hubbard Model

CHAPTER 6

INTRODUCTION

Superconductivity is the macroscopic quantum phenomenon corresponding to zero electrical resistance and perfect diamagnetism, where the latter is known as the Meissner effect [1]. The first superconductors were phonon mediated [54, 55], described by the formation of Cooper pairs [39] and subsequent condensation in the BCS solution [4]. In these materials Coulomb repulsion can be sidestepped, as the correlation length in these superconductors was large, allowing the electrons to be attracted at a distance where Coulomb is screened. Only electrons very close to the Fermi surface participate, within a Debye energy or so. The next generation of superconductors were strongly correlated and do not fit naturally into this picture. The Coulomb repulsion is dominant and so the interactions are both repulsive and not weak, the coherence length is quite small and so the electrons are not naturally well separated. There is also evidence that all the charge carriers participate and the phenomenon is not restricted to a tiny energy region around the Fermi surface [56] (see figure 6.1 on page 42). We investigate a strongly correlated model which is susceptible to superconductivity with these strongly-correlated hallmarks.

The physics of the cuprates is that of doping a Mott insulator [22]. The Coulomb interaction dominates the chemical bonding and the electrons are localised even though the non-interacting picture would offer a metal. This Mott insulator is usually an antiferromagnet, caused by the residual effects of the chemical bonding and the fact that the

Figure 6.1: Uemura Plot

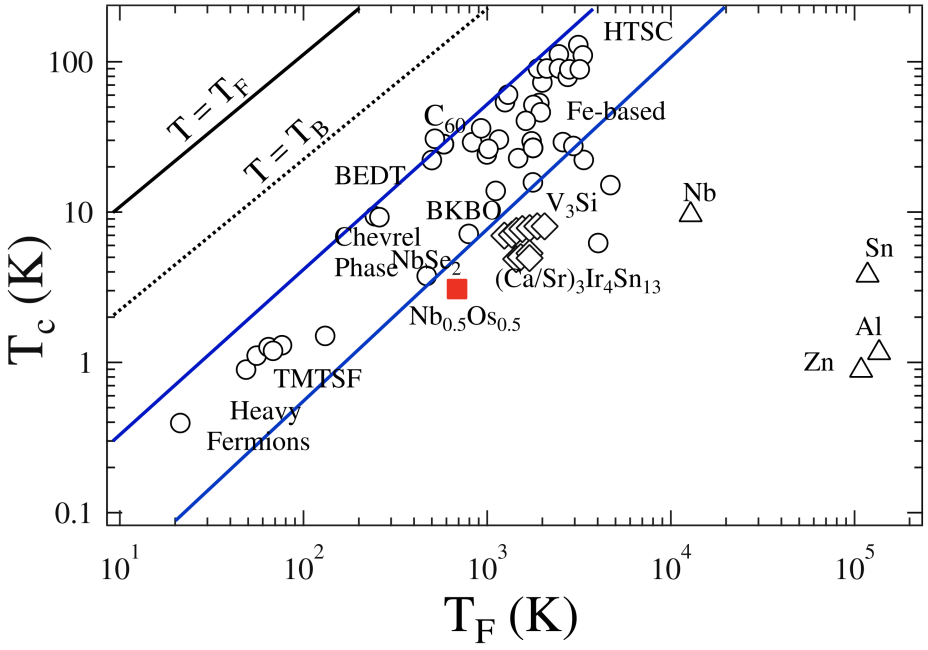

Superconducting transition temperature versus effective Fermi temperature. $T_C = T_F$ would correspond to the entire band of electrons contributing to the superconductivity. Taken from [57].

Coulomb interaction is not infinite known as super-exchange [22]. We will take the mathematical limit that the Coulomb interaction is divergent, eliminating this magnetism, and only reintroduce it as an afterthought; our target is really the superconductivity. Strongly correlated systems are not all superconductors and a variety of phenomena are observed. We also observe a phase which corresponds to the ferromagnetism in the manganites, and the overall picture is a direct competition between this ferromagnet and the superconductor, with the ferromagnet winning in the limit of extreme Coulomb interaction, physically reminiscent of Nagaoka ferromagnetism [52].

Superconductivity is a tricky property to investigate mathematically. The fundamental issue is that of correlations. In metals we know how to describe a non-interacting state in terms of a Fermi surface and occupancy, but in the presence of interactions we might expect a Fermi-liquid description but we only have vague renormalisation arguments to suggest which correlations might be relevant at low energy. On a more practical level, we have mean-field theory which targets the best non-interacting state to approximate

the Fermi-liquid. The positive characteristic of mean-field theory is that it only provides order if the system is susceptible to that order, and the negative characteristic is that if the system is susceptible to order then the technique will offer the order even when there are better correlated states available to the system. We will employ the assumption that if the system is susceptible to superconductivity then mean-field theory will predict this and that only low dimensional fluctuations would be expected to destabilise this order via the Mermin-Wagner theorem [58].

Obviously, mean-field theory is only credible when the interactions are weak, but we are studying a model with divergent repulsion, so we need some non-trivial mathematics to deal with this. Our first step is to map our original strongly correlated Hamiltonian onto another weakly interacting Hamiltonian. This step is exact and is accomplished by a non-linear fermion transformation [59]. The resulting description usually has weak interactions and so the mean-field theory should be credible; in addition we have a comparison with an exact diagonalisation study which shows good agreement. Since we are restricted to mean-field theory to demonstrate pairing, we have elected to work in one-dimension. This has the advantage that we can compare with our exact diagonalisation, which is restricted to small systems, but has the disadvantage that long-range phase fluctuations would physically be expected to eliminate any long-range order [58]. The mean-field theory erroneously promotes the long-range order, which would be correct in three dimensions, but these weak power-law promoting fluctuations are an irrelevance to the physical interactions which locally promote the superconducting correlations.

Physically, the mechanism that induces the superconductivity is surprisingly simple. The strong repulsion means that situations with extra local charge have restricted motion, they have to avoid paying the repulsive energy penalty. Situations with less local charge can move around more freely. It can be advantageous to allow local charge fluctuations because the rarefied configurations together with the denser blocked regions gain more from the hopping than the homogeneous average. This is depicted in figure 8.1 on page 67. Obviously this requires non-linearity, with the almost vacant being strongly preferred over

both the average and the dense configurations. This non-linearity is provided by correlated hopping: the chemical bonding that depends on the local occupancy of the site bonded to. This correlated hopping is a generic consequence of non-linear fermion transformations.

Mathematically we employ three independent techniques; non-linear fermion transformations [59], exact diagonalisation [60] and resolvent formalism [61]. The first technique has the crucial advantage that provides mathematical control. Exact diagonalisation is a standard numerical technique that provides the exact solution to a small finite system. The infinite system is then analysed through finite-size scaling, a form of extrapolation. Resolvent formalism is a technique for finding the exact solution to an eigenvalue problem where, in some basis, there is a trivially completely solvable problem that is only different from the desired problem in its action on a finite number of basis states. For metallic systems, translational invariance controls one particle and then the interactions with a second are local in real space and may be solved using resolvent formalism. We can exactly solve the two-hole problem, allowing a rigorous proof of hole pairing.

The technique of non-linear fermion transformations allows access to a very particular issue: in strongly correlated systems the Coulomb interaction is dominant. Although one electron can naturally occupy a state, a second is strongly repelled by this Coulomb repulsion and avoids double occupancy. If there is another doubly occupied state with less repulsive losses, then a Fermi-liquid can be constructed using quite different single-particle and two-particle states using a non-linear fermion transformation. The choice of such states is usually quite subtle, but we provide an example where there is a unique choice. Note that high temperature superconductivity supplies an excellent example of this problem, one particle occupies a copper orbital but a second sits in an oxygen orbital and forms a Zhang-Rice singlet [41].

This part is composed of seven chapters which, when put together, show that our Hubbard model exhibits superconductivity. In chapter 7 we present the model in question. This is a minimal model which encapsulates the physics of unconventional superconductors: a Hubbard model with two atoms per unit cell. In the next chapter we exactly take

the physical limit of divergent Coulomb repulsion to constrain the problem to one energy scale and reduce the local state space. This is done with a non-linear fermion transformation [59] and is the key technique in the analysis. Using this, a problem involving divergent energy scales is transformed into one of moderate interactions. In the chapter 9 we exactly show that two holes at the Mott point bind. This is followed up with mean field analysis in chapter 10. Where the results are not exact, we corroborate using exact diagonalisation and will find good agreement seen in chapter 11. All results will then point to this system exhibiting superconductivity. In the penultimate chapter we make the physical extension to non-diverging Coulomb repulsion and find that superconductivity is enhanced.

CHAPTER 7

THE PARTICULAR HUBBARD MODEL

Like all good theoretical stories, ours begins with a Hamiltonian. Unconventional superconductors are dominated by two short range interactions: chemical bonding and local Coulomb repulsion. With its elementary treatment of these two interactions the Hubbard model is the natural starting point when modelling unconventional superconductivity. Moreover this is a physically motivated choice as shown by Zhang and Rice when they demonstrated the copper-oxide planes in the cuprates can be modelled with a 2D square lattice Hubbard model.

In this section we will introduce the Hamiltonian. Our model is designed to give us precise mathematical control and therefore appears slightly contrived. This control comes in the form of a local symmetry which we will detail and extract. This will split the local state space in two: states that are symmetric or anti-symmetric under the transformation.

7.1 The Model

The model with which we begin is

$$H = -t_1 \sum_{\langle ij\rangle\sigma} (t^\dagger_{i\sigma} + b^\dagger_{i\sigma})(t_{j\sigma} + b_{j\sigma}) - t_0 \sum_{i\sigma} (t^\dagger_{i\sigma} b_{i\sigma} + b^\dagger_{i\sigma} t_{i\sigma}) + U \sum_i (t^\dagger_{i\uparrow} t_{i\uparrow} t^\dagger_{i\downarrow} t_{i\downarrow} + b^\dagger_{i\uparrow} b_{i\uparrow} b^\dagger_{i\downarrow} b_{i\downarrow}), \quad (7.1)$$

where $t^\dagger_{i\sigma}$, $b^\dagger_{i\sigma}$, $t_{i\sigma}$, and $b_{i\sigma}$ are standard independent fermionic creation and annihilation operators, t_0 and t_1 are hopping parameters and U is the Coulomb repulsion.

This is an ordinary Hubbard model but on a peculiar geometry. We can physically realise this geometry in multiple ways, a select few are depicted in figures 7.1 on page 49, 7.2 on page 49, and 7.3 on page 50. Figure 7.1 on page 49 depicts a system where this Hamiltonian is geometrically 'literally' (in the sense bond strength is directly proportional to bond length) where the system is formed of edge sharing tetrahedra. Figure 7.2 on page 49 depicts it as a 1D ladder which is easier to visualise but is less physical as diagonal and horizontal bonds are the same strength. Figure 7.3 on page 50 depicts the system as two coupled square lattices.

Next we move on to analysing the symmetry within this Hamiltonian which is key in tackling the problem.

7.2 A Set of Local Symmetries

Symmetries are imperative in physics. Frequently, these simplify the problem to a solvable form. In our case the symmetry is what allows us to tackle the problem and is crucial in our analysis.

The symmetry in question is

$$t_{i\sigma} \leftrightarrow b_{i\sigma}, \quad (7.2)$$

for each site i with both spins σ and $\bar{\sigma}$. This is a *local* symmetry and corresponds to

Figure 7.1: Geometric Representation of the Model

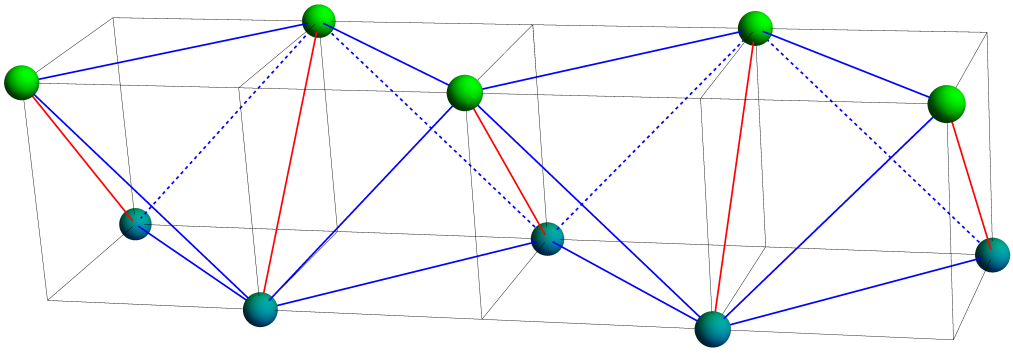

Geometric representation of the model if taken 'literally'. A system of edge sharing tetrahedra. 'Top' green sites corresponds to $t^\dagger_{i\sigma}$ operators and 'bottom' blue sites $b^\dagger_{i\sigma}$. Blue lines correspond to t_1 hopping and red lines correspond to t_0 hopping.

Figure 7.2: Ladder Representation of the Model

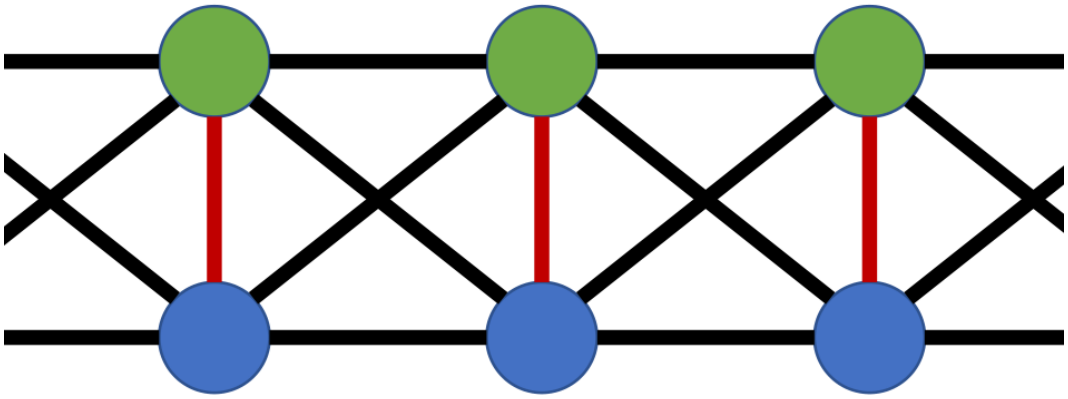

Coupled ladder with contrived hopping which is easier to visualise. 'Top' green sites corresponds to $t^\dagger_{i\sigma}$ operators and 'bottom' blue sites $b^\dagger_{i\sigma}$. Black lines correspond to t_1 hopping and red lines correspond to t_0 hopping.

Figure 7.3: 2D Coupled Square Lattice Representation of the Model

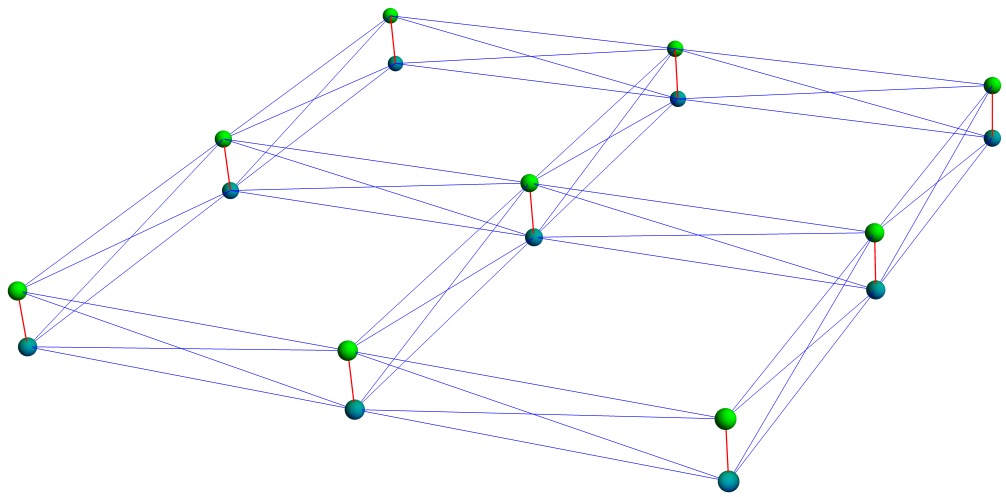

Representation where two 2D square lattices are coupled in an interesting manner. Reminiscent of the two copper oxide layers in YBCO. 'Top' green sites corresponds to $t^{\dagger}_{i\sigma}$ operators and 'bottom' blue sites $b^{\dagger}_{i\sigma}$. Blue lines correspond to t_1 hopping and red lines correspond to t_0 hopping.

swapping top and bottom sites via the t_0 (red bond in figures) bond. Analytically this is trivially checked. Physically we can see the source of this symmetry is the 'horizontal' and 'diagonal' bonds being the same in figure 7.2 on page 49.

In the following sections we will see the affect of the symmetry on the states and Hamiltonian.

7.2.1 The States

So the Hamiltonian is symmetric but what about the states that occupy it? As this is a local symmetry, we examine the basis states. There are 16 basis states in this Hamiltonian

given by

$$|0\rangle\,, \tag{7.3}$$

$$t^\dagger_{i\uparrow}|0\rangle\,, \quad t^\dagger_{i\downarrow}|0\rangle\,, b^\dagger_{i\uparrow}|0\rangle\,, b^\dagger_{i\downarrow}|0\rangle\,, \tag{7.4}$$

$$t^\dagger_{i\uparrow}t^\dagger_{i\downarrow}|0\rangle\,, t^\dagger_{i\uparrow}b^\dagger_{i\downarrow}|0\rangle\,, t^\dagger_{i\downarrow}b^\dagger_{i\uparrow}|0\rangle\,, t^\dagger_{i\uparrow}b^\dagger_{i\uparrow}|0\rangle\,, t^\dagger_{i\downarrow}b^\dagger_{i\downarrow}|0\rangle\,, b^\dagger_{i\uparrow}b^\dagger_{i\downarrow}|0\rangle\,, \tag{7.5}$$

$$b^\dagger_{i\uparrow}t^\dagger_{i\uparrow}t^\dagger_{i\downarrow}|0\rangle\,, \quad b^\dagger_{i\downarrow}t^\dagger_{i\uparrow}t^\dagger_{i\downarrow}|0\rangle \quad t^\dagger_{i\uparrow}b^\dagger_{i\uparrow}b^\dagger_{i\downarrow}|0\rangle\,, \quad t^\dagger_{i\downarrow}b^\dagger_{i\uparrow}b^\dagger_{i\downarrow}|0\rangle\,, \tag{7.6}$$

$$t^\dagger_{i\uparrow}t^\dagger_{i\downarrow}b^\dagger_{i\uparrow}b^\dagger_{i\downarrow}|0\rangle\,, \tag{7.7}$$

where we have grouped states by particle number. Obviously dealing with 16 states is rather unwieldy but the symmetry is here to help.

We know that $t_{i\sigma} \leftrightarrow b_{i\sigma}$ is a symmetry of the Hamiltonian, therefore the states must respect the symmetry. Written as they are currently they do not respect the symmetry and are clearly not the optimal basis to use. The correct operators to use are

$$s^\dagger_{i\sigma} = \frac{1}{\sqrt{2}}[t^\dagger_{i\sigma} + b^\dagger_{i\sigma}] \quad \text{and} \quad a^\dagger_{i\sigma} = \frac{1}{\sqrt{2}}[t^\dagger_{i\sigma} - b^\dagger_{i\sigma}], \tag{7.8}$$

where the operator $s^\dagger_{i\sigma}$ is symmetric and $a^\dagger_{i\sigma}$ is anti-symmetric under the transformation. Mathematically $s^\dagger_{i\sigma} \to s^\dagger_{i\sigma}$ and $a^\dagger_{i\sigma} \to -a^\dagger_{i\sigma}$ under $t_{i\sigma} \leftrightarrow b_{i\sigma}$.

Generating the local state space again we see that of the 16 states, 8 are symmetric and 8 are anti-symmetric under the transformation. The symmetric basis states are given by

$$|0\rangle = |0\rangle\,, \tag{7.9}$$

$$s^\dagger_{i\uparrow}|0\rangle = \frac{1}{\sqrt{2}}[t^\dagger_{i\uparrow} + b^\dagger_{i\uparrow}]\,|0\rangle\,, \tag{7.10}$$

$$s^\dagger_{i\downarrow}|0\rangle = \frac{1}{\sqrt{2}}[t^\dagger_{i\downarrow} + b^\dagger_{i\downarrow}]\,|0\rangle\,, \tag{7.11}$$

$$s^\dagger_{i\uparrow}s^\dagger_{i\downarrow}|0\rangle = \frac{1}{2}[t^\dagger_{i\uparrow}t^\dagger_{i\downarrow} + b^\dagger_{i\uparrow}t^\dagger_{i\downarrow} + t^\dagger_{i\uparrow}b^\dagger_{i\downarrow} + b^\dagger_{i\uparrow}b^\dagger_{i\downarrow}]\,|0\rangle\,, \tag{7.12}$$

$$a^\dagger_{i\uparrow}a^\dagger_{i\downarrow}|0\rangle = \frac{1}{2}[t^\dagger_{i\uparrow}t^\dagger_{i\downarrow} - b^\dagger_{i\uparrow}t^\dagger_{i\downarrow} - t^\dagger_{i\uparrow}b^\dagger_{i\downarrow} + b^\dagger_{i\uparrow}b^\dagger_{i\downarrow}]\,|0\rangle\,, \tag{7.13}$$

$$s^\dagger_{i\uparrow}a^\dagger_{i\uparrow}a^\dagger_{i\downarrow}\left|0\right\rangle = \frac{1}{\sqrt{2}}[b^\dagger_{i\uparrow}t^\dagger_{i\uparrow}t^\dagger_{i\downarrow} + t^\dagger_{i\uparrow}b^\dagger_{i\uparrow}b^\dagger_{i\downarrow}]\left|0\right\rangle, \tag{7.14}$$

$$s^\dagger_{i\downarrow}a^\dagger_{i\uparrow}a^\dagger_{i\downarrow}\left|0\right\rangle = \frac{1}{\sqrt{2}}[b^\dagger_{i\downarrow}t^\dagger_{i\uparrow}t^\dagger_{i\downarrow} + t^\dagger_{i\downarrow}b^\dagger_{i\uparrow}b^\dagger_{i\downarrow}]\left|0\right\rangle, \tag{7.15}$$

$$s^\dagger_{i\uparrow}s^\dagger_{i\downarrow}a^\dagger_{i\uparrow}a^\dagger_{i\downarrow}\left|0\right\rangle = t^\dagger_{i\uparrow}t^\dagger_{i\downarrow}b^\dagger_{i\uparrow}b^\dagger_{i\downarrow}\left|0\right\rangle, \tag{7.16}$$

and the anti-symmetric basis states are given by

$$a^\dagger_\uparrow\left|0\right\rangle = \frac{1}{\sqrt{2}}[t^\dagger_\uparrow - b^\dagger_\uparrow]\left|0\right\rangle, \tag{7.17}$$

$$a^\dagger_\downarrow\left|0\right\rangle = \frac{1}{\sqrt{2}}[t^\dagger_\downarrow - b^\dagger_\downarrow]\left|0\right\rangle, \tag{7.18}$$

$$s^\dagger_\uparrow a^\dagger_\uparrow\left|0\right\rangle = t^\dagger_\uparrow b^\dagger_\uparrow\left|0\right\rangle, \tag{7.19}$$

$$s^\dagger_\downarrow a^\dagger_\downarrow\left|0\right\rangle = t^\dagger_\downarrow b^\dagger_\downarrow\left|0\right\rangle, \tag{7.20}$$

$$s^\dagger_\uparrow a^\dagger_\downarrow\left|0\right\rangle = \frac{1}{2}[t^\dagger_\uparrow t^\dagger_\downarrow + b^\dagger_\uparrow t^\dagger_\downarrow + b^\dagger_\downarrow t^\dagger_\uparrow + b^\dagger_\uparrow b^\dagger_\downarrow]\left|0\right\rangle, \tag{7.21}$$

$$s^\dagger_\downarrow a^\dagger_\uparrow\left|0\right\rangle = \frac{1}{2}[t^\dagger_\downarrow t^\dagger_\uparrow + b^\dagger_\downarrow t^\dagger_\uparrow + b^\dagger_\uparrow t^\dagger_\downarrow + b^\dagger_\downarrow b^\dagger_\uparrow]\left|0\right\rangle, \tag{7.22}$$

$$s^\dagger_\uparrow s^\dagger_\downarrow a^\dagger_\uparrow\left|0\right\rangle = \frac{1}{\sqrt{2}}[t^\dagger_{i\uparrow}b^\dagger_{i\uparrow}b^\dagger_{i\downarrow} - b^\dagger_{i\uparrow}t^\dagger_{i\uparrow}t^\dagger_{i\downarrow}]\left|0\right\rangle, \tag{7.23}$$

$$s^\dagger_\uparrow s^\dagger_\downarrow a^\dagger_\downarrow\left|0\right\rangle = \frac{1}{\sqrt{2}}[t^\dagger_{i\downarrow}b^\dagger_{i\uparrow}b^\dagger_{i\downarrow} - b^\dagger_{i\downarrow}t^\dagger_{i\uparrow}t^\dagger_{i\downarrow}]\left|0\right\rangle. \tag{7.24}$$

We have dramatically simplified the states. Now we move to the Hamiltonian.

7.2.2 The Hamiltonian

In its current form the Hamiltonian is not very useful. When applying it to our new representations we would have to convert the states to the original basis, calculate, and convert back. Instead we recast the Hamiltonian in terms of $s^\dagger_{i\sigma}$ and $a^\dagger_{i\sigma}$. Note, that we can take pairs of creation or annihilation operators in the original basis to make this

calculation easier, for example $t^\dagger_\uparrow t^\dagger_\downarrow + b^\dagger_\uparrow b^\dagger_\downarrow = s^\dagger_\uparrow s^\dagger_\downarrow + a^\dagger_\uparrow a^\dagger_\downarrow$. The Hamiltonian becomes

$$H = -2t_1 \sum_{\langle ij\rangle\sigma} s^\dagger_{i\sigma} s_{j\sigma} - t_0 \sum_{i\sigma} (s^\dagger_{i\sigma} s_{i\sigma} - a^\dagger_{i\sigma} a_{i\sigma}) \\ + \frac{U}{2} \sum_i \Big[(s^\dagger_{i\uparrow} s^\dagger_{i\downarrow} + a^\dagger_{i\uparrow} a^\dagger_{i\downarrow})(s_{i\downarrow} s_{i\uparrow} + a_{i\downarrow} a_{i\uparrow}) + (s^\dagger_{i\uparrow} a^\dagger_{i\downarrow} - s^\dagger_{i\downarrow} a^\dagger_{i\uparrow})(a_{i\downarrow} s_{i\uparrow} - a_{i\uparrow} s_{i\downarrow}) \Big]. \quad (7.25)$$

Note the hopping has become simple but the Hubbard term is more involved. The t_0 hopping simply returns the difference between the number of $s^\dagger_{i\sigma}$ and $a^\dagger_{i\sigma}$ states. Interestingly, the t_1 term only hops $s^\dagger_{i\sigma}$ states from one site to the next. This means the $a^\dagger_{i\sigma}$ states are localised and cannot move. This is reminiscent of the Anderson lattice model discussed in section 4.5.

With the basis states and Hamiltonian respecting the symmetry, we move our attention to the entire state space.

7.2.3 Separating the State Spaces

Currently we have used the symmetry to classify the basis states into two sets, and recast the Hamiltonian. In this section we will apply this symmetry to the system and argue that there are only two symmetry configurations to consider: systems composed of the same symmetry set on each site.

Let's consider a one dimensional ladder for ease of visualisation. The symmetry allows us to describe each pair of sites ($t_{i\sigma}$ and $b_{i\sigma}$) connected by t_0 (red bond in figures) as one site (labelled by the index i) with 16 degrees of freedom. This will be called a p-site from here on in. On each p-site there exists a state which is either symmetric or anti-symmetric under the transformation. We can independently label each p-site with an 'S' or 'A' for the symmetry of the state that occupies it. Both S and A have 8 degrees of freedom. In principle any configurations of S and A systems could exist, but this is not what we see. When examining this system with exact diagonalization (see Appendix C if unfamiliar), we find that only one of two situations occur. Either the system is fully configured of Ss

Figure 7.4: Symmetry Extraction Process

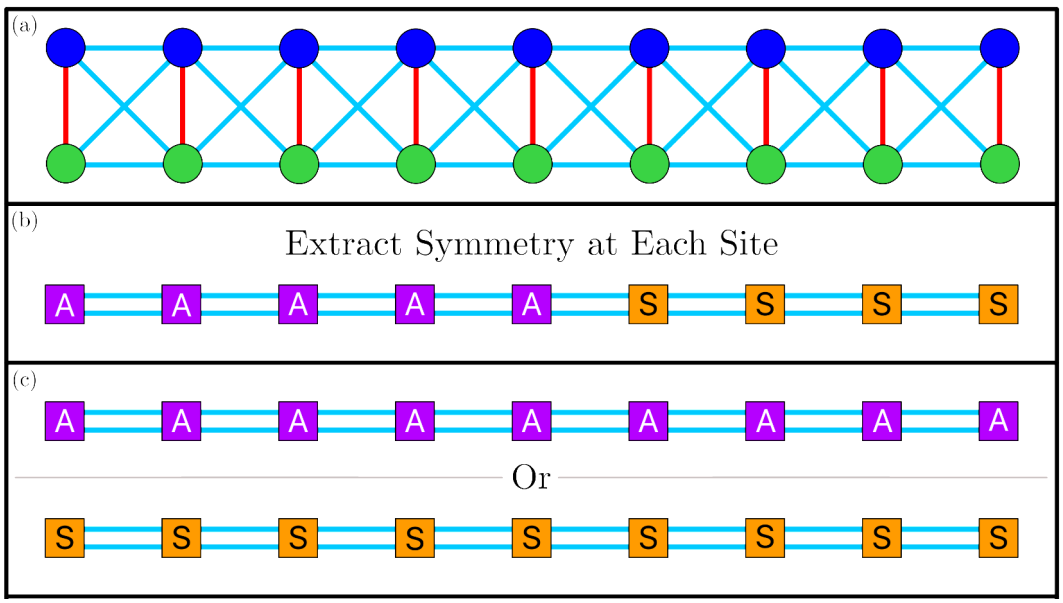

The process begins with diagram (a), where on any red bond we can switch green and blue sites as the system is symmetric under that transformation. Upon extracting the symmetry we are left with diagram (b), where each p-site is labelled either 'S' or 'A' for the symmetry of the state that occupies it. From exact diagonalization results we discover systems are formed of purely 'S' or 'A', or a phase separated mixture of the two. We arrive at (c) where we examine pure configurations and Maxwell construct where required.

or As, or the system is split into two regions with Ss in one region and As in the other. This is a phase separated mixture. We will see that these phase separated systems are accurately described by a Maxwell construction (discussed in detail in section 11.1).

This motivates us to consider two systems: one with an S on each site which we call the symmetric subspace, the other with an A on each site which we call the anti-symmetric subspace. When a phase separated mixture would occur we use a Maxwell construction between the symmetric and anti-symmetric subspaces. This process is depicted in figure 7.4 on page 54.

In this chapter we introduced the Hamiltonian and its key local symmetry. This symmetry was used to split the set of basis states in two. The reduced basis states were either symmetric or anti-symmetric under the transformation. The Hamiltonian was recast to respect the symmetry and we found that $s^\dagger_{i\sigma}$ states we able to move while $a^\dagger_{i\sigma}$ states were localised. Finally we argued why we only need to consider two symmetry

configurations. We now move on to a physically motivated limit that greatly simplifies the problem.

CHAPTER 8

SETTING U = ∞ — NON-LINEAR FERMION TRANSFORMATIONS

The Hubbard model is notoriously difficult to tackle, highlighted by the fact that an exact solution only exists for a linear chain[62]. As the cuprates can be modelled by an ordinary Hubbard model [41], people have been motivated to solve it on a 2D square lattice for decades, but they have not got far. People believe this difficulty is due to the strongly correlated nature of the problem [63]. To know how one particle will behave we need to know how they will all behave. On the 1D chain it is possible to consider the problem in terms of three particle scattering thanks to the Yang-Baxter equation [64], allowing the model to be solved. In short, when considering three particle scattering the order of operation does not matter: the scattering of particle 1 and 2 does not affect the scattering of 2 and 3. This is not true for higher dimensions.

So how can we simplify this problem? One way is to eliminate one of the energy scales. Of course we set either t or U to zero; this results in a trivially solvable problem. A better approach is to be physically motivated and take limiting procedures, which keeps the physics of the problem intact. In unconventional superconductors the Coulomb repulsion is usually an order of magnitude larger than chemical bonding [48]. To physically simulate this we could take the limit of divergent Coulomb. Indeed, this is what motivates us to

take the limit $U = \infty$. In this limit double occupation of a single site is prohibited. Pauli exclusion prohibits double occupation of a site with the same spin, and $U = \infty$ prohibits double occupation of a site with opposite spins. Immediately we are in a more fortunate position, as not only do we have fewer degrees of freedom per site but we have also removed a variable.

This alone would not make things easier. We require a mathematical formalism to aid in this physical choice. Fortunately, we have this in the form of 'Non-Linear Fermion Transformations' [59]. This is an exact transformation that allows one to arbitrarily change the basis being worked in. This powerful technique will allow us write down a Hamiltonian that exactly describes the system of states that remain accessible after taking this limit.

In the remainder of this chapter we will give an overview of non-linear fermion transformations (including a simple example) and apply this technique on both the symmetric and anti-symmetric subspaces.

8.1 Non-Linear Fermion Transformations — How and When to Apply Them

A non-linear fermion transformation is an exact technique by which to transform into an arbitrary basis. The process is outlined as:

1. Choose a representation and *define* how they correspond to the original states.

2. Recast the Hamiltonian.

These steps are detailed below.

Let's consider a rather contrived example which highlights why one would use a non-linear fermion transformation. The Hamiltonian is given by

$$H_{Strange} = -t \sum_{\langle ij \rangle \sigma} (1 - 2c^{\dagger}_{i\bar{\sigma}} c_{i\bar{\sigma}}) c^{\dagger}_{i\sigma} c_{j\sigma} (1 - 2c^{\dagger}_{j\bar{\sigma}} c_{j\bar{\sigma}}). \tag{8.1}$$

Step 1

In this part we have a real choice, we can choose whatever basis we want to describe this problem. Some choices are smarter than others, but we will choose a representation that remarkably simplifies the problem.

$$|0\rangle_p = |0\rangle_c\,, \quad p_\uparrow^\dagger |0\rangle_p = c_\uparrow^\dagger |0\rangle_c\,, \quad p_\downarrow^\dagger |0\rangle_p = c_\downarrow^\dagger |0\rangle_c\,, \quad p_\uparrow^\dagger p_\downarrow^\dagger |0\rangle_p = -c_\uparrow^\dagger c_\downarrow^\dagger |0\rangle_c\,. \tag{8.2}$$

We can immediately see that this transformation is not linear as when we have one particle $p_\downarrow^\dagger |0\rangle_p = c_\downarrow^\dagger |0\rangle_c$, but when we add a second particle $p_\uparrow^\dagger p_\downarrow^\dagger |0\rangle_p \neq c_\uparrow^\dagger c_\downarrow^\dagger |0\rangle_c$. This transformation is both particle and spin conserving hence it is clear that these new p operators are still fermions and obey the appropriate commutation relations [59].

Step 2

Now we recast the Hamiltonian. This is done by:

1. Applying the original operators to the new states.

2. Use the definitions to change back to the original basis.

3. Calculate the operation and use the definitions to transform back.

4. Adding linear combinations of the results to ensure the correct mathematics.

When doing this transformation we consider diagonal operators together, and off diagonal operators by their composite operators separately. As the strange hopping is off diagonal we only need to consider $c_\sigma(1 - 2c_{\bar\sigma}^\dagger c_{\bar\sigma})$ and $(1 - 2c_{\bar\sigma}^\dagger c_{\bar\sigma})c_\sigma^\dagger$ separately. We will do one example in detail and show the results for the rest. Consider acting $(1 - 2c_{\bar\sigma}^\dagger c_{\bar\sigma})c_\sigma^\dagger$ on $p_{\bar\sigma}^\dagger |0\rangle_p$. Step one is to apply the operator to the new state, therefore we are calculating $(1-2c_{\bar\sigma}^\dagger c_{\bar\sigma})c_\sigma^\dagger p_{\bar\sigma}^\dagger |0\rangle_p$. Step two is to use the definitions to change back to the original basis. As $p_{\bar\sigma}^\dagger |0\rangle_p \equiv c_{\bar\sigma}^\dagger |0\rangle_c$ we have $(1-2c_{\bar\sigma}^\dagger c_{\bar\sigma})c_\sigma^\dagger p_{\bar\sigma}^\dagger |0\rangle_p \equiv (1-2c_{\bar\sigma}^\dagger c_{\bar\sigma})c_\sigma^\dagger c_{\bar\sigma}^\dagger |0\rangle_c$. The bracketed term notices $c_{\bar\sigma}^\dagger$ and adds a minus sign. The result is therefore $(1-2c_{\bar\sigma}^\dagger c_{\bar\sigma})c_\sigma^\dagger p_{\bar\sigma}^\dagger |0\rangle_p \equiv -c_\sigma^\dagger c_{\bar\sigma}^\dagger |0\rangle_c$.

Using our definition of $p^\dagger_\sigma p^\dagger_{\bar{\sigma}} \left|0\right\rangle_p = -c^\dagger_\sigma c^\dagger_{\bar{\sigma}} \left|0\right\rangle_c$ gives

$$(1 - 2c^\dagger_{\bar{\sigma}} c_{\bar{\sigma}}) c^\dagger_\sigma p^\dagger_{\bar{\sigma}} \left|0\right\rangle_p \equiv -c^\dagger_\sigma c^\dagger_{\bar{\sigma}} \left|0\right\rangle_c \equiv p^\dagger_\sigma p^\dagger_{\bar{\sigma}} \left|0\right\rangle_p \tag{8.3}$$

Repeating this process for all states and the operator c_σ yields

$$(1 - 2c^\dagger_{\bar{\sigma}} c_{\bar{\sigma}}) c_\sigma \left|0\right\rangle_p \equiv (1 - 2c^\dagger_{\bar{\sigma}} c_{\bar{\sigma}}) c_\sigma \left|0\right\rangle_c \equiv 0, \tag{8.4}$$

$$(1 - 2c^\dagger_{\bar{\sigma}} c_{\bar{\sigma}}) c_\sigma p^\dagger_\sigma \left|0\right\rangle_p \equiv (1 - 2c^\dagger_{\bar{\sigma}} c_{\bar{\sigma}}) c_\sigma c^\dagger_\sigma \left|0\right\rangle_c \equiv \left|0\right\rangle_p, \tag{8.5}$$

$$(1 - 2c^\dagger_{\bar{\sigma}} c_{\bar{\sigma}}) c_\sigma p^\dagger_{\bar{\sigma}} \left|0\right\rangle_p \equiv (1 - 2c^\dagger_{\bar{\sigma}} c_{\bar{\sigma}}) c_\sigma c^\dagger_{\bar{\sigma}} \left|0\right\rangle_c \equiv 0, \tag{8.6}$$

$$(1 - 2c^\dagger_{\bar{\sigma}} c_{\bar{\sigma}}) c_\sigma p^\dagger_\sigma p^\dagger_{\bar{\sigma}} \left|0\right\rangle_p \equiv (1 - 2c^\dagger_{\bar{\sigma}} c_{\bar{\sigma}}) c_\sigma (-c^\dagger_\sigma c^\dagger_{\bar{\sigma}}) \left|0\right\rangle_c \equiv p^\dagger_{\bar{\sigma}} \left|0\right\rangle_p. \tag{8.7}$$

Similarly for $c^\dagger_\sigma$ we have

$$(1 - 2c^\dagger_{\bar{\sigma}} c_{\bar{\sigma}}) c^\dagger_\sigma \left|0\right\rangle_p \equiv (1 - 2c^\dagger_{\bar{\sigma}} c_{\bar{\sigma}}) c^\dagger_\sigma \left|0\right\rangle_c \equiv p^\dagger_\sigma \left|0\right\rangle_p, \tag{8.8}$$

$$(1 - 2c^\dagger_{\bar{\sigma}} c_{\bar{\sigma}}) c^\dagger_\sigma p^\dagger_\sigma \left|0\right\rangle_p \equiv (1 - 2c^\dagger_{\bar{\sigma}} c_{\bar{\sigma}}) c^\dagger_\sigma c^\dagger_\sigma \left|0\right\rangle_c \equiv 0, \tag{8.9}$$

$$(1 - 2c^\dagger_{\bar{\sigma}} c_{\bar{\sigma}}) c^\dagger_\sigma p^\dagger_{\bar{\sigma}} \left|0\right\rangle_p \equiv (1 - 2c^\dagger_{\bar{\sigma}} c_{\bar{\sigma}}) c^\dagger_\sigma c^\dagger_{\bar{\sigma}} \left|0\right\rangle_c \equiv p^\dagger_\sigma p^\dagger_{\bar{\sigma}} \left|0\right\rangle_p, \tag{8.10}$$

$$(1 - 2c^\dagger_{\bar{\sigma}} c_{\bar{\sigma}}) c^\dagger_\sigma p^\dagger_\sigma p^\dagger_{\bar{\sigma}} \left|0\right\rangle_p \equiv (1 - 2c^\dagger_{\bar{\sigma}} c_{\bar{\sigma}}) c^\dagger_\sigma (-c^\dagger_\sigma c^\dagger_{\bar{\sigma}}) \left|0\right\rangle_c \equiv 0. \tag{8.11}$$

It's not difficult to see we can recast these operators as

$$(1 - 2c^\dagger_{\bar{\sigma}} c_{\bar{\sigma}}) c^\dagger_\sigma = p^\dagger_\sigma \quad \text{and} \quad (1 - 2c^\dagger_{\bar{\sigma}} c_{\bar{\sigma}}) c_\sigma = p_\sigma. \tag{8.12}$$

This turns the Hamiltonian 8.1 into

$$H_{Strange} = -t \sum_{\langle ij \rangle \sigma} p^\dagger_{i\sigma} p_{j\sigma}. \tag{8.13}$$

There are two incredible benefits to this result. Firstly, this result is exact. Any analysis done on this model is not contingent on the validity of this result. Secondly, the transformation has resulted in a Hamiltonian that is exactly solvable. In this case the

result is just a tight binding Hamiltonian in p.

In fact we can quantify how much of a success this result is. To see how, let's attempt Hartree-Fock mean field theory on this Hamiltonian. If this technique is unfamiliar to you please see appendix D, where it is explained in detail. The details of the derivation are irrelevant for this point so we only present the result.

$$E_{MF} = -2tN\left[(1-2n_0)^2\frac{\sin(\pi n_0)}{\pi} - 4\frac{\sin^3(\pi n_0)}{\pi^3}\right] \tag{8.14}$$

where $n_0 = \langle p^\dagger_{i\sigma}p_{i\sigma}\rangle = \langle p^\dagger_{i\bar{\sigma}}p_{i\bar{\sigma}}\rangle$ is the occupation fraction. However, the exact result is

$$E_{Exact} = -2tN\frac{\sin(\pi n_0)}{\pi}. \tag{8.15}$$

The ratio of the two is

$$\frac{E_{MF}}{E_{Exact}} = (1-2n_0)^2 - 4\frac{\sin^2(\pi n_0)}{\pi^2}. \tag{8.16}$$

At the extreme ends of occupation the difference is reasonable, but in the middle the mean field result is terrible! The non-linear fermion transformation has saved us.

In this example the non-linear fermion transformation has been very successful but this success is not guaranteed. Though the result will always be exact, any approximation procedures that follow may not succeed. We could imagine doing this example in reverse, going from the tight binding model to a strange model. The incredible success would now become an incredible failure. The choice of definitions in step one are crucial.

In this thesis we will use non-linear fermion transformations to constrain our Hamiltonian after taking the limit $U = \infty$. Success here is dependent on external factors. To see why, let's consider the t-model

$$H^t = -t\sum_{\langle ij\rangle\sigma}(1-c^\dagger_{i\bar{\sigma}}c_{i\bar{\sigma}})c^\dagger_{i\sigma}c_{j\sigma}(1-c^\dagger_{j\bar{\sigma}}c_{j\bar{\sigma}}). \tag{8.17}$$

Though this Hamiltonian exactly projects doubly occupied states, mean field theory on it will always fail. After performing Hartree-Fock mean field theory on this Hamiltonian,

we get the effective single particle Hamiltonian

$$H^t_{eff} = -t \sum_{\langle ij \rangle \sigma} [(1 - n_0)^2 - 3n_1^2] c^\dagger_{i\sigma} c_{j\sigma} + 2n_1(n_0 - n_1) c^\dagger_{i\sigma} c_{i\sigma}, \tag{8.18}$$

where $n_0 = \langle c^\dagger_{i\sigma} c_{i\sigma} \rangle = \langle c^\dagger_{i\bar{\sigma}} c_{i\bar{\sigma}} \rangle$ and $n_1 = \langle c^\dagger_{i\sigma} c_{j\sigma} \rangle = \langle c^\dagger_{i\bar{\sigma}} c_{j\bar{\sigma}} \rangle$. Note that this Hamiltonian can create doubly occupied pairs of electrons (i.e $c^\dagger_\uparrow c^\dagger_\downarrow$) as this is just a tight binding model; nothing is stopping it. The approximation does not respect the constraints of the original problem!

This occurs because approximations inherently try to convert a many body problem into a single particle problem, but the operators that restrict the subspace are many body by construction. The *only* way to mitigate this issue is to use a basis which completely covers the accessible states. In this example we were left with three accessible states, but the transformed basis permitted four states. As fermions bring with them two degrees of freedom, either occupied or not, this example cannot be transformed into one containing only fermions. Simply put, two does not divide three. Instead we must use a description for which there are three states. A possibility is to consider a spin-zero vacuum and spin-half particle, along with exchange operators. For example we could write

$$H = -t \sum_{\langle ij \rangle} \Sigma_{ij}, \tag{8.19}$$

where the basis states are

$$|0\rangle = |0\rangle\,, \quad c^\dagger_\sigma |0\rangle = |\uparrow\rangle\,, \quad c^\dagger_{\bar{\sigma}} |0\rangle = |\downarrow\rangle\,, \tag{8.20}$$

and the operator Σ_{ij} is the exchange operator which swaps the spins sites i and j. Unfortunately, mean field techniques are not well developed for these types of problems.

In the following sections we will perform a non-linear fermion transformation on the symmetric and attempt to on the anti-symmetric subspace but decide not to. We will discover that the symmetric subspace can be successfully transformed in a way where the

states are mapped onto a spin-half system, and that the anti-symmetric subspace cannot.

8.2 The Symmetric State Space

In this section we take the limit $U = \infty$ and perform a non-linear fermion transformation on the symmetric subspace. We begin by writing down the states. For the symmetric subspace, the eight local states and their representations in the original basis are

$$|0\rangle = |0\rangle\,, \tag{8.21}$$

$$s_\uparrow^\dagger |0\rangle = \frac{1}{\sqrt{2}}[t_\uparrow^\dagger + b_\uparrow^\dagger]\,|0\rangle\,, \tag{8.22}$$

$$s_\downarrow^\dagger |0\rangle = \frac{1}{\sqrt{2}}[t_\downarrow^\dagger + b_\downarrow^\dagger]\,|0\rangle\,, \tag{8.23}$$

$$\frac{1}{\sqrt{2}}[s_\uparrow^\dagger s_\downarrow^\dagger - a_\uparrow^\dagger a_\downarrow^\dagger]\,|0\rangle = \frac{1}{\sqrt{2}}[t_\uparrow^\dagger b_\downarrow^\dagger - t_\downarrow^\dagger b_\uparrow^\dagger]\,|0\rangle\,, \tag{8.24}$$

$$\frac{1}{\sqrt{2}}[s_\uparrow^\dagger s_\downarrow^\dagger + a_\uparrow^\dagger a_\downarrow^\dagger]\,|0\rangle = \frac{1}{\sqrt{2}}[t_\uparrow^\dagger t_\downarrow^\dagger + b_\uparrow^\dagger b_\downarrow^\dagger]\,|0\rangle^\Delta\,, \tag{8.25}$$

$$s_{i\uparrow}^\dagger a_{i\uparrow}^\dagger a_{i\downarrow}^\dagger |0\rangle = \frac{1}{\sqrt{2}}[b_{i\uparrow}^\dagger t_{i\uparrow}^\dagger t_{i\downarrow}^\dagger + t_{i\uparrow}^\dagger b_{i\uparrow}^\dagger b_{i\downarrow}^\dagger]\,|0\rangle^\Delta\,, \tag{8.26}$$

$$s_{i\downarrow}^\dagger a_{i\uparrow}^\dagger a_{i\downarrow}^\dagger |0\rangle = \frac{1}{\sqrt{2}}[b_{i\downarrow}^\dagger t_{i\uparrow}^\dagger t_{i\downarrow}^\dagger + t_{i\downarrow}^\dagger b_{i\uparrow}^\dagger b_{i\downarrow}^\dagger]\,|0\rangle^\Delta\,, \tag{8.27}$$

$$s_{i\uparrow}^\dagger s_{i\downarrow}^\dagger a_{i\uparrow}^\dagger a_{i\downarrow}^\dagger |0\rangle = t_{i\uparrow}^\dagger t_{i\downarrow}^\dagger b_{i\uparrow}^\dagger b_{i\downarrow}^\dagger\,|0\rangle^\Delta\,, \tag{8.28}$$

where states labelled by Δ are doubly occupied and are hence projected away by the limit $U = \infty$. As both $s_\uparrow^\dagger s_\downarrow^\dagger$ and $a_\uparrow^\dagger a_\downarrow^\dagger$ contain states that are both projected and allowed, we have taken linear combinations of them to create states that are either completely projected or allowed.

Fortunately, the number of states that are allowed in this subspace is four, which is divisible by two. This means we can use a non-linear fermion transformation to restrict us within this state space. We choose to do this with two spin half fermions with the

following definition

$$|0\rangle_c = |0\rangle\,, \tag{8.29}$$

$$c_\uparrow^\dagger |0\rangle_c = s_\uparrow^\dagger |0\rangle\,, \tag{8.30}$$

$$c_\downarrow^\dagger |0\rangle_c = s_\downarrow^\dagger |0\rangle\,, \tag{8.31}$$

$$c_\uparrow^\dagger c_\downarrow^\dagger |0\rangle_c = \frac{1}{\sqrt{2}}[s_\uparrow^\dagger s_\downarrow^\dagger - a_\uparrow^\dagger a_\downarrow^\dagger]\,|0\rangle\,. \tag{8.32}$$

We have chosen this definition as it conserves number and spin.

The next step is to recast the Hamiltonian. Let's consider the t_1 hopping term, as it is off-diagonal we only need to examine $s_\sigma^\dagger$ and s_σ terms separately. Remember the steps are: apply the operator, convert using the definitions, calculate and project, and transform back. Using '$\rightarrow$' as a shorthand for projection, for $s_\sigma^\dagger$ this is given by

$$s_\sigma^\dagger |0\rangle_c \equiv s_\sigma^\dagger |0\rangle \equiv c_\sigma^\dagger |0\rangle_c\,, \tag{8.33}$$

$$s_\sigma^\dagger c_\sigma^\dagger |0\rangle_c \equiv s_\sigma^\dagger s_\sigma^\dagger |0\rangle \equiv 0, \tag{8.34}$$

$$\begin{aligned} s_\sigma^\dagger c_{\bar\sigma}^\dagger |0\rangle_c \equiv s_\sigma^\dagger s_{\bar\sigma}^\dagger |0\rangle &= \frac{1}{2}[t_\sigma^\dagger t_{\bar\sigma}^\dagger + t_\sigma^\dagger b_{\bar\sigma}^\dagger - t_{\bar\sigma}^\dagger b_\sigma^\dagger + b_\sigma^\dagger b_{\bar\sigma}^\dagger]\,|0\rangle \\ &\rightarrow \frac{1}{2}[t_\sigma^\dagger b_{\bar\sigma}^\dagger - t_{\bar\sigma}^\dagger b_\sigma^\dagger]\,|0\rangle \equiv \frac{1}{\sqrt{2}} c_\sigma^\dagger c_{\bar\sigma}^\dagger |0\rangle_c\,, \end{aligned} \tag{8.35}$$

$$\begin{aligned} s_\sigma^\dagger c_\sigma^\dagger c_{\bar\sigma}^\dagger |0\rangle_c \equiv s_\sigma^\dagger \frac{1}{\sqrt{2}}[s_\sigma^\dagger s_{\bar\sigma}^\dagger - a_\sigma^\dagger a_{\bar\sigma}^\dagger]\,|0\rangle &= -\frac{1}{\sqrt{2}} s_\sigma^\dagger a_\sigma^\dagger a_{\bar\sigma}^\dagger |0\rangle \\ &\rightarrow 0 \equiv 0. \end{aligned} \tag{8.36}$$

For s_σ this is given by

$$s_\sigma |0\rangle_c \equiv s_\sigma |0\rangle \equiv 0, \tag{8.37}$$

$$s_\sigma c_\sigma^\dagger |0\rangle_c \equiv s_\sigma s_\sigma^\dagger |0\rangle \equiv |0\rangle_c\,, \tag{8.38}$$

$$s_\sigma c_{\bar\sigma}^\dagger |0\rangle_c \equiv s_\sigma s_{\bar\sigma}^\dagger |0\rangle \equiv 0 \tag{8.39}$$

$$s_\sigma c_\sigma^\dagger c_{\bar\sigma}^\dagger |0\rangle_c \equiv s_\sigma \frac{1}{\sqrt{2}}[s_\sigma^\dagger s_{\bar\sigma}^\dagger - a_\sigma^\dagger a_{\bar\sigma}^\dagger]\,|0\rangle = \frac{1}{\sqrt{2}} s_\sigma^\dagger |0\rangle \equiv \frac{1}{\sqrt{2}} c_\sigma^\dagger |0\rangle_c\,. \tag{8.40}$$

Combining these results, using $s_\sigma^\dagger = \alpha(1 - c_{\bar{\sigma}}^\dagger c_{\bar{\sigma}})c_\sigma^\dagger + \beta c_{\bar{\sigma}}^\dagger c_{\bar{\sigma}} c_\sigma^\dagger$ and solving for α and β, gives

$$s_\sigma^\dagger = (1 - \eta c_{\bar{\sigma}}^\dagger c_{\bar{\sigma}})c_\sigma^\dagger \quad \text{and} \quad s_\sigma = c_\sigma(1 - \eta c_{\bar{\sigma}}^\dagger c_{\bar{\sigma}}), \tag{8.41}$$

where $\eta = 1 - \frac{1}{\sqrt{2}}$ is the degree of non-linearity. Note that $\eta \approx 0.3$ is moderate compared to 1. The transformation has recast the problem from divergent interactions to moderate ones. Compare this to the original Hubbard model where the equivalent object is $\frac{U}{t}$. Now that this is the case, it is reasonable to perform mean field theory on this Hamiltonian, which will be done in chapter 10.

We now turn to the t_0 term and perform the transformation. This term is diagonal and hence we cannot consider each operator individually and must consider the term in its entirety. The term we need to consider is

$$-t_0 \sum_{i\sigma} (s_{i\sigma}^\dagger s_{i\sigma} - a_{i\sigma}^\dagger a_{i\sigma}). \tag{8.42}$$

Applying this to the states gives

$$(s_\sigma^\dagger s_\sigma - a_\sigma^\dagger a_\sigma) \left|0\right\rangle_c = 0, \tag{8.43}$$

$$(s_\sigma^\dagger s_\sigma - a_\sigma^\dagger a_\sigma) c_\sigma^\dagger \left|0\right\rangle_c = c_\sigma^\dagger \left|0\right\rangle_c, \tag{8.44}$$

$$(s_\sigma^\dagger s_\sigma - a_\sigma^\dagger a_\sigma) c_{\bar{\sigma}}^\dagger \left|0\right\rangle_c = 0, \tag{8.45}$$

$$\begin{aligned} (s_\sigma^\dagger s_\sigma - a_\sigma^\dagger a_\sigma) c_\sigma^\dagger c_{\bar{\sigma}}^\dagger \left|0\right\rangle_c &\equiv (s_\sigma^\dagger s_\sigma - a_\sigma^\dagger a_\sigma) \frac{1}{\sqrt{2}} [s_\sigma^\dagger s_{\bar{\sigma}}^\dagger - a_\sigma^\dagger a_{\bar{\sigma}}^\dagger] \left|0\right\rangle \\ &= \frac{1}{\sqrt{2}} [s_\sigma^\dagger s_{\bar{\sigma}}^\dagger + a_\sigma^\dagger a_{\bar{\sigma}}^\dagger] \left|0\right\rangle \to 0. \end{aligned} \tag{8.46}$$

Which means the term can be recast as

$$-t_0 \left[\sum_{i\sigma} c_{i\sigma}^\dagger c_{i\sigma} - 2 \sum_i c_{i\uparrow}^\dagger c_{i\uparrow} c_{i\downarrow}^\dagger c_{i\downarrow} \right]. \tag{8.47}$$

The t_0 term has become a Hubbard-like term. Note that the value of t_0 can be negative, and it is known that the negative U Hubbard model exhibits superconductivity [65].

Though it is true that the symmetric-subspace has a superconducting phase for negative values of t_0, this does not apply to the system as a whole. To understand why, we need to understand the effect of t_0 on the anti-symmetric subspace. There is competition between the two subspaces and we are required to investigate which of the two subspaces is the ground state. This will be discussed at length in chapter 10.

Putting everything together we get the Hamiltonian for the symmetric subspace to be

$$H_S = -2t_1 \sum_{\langle ij \rangle \sigma} (1 - \eta c^\dagger_{i\bar{\sigma}} c_{i\bar{\sigma}}) c^\dagger_{i\sigma} c_{j\sigma} (1 - \eta c^\dagger_{j\bar{\sigma}} c_{j\bar{\sigma}}) - t_0 \sum_{i\sigma} c^\dagger_{i\sigma} c_{i\sigma} + 2t_0 \sum_i c^\dagger_{i\uparrow} c_{i\uparrow} c^\dagger_{i\downarrow} c_{i\downarrow}. \quad (8.48)$$

At this point let's discuss the nature of the non-linear hopping depicted in figure 8.1 on page 67. At low occupation the system is dominantly described via (a) and (b), where $U = \infty$ penalises particles next to one another with a decreased hopping. However, at high occupation the system must decide between (c) and (d). With the latter being penalised the system has no choice but to form pairs and keep them closely bound (c) to circumvent the Coulomb penalty. From this we can infer (from physical intuition, not proof) that at low occupation particles would like to be spread out, in order to gain as much hopping energy as possible. At the other end, as this Hamiltonian is not particle hole symmetric, holes would like to pair up (rather than be uniformly distributed) in order to gain hopping energy. This is the first indication that holes in the symmetric subspace would like to form pairs.

Figure 8.1: Correlated Motion of Electrons

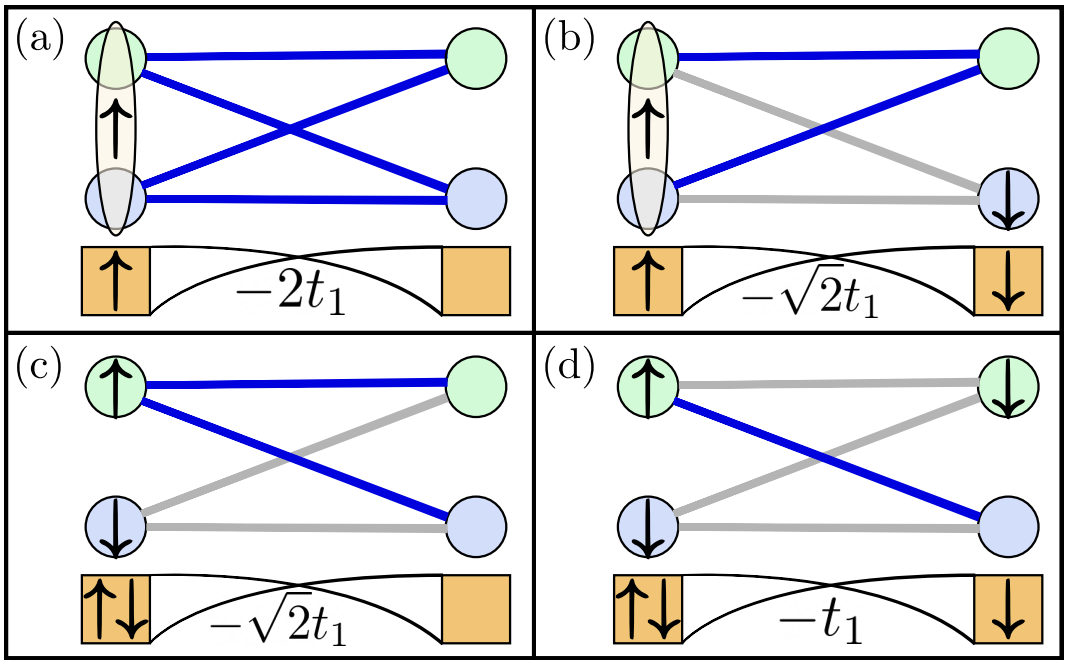

The energy gain for hopping a particle with spin ↑ from the left site to the right. Accessible hops are highlighted in blue. Green rings describe a superposition over both top and bottom sites. In sub-figures b and d states on the right are not symmetric for ease of visualisation.

8.3 The Anti-Symmetric State Space

For the anti-symmetric subspace, the eight local states and their original representations are

$$a_\uparrow^\dagger |0\rangle = \frac{1}{\sqrt{2}}[t_\uparrow^\dagger - b_\uparrow^\dagger] |0\rangle , \tag{8.49}$$

$$a_\downarrow^\dagger |0\rangle = \frac{1}{\sqrt{2}}[t_\downarrow^\dagger - b_\downarrow^\dagger] |0\rangle , \tag{8.50}$$

$$s_\uparrow^\dagger a_\uparrow^\dagger |0\rangle = t_\uparrow^\dagger b_\uparrow^\dagger |0\rangle , \tag{8.51}$$

$$s_\downarrow^\dagger a_\downarrow^\dagger |0\rangle = t_\downarrow^\dagger b_\downarrow^\dagger |0\rangle , \tag{8.52}$$

$$\frac{1}{\sqrt{2}}(s_\uparrow^\dagger a_\downarrow^\dagger + s_\downarrow^\dagger a_\uparrow^\dagger) |0\rangle = \frac{1}{\sqrt{2}}[b_\uparrow^\dagger t_\downarrow^\dagger + b_\downarrow^\dagger t_\uparrow^\dagger] |0\rangle , \tag{8.53}$$

$$\frac{1}{\sqrt{2}}(s_\uparrow^\dagger a_\downarrow^\dagger - s_\downarrow^\dagger a_\uparrow^\dagger) |0\rangle = \frac{1}{\sqrt{2}}[t_\uparrow^\dagger t_\downarrow^\dagger - b_\uparrow^\dagger b_\downarrow^\dagger] |0\rangle^\Delta , \tag{8.54}$$

$$s_\uparrow^\dagger s_\downarrow^\dagger a_\uparrow^\dagger |0\rangle = \frac{1}{2\sqrt{2}}[t_\uparrow^\dagger + b_\uparrow^\dagger][t_\downarrow^\dagger + b_\downarrow^\dagger][t_\uparrow^\dagger - b_\uparrow^\dagger] |0\rangle^\Delta , \tag{8.55}$$

$$s_\uparrow^\dagger s_\downarrow^\dagger a_\downarrow^\dagger |0\rangle = \frac{1}{2\sqrt{2}}[t_\uparrow^\dagger + b_\uparrow^\dagger][t_\downarrow^\dagger + b_\downarrow^\dagger][t_\downarrow^\dagger - b_\downarrow^\dagger] |0\rangle^\Delta , \tag{8.56}$$

where Δ denotes a state that is projected away. We can instantly tell that a non-linear fermion transformation on this subspace will not be as effective as before. This is because there are five allowed states, and five is not divisible by two. Instead we must rely on the energetics to generate an effective Hamiltonian.

Consider a pair of neighbouring sites. From the Hamiltonian (7.25) we know that only the s_σ particles are mobile. If both of these sites are singly or doubly occupied then the particles cannot move. This is due to the Hamiltonian and limit $U = \infty$ respectively. So when contemplating electron motion, we need only consider the case where one site is singly occupied and the other is doubly occupied. As all singly occupied sites are total spin half and all doubly occupied are total spin one, the pair can only have total spin of $\frac{3}{2}$ or $\frac{1}{2}$. The following is a calculation where we apply the hopping Hamiltonian to the pair of possible states and project away disallowed states (the vacuum has been omitted to save space but is in each state)

$$s^\dagger_{1\uparrow}a^\dagger_{1\uparrow}a^\dagger_{2\uparrow} \to -a^\dagger_{1\uparrow}s^\dagger_{2\uparrow}a^\dagger_{2\uparrow}, \tag{8.57}$$

$$s^\dagger_{1\downarrow}a^\dagger_{1\downarrow}a^\dagger_{2\downarrow} \to -a^\dagger_{1\downarrow}s^\dagger_{2\downarrow}a^\dagger_{2\downarrow}, \tag{8.58}$$

$$s^\dagger_{1\uparrow}a^\dagger_{1\uparrow}a^\dagger_{2\downarrow} \to -a^\dagger_{1\uparrow}s^\dagger_{2\uparrow}a^\dagger_{2\downarrow} = -\frac{1}{2}a^\dagger_{1\uparrow}(s^\dagger_{2\uparrow}a^\dagger_{2\downarrow} + s^\dagger_{2\downarrow}a^\dagger_{2\uparrow}), \tag{8.59}$$

$$s^\dagger_{1\downarrow}a^\dagger_{1\downarrow}a^\dagger_{2\uparrow} \to -a^\dagger_{1\downarrow}s^\dagger_{2\downarrow}a^\dagger_{2\uparrow} = -\frac{1}{2}a^\dagger_{1\downarrow}(s^\dagger_{2\uparrow}a^\dagger_{2\downarrow} + s^\dagger_{2\downarrow}a^\dagger_{2\uparrow}), \tag{8.60}$$

$$\frac{1}{\sqrt{2}}(s^\dagger_{1\uparrow}a^\dagger_{1\downarrow} + s^\dagger_{1\downarrow}a^\dagger_{1\uparrow})a^\dagger_{2\uparrow} \to -\frac{1}{\sqrt{2}}(a^\dagger_{1\downarrow}s^\dagger_{2\uparrow}a^\dagger_{2\uparrow} + a^\dagger_{1\uparrow}s^\dagger_{2\downarrow}a^\dagger_{2\uparrow}) \tag{8.61}$$

$$= -\frac{1}{\sqrt{2}}(a^\dagger_{1\downarrow}s^\dagger_{2\uparrow}a^\dagger_{2\uparrow} + a^\dagger_{1\uparrow}\frac{1}{2}(s^\dagger_{2\uparrow}a^\dagger_{2\downarrow} + s^\dagger_{2\downarrow}a^\dagger_{2\uparrow})),$$

$$\frac{1}{\sqrt{2}}(s^\dagger_{1\uparrow}a^\dagger_{1\downarrow} + s^\dagger_{1\downarrow}a^\dagger_{1\uparrow})a^\dagger_{2\downarrow} \to -\frac{1}{\sqrt{2}}(a^\dagger_{1\downarrow}s^\dagger_{2\uparrow}a^\dagger_{2\downarrow} + a^\dagger_{1\uparrow}s^\dagger_{2\downarrow}a^\dagger_{2\downarrow}) \tag{8.62}$$

$$= -\frac{1}{\sqrt{2}}(a^\dagger_{1\downarrow}\frac{1}{2}(s^\dagger_{2\uparrow}a^\dagger_{2\downarrow} + s^\dagger_{2\downarrow}a^\dagger_{2\uparrow}) + a^\dagger_{1\uparrow}s^\dagger_{2\downarrow}a^\dagger_{2\downarrow}),$$

Where we have used the fact

$$s^\dagger_\sigma a^\dagger_{\bar\sigma} = \frac{1}{2}(t^\dagger_\sigma {t^\dagger_{\bar\sigma}}^\Delta - t^\dagger_\sigma b^\dagger_{\bar\sigma} + b^\dagger_\sigma t^\dagger_{\bar\sigma} - b^\dagger_\sigma {b^\dagger_\sigma}^\Delta) \tag{8.63}$$

$$\rightarrow \frac{1}{2}(-t^\dagger_\sigma b^\dagger_{\bar\sigma} + b^\dagger_\sigma t^\dagger_{\bar\sigma}) \tag{8.64}$$

$$= \frac{1}{2}(s^\dagger_\sigma a^\dagger_{\bar\sigma} + s^\dagger_{\bar\sigma} a^\dagger_\sigma). \tag{8.65}$$

In its current form things are not as transparent as they could be. Clearly the physics of this problem is based around spin, so lets cast this to a spin problem. This is done by defining

$$a^\dagger_\uparrow |0\rangle = |\uparrow\rangle\,, \quad a^\dagger_\downarrow |0\rangle = |\downarrow\rangle\,, \tag{8.66}$$

$$s^\dagger_\uparrow a^\dagger_\uparrow |0\rangle = |1\rangle\,, \quad \frac{1}{\sqrt{2}}(s^\dagger_\uparrow a^\dagger_\downarrow + s^\dagger_\downarrow a^\dagger_\uparrow) = |0\rangle\,, \quad s^\dagger_\downarrow a^\dagger_\downarrow |0\rangle = |\bar 1\rangle \tag{8.67}$$

where the spin-one states are labelled by their spin projection. The above results can be rewritten as

$$H\,|1\uparrow\rangle = -2t_1\,|\uparrow 1\rangle\,, \tag{8.68}$$

$$H\,|\bar 1\downarrow\rangle = -2t_1\,|\downarrow \bar 1\rangle\,, \tag{8.69}$$

$$H\,|1\downarrow\rangle = -\sqrt{2}t_1\,|\uparrow 0\rangle\,, \tag{8.70}$$

$$H\,|\bar 1\uparrow\rangle = -\sqrt{2}t_1\,|\downarrow 0\rangle\,, \tag{8.71}$$

$$H\,|0\uparrow\rangle = -\sqrt{2}t_1\,|\downarrow 1\rangle - t_1\,|\uparrow 0\rangle\,, \tag{8.72}$$

$$H\,|0\downarrow\rangle = -\sqrt{2}t_1\,|\uparrow \bar 1\rangle - t_1\,|\downarrow 0\rangle\,. \tag{8.73}$$

From this it can easily be shown that

$$H = -t_1 \sum_{\langle ij\rangle} [1 + 2\mathbf{s}_i \cdot \mathbf{S}_j]\,\Sigma_{ij}, \tag{8.74}$$

where $\mathbf{s}$ and $\mathbf{S}$ are the standard spin operators acting on the spin-half and spin-one states

respectively, and Σ_{ij} exchanges states on sites i and j. To see this expand, the Hamiltonian in terms of ladder operators giving

$$H = -t_1 \sum_{\langle ij \rangle} \left[1 + 2\left(s_i^Z S_j^Z + 2\left(s_i^+ S_j^- + s_i^- S_j^+\right)\right)\right] \Sigma_{ij}, \tag{8.75}$$

along with the spin relations

$$s^Z |\uparrow\rangle = \frac{1}{2} |\uparrow\rangle \qquad s^+ |\uparrow\rangle = 0 \qquad s^- |\uparrow\rangle = |\downarrow\rangle, \tag{8.76}$$

$$s^Z |\downarrow\rangle = -\frac{1}{2} |\downarrow\rangle \qquad s^+ |\downarrow\rangle = |\uparrow\rangle \qquad s^- |\downarrow\rangle = 0, \tag{8.77}$$

$$S^Z |1\rangle = |1\rangle \qquad S^+ |1\rangle = 0 \qquad S^- |1\rangle = \sqrt{2} |0\rangle, \tag{8.78}$$

$$S^Z |0\rangle = 0 \qquad S^+ |0\rangle = \sqrt{2} |1\rangle \qquad S^- |0\rangle = \sqrt{2} |\bar{1}\rangle, \tag{8.79}$$

$$S^Z |\bar{1}\rangle = -|\bar{1}\rangle \qquad S^+ |\bar{1}\rangle = \sqrt{2} |0\rangle \qquad S^- |\bar{1}\rangle = 0. \tag{8.80}$$

By expanding $(\mathbf{s}_i + \mathbf{S}_j)^2$ it can be shown that $\mathbf{s}_i \cdot \mathbf{S}_j = -\frac{1}{2}$ for total spin $\frac{1}{2}$ and $\mathbf{s}_i \cdot \mathbf{S}_j = \frac{1}{2}$ for total spin $\frac{3}{2}$. From this set of equations we can see that if the total spin of the pair of sites is $\frac{3}{2}$ then it hops with twice the amplitude of when the pair of sites is total spin $\frac{1}{2}$. This implies the hopping energetically favours ferromagnetism. This is corroborated with our exact diagonalisation results. We see that every anti-symmetric system examined has maximal spin. Of course this ferromagnetism must be stable to frustration to be a 'true' ferromagnet, but in our case there is no structural frustration that can affect our system.

The Hamiltonian for the remaining ferromagnet is

$$H_A = -2t_1 \sum_{\langle ij \rangle} s_{i\uparrow}^\dagger s_{j\uparrow} - t_0 \sum_i \left(1 - s_{i\uparrow}^\dagger s_{i\uparrow}\right), \tag{8.81}$$

where the vacuum is given by $|0\rangle_A = \prod_i a_{i\uparrow}^\dagger |0\rangle$.

In this chapter we took the physically motivated limit of divergent Coulomb limit given by $U = \infty$. This limit was taken exactly using a non-linear fermion transformation. We

found that the symmetric subspace was well behaved under the transformation, and the problem was recast to one with moderate interactions. In the anti-symmetric subspace things were not as effective, because there were five states remaining after the $U = \infty$ projection. We had to examine the energetics of problem and discovered the anti-symmetric subspace is described as a ferromagnet.

In the next chapter we will examine an exact solution of hole pairing using resolvent formalism.

CHAPTER 9

IMPURITY THEORY — AN EXACT SOLUTION FOR TWO HOLES AT THE MOTT POINT

In noteworthy physical problems the Hamiltonian is rarely solved trivially. Exact solutions are usually impossible. In this section we will present a rare case where the system can be solved exactly. We will show that two holes at the Mott point bind to form a localised pair.

After applying the limit $U = \infty$ the symmetric subspace is left with 4 of the 8 basis states it began with. These are exactly described by the non-linear fermion transformation. Therefore full occupation in the new $c^\dagger_{i\sigma}$ basis corresponds to the Mott point in the original $t^\dagger_{i\sigma}$, $b^\dagger_{i\sigma}$ basis.

The technique used in this chapter is called impurity theory or resolvent formalism [66]. It is a standard technique hence if this is unfamiliar see appendix E. Nevertheless, here is a *very brief* overview of the technique. First split the Hamiltonian in two: an exactly solvable component H_E and an 'impurity' H_I that only affects a small number of states $H = H_E + H_I$. This method relies on understanding and dealing with the resolvent

$G(\epsilon) = [\epsilon - H]^{-1}$. Using completeness this can be rewritten as

$$G(\epsilon)_{ii'} = \sum_{nn'} |\psi_i^{(n)}\rangle \, G(\epsilon)_{nn'} \, \langle \psi_{i'}^{(n')}| = \sum_n \frac{|\psi_i^{(n)}\rangle \, \langle \psi_{i'}^{(n)}|}{\epsilon - E_n}, \tag{9.1}$$

where $|\psi_i^{(n)}\rangle$ are the eigenvectors of H. Note that there are poles at the eigenvalues of H, whose residues are their corresponding eigenfunctions. By defining $G_E(\epsilon) = [\epsilon - H_E]^{-1}$ it can be shown that $G(\epsilon) = G_E(\epsilon) + G_E(\epsilon)\Sigma(\epsilon)G_E(\epsilon)$, where $\Sigma(\epsilon) = H_I[1 - G_E(\epsilon)H_I]^{-1}$. We can see that the poles, and hence the energy eigenvalues, of $G(\epsilon)$ are either poles of $G_E(\epsilon)$ or of $\Sigma(\epsilon)$. We are only interested in 'new' poles as they correspond to energies due to the addition of H_I. Therefore, we must calculate the poles of $\Sigma(\epsilon)$ which is equivalent to solving the equation

$$|\Phi\rangle = G_E(\epsilon) H_I \, |\Phi\rangle \, . \tag{9.2}$$

This calculation involves a finite dimensional inverse, controlled by the non-zero eigenbasis of H_I, and is tractable for small matrices. If this energy ϵ is lower than the ground state energy of H_E there is a bound state.

It can also be shown (see appendix E) that the wavefunction of the bound state is given by

$$|\psi_i^{(n')}\rangle = G_E(E_{n'}) \, |\varphi^{(n')}\rangle \, , \tag{9.3}$$

where $E_{n'}$ is the bound state energy and $|\varphi^{(n')}\rangle$ is found by calculating the residue of $\Sigma(\epsilon)$ at $\epsilon = E_{n'}$ giving $|\varphi^{(n')}\rangle \, \langle \varphi^{(n')}|$.

We will calculate the energy, dispersion, and correlation length of the pair. Then we will extend the energy results to two dimensions.

9.1 Binding Energy — Two Holes at the Mott Point Bind

In this section we will calculate the binding energy of two holes at the Mott point. We will set up the state, apply the Hamiltonian, and split it in the required manner. Then we will use impurity theory to calculate the binding energy.

The state in question, two holes at the Mott point, is given by

$$|m\rangle = \frac{1}{\sqrt{N}} \sum_j h^\dagger_{j,\uparrow} h^\dagger_{j+m,\downarrow} |\Psi\rangle_{Mott} \,, \tag{9.4}$$

where $h^\dagger_{i\sigma} = c_{i\sigma}$ is the hole creation operator, m is the separation of the holes, and $|\Psi\rangle_{Mott} = \prod_i c^\dagger_{i\uparrow} c^\dagger_{i\downarrow} |0\rangle$ is the Mott state in the original $(t_{i\sigma}, b_{i\sigma})$ basis and a band insulator in this basis.

As the state is written in terms of hole operators we rewrite the Hamiltonian in terms of $h^\dagger_{i\sigma}$. This gives

$$H_S = -t_0 \sum_{j\sigma} h^\dagger_{j\sigma} h_{j\sigma} + 2t_0 \sum_j h^\dagger_{j\uparrow} h_{j\uparrow} h^\dagger_{j\downarrow} h_{j\downarrow} + t_1 \sum_{\langle jj'\rangle\sigma} h^\dagger_{j\sigma} h_{j'\sigma} \left(1 + \chi h^\dagger_{j\bar{\sigma}} h_{j\bar{\sigma}}\right) \left(1 + \chi h^\dagger_{j'\sigma} h_{j'\sigma}\right), \tag{9.5}$$

where $\chi = \sqrt{2} - 1$. Next we apply this to our state $|m\rangle$, using the shorthand $\bar{m} = -m$, which gives

$$H_S |m\rangle = -2t_0 |m\rangle + 2t_1(|m+1\rangle + |m-1\rangle), \qquad \forall m \neq 1, 0, \bar{1}, \tag{9.6}$$

$$H_S |1\rangle = -2t_0 |1\rangle + 2t_1(|2\rangle + |0\rangle) + 2t_1\chi |0\rangle \,, \tag{9.7}$$

$$H_S |0\rangle = 2t_1(|1\rangle + |\bar{1}\rangle) + 2t_1\chi(|1\rangle + |\bar{1}\rangle), \tag{9.8}$$

$$H_S |\bar{1}\rangle = -2t_0 |\bar{1}\rangle + 2t_1(|0\rangle + |\bar{2}\rangle) + 2t_1\chi |0\rangle \,. \tag{9.9}$$

This can be rewritten as $H_S = H_E + H_I$, where in matrix form

$$H_E = \begin{bmatrix} \ddots & \ddots & & & \\ \ddots & -2t_0 & 2t_1 & & \\ & 2t_1 & -2t_0 & 2t_1 & \\ & & 2t_1 & -2t_0 & \ddots \\ & & & \ddots & \ddots \end{bmatrix} \quad \text{and} \quad H_I = \begin{bmatrix} \ddots & 0 & 0 & 0 & 0 \\ 0 & 0 & 2\chi t_1 & 0 & 0 \\ 0 & 2\chi t_1 & 2t_0 & 2\chi t_1 & 0 \\ 0 & 0 & 2\chi t_1 & 0 & 0 \\ 0 & 0 & 0 & 0 & \ddots \end{bmatrix}, \tag{9.10}$$

which is exactly what is required to perform impurity theory.

We diagonalise H_E with a Bloch transformation giving G_E in its diagonal basis as

$$G_E(\epsilon)_{kk'} = \frac{\delta_{kk'}}{(\epsilon + 2t_0) - 4t_1 \cos k}, \tag{9.11}$$

and in real space this is given by

$$G_E(\epsilon)_{jj'} = \frac{1}{N} \sum_k \frac{e^{ik(j-j')}}{(\epsilon + 2t_0) - 4t_1 \cos k}. \tag{9.12}$$

Taking the continuum limit it gives

$$G_E(\epsilon)_{jj'} = \int_{-\pi}^{\pi} \frac{dk}{2\pi} \frac{e^{ik(j-j')}}{(\epsilon + 2t_0) - 4t_1 \cos k}. \tag{9.13}$$

This is solved with complex analysis and gives

$$G_E(\epsilon)_{jj'} = \frac{-(x_-)^{|j-j'|}}{2t_0 (x_- - x_+)}. \tag{9.14}$$

where

$$x_\mp = \frac{(\epsilon + 2t_0) \pm \left[(\epsilon + 2t_0)^2 - 16t_1^2\right]^{1/2}}{4t_1}. \tag{9.15}$$

The matrix G_E is symmetric, i.e. $G_E(\epsilon)_{jj'} = G_E(\epsilon)_{j'j}$, so we will label the elements of

G_E with its corresponding displacement. In our case Equation 9.2 is given by

$$\begin{bmatrix} a \\ b \\ a \end{bmatrix} = \begin{bmatrix} G_0 & G_1 & G_2 \\ G_1 & G_0 & G_1 \\ G_2 & G_1 & G_0 \end{bmatrix} \begin{bmatrix} 0 & 2\chi t_1 & 0 \\ 2\chi t_1 & 2t_0 & 2\chi t_1 \\ 0 & 2\chi t_1 & 0 \end{bmatrix} \begin{bmatrix} a \\ b \\ a \end{bmatrix}. \tag{9.16}$$

$$\begin{bmatrix} a \\ b \\ a \end{bmatrix} = \begin{bmatrix} G_0 & G_1 & G_2 \\ G_1 & G_0 & G_1 \\ G_2 & G_1 & G_0 \end{bmatrix} \begin{bmatrix} 2\chi t_1 b \\ 4\chi t_1 a + 2t_0 b \\ 2\chi t_1 b \end{bmatrix}. \tag{9.17}$$

This gives

$$a = 2\chi t_1 b(G_0 + G_2) + G_1(4\chi t_1 a + 2t_0 b) \tag{9.18}$$

$$b = 4\chi t_1 b G_1 + G_0(4\chi t_1 a + 2t_0 b) \tag{9.19}$$

We can also use the definition of $(\epsilon - H_E)G_E = 1$

$$\begin{bmatrix} \epsilon & -2t_1 & 0 \\ -2t_1 & \epsilon + 2t_0 & -2t_1 \\ 0 & -2t_1 & \epsilon \end{bmatrix} \begin{bmatrix} G_0 & G_1 & G_2 \\ G_1 & G_0 & G_1 \\ G_2 & G_1 & G_0 \end{bmatrix} = \begin{bmatrix} 1 & 0 & 0 \\ 0 & 1 & 0 \\ 0 & 0 & 1 \end{bmatrix}, \tag{9.20}$$

which gives

$$(\epsilon + 2t_0)G_0 - 4t_1 G_1 = 1 \tag{9.21}$$

$$\epsilon G_1 - 2t_2(G_0 + G_2) = 0 \tag{9.22}$$

The eigenvalue equation is solved to give

$$G_E(\epsilon)_{00} = \frac{2}{\epsilon + 4t_0}. \tag{9.23}$$

Figure 9.1: Exact Binding Energy of Two Holes at the Mott Point — 1D

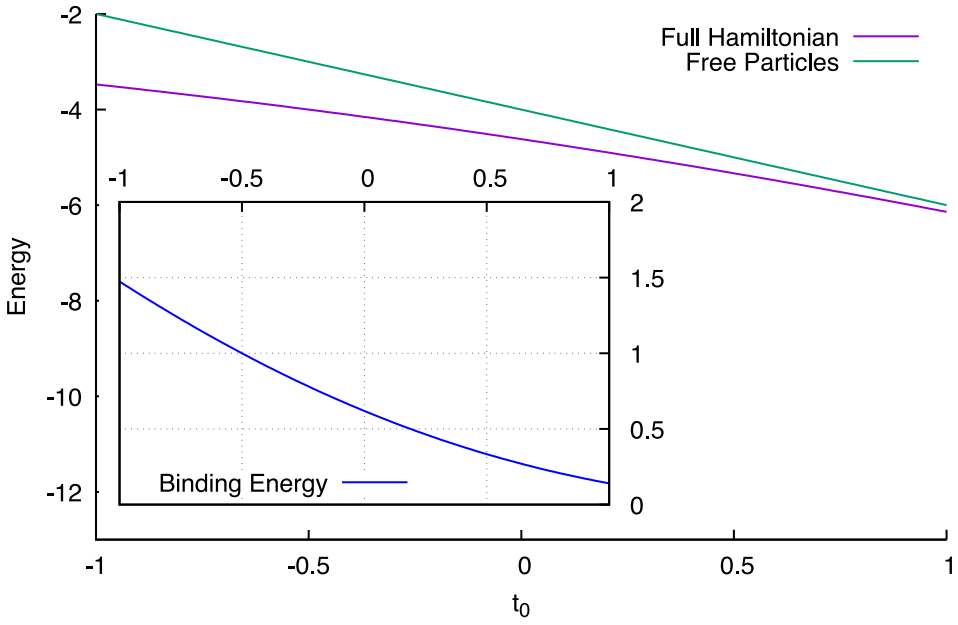

Total energy for two holes with Hamiltonian H_E, labelled free particles, and exact solution labelled full Hamiltonian. The difference of the two is the binding energy. The units of energy are the same as t_0.

Equating 9.14 and 9.23 yields the bound state energy as

$$\epsilon_B = \frac{4}{3}\left[-t_0 - \sqrt{t_0^2 + 12t_1^2}\right], \tag{9.24}$$

and therefore the binding energy is given by

$$\Delta = \frac{4}{3}\left[-t_0 - \sqrt{t_0^2 + 12t_1^2}\right] + 2t_0 + 4t_1. \tag{9.25}$$

This is depicted in figure 9.1 on page 78. Note this system is not always bound. At $t_0 = 2$ both energies become equal and the gap becomes zero.

In this section we calculated the binding energy of two holes at the Mott point and showed they are bound for a wide range of t_0. In the following section we will extend this calculation to include momentum.

9.2 Centre of Mass Momentum — Binding as a Function of Momentum

We have solved the case where the momentum of the pair is zero. Now we will add momentum to the centre of mass of the pair and see the effects. This is as simple as adding a phase to the definition of the pair. The states are now defined as

$$|m\rangle_q = \frac{1}{\sqrt{N}} \sum_j e^{iq\left(j+\frac{m}{2}\right)} h_{j,\uparrow} h_{j+m,\downarrow} |\Psi_{\text{Mott}}\rangle \,, \tag{9.26}$$

where q is the centre of mass momentum of the pair.

This trivially updates the prior calculation in the following manner

$$\begin{aligned} t_0 &\to t_0, \\ t_1 &\to t_1 \cos\left[\tfrac{q}{2}\right], \end{aligned} \tag{9.27}$$

and therefore the binding energy is given by

$$\Delta = \frac{4}{3}\left[-t_0 - \sqrt{t_0^2 + 12t_1^2 \cos^2\left[\frac{q}{2}\right]}\right] + 2t_0 - 4t_1 \cos\left[\frac{q}{2}\right]. \tag{9.28}$$

This is depicted in figure 9.2 on page 80.

In this section we showed that two holes are bound at the Mott point even with momentum. We now move on to calculating the correlation length of the bound pair.

9.3 Correlation Length — The Holes are Tightly Bound

To calculate the correlation length we must first find the wavefunction. This calculation requires solving

$$|\psi^{(n')}\rangle = G_E(E_{n'}) \, |\varphi^{(n')}\rangle \,, \tag{9.29}$$

Figure 9.2: Exact Dispersion of Two Holes at the Mott Point — 1D

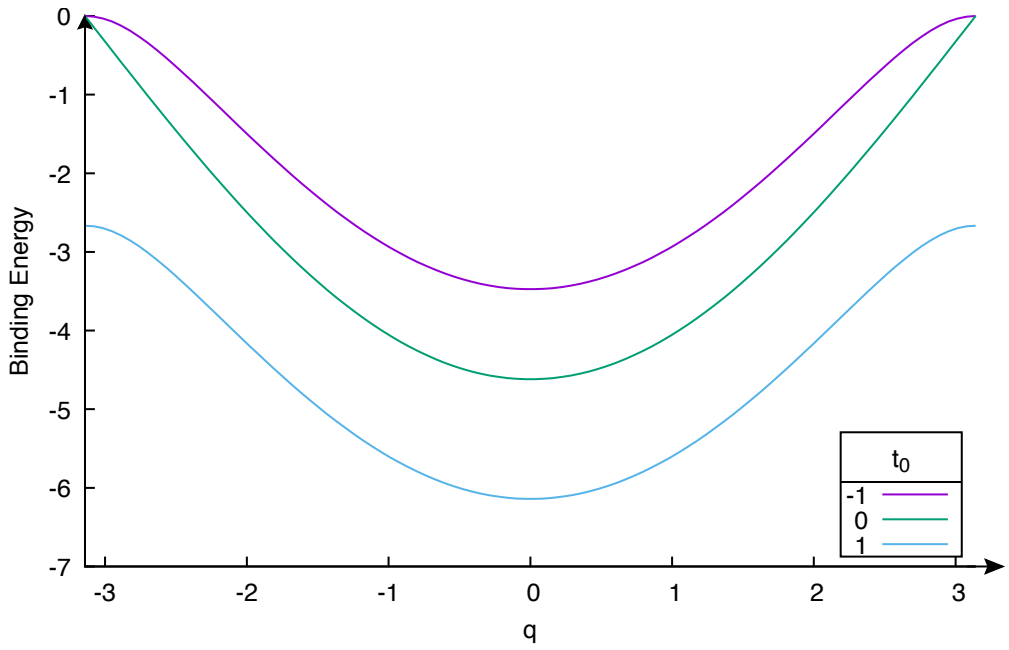

The total energy as a function of centre of mass momentum. Energy is in the same units of t_0.

which requires solving a three dimensional eigenvalue equation. The process of calculating the wavefunction using impurity theory is detailed in Appendix E. This gives

$$|\psi\rangle \propto \sum_n \left[\left(\frac{\epsilon_B}{\chi+2} + \frac{2t_0}{\chi} \right) G_n + t_1 \left(G_{n+1} + G_{n-1} \right) \right] |n\rangle \,. \tag{9.30}$$

From equation 9.14 it can be seen that

$$G_n = G_0 x_+^{|n|}, \tag{9.31}$$

and therefore

$$|\psi\rangle \propto \sum_n \left[\left(\frac{\epsilon_B}{\chi+2} + \frac{2t_0}{\chi} \right) + t_1 \left(x_+ + \frac{1}{x_+} \right) \right] G_0 x_+^{|n|} |n\rangle \,. \tag{9.32}$$

To calculate the correlation length we state

$$\psi_n \propto e^{-\frac{|n|}{\xi}} |n\rangle \,, \tag{9.33}$$

Figure 9.3: Exact Correlation Length of Two Holes at the Mott Point — 1D

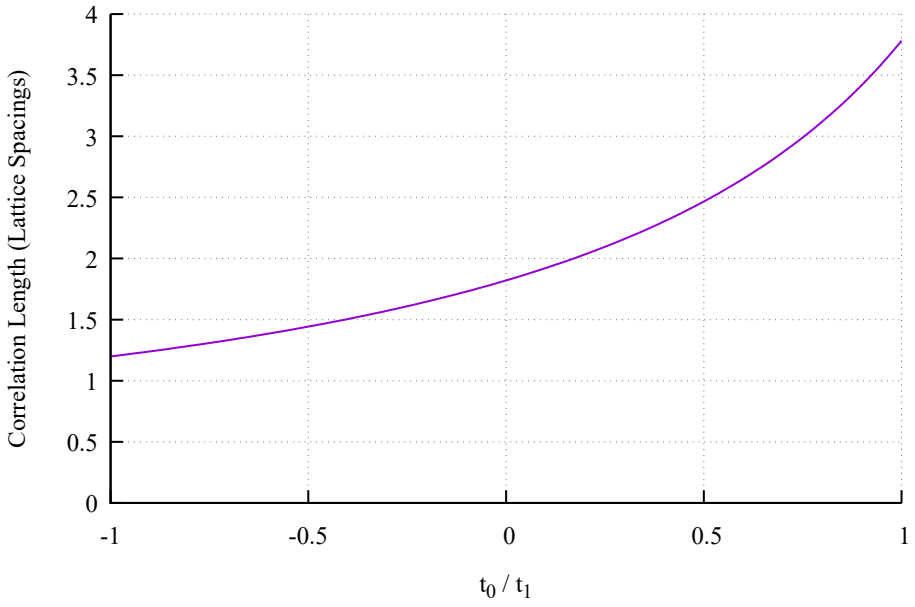

Correlation length of the pair, setting $t_1 = 1$ *and varying* t_0.

which is trivially solved to give the correlation length as

$$\frac{1}{\xi} = \ln \left| \frac{6}{\tau + \sqrt{\tau^2 + 12}} \right|, \tag{9.34}$$

where $\tau = \frac{t_0}{t_1}$. This is depicted in figure 9.3 on page 81. Note $\tau = 2$ is special as this is the critical point where the correlation length diverges.

9.4 Extending Results to Two Dimensions

This calculation is trivially extended to higher dimensions. The only issue is the inability to analytically perform the integration. As a result we rely on numerical integration.

We are required to solve

$$\frac{1}{N} \sum_{\mathbf{k}} \frac{1}{\epsilon - 2t_1 Z \gamma_{\mathbf{k}} + 2t_0} = \frac{2}{\epsilon + 4t_0}, \tag{9.35}$$

Figure 9.4: Exact Binding Energy of Two Holes at the Mott Point — 2D

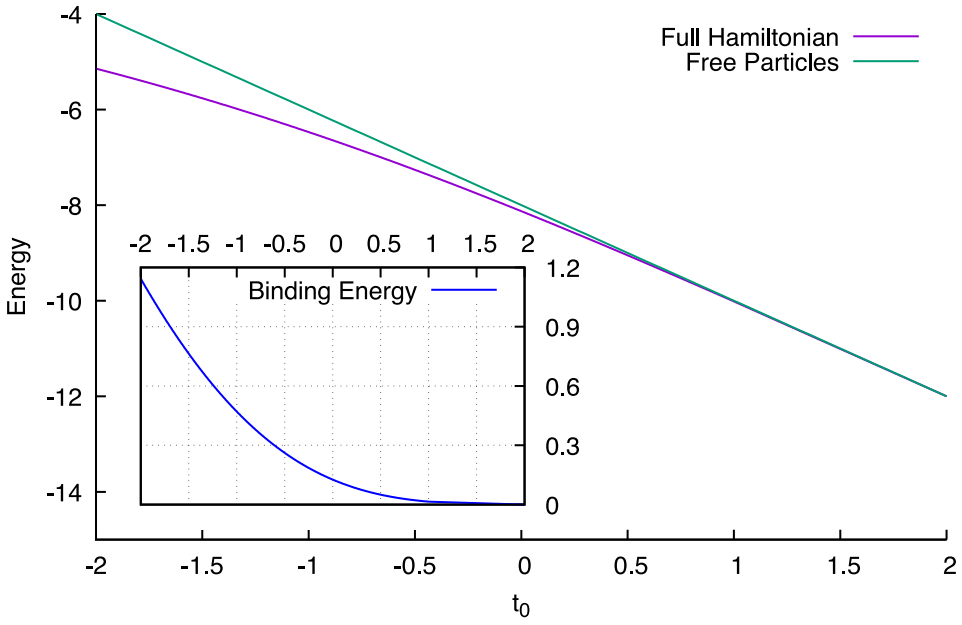

Total energy for two holes with Hamiltonian H_E, labelled free particles, and exact solution labelled full Hamiltonian. The difference of the two is the binding energy. Calculated on the 2D square lattice. Energy is in the same units as t_0.

where $\gamma_{\mathbf{k}}$ is the structure factor and Z is the co-ordination number (the number of nearest neighbours). In figure 9.4 on page 82 we depict the binding energy of two holes at the Mott point for the 2D square lattice.

In this chapter we showed exactly that two holes form a closely bound pair. This was qualitatively analogous to the Cooper problem. As exact solutions with more holes are not tractable in the next chapter we use mean field theory.

CHAPTER 10

MEAN FIELD THEORY — AN APPROXIMATE SOLUTION FOR ARBITRARY OCCUPATION

Exact solutions with more holes are not tractable. Therefore we use mean field theory [67]. In the anti-symmetric subspace this is an exact solution as H_A is non-interacting. In the symmetric subspace this is an appropriate technique as, thanks to the non-linear fermion transformation, interactions are now moderate. Nevertheless we will compare our results to exact diagonalization in chapter 11 and find good agreement.

As this technique is standard we have detailed and introduced it in appendix D. Here is a *very brief* overview of the process.

1. Decide what physics you are examining. This restricts the allowed correlations.
2. Calculate the average energy $\bar{E} = \langle H \rangle$ using Slater determinants [68] where necessary.
3. Use Wick's theorem [69] to create an effective single particle Hamiltonian H^{eff}.
4. Use the resolvent $G(\epsilon) = [\epsilon - H^{eff}]^{-1}$ to self consistently determine the fields which are permitted.

The first calculation is the ferromagnetic phase in the anti-symmetric subspace.

10.1 Anti-Symmetric Subspace

Note that this process is exact for the anti-symmetric subspace, as H_A is a single particle Hamiltonian. The anti-symmetric subspace Hamiltonian is

$$H_A = -2t_1 \sum_{\langle ij \rangle} s^\dagger_{i\uparrow} s_{j\uparrow} - t_0 \sum_i \left(1 - s^\dagger_{i\uparrow} s_{i\uparrow}\right). \tag{10.1}$$

We assume translational invariance in this calculation, so the only correlations allowed are $n_0^A = \langle s^\dagger_{i\uparrow} s^\dagger_{i\uparrow} \rangle$ and $n_1^A = \langle s^\dagger_{i\uparrow} s^\dagger_{j\uparrow} \rangle$. The average energy per site is therefore

$$\bar{E}_A = -2t_1 Z n_1^A - t_0(1 - n_0^A), \tag{10.2}$$

where Z is the co-ordination number (the number of nearest neighbours). The Hamiltonian is already single particle so we do not require Wick's theorem. We diagonalise H_A with a Bloch transform which gives the resolvent as

$$G_A(\epsilon) = \frac{\delta_{\mathbf{k}\mathbf{k}'}}{\epsilon + 2t_1 Z \gamma_{\mathbf{k}} + t_0}, \tag{10.3}$$

where $\gamma_{\mathbf{k}}$ is the nearest neighbour structure factor. The only quantities required to be calculated are n_0^A and n_1^A, with the former given by

$$\begin{aligned} n_0^A &= \langle s^\dagger_{i\uparrow} s_{i\uparrow} \rangle = \sum_{\mathbf{k}} \langle s^\dagger_{\mathbf{k}\uparrow} s_{\mathbf{k}\uparrow} \rangle & (10.4)\\ &= \sum_{\mathbf{k}} \int_C \frac{\mathrm{d}\epsilon}{2\pi i} f(\epsilon - \mu) G_A(\epsilon) & (10.5)\\ &= \sum_k \int_C \frac{\mathrm{d}\epsilon}{2\pi i} f(\epsilon - \mu) \frac{1}{\epsilon + 2t_1 Z \gamma_{\mathbf{k}} + t_0} & (10.6)\\ &= \sum_k f\left(-2t_1 Z \gamma_{\mathbf{k}} - t_0 - \mu\right) & (10.7) \end{aligned}$$

$$= \int_{-\pi}^{\pi} \frac{\mathrm{d}^d\mathbf{k}}{(2\pi)^d} f\left(-2t_1 Z\gamma_{\mathbf{k}} - t_0 - \mu\right), \tag{10.8}$$

where $f(x)$ is the Fermi function, and in the final step we took the continuum limit. Similarly for n_1^A we have

$$n_1^A = \int_{-\pi}^{\pi} \frac{\mathrm{d}^d\mathbf{k}}{(2\pi)^d} f\left(-2t_1 Z\gamma_{\mathbf{k}} - t_0 - \mu\right)\gamma_{\mathbf{k}}. \tag{10.9}$$

This result is depicted and discussed in chapter 11.

We now move on to the symmetric subspace, in which a superconducting phase can be found.

10.2 Symmetric Subspace

In this section we will calculate the paramagnetic and superconducting mean field energy. The paramagnetic solution is standard, but the superconducting solution must be diagonalised via a Bogoliubov-Valatin [40] transformation. This is standard for BCS theory.

10.2.1 Paramagnetic Calculation

In this calculation we will assume translational invariance and paramagnetism. The correlations that are in this calculation are $n_0^S = \langle c_{i\sigma}^\dagger c_{i\sigma}\rangle$ and $n_1^S = \langle c_{i\sigma}^\dagger c_{j\sigma}\rangle$. There is no magnetism as spin up and down are treated equally. The Hamiltonian is

$$H_S = -2t_1 \sum_{\langle ij\rangle\sigma} (1-\eta c_{i\bar{\sigma}}^\dagger c_{i\bar{\sigma}}) c_{i\sigma}^\dagger c_{j\sigma} (1-\eta c_{j\bar{\sigma}}^\dagger c_{j\bar{\sigma}}) - t_0 \sum_{i\sigma} c_{i\sigma}^\dagger c_{i\sigma} + 2t_0 \sum_i c_{i\uparrow}^\dagger c_{i\uparrow} c_{i\downarrow}^\dagger c_{i\downarrow}. \quad (10.10)$$

The average energy per spin per site is therefore

$$\bar{E}_S = -4t_1 Z n_1^S \left(\left(1-\eta n_0^S\right)^2 - \eta^2 n_1^{S^2} \right) - t_0 n_0^S \left(n_0^S - 1\right). \quad (10.11)$$

Using Wick's theorem this gives an effective single particle Hamiltonian of

$$H_S^{eff} = \alpha_S \sum_{j\sigma} c_{j\sigma}^\dagger c_{j\sigma} + \beta_S \sum_{\langle jj'\rangle\sigma} c_{j\sigma}^\dagger c_{j'\sigma}, \quad (10.12)$$

where $\alpha_S = 4Zt_1\eta n_1^S \left(1-\eta n_0^S\right) + t_0\left(2n_0^S - 1\right)$ and $\beta_S = -4Zt_1\left(\left(1-\eta n_0^S\right)^2 - 3\eta^2 n_1^{S^2} \right)$. This is diagonalised using a Bloch transformation and gives the resolvent

$$G_S(\epsilon) = \frac{\delta_{\mathbf{k}\mathbf{k}'}}{\epsilon - \beta_S Z \gamma_{\mathbf{k}} - \alpha_S}. \quad (10.13)$$

Using this we can self consistently define our fields, which gives

$$n_0^S = \int_{-\pi}^{\pi} \frac{\mathrm{d}^d\mathbf{k}}{(2\pi)^d} f\left(-\beta_S Z\gamma_{\mathbf{k}} - \alpha - \mu\right), \quad (10.14)$$

$$n_1^S = \int_{-\pi}^{\pi} \frac{\mathrm{d}^d\mathbf{k}}{(2\pi)^d} f\left(-\beta_S Z\gamma_{\mathbf{k}} - \alpha - \mu\right)\gamma_{\mathbf{k}}. \tag{10.15}$$

This is depicted and discussed in chapter 11. Next we look at the superconducting solution.

10.2.2 Superconducting Calculation

In this calculation we assume translational invariance, spin symmetry, and the existence of the superconducting fields δ_0, δ_0^*, δ_1, and δ_1^*. This

$$n_0^{SC} = \langle c_{i\sigma}^\dagger c_{i\sigma}\rangle, \quad n_1^{SC} = \langle c_{i\sigma}^\dagger c_{j\sigma}\rangle \tag{10.16}$$

$$\delta_0 = \langle \sigma c_{i\sigma}^\dagger c_{i\bar{\sigma}}^\dagger\rangle, \quad \delta_0^* = \langle \sigma c_{i\bar{\sigma}} c_{i\sigma}\rangle \tag{10.17}$$

$$\delta_1 = \langle \sigma c_{i\sigma}^\dagger c_{j\bar{\sigma}}^\dagger\rangle, \quad \delta_1^* = \langle \sigma c_{i\bar{\sigma}} c_{j\sigma}\rangle, \tag{10.18}$$

where we have used the shorthand $\sigma = +/-$ for spins $\sigma = \uparrow / \downarrow$. Without loss of generality we can choose a phase such that $\delta_0 = \delta_0^*$ and $\delta_1 = \delta_1^*$. This gives the average energy per site as

$$\begin{aligned}\bar{E}^{SC} = -4t_1 Z n_1^{SC}\left(\left(1-\eta n_0^{SC}\right)^2 - \eta^2 {n^{SC}}_1^2\right) - 2t_0 n_0^{SC}\left(1-n_0^{SC}\right) + 2t_0\delta_0^2 \\ + 4t_1 Z\left(2\eta\delta_0\delta_1\left(1-\eta n_0^{SC}\right) + \eta^2 n_1^{SC}\left(\delta_0^2+\delta_1^2\right)\right).\end{aligned} \tag{10.19}$$

Using Wick's theorem this gives an effective Hamiltonian as

$$\begin{aligned}H_{SC}^{eff} = \alpha_{SC}\sum_{j\sigma} c_{j\sigma}^\dagger c_{j\sigma} + \beta_{SC}\sum_{\langle jj'\rangle\sigma} c_{j\sigma}^\dagger c_{j'\sigma} \\ + \nu_{SC}\sum_{j\sigma}\left(c_{j\sigma}^\dagger c_{j\bar{\sigma}}^\dagger + c_{j\bar{\sigma}}c_{j\sigma}\right) + \lambda_{SC}\sum_{\langle jj'\rangle\sigma}\left(c_{j\sigma}^\dagger c_{j'\bar{\sigma}}^\dagger + c_{j'\bar{\sigma}}c_{j\sigma}\right),\end{aligned} \tag{10.20}$$

where

$$\alpha_{SC} = 2t_0\left(2n_0 - 1\right) + 16t_1\eta\left(n_1\left(1 - \eta n_0\right) - \eta\delta_0\delta_1\right), \tag{10.21}$$

$$\beta_{SC} = -8t_1\left(\left(1 - \eta n_0\right)^2 - \eta^2\left(3n_1^2 + \delta_0^2 + \delta_1^2\right)\right), \tag{10.22}$$

$$\nu_{SC} = 4t_0\delta_0 + 16t_1\eta\left(\delta_1\left(1 - \eta n_0\right) + \eta n_1\delta_0\right), \tag{10.23}$$

$$\lambda_{SC} = 16t_1\eta\left(\delta_0\left(1 - \eta n_0\right) + \eta n_1\delta_1\right). \tag{10.24}$$

After a Bloch transformation and Bogoliubov-Valatin transformation we cast H_{SC}^{eff} as the following matrix

$$H_{SC}^{eff} = \sum_{\mathbf{k}\sigma}\begin{bmatrix} c_{\mathbf{k}\sigma}^\dagger & c_{-\mathbf{k}\bar{\sigma}} \end{bmatrix}\begin{bmatrix} A_{\mathbf{k}} & B_{\mathbf{k}} \\ B_{\mathbf{k}} & -A_{\mathbf{k}} \end{bmatrix}\begin{bmatrix} c_{\mathbf{k}\sigma} \\ c_{-\mathbf{k}\bar{\sigma}}^\dagger \end{bmatrix} + A_{\mathbf{k}}, \tag{10.25}$$

where $A_{\mathbf{k}} = \alpha_{SC} + \beta_{SC}Z\gamma_{\mathbf{k}}$ and $B_{\mathbf{k}} = \nu_{SC} + \lambda_{SC}Z\gamma_{\mathbf{k}}$. Diagonalising this matrix gives the expected gapped BCS dispersion

$$E_{\mathbf{k}}^{\pm} = \pm\sqrt{A_{\mathbf{k}}^2 + B_{\mathbf{k}}^2}. \tag{10.26}$$

Again, we generate the resolvent

$$G_{SC}(\epsilon) = \frac{1}{\epsilon^2 - A_{\mathbf{k}}^2 + B_{\mathbf{k}}^2}\begin{bmatrix} \epsilon + A_{\mathbf{k}} & -B_{\mathbf{k}} \\ -B_{\mathbf{k}} & \epsilon - A_{\mathbf{k}} \end{bmatrix}, \tag{10.27}$$

which is used to generate the fields

$$n_0^{SC} = \int_{-\pi}^{\pi} \frac{\mathrm{d}^d\mathbf{k}}{(2\pi)^d} \frac{1}{2} f(E_{\mathbf{k}}^+) \left(1 - \frac{A_{\mathbf{k}}}{E_{\mathbf{k}}^+}\right), \tag{10.28}$$

$$n_1^{SC} = \int_{-\pi}^{\pi} \frac{\mathrm{d}^d\mathbf{k}}{(2\pi)^d} \frac{1}{2} f(E_{\mathbf{k}}^+) \left(1 - \frac{A_{\mathbf{k}}}{E_{\mathbf{k}}^+}\right) \gamma_k, \tag{10.29}$$

$$\delta_0 = \int_{-\pi}^{\pi} \frac{\mathrm{d}^d\mathbf{k}}{(2\pi)^d} f(E_{\mathbf{k}}^+) \left(\frac{-B_{\mathbf{k}}}{2E_{\mathbf{k}}^+}\right), \tag{10.30}$$

$$\delta_1 = \int_{-\pi}^{\pi} \frac{\mathrm{d}^d\mathbf{k}}{(2\pi)^d} f(E_{\mathbf{k}}^+) \left(\frac{-B_{\mathbf{k}}}{2E_{\mathbf{k}}^+}\right) \gamma_k, \tag{10.31}$$

where in these equations $A_{\mathbf{k}} \to A_{\mathbf{k}} - \mu$ to control the number of particles in the Grand Canonical picture with the chemical potential μ.

In this chapter we performed Hartree-Fock mean field theory on both the symmetric and anti-symmetric subspace. We calculated for a paramagnetic and superconducting phase for the symmetric subspace. This analysis is exact for the ferromagnet in the anti-symmetric subspace. In the next chapter we present the results.

CHAPTER 11

RESULTS

In this chapter we will present the total energy and specific correlations from different phases in the model. In the anti-symmetric subspace we will only present a ferromagnetic phase, as this is the only phase by construction. In the symmetric subspace we will consider a paramagnetic and superconducting phase generated in the previous chapter. The correlations we consider are excess pairing, occupation factor, and the superconducting gap.

Initial calculations are performed in 1D, as exact diagonalization finite scales best in 1D [70]. However, we know that long range order is not permitted in 1D due to the Mermin Wagner theorem. For this reason we do further calculations in 2 dimensions. It is important to note that we are at the level of BCS with these results. Hartree-Fock mean field theory is a variational solution and finds the best single particle solution to a many body problem.

Before we present our main results let's discuss the competition between the two subspaces.

11.1 Maxwell Construction — Bridging the Gap Between Subspaces

In chapter 7, we discussed the role of symmetry in this model. Specifically, that we need only consider two symmetry configurations: purely S on each site or A on each site. In this section we discuss the motivation behind this approach.

The complete system of 9 degrees of freedom is rather unwieldy. From energy arguments we saw that two neighbouring anti-symmetric states would like to have maximal spin and exchange. This energy gain can occur en masse if all the anti-symmetric states are together in real space. To test this hypothesis we used exact diagonalisation on the complete system of 9 degrees of freedom, and we extracted the symmetry at each site. As there is translational invariance the ground state is a linear superposition of translated copies. Therefore to extract the symmetry we: calculate the ground state vector, apply the symmetry transformation on each site, and project into the untranslated configuration i.e. $|GS\rangle \to \frac{1}{2}(1+\hat{T}_i)\,|GS\rangle$, where $\hat{T}_i$ is $t^\dagger_{i\sigma} \leftrightarrow b^\dagger_{i\sigma}$ on site i. This provided a set of labels for each system which is shown in table 11.1 on page 93.

Our hypothesis was correct! The system phase separates to gain the most energy it can. When this occurs it is frequently described mathematically by a Maxwell construction (see appendix G if unfamiliar). We separated the state space, into the symmetric and anti-symmetric subspaces, and performed a Maxwell construction between them. This is depicted in figure 11.1 on page 94. Note the agreement between the Maxwell construction and the exact diagonalisation. Add to that when the ground state is described by one of the two subspaces, the two exact diagonalisation calculation energies agrees to numerical accuracy.

There is one caveat however, and that is the effect of long range Coulomb. Our model only takes into account local Coulomb repulsion; this is usually appropriate thanks to screening. However, when phase separation occurs in this model it is between states with different occupation numbers. Having phase separation on a macroscopic scale would

correspond to 10^{23} extra electrons on one side of the crystal. This would incur a *massive* long range Coulomb penality. Instead there would be a balance between the gain from phase separation and the penalty from long range Coulomb such that the phase separation would occur on a micro- or meso-scopic scale. This has been seen experimentally, one such system is $Sr_{0.5}Ce_{0.5}FBiS_{2-x}Se_x$ where ferromagnetism and superconductivity were shown to co-exist [71].

We can therefore consider both subspaces independently, allowing us to examine larger systems numerically. Now we move on to the rest of the results starting with total energy as a function of occupation.

Table 11.1: Phase Separation in the Model: Symmetry Extracted States from Exact Diagonalisation on Systems with Periodic Boundary Conditions

No of Particles	Symmetry Configuration	No of Particles	Symmetry Configuration
0	SSSSSSSSSS	11	SSSSSSSSSS
1	SSSSSSSSSS	12	SSSSSSSSSS
2	SSSSSSSSSS	13	SSSAAASSSS
3	SSSSSSSSSS	14	SSSSSAAAAA
4	SSSSSSSSSS	15	AAAAASSSAA
5	SSSSSSSSSS	16	AAAAAAAAAA
6	SSSSSSSSSS	17	AAAAAAAAAA
7	SSSSSSSSSS	18	AAAAAAAAAA
8	SSSSSSSSSS	19	AAAAAAAAAA
9	SSSSSSSSSS	20	AAAAAAAAAA
10	SSSSSSSSSS		

Figure 11.1: Maxwell Construction Fit to Phase Separation

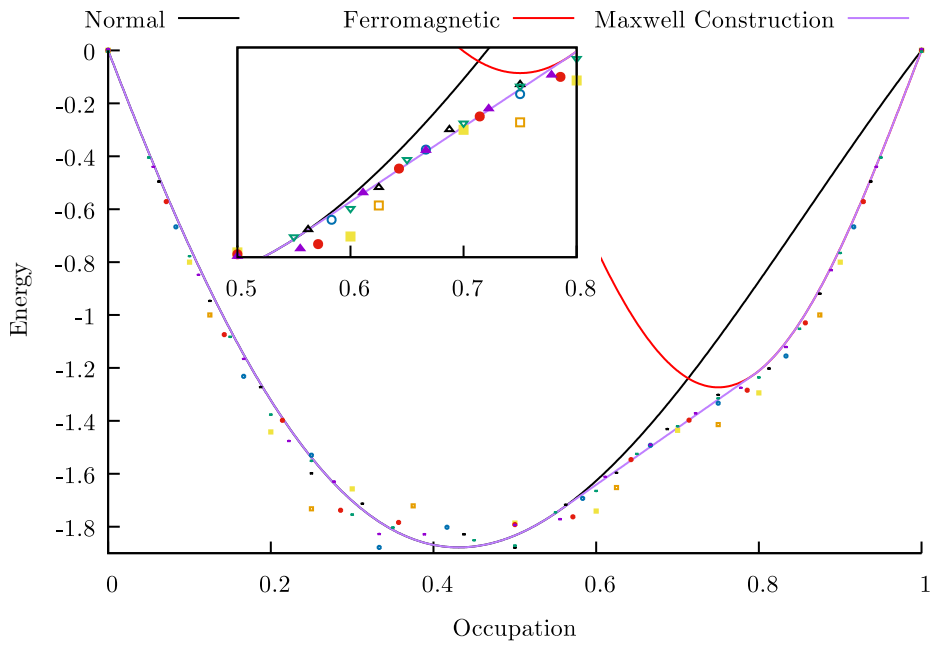

Energy per site as a function of occupation, comparing mean field theory to diagonalisation of finite systems of size 8 to 10 (each system size is a different point) with $t_0 = 0$ and $t_1 = 1$. The three systems examined are the full system, symmetric, and anti-symmetric. Predominantly the pure symmetry configurations energies match the full system. When these systems are in competition a Maxwell construction between the subspaces shows good agreement to the data.

11.2 Total Energy as a Function of Occupation

In this section we present total energy results from which a zero temperature phase diagram can be generated. Each phase has an associated total energy which can be compared to find the ground state phase of the system. As we vary the chemical potential μ we self consistently solve for the correlations numerically. This allows us to find the phase of the system as a function of occupation.

Figures 11.2 on page 96, 11.3 on page 97, and 11.4 on page 98 depict the average energy as a function of occupation for $t_0 = 0, 1$, and -1 respectively. As can be seen the interplay between magnetism, paramagnetism, and superconductivity is controlled by t_0. While decreasing t_0 strengthens the superconductivity it also strengthens the ferromagnetism. When $t_0 = 1$ the ferromagnetism is completely suppressed, the symmetric subspace is the ground state for all occupation, and close to the Mott point superconductivity prevails. Note the quality of the agreement between exact diagonalisation and mean field theory in every figure. As they are two independent techniques and the exact diagonalisation is 'correct', the agreement signifies the validity of the mean-field solution.

In this section we showed the total energy results which generated the zero temperature phase diagram of this system. We now move on to calculating correlations.

Figure 11.2: Total Energy as a Function of Occupation $t_0 = 0$, $t_1 = 1$ — 1D

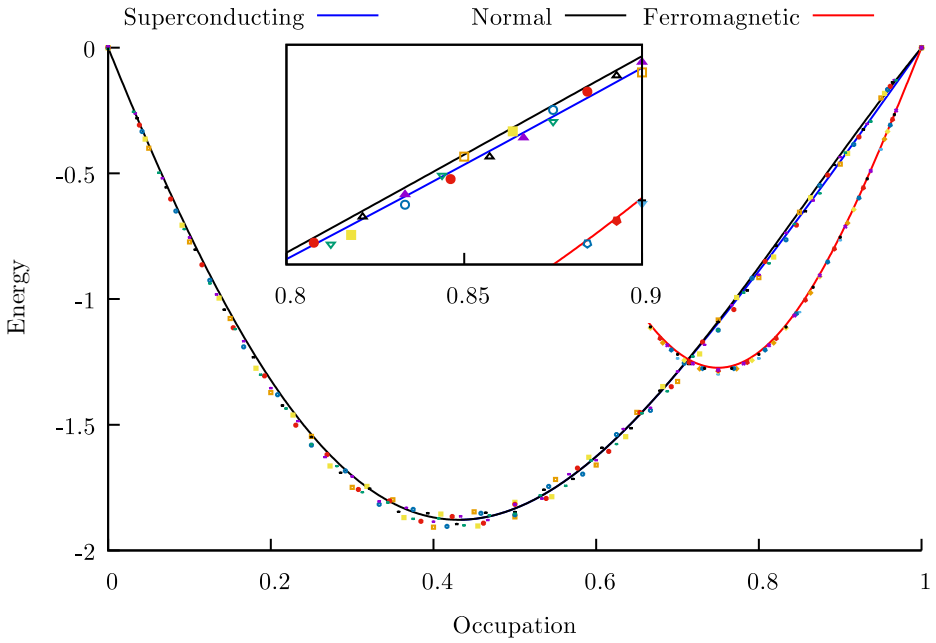

Energy per site per spin as a function of occupation, comparing mean field theory to diagonalisation of finite systems of size 10 to 14 with $t_0 = 0$ with $t_1 = 1$. There is competition between the subspaces i.e. the superconductivity and ferromagnetism do coexist.

Figure 11.3: Total Energy as a Function of Occupation $t_0 = 1$, $t_1 = 1$ — 1D

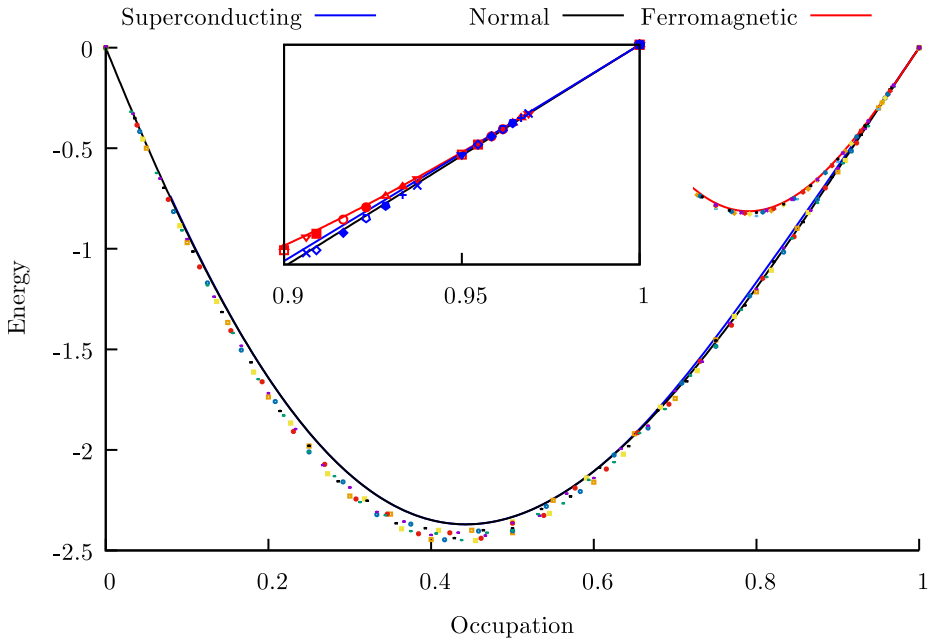

Energy per site per spin as a function of occupation, comparing mean field theory to diagonalisation of finite systems of size 10 to 14 with $t_0 = t_1$ with $t_1 = 1$. Superconductivity, paramagnetism, and ferromagnetism are competitive close to the Mott point, however superconductivity is the ground state of the system. As there is no competition between the subspaces, this is a pure example of a superconducting system.

Figure 11.4: Total Energy as a Function of Occupation $t_0 = -1$, $t_1 = 1$ — 1D

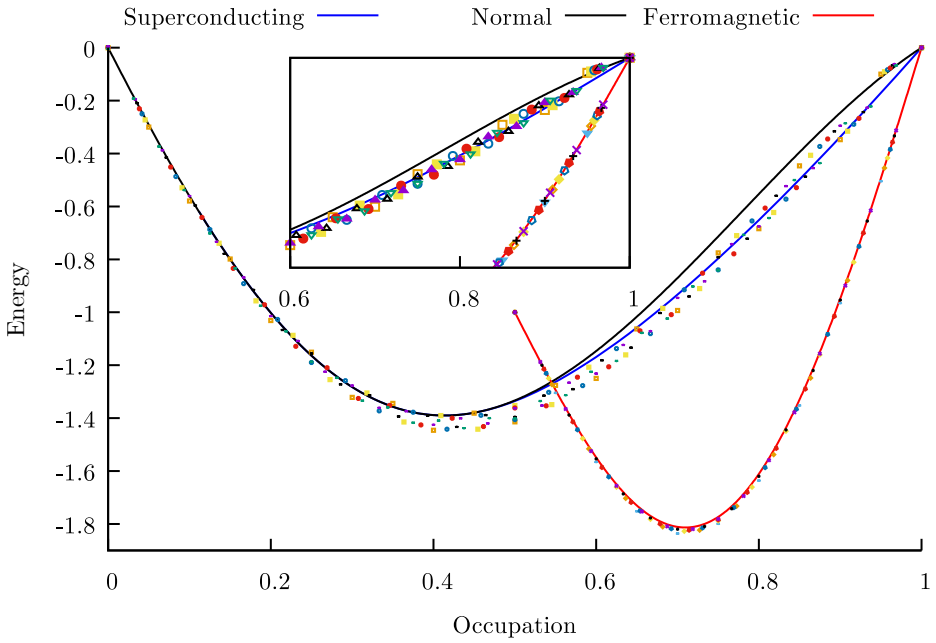

Energy per site per spin as a function of occupation, comparing mean field theory to diagonalisation of finite systems of size 10 to 14 with $t_0 = -t_1$ with $t_1 = 1$. Superconducting mean field theory, existing within the symmetric subspace, provides better agreement for diagonalisation results. Ferromagnetism is the phase within the anti-symmetric subspace and is energetically dominant over superconductivity.

11.3 Superconducting Correlations — Going Beyond Total Energy

The total energy is an extensive quantity and hence finite scales well with exact diagonalisation. Superconductivity has microscopic quantities associated with it. In this thesis we examine three such correlations: pair formation, occupation factor, and superconducting gap. For each quantity we compare the mean field prediction to exact diagonalisation and find good agreement.

11.3.1 Pair Formation

In superconductors pairs form more frequently than in an uncorrelated system [72]. In this subsection we examine the excess pairing given by

$$P = \frac{1}{N} \sum_i \left\langle \left(c^\dagger_{i\uparrow} c_{i\uparrow} - \left\langle c^\dagger_{i\uparrow} c_{i\uparrow} \right\rangle \right) \left(c^\dagger_{i\downarrow} c_{i\downarrow} - \left\langle c^\dagger_{i\downarrow} c_{i\downarrow} \right\rangle \right) \right\rangle , \tag{11.1}$$

where P counts the number of pairs in excess of uncorrelated. This is depicted in figure 11.5 on page 100 and shows that excess pairing, and therefore superconductivity, strengthens with the reduction of t_0. For low occupation the system is strongly correlated against pair formation as discussed in figure 8.1 on page 67. Mean field theory's failure for these types of systems is well known, and so the best it can do is be zero in this region. For higher occupation the system prefers pair formation, which agrees with the BCS superconducting solution. This is a local quantity and as a result finite size scales well.

Figure 11.5: Excess Pair Formation — 1D

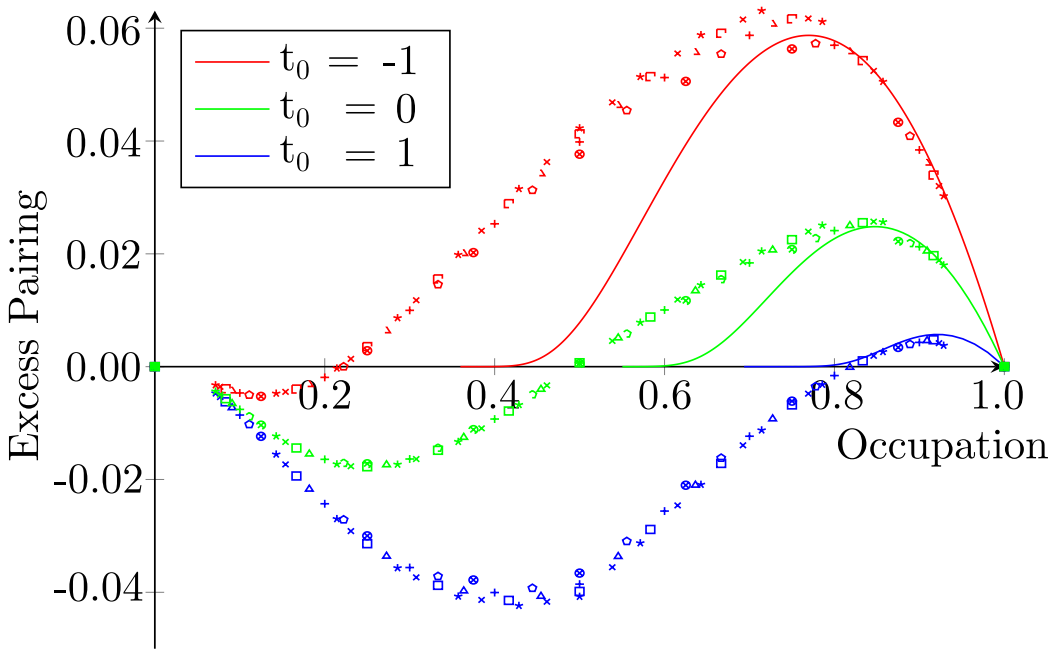

Excess pairing probability, P, against occupation for the 1D lattice with $t_1 = 1$ and varying t_0, comparing mean field theory to diagonalisation of a finite system of size 8 to 14. Mean field theory shows good agreement to diagonalisation results, where superconductivity exists close to the Mott point.

11.3.2 Occupation Factor

The occupation factor provides a measure to what degree a system is a Fermi liquid. If it is, then there will be a sharp discontinuity. In superconductors however, pairs form in a window around the Fermi surface. This distorts the Fermi discontinuity, making it continuous so that superconductivity can manifest.

For our system we have the original $s^\dagger_{i\sigma}$ operators to calculate the occupation factor. This is given by

$$n^S_k = \sum_\sigma \langle s^\dagger_{k\sigma} s_{k\sigma} \rangle, \tag{11.2}$$

which when Bloch transformed is equal to

$$n^S_k = \frac{1}{N} \sum_{jj'\sigma} e^{ik(j-j')} \langle s^\dagger_{j\sigma} s_{j'\sigma} \rangle, \tag{11.3}$$

$$= \sum_{j'\sigma} e^{-ikj'} \langle s^\dagger_{0\sigma} s_{j'\sigma} \rangle, \tag{11.4}$$

where we have used translational invariance in the final step. We then substitute the non-linear fermion transformation, however this needs to be done carefully. Our definitions of $s^\dagger_{i\sigma}$ are only true when the operators are off diagonal. When $j = j'$ we have

$$s^\dagger_{j\sigma} s_{j\sigma} = c^\dagger_{j\sigma} c_{j\sigma} - \frac{1}{2} c^\dagger_{j\sigma} c_{j\sigma} c^\dagger_{j\bar{\sigma}} c_{j\bar{\sigma}}. \tag{11.5}$$

Combined this gives

$$\begin{aligned} n^S_k = \sum_{j'\sigma} e^{-ikj'} \langle (1 - \eta c^\dagger_{0\bar{\sigma}} c_{0\bar{\sigma}}) c^\dagger_{0\sigma} c_{j'\sigma} (1 - \eta c^\dagger_{j'\bar{\sigma}} c_{j'\bar{\sigma}}) \rangle \\ - \langle (1 - \eta c^\dagger_{0\bar{\sigma}} c_{0\bar{\sigma}}) c^\dagger_{0\sigma} c_{0\sigma} (1 - \eta c^\dagger_{0\bar{\sigma}} c_{0\bar{\sigma}}) \rangle + \langle c^\dagger_{0\sigma} c_{0\sigma} \rangle - \frac{1}{2} \langle c^\dagger_{0\sigma} c_{0\sigma} \rangle \langle c^\dagger_{0\bar{\sigma}} c_{0\bar{\sigma}} \rangle \end{aligned} \tag{11.6}$$

$$= n_k (1 - \eta n_0)^2 - \eta^2 \frac{1}{4} \frac{1}{N^2} \sum_{k_1 k_2} n_{k_1} n_{k_2} n_{k+k_1+k_2} + (2\eta - \frac{1}{2}) n_0^2, \tag{11.7}$$

where $n_k = \sum_\sigma \langle c^\dagger_\sigma c_\sigma \rangle$. Figures 11.8 on page 104, 11.9 on page 105, 11.10 on page 106 depict the occupation factor for $t_0 = 1, -1, 0$ respectively for varying occupation. This

result also agrees with the existence of a superconducting phase. Note, that this analytical result gives access the renormalised Fermi liquid discontinuity Z. This is plotted in figures 11.6 on page 102 and 11.7 on page 103. We find that Z tends to $\frac{1}{2}$ close to the Mott point as is expected theoretically.

Figure 11.6: Fermi Liquid Discontinuity as a Function of Occupation

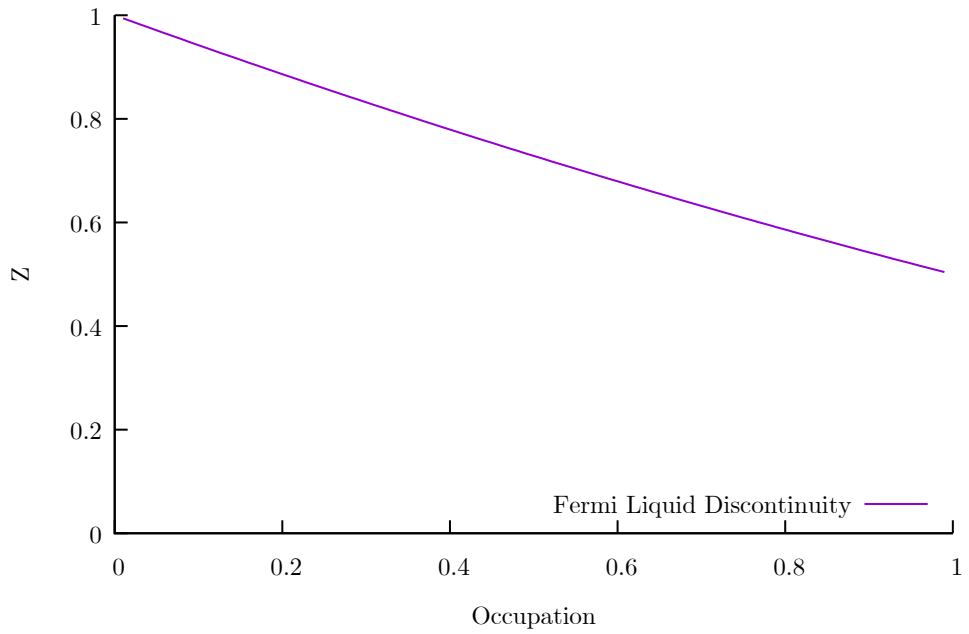

Renormalised Fermi liquid discontinuity as a function of occupation. At low occupation there is little interaction and hence is close to 1, whilst closer to the Mott point $Z \to 0.5$ as is theoretically expected.

Figure 11.7: Occupation Factor Analytical $t_0 = 1$

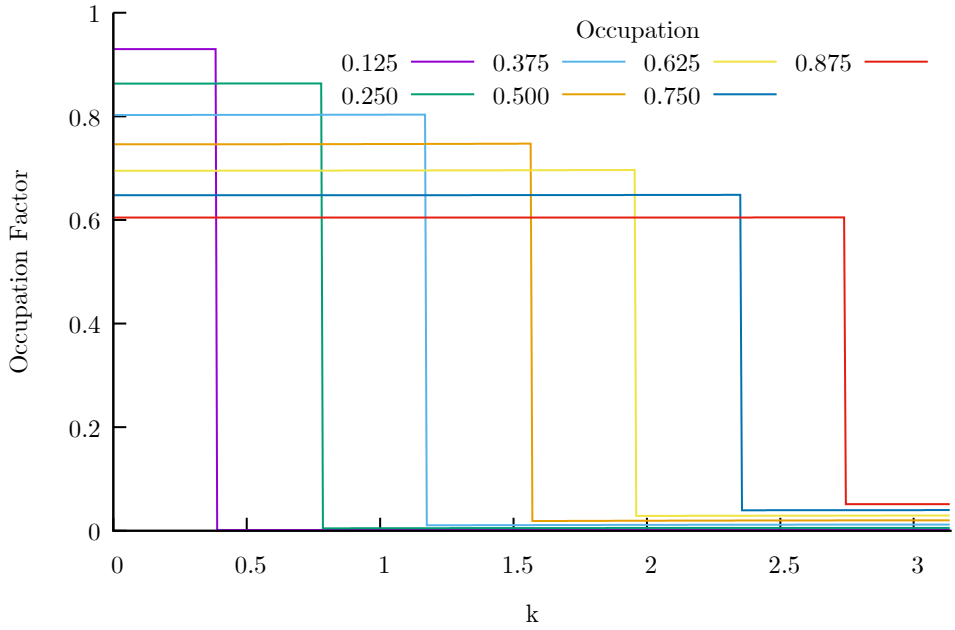

Analytical occupation factor n_k for $t_0 = 1$ and various occupation. In a perfect Fermi liquid $n_k = 1$ until $k = k_F$ then $n_k = 0$. In systems with interactions this discontinuity is renormalised which is called Z.

Figure 11.8: Occupation Factor Numerical $t_0 = 1$

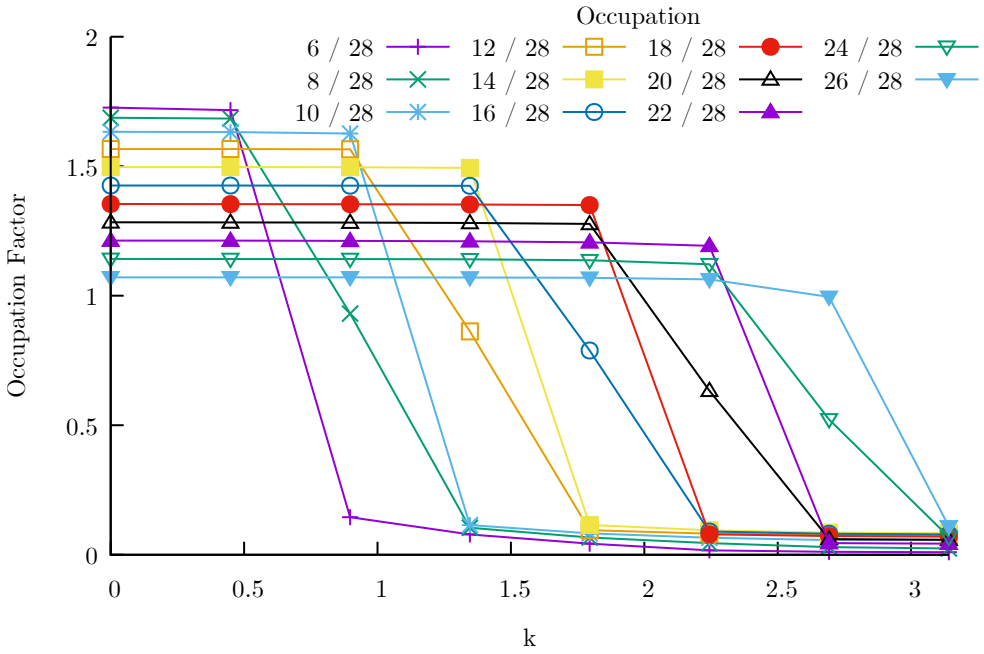

Numerical occupation factor n_k for $t_0 = 1$ and various occupation. If the system was a metal we'd expect constant n_k until k_F with a sharp drop to a lower constant. However we see that as the system exhibits superconductivity there is a 'softening' of the Fermi surface, as expected.

Figure 11.9: Occupation Factor Numerical $t_0 = -1$

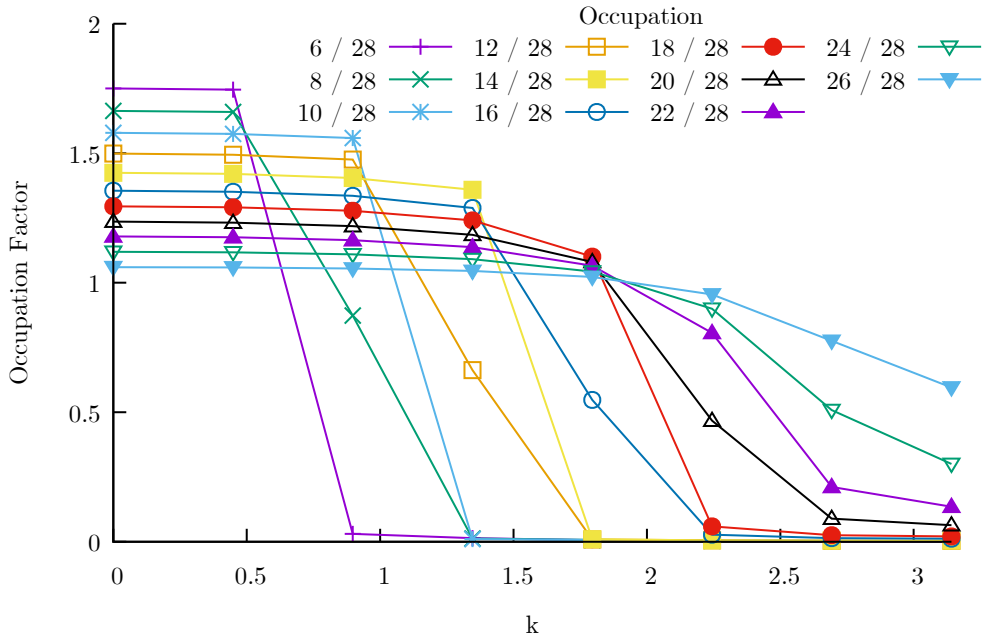

Numerical occupation factor n_k for $t_0 = -1$ and various occupation. If the system was a metal we'd expect constant n_k until k_F with a sharp drop to a lower constant. However we see that as the system exhibits superconductivity there is a 'softening' of the Fermi surface, as expected.

Figure 11.10: Occupation Factor $t_0 = 0$

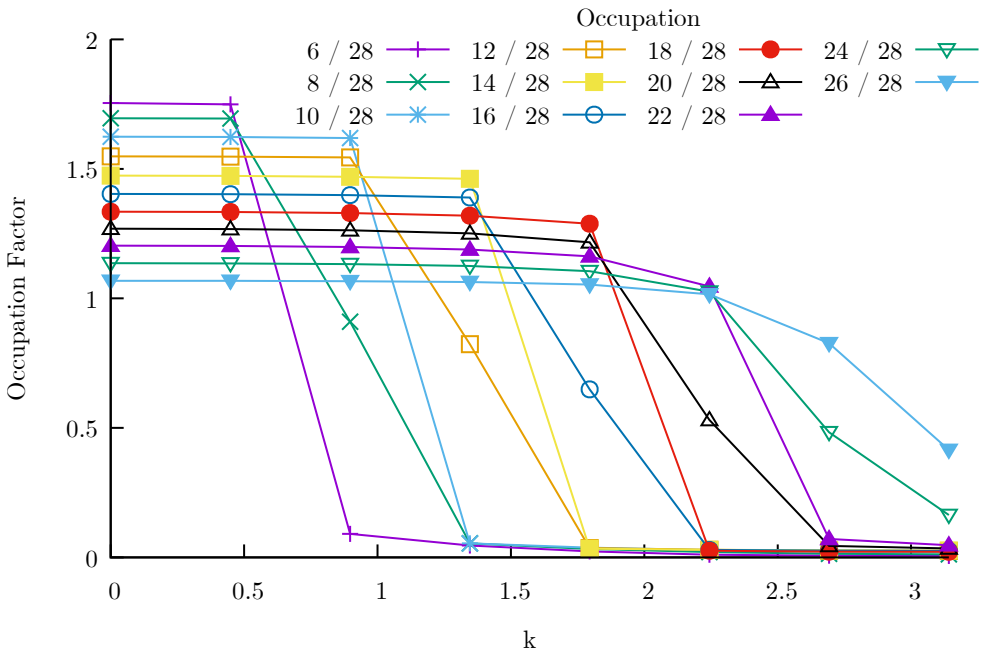

Numerical occupation factor n_k for $t_0 = 1$ and various occupation. If the system was a metal we'd expect $n_k = 1$ until k_F with a sharp drop to zero. However we see that as the system exhibits superconductivity there is a 'softening' of the Fermi surface, as expected.

11.3.3 Superconducting Gap

A cornerstone of superconductivity is the superconducting gap: the excess energy gained from pair formation. We calculate the gap from exact diagonalisation by comparing the energy difference for even and odd particles

$$\Delta_N = |E_{N-1} - 2E_N + E_{N+1}|. \tag{11.8}$$

This is depicted in figures 11.11 on page 108, 11.12 on page 109, and 11.13 on page 110. This is the most sensitive calculation of all in this thesis as the gap is global property of the system. It is incredibly sensitive to occupation and system size, and as a result we use finite size extrapolation to infer how an infinite system would behave. As each occupation ratio may only be attained with certain system sizes we are extrapolate with differing, but the maximal, number of points for each occupation. The gap has good agreement with the mean field solution. When the mean field results predicts no gap so does the extrapolation, the onset is approximately at the right point, and the size is of the correct order of magnitude. Finally, the Mott point agrees incredibly well and tends to the bound hole-pair state energy, showing the strength of the calculation at this point. Experimentally the superconducting transition temperature is directly related to the size of the gap. In our systems superconducting solutions occur close to $t_0 = 1$ (see Figure 11.13 on page 110) for which the gap ranges from 0 to 0.15eV. Therefore we find the transition temperature would be of order 100K, similar to those seen in experiments.

Figure 11.11: Superconducting Gap — 1D $t_0 = 1$

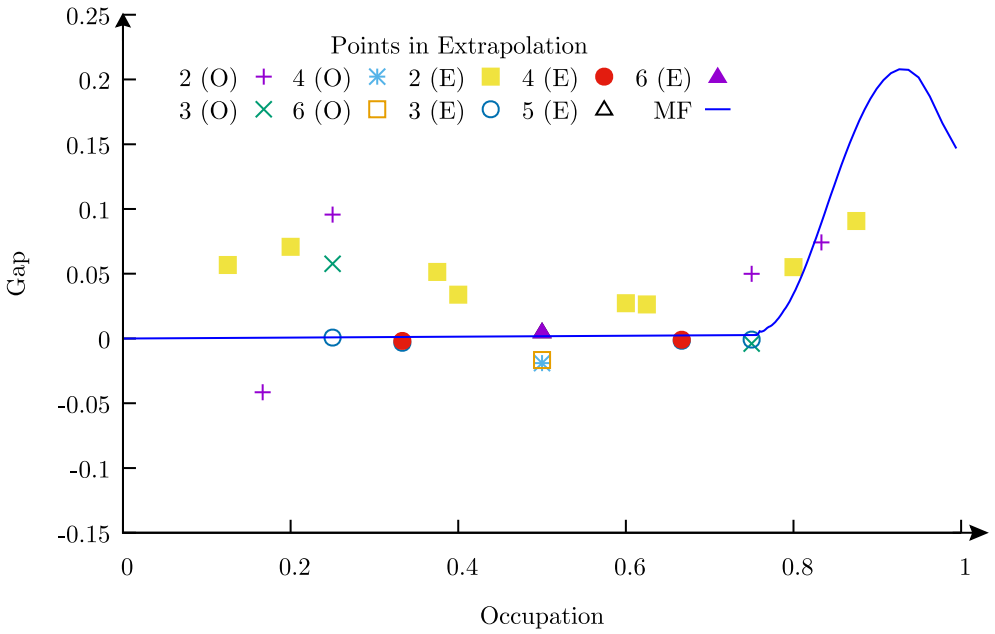

Superconducting gap as a function of occupancy, comparing mean field theory to polynomial extrapolation of diagonalisation of finite systems. The number of points we can extrapolate from is a function of occupation as certain ratios only occur for particular system sizes. O stands for odd system sizes, E for even system sizes, whilst straight lines are the mean field prediction.

Figure 11.12: Superconducting Gap — 1D $t_0 = 0$

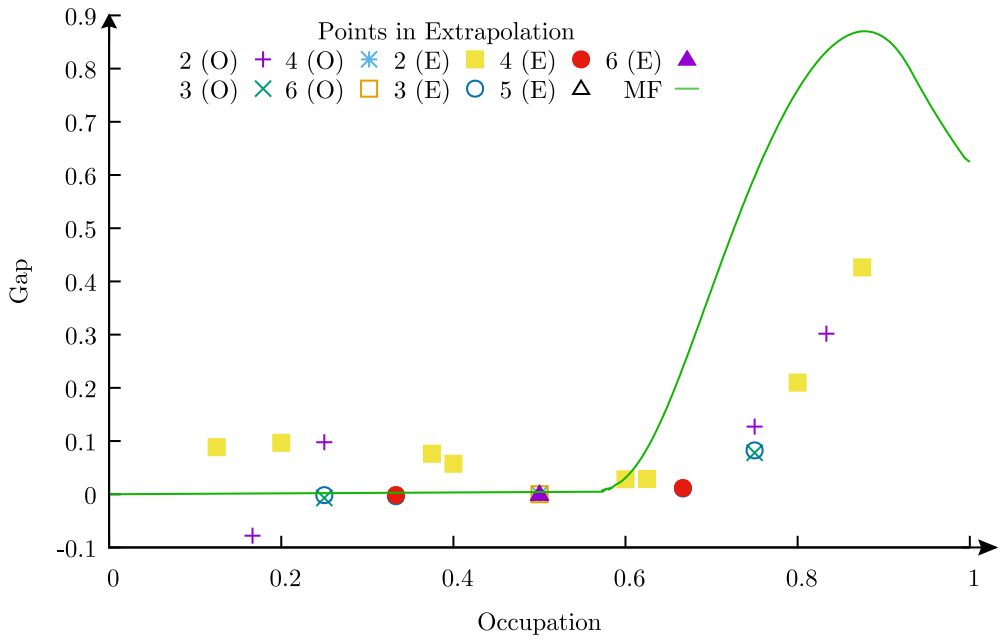

Superconducting gap as a function of occupancy, comparing mean field theory to polynomial extrapolation of diagonalisation of finite systems. The number of points we can extrapolate from is a function of occupation as certain ratios only occur for particular system sizes. O stands for odd system sizes, E for even system sizes, whilst straight lines are the mean field prediction.

Figure 11.13: Superconducting Gap — 1D $t_0 = -1$

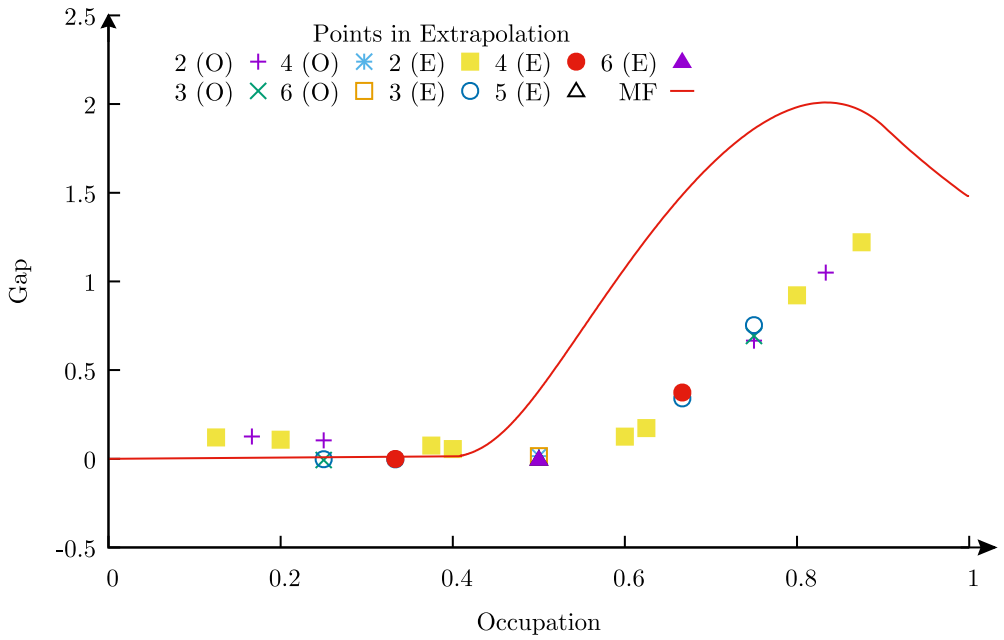

Superconducting gap as a function of occupancy, comparing mean field theory to polynomial extrapolation of diagonalisation of finite systems. The number of points we can extrapolate from is a function of occupation as certain ratios only occur for particular system sizes. O stands for odd system sizes, E for even system sizes, whilst straight lines are the mean field prediction.

In this section we showed total energy and correlation results for a one dimensional system. We know however that long range order is not permitted in one dimension but quasi-long range order is, which boasts qualitatively similar results. In the next section we extend these results to two dimensions for which long range order is permitted at zero temperature.

11.4 Extending Results to Two Dimensions

In this section we extend the previous results to the 2D square lattice. For the mean field theory this is trivially done by changing the structure factor in the calculations. Unfortunately, the exact diagonalisation is limited for two dimensions as the systems sizes are comparatively much smaller. Nevertheless we find good agreement, given the limitations.

Figures 11.14 on page 111, 11.15 on page 112, 11.16 on page 113, depict the total energy as a function of occupation for $t_0 = 0, 2$ and -2 respectively. Again t_0 controls the interplay between superconductivity, paramagnetism, and ferromagnetism. With fewer and proportionally smaller systems when compared to 1D the agreement of the numerics is less satisfactory than before. Nevertheless, systems which are strongly superconducting show good agreement with the numerics.

Figure 11.14: Total Energy as a Function of Occupation $t_0 = 0$, $t_1 = 1$ — 2D

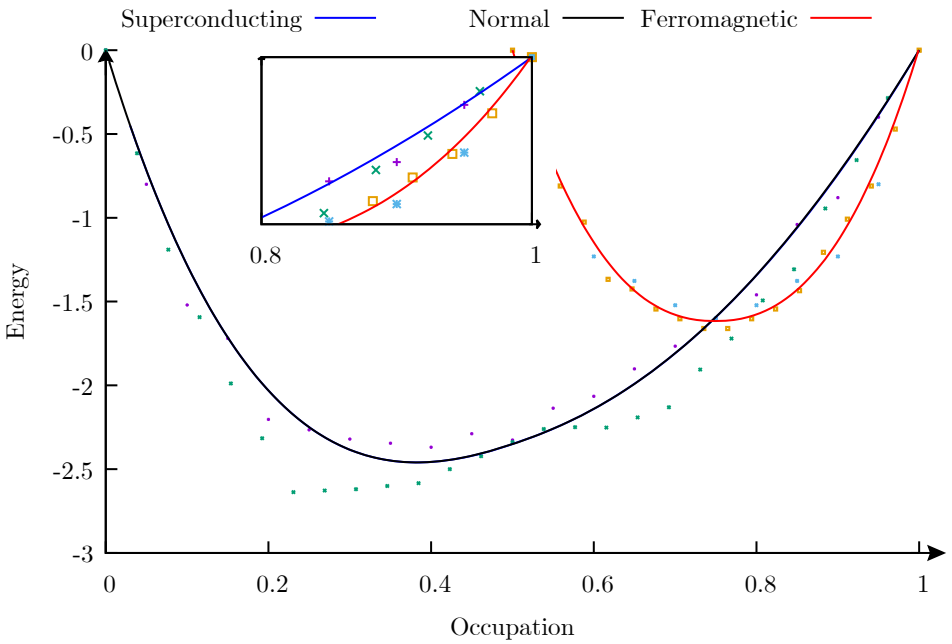

Energy per site as a function of occupation, comparing mean field theory to diagonalisation of a finite system of size 3×3 *and* 3×4 *with* $t_0 = 0$ *and* $t_1 = 1$. *There is competition between all the phases.*

Figure 11.15: Total Energy as a Function of Occupation $t_0 = 2$, $t_1 = 1$ — 2D

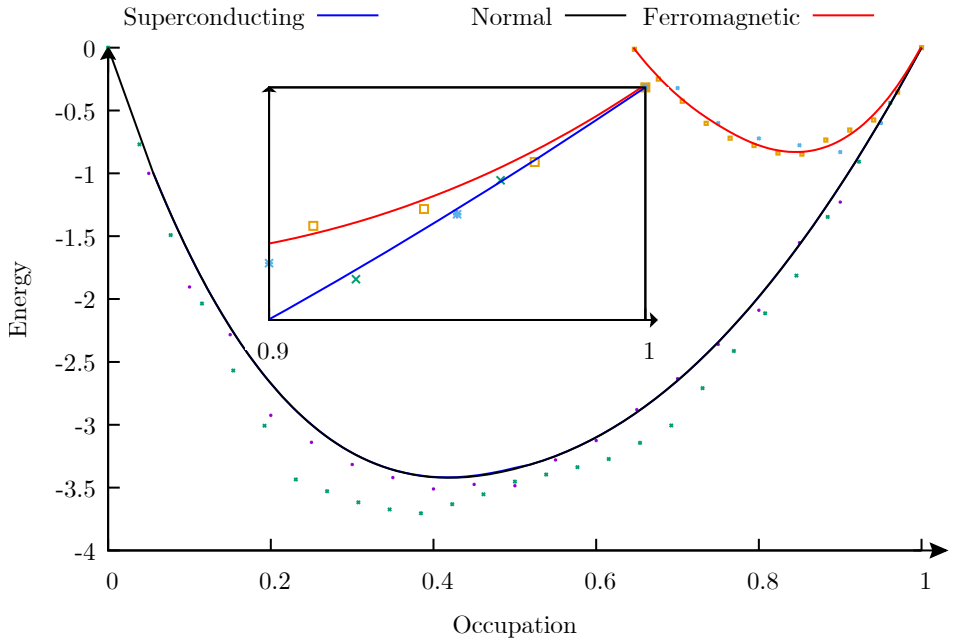

Energy per site as a function of occupation, comparing mean field theory to diagonalisation of a finite system of size 3×3 *and* 3×4 *with* $t_0 = 2$ *and* $t_1 = 1$. *Superconductivity is the favourable phase close to the Mott point where it competes with paramagnetism and ferromagnetism. This is an example of a 2D system which is superconducting.*

Figure 11.16: Total Energy as a Function of Occupation $t_0 = -2$, $t_1 = 1$ — 2D

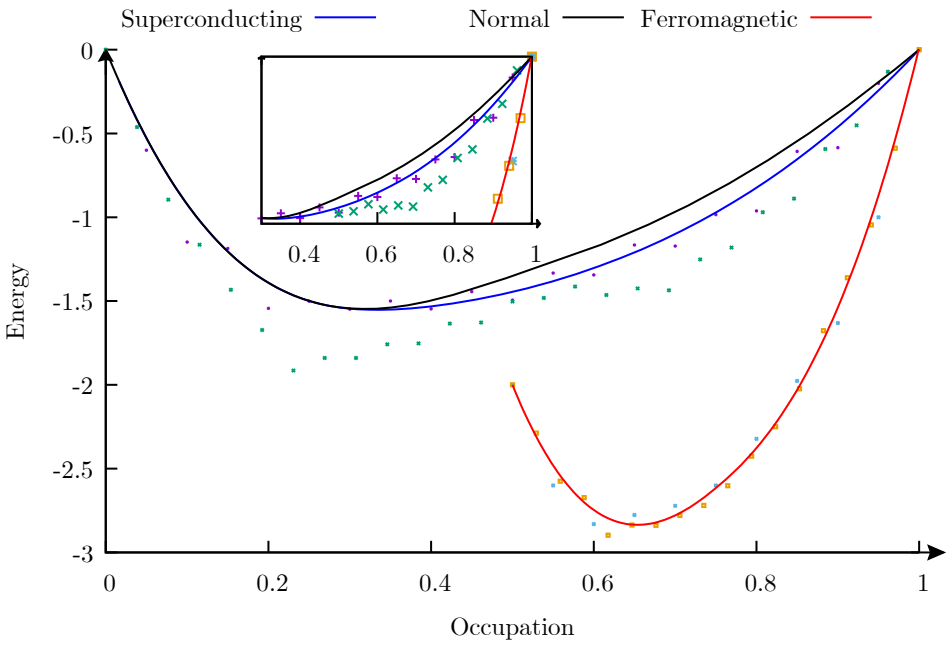

Energy per site as a function of occupation, comparing mean field theory to diagonalisation of a finite system of size 3×3 *and* 3×4 *with* $t_0 = -2$ *and* $t_1 = 1$. *Superconductivity has better agreement over paramagnetism, both existing within the symmetric subspace. The anti-symmetric subspace is ferromagnetic and energetically dominant in the region where superconductivity is prevalent, hence this system is not superconducting.*

Figures 11.18 on page 115 and 11.17 on page 114 depict the excess pair formation and superconducting gap for two dimensional systems. Again the pairing agrees well close to the Mott point, where the superconductivity exists. Additionally, as the superconducting gap calculation was the most sensitive numerical calculation in the previous section it is reasonable that it will not perform as well in 2D. We would only have two points to extrapolate from and this would definitely be unscientific.

In this chapter we presented results that rigorously demonstrated superconductivity in this model. We controlled the interplay between magnetism and superconductivity with t_0. When extending the calculation to two dimensions we found little qualitative difference. In the following chapter we will extend this calculation to finite Coulomb repulsion using perturbation theory.

Figure 11.17: Excess Pair Formation — 2D

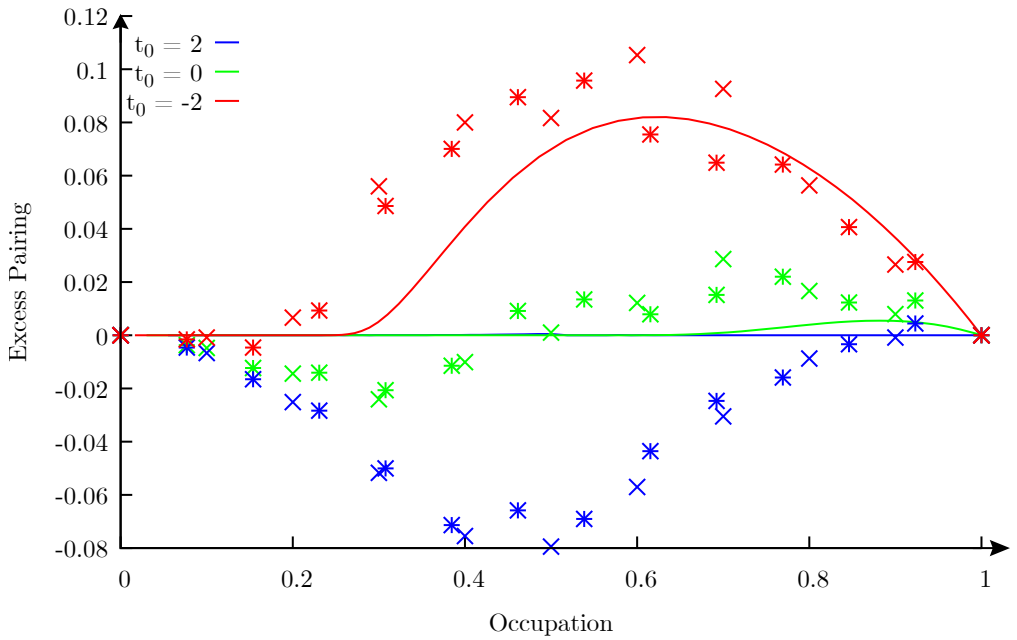

Excess pairing probability, P, against occupation for the 2D square lattice with $t_1 = 1$ *and varying* t_0*, comparing mean field theory to diagonalisation of a finite system of size* 3×3 *and* 3×4*. Mean field theory shows good agreement to diagonalisation results, where superconductivity exists close to the Mott point.*

Figure 11.18: Superconducting Gap — 2D

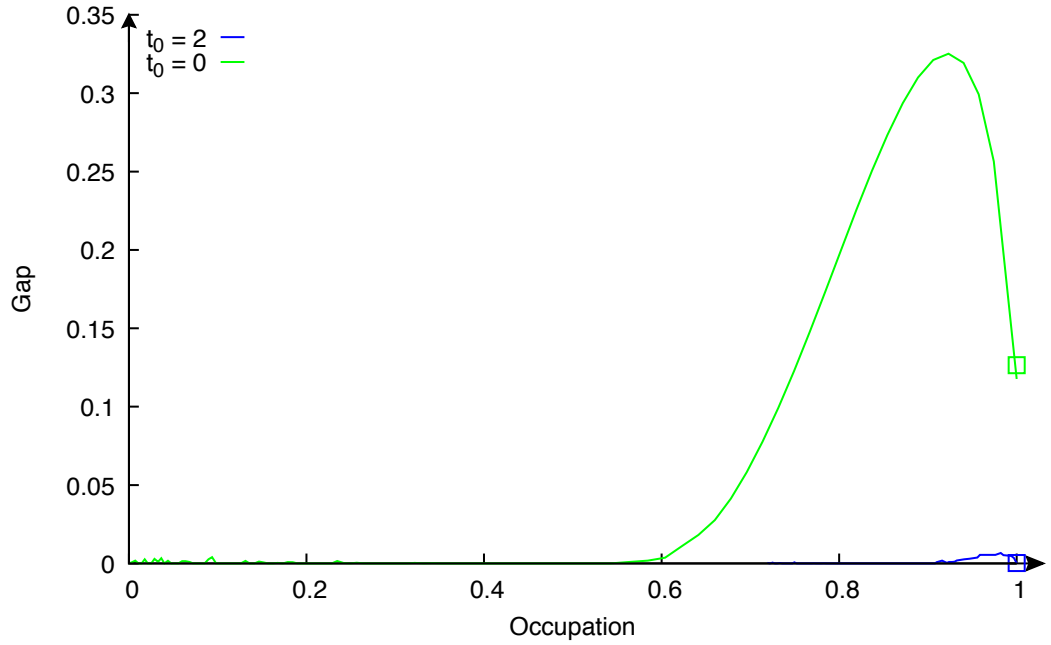

Superconducting gap, against occupation for the 2D square lattice with $t_1 = 1$ and varying t_0. We are unable to compare against finite sized diagonalisation as there is not enough data to finite size scale. However, the exact solution at the Mott point agrees well.

CHAPTER 12

PERTURBATION THEORY — HEISENBERG CORRECTIONS FROM LARGE BUT FINITE U

All prior work has focused on the $U = \infty$ limit. It could be argued that his limit was pathological, but it gave us access to exact results analytically and numerical simulations on larger systems. However in real materials U is not infinite, it is only large; for example, in the cuprates $U \approx 8t$ [73]. How can we reconcile this in our work? We will lift this limit perturbatively in the large U limit. This will be done using second order perturbation theory which gives Heisenberg corrections [74]. This is a standard technique and is detailed in appendix F.

In this chapter we will generate the Hamiltonian perturbatively for the symmetric-subspace and replicate the equivalent results from the previous chapter. We are not able to prove hole binding at the Mott point in this system. Instead we rely on mean-field and exact diagonalization.

Things are worse for the anti-symmetric subspace. Here virtual hopping is to states that are total spin zero. This reduces the total spin of the system resulting in a breakdown of the ferromagnet. Note that this occurs at high occupation and hence we expect a

Figure 12.1: Perturbative Hops Allowed

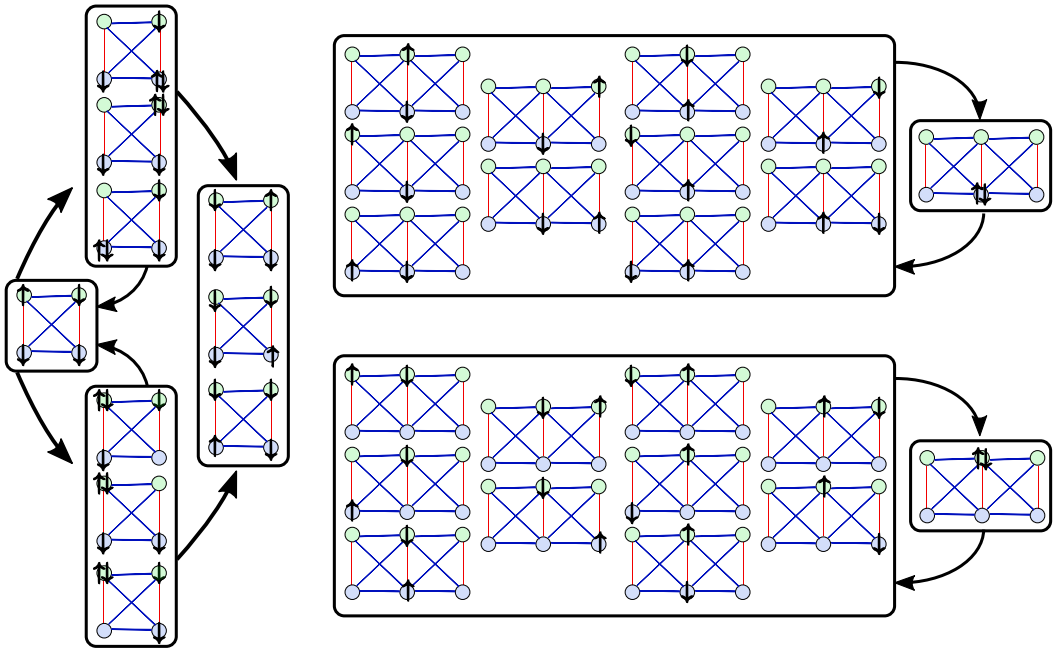

Diagrams of allowed hops in perturbative expansion. Arrows denote sequence of hops. Intermediate states pay on-site Coulomb penalty.

ferromagnetic to anti-ferromagnetic transition with doping. This is exactly what we see numerically. Analytically things are much more difficult as all 8 anti-symmetric states play a role, and as a result we do not have a manageable theory.

The first thing to do is calculate the Hamiltonian.

12.1 The Resulting Hamiltonian

This process is simple but algebraically taxing. As a result we simply present the result, and the general process is detailed in appendix F, with the allowed hops being depicted in figure 12.1 on page 118. The Hamiltonian becomes

$$H_S \to H_S - \frac{1}{U}\sum_j H_j^U, \tag{12.1}$$

where

$$H_j^U = \left[2t_0 c_{j\uparrow}^\dagger c_{j\downarrow}^\dagger + \sum_{n_2} \sqrt{2} t_1 \sum_{\langle jj_2\rangle_{n_2}} \left(s_{j_2\uparrow}^\dagger c_{j\downarrow}^\dagger + c_{j\uparrow}^\dagger s_{j_2\downarrow}^\dagger\right)\right] \times \left[2t_0 c_{j\downarrow} c_{j\uparrow} + \sum_{n_1} \sqrt{2} t_1 \sum_{\langle jj_1\rangle_{n_1}} (c_{j\downarrow} s_{j_1\uparrow} + s_{j_1\downarrow} c_{j\uparrow})\right], \quad (12.2)$$

where $\langle jj_1\rangle_{n_1}$ and $\langle jj_2\rangle_{n_2}$ denote the first and second neighbours of j. Repeating the mean field procedure yields the average energy

$$\begin{aligned}\bar{E}_{SC_U} = \bar{E}_{SC} - \frac{8{t_1}^2}{U}\Bigg[&\frac{1}{2}\Big[n_0(-({\delta_0}^2 + {\delta_1}^2)) + 2\delta_0\delta_1 n_1 - n_0({n_0}^2 - {n_1}^2)\Big] \\ &+ \Big[{\delta_1}^2 + {n_1}^2\Big]\Big[\eta^2(\delta_0 - \delta_2)^2 + (1 - \eta(n_0 - n_2))^2\Big] \\ &+ \eta^2\Big[\delta_0 - \delta_2\Big]^2\Big[1 - \eta(n_0 - n_2)\Big]\Big[{n_1}^2 - n_0 n_2\Big]\Big[2\delta_1\eta n_1(\delta_0 + \delta_2) - 2\delta_0\delta_2\eta n_0 \\ &+ ({\delta_1}^2 + n_0 n_2)(1 - \eta(n_0 - n_2)) + 2\eta {n_1}^2 n_2\Big] \\ &+ 2{\delta_1}^2 + {n_0}^2 + {n_1}^2\Bigg] - 8t_1\Bigg[n_1\Big[(1 - \eta n_0)^2 - \eta^2({\delta_0}^2 + {\delta_1}^2 + {n_1}^2)\Big] \\ - \frac{8\sqrt{2}t_0 t_1}{U}\Bigg[&- \eta\Big[-n_1({\delta_0}^2 + {\delta_1}^2) + 2\delta_0\delta_1 n_0 + n_1({n_0}^2 - {n_1}^2)\Big] + \delta_0\delta_1 + n_0 n_1\Bigg] \\ &- \frac{4{t_0}^2}{U}\Big[{\delta_0}^2 + {n_0}^2\Big] - 2t_0\Big[(1 - n_0)n_0 - {\delta_0}^2\Big], \quad (12.3)\end{aligned}$$

where $n_2 = \langle c_{j\sigma}^\dagger c_{\sigma j_2}\rangle$ and $\delta_2 = \langle \sigma c_{j\sigma}^\dagger c_{\bar{\sigma} j_2}^\dagger\rangle$ are now introduce. This is used to generate the self consistent parameters with the exact same procedure in chapter 10.

12.2 Modified Results

In this section we present the equivalent results from the previous chapter but with finite U. Figure 12.4 on page 123 demonstrates a case where the symmetric subspace is the true ground state. Again in this system superconductivity occurs close to the Mott point. In these results the perturbative expansion consistently produces an overestimate for the

energy gained due to virtual hopping. In principle this can be remedied by adding higher order terms such as t^3/U^2, but it is not done in this work.

For the symmetric subspace these fluctuations allow for energy to be gained, as is expected from similar $t - J$ models. The interesting thing however is that because we have dealt with the hopping exactly, we are not erroneously adding superconducting fluctuations. Whilst in the anti-symmetric subspace these fluctuations break the ferromagnet, and the resulting anti-ferromagnet does not gain that much energy while being localised close to the Mott point. Whilst we cannot analytically examine the anti-symmetric subspace, we can numerically study it.

The superconducting gap is calculated in the same way as previous calculations and is depicted in figures 12.5 on page 124, 12.6 on page 124, 12.7 on page 125. Again we are limited by system size for extrapolation, but the trend seems to agree well with the mean field data.

In this chapter we extended results to finite Coulomb repulsion using second order perturbation theory. The analysis was identical to previous chapters, but we were limited numerically by reduced system size. Nevertheless results showed good agreement. There was competition between paramagnetism, superconductivity, and anti-ferromagnetism which could be controlled by t_0. This model still exhibits superconductivity at finite U. In the next chapter we conclude the work done in this part.

Figure 12.2: Total Energy as a Function of Occupation $U = 10$, $t_0 = 0$, $t_1 = 1$ — Finite U

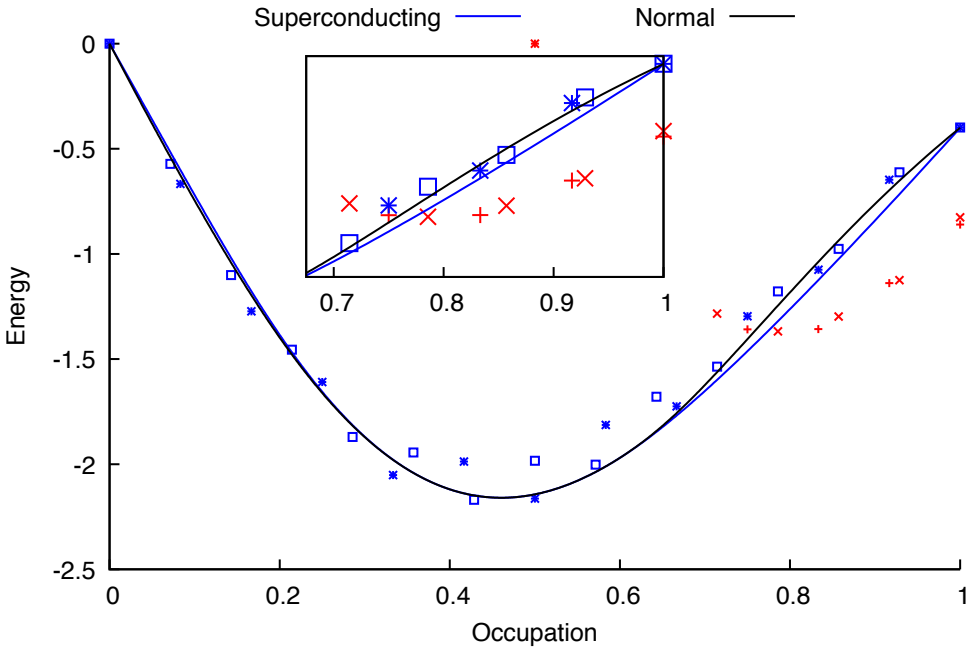

Energy per site as a function of occupation, comparing perturbative mean field theory to exact diagonalisation of finite systems of size 8 and 9 with $U = 10$, $t_0 = 0$ and $t_1 = 1$. The anti-symmetric subspace cannot be characterized, however there is a phase transition from ferromagnetism to anti-ferromagnetism close to the Mott point. Mean field theory has good agreement to the diagonalisation data, with superconductivity being favourable over paramagnetism but not the anti-symmetric subspace.

Figure 12.3: Total Energy as a Function of Occupation $U = 10$, $t_0 = -1$, $t_1 = 1$ — Finite U

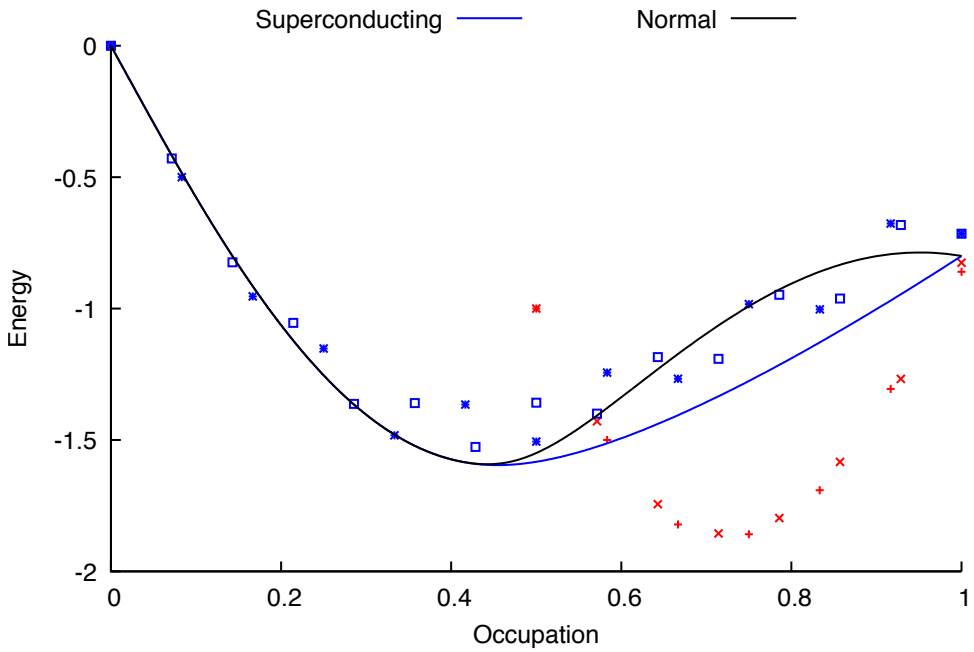

Energy per site as a function of occupation, comparing perturbative mean field theory to exact diagonalisation of finite systems of size 8 and 9 with $U = 10$, $t_0 = -1$ and $t_1 = 1$. The anti-symmetric subspace cannot be characterized, however there is a phase transition from ferromagnetism to anti-ferromagnetism close to the Mott point. This system is dominated by the anti-symmetric subspace.

Figure 12.4: Total Energy as a Function of Occupation $U = 10$, $t_0 = 1$, $t_1 = 1$ — Finite U

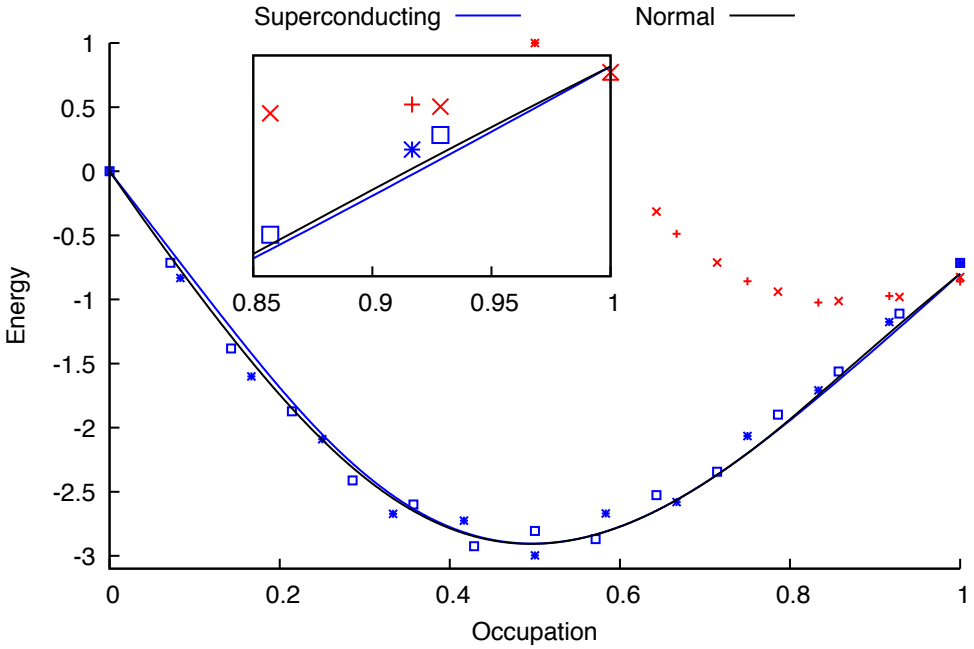

Energy per site as a function of occupation, comparing perturbative mean field theory to exact diagonalisation of a finite system of size 8 and 9 with $U = 10$, $t_0 = 1$ and $t_1 = 1$. Superconductivity is the favoured phase, close to the Mott point, while competing with anti-ferromagnetism (from the anti-symmetric subspace) and paramagnetism (from the symmetric subspace).

Figure 12.5: Superconducting Gap as a Function of Occupation — Finite U $t_0 = 1$

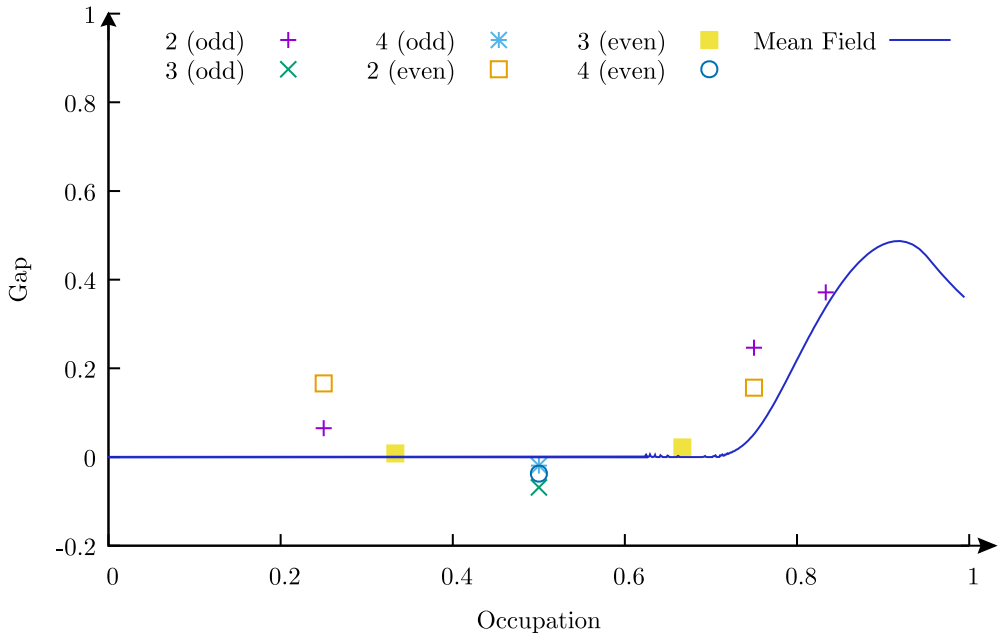

Superconducting gap of a system with $U = 10$, and $t_0 = 1$. We only have access to smaller systems and hence have limited finite sized scaling. Despite this there is still good agreement.

Figure 12.6: Superconducting Gap as a Function of Occupation — Finite U $t_0 = 0$

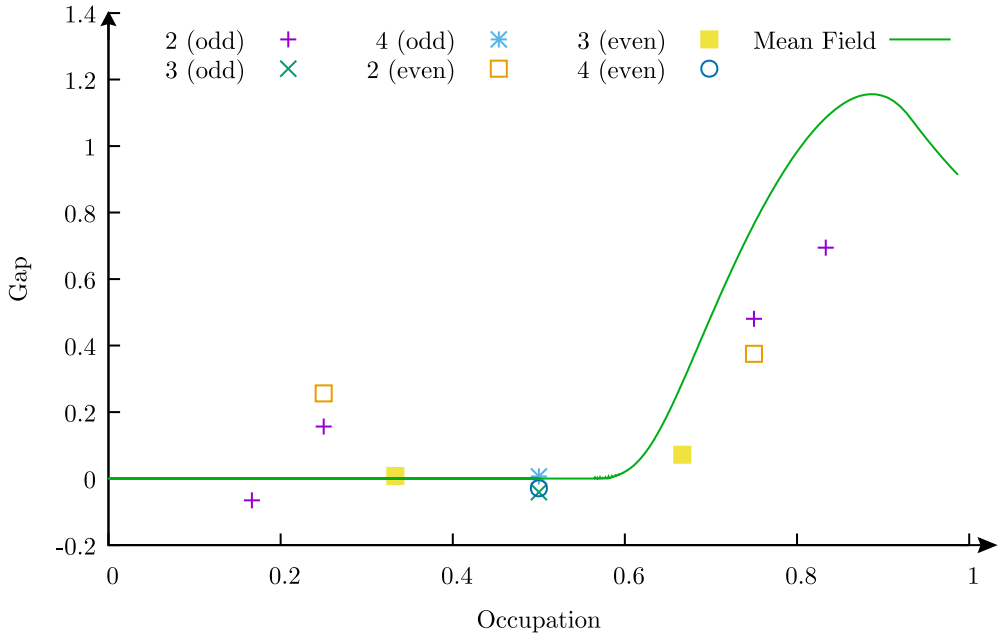

Superconducting gap of a system with $U = 10$, and $t_0 = 0$. We only have access to smaller systems and hence have limited finite sized scaling. Despite this there is still good agreement.

Figure 12.7: Superconducting Gap as a Function of Occupation — Finite U $t_0 = -1$

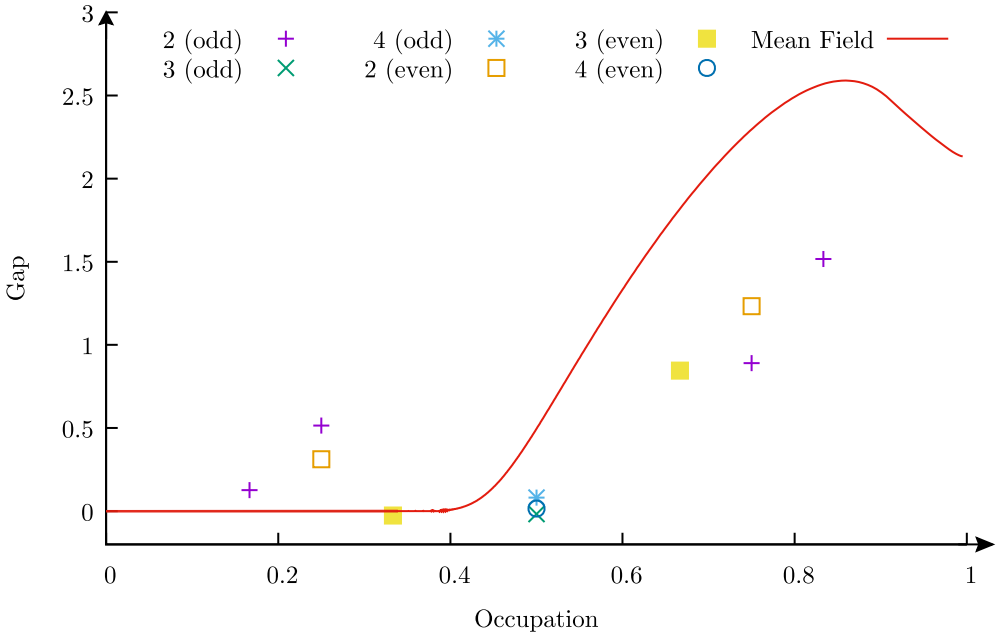

Superconducting gap of a system with $U = 10$, and $t_0 = -1$. We only have access to smaller systems and hence have limited finite sized scaling. Despite this there is still good agreement.

CHAPTER 13

SUMMARY

We have rigorously demonstrated that this repulsive Hubbard model exhibits pairing and presumably superconductivity. We began with an ordinary Hubbard model with a collection of local symmetries. These were extracted resulting in two subspaces, symmetric and anti-symmetric. We then took the physically motivated limit of divergent Coulomb exactly. This reduced the state space, simplifying the problem further, and showed the anti-symmetric subspace is ferromagnetic. We exactly showed that two holes at the Mott point bind, which formed the basis of a BCS mean field solution. The mean field results of total energy, excess pairing, and the superconducting gap showed good agreement with exact diagonalisation. Finally we extended our results to finite but large U using perturbation theory. This opened up an anti-ferromagnetic phase in the anti-symmetric subspace at the Mott point as the ferromagnetism cannot gain from the Heisenberg corrections.. Our model manifests the phase diagram of the cuprates, as seen in figure 13.1 on page 129.

We are left asking whether this toy model contains the core physics behind unconventional superconductivity. Possibly this model is to unconventional superconductivity as the Ising model is to magnetism. Is the physics of the cuprates Anderson's resonating valence bond theory? For our model, the ground state at the Mott point is a valence bond solid, a more controlled version of the former. Anderson hypothesises that upon doping

these valence bonds will gain kinetic energy, condense and superconduct. This is exactly what occurs in our model.

Our model also shines light on the interplay between magnetism and superconductivity. There are theories stating that magnetic excitations couple electrons in the same manner as phonons in conventional superconductors. However, in our model magnetism and superconductivity occur in different symmetry protected subspaces. They do not talk to each other.

What about the more interesting phases such as the pseudogap and strange metal? The analysis in this thesis is at zero temperature, and as a result we cannot comment if these exotic phases are encapsulated in our model. This could possibly be an extension for further work.

The final comment is that of particle-hole asymmetry. Our model is *not* particle-hole symmetric. In the cuprates there is only qualitative symmetry between particles and holes in the phase diagram. Though both can be broadly described as *'strong anti-ferromagnets at the Mott point which die and give rise to superconductivity upon doping'*, it is a fact that there is quantitative asymmetry. In the hole doped cuprates superconductivity occurs sooner and is stronger than in the particle doped case. This cannot be examined with the techniques we have used. There is debate on whether the hole doped cuprates are described by a three band Hubbard model or a single band model. Until we can deal with both sides of the Mott point with the same level of rigour, our work cannot comment on this debate.

Figure 13.1: Schematic Phase Diagram of All Systems Considered

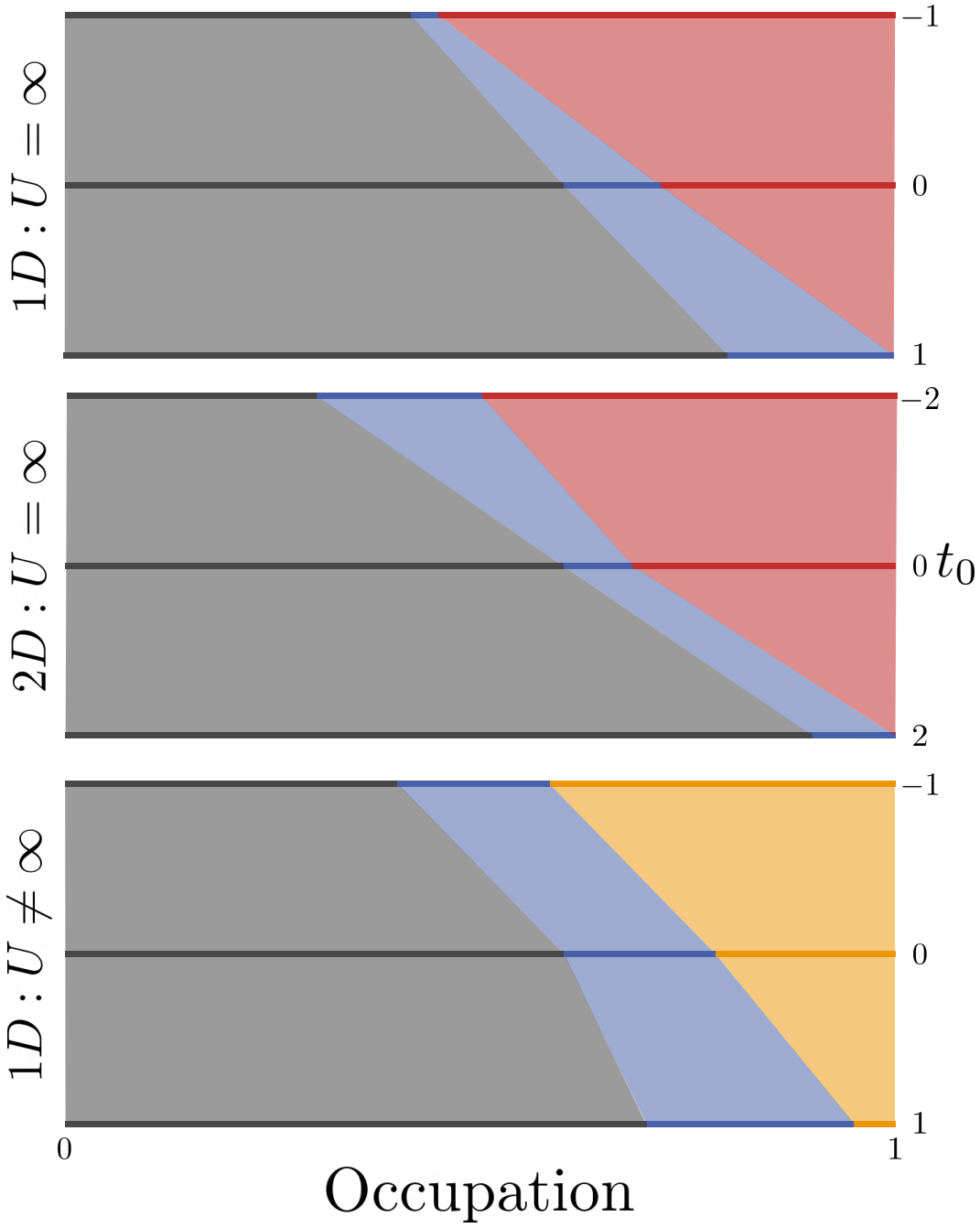

Phase diagrams for the three systems we consider in this thesis: 1D chain with $U = \infty$, 2D square lattice with $U = \infty$, and 1D chain with $U = 10$. In these diagrams the grey region is normal, blue is superconducting, red is ferromagnetic, and amber is anti-ferromagnetic. For each of the systems we have calculated three values of t_0, the intermediate regions are linear interpolations and a guide to the eye.

Part III

Self-Consistent Distribution Theory — Dealing With Finite U With Remarkable Accuracy

CHAPTER 14

INTRODUCTION

Most non-trivial problems do not yet have exact solutions. For this reason the community relies on computational and perturbative techniques. Unfortunately, accurate computational methods are often expensive in both time and memory [75] and hence are limited to small systems. A state of the art technique in strongly interacting problems is perturbation theory. Take the Hubbard model

$$H = -t \sum_{\langle ij \rangle \sigma} c^\dagger_{i\sigma} c_{j\sigma} + U \sum_i c^\dagger_{i\uparrow} c_{i\uparrow} c^\dagger_{i\downarrow} c_{i\downarrow}. \tag{14.1}$$

One can tackle this model in the limit $U = \infty$ or in the limit $U = 0$, and then U or U^{-1} can be reintroduced perturbatively. This is a *limited* process. The perturbations are only valid in the vicinity of the limit and breakdown rather quickly. Currently there are two ways to deal with this: either stay in the region of validity, or add higher order corrections to our perturbation scheme. Neither of these options are ideal.

In principle non-perturbative techniques could do wonders here, but they are few and far between. We will present a self-consistent, non-perturbative method which provides remarkably accurate results.

In this part we will formulate and implement the technique. The core principle is rather simple. If we use a non-orthogonal operator, defined by a distribution over the lattice, would this encapsulate the long range perturbative corrections? The answer is

yes.

We begin with the Hubbard model from the previous part for which the focus was predominantly on the limit $U = \infty$, and we only examined finite U perturbatively. In this part we will examine the finite U limit using a non-perturbative approach. In physical systems a lot of interesting physics occurs at the Mott point, including but not limited to high temperature superconductivity, spin glasses, and anti-ferromagnetism [76]. For this reason we begin our analysis at the Mott point in section 15.2 and enforce certain symmetry properties. This defines a new non-orthogonal operator which is key within the method for this part. This method, which is discussed in section 15.3, is simple though algebraically tedious. Due to certain properties of the Mott point, the two operator ($s^\dagger_{i\sigma}$ and $a^\dagger_{i\sigma}$) species system can be exactly mapped onto a single operator system. The new non-orthogonal prescription describes fluctuations which the original does not, these are then taken into account. At this point paramagnetic averages are taken in order to create a single particle picture. Finally appropriate commutators are calculated to describe the dispersion for adding and subtracting a particle. With this description we find that the occupation factor is not set, *it is solved for*. This allows us to examine the Fermi-liquid discontinuity which is discussed in section 15.5, along with results and supporting numerical work.

CHAPTER 15

SOLVING THE PROBLEM AT THE MOTT POINT

New procedures require precision and control. For this reason we begin by solving the problem at the Mott point. Control here comes from the fact that, in our system, at $U = \infty$ the Mott state is known *exactly*. From this we can generate an intelligent ansatz for our non-orthogonal operators. In our case these will be a weighted distribution of the original operators over the lattice.

In this chapter we will formulate and apply the theory to our model. In the first section we will map the Hamiltonian to a pseudospin Hamiltonian exactly. This prescription dramatically simplifies the problem. In the following section we examine the state at the Mott point. Here we will extract the local symmetry. Before taking a journey through arduous algebra we will detail the method, which is conceptually surprisingly simple. In the final section we will present the fruits of our labour, the results, and highlight their remarkable accuracy.

15.1 Exact Mapping to a Pseudospin Hamiltonian

In this section we will map the original Hamiltonian to a pseudospin model exactly. This is a rather trivial process and only requires noticing the structure of the basis states. We

will find that the symmetric and anti-symmetric subspaces (recall $t_{i\sigma} \leftrightarrow b_{i\sigma}$) have the same structure except for one small difference. The benefit of doing this will become clear in section 15.3 but for now can be summarised as 'equivalence principles'.

To recap, the original Hamiltonian is given by

$$H = -t_1 \sum_{\langle ij\rangle\sigma} \Big[t^\dagger_{i\sigma}+b^\dagger_{i\sigma}\Big]\Big[t_{j\sigma}+b_{j\sigma}\Big] - t_0 \sum_{i\sigma} \Big[t^\dagger_{i\sigma}b_{i\sigma}+b^\dagger_{i\sigma}t_{i\sigma}\Big] + U\sum_j \Big[t^\dagger_{j\uparrow}t_{j\uparrow}t^\dagger_{j\downarrow}t_{j\downarrow}+b^\dagger_{j\uparrow}b_{j\uparrow}b^\dagger_{j\downarrow}b_{j\downarrow}\Big], \tag{15.1}$$

which has a local symmetry $t_{i\sigma} \leftrightarrow b_{i\sigma}$ allowing the Hamiltonian to be recast using the operators

$$s_{j\sigma} = \frac{1}{\sqrt{2}}\Big[t_{j\sigma} + b_{j\sigma}\Big], \quad a_{j\sigma} = \frac{1}{\sqrt{2}}\Big[t_{j\sigma} - b_{j\sigma}\Big], \tag{15.2}$$

giving

$$\begin{aligned} H = &-2t_1 \sum_{\langle ij\rangle\sigma} s^\dagger_{i\sigma}s_{j\sigma} - t_0 \sum_{i\sigma}\Big[s^\dagger_{i\sigma}s_{i\sigma} - a^\dagger_{i\sigma}a_{i\sigma}\Big] \\ &+ \frac{U}{2}\sum_j \Bigg[\Big[s^\dagger_{j\uparrow}s^\dagger_{j\downarrow} + a^\dagger_{j\uparrow}a^\dagger_{j\downarrow}\Big]\Big[s_{j\downarrow}s_{j\uparrow} + a_{j\downarrow}a_{j\uparrow}\Big] + \Big[s^\dagger_{j\uparrow}a^\dagger_{j\downarrow} - s^\dagger_{j\downarrow}a^\dagger_{j\uparrow}\Big]\Big[a_{j\downarrow}s_{j\uparrow} - a_{j\uparrow}s_{j\downarrow}\Big]\Bigg]. \end{aligned} \tag{15.3}$$

There are 16 basis states, 8 of which are symmetric under the transformation and are given by

$$|0\rangle, \quad s^\dagger_{j\uparrow}|0\rangle, \quad s^\dagger_{j\downarrow}|0\rangle, \quad s^\dagger_{j\uparrow}s^\dagger_{j\downarrow}|0\rangle, \tag{15.4}$$

$$a^\dagger_{j\uparrow}a^\dagger_{j\downarrow}|0\rangle, \quad s^\dagger_{j\uparrow}a^\dagger_{j\uparrow}a^\dagger_{j\downarrow}|0\rangle, \quad s^\dagger_{j\downarrow}a^\dagger_{j\uparrow}a^\dagger_{j\downarrow}|0\rangle, \quad s^\dagger_{j\uparrow}s^\dagger_{j\downarrow}a^\dagger_{j\uparrow}a^\dagger_{j\downarrow}|0\rangle, \tag{15.5}$$

and 8 are anti-symmetric under the transformation and are given by

$$a^\dagger_{j\uparrow}|0\rangle, \quad s^\dagger_{j\uparrow}a^\dagger_{j\uparrow}|0\rangle, \quad s^\dagger_{j\downarrow}a^\dagger_{j\uparrow}|0\rangle, \quad s^\dagger_{j\uparrow}s^\dagger_{j\downarrow}a^\dagger_{j\uparrow}|0\rangle, \tag{15.6}$$

$$a^\dagger_{j\downarrow}|0\rangle, \quad s^\dagger_{j\uparrow}a^\dagger_{j\downarrow}|0\rangle, \quad s^\dagger_{j\downarrow}a^\dagger_{j\downarrow}|0\rangle, \quad s^\dagger_{j\uparrow}s^\dagger_{j\downarrow}a^\dagger_{j\downarrow}|0\rangle. \tag{15.7}$$

We can map the 16 basis states onto pseudo and real spin for the symmetric and anti-

symmetric states respectively. Note that half of the symmetric basis states are occupied by $a^\dagger_\uparrow a^\dagger_\downarrow$ while the other half are not. These form our pseudospin, given by $|\downarrow_S\rangle = |0\rangle$ and $|\uparrow_S\rangle = a^\dagger_{j\uparrow} a^\dagger_{j\downarrow} |0\rangle$. For the anti-symmetric basis states the spin is real, given by $|\uparrow_A\rangle = a^\dagger_{j\uparrow}$ and $|\downarrow_A\rangle = a^\dagger_{j\downarrow}$. Half of the anti-symmetric basis states are occupied by $a^\dagger_\uparrow$ and the other half by $a^\dagger_\downarrow$. This allows us to recast the states to

$$|\tau_\alpha\rangle\,, \quad s^\dagger_{j\uparrow}|\tau_\alpha\rangle\,, \quad s^\dagger_{j\downarrow}|\tau_\alpha\rangle\,, \quad s^\dagger_{j\uparrow}s^\dagger_{j\downarrow}|\tau_\alpha\rangle\,, \tag{15.8}$$

where in the symmetric subspace $|\tau_\alpha\rangle$ is a pseudospin and in the anti-symmetric subspace is a real spin. This is expressed by $|\downarrow_S\rangle = |0\rangle$, $|\uparrow_S\rangle = a^\dagger_{j\uparrow} a^\dagger_{j\downarrow} |0\rangle$, $|\uparrow_A\rangle = a^\dagger_{j\uparrow}$, and $|\downarrow_A\rangle = a^\dagger_{j\downarrow}$.

In this part of the thesis we are focused on the symmetric subspace: states which are occupied by a symmetric basis state on each site. For the symmetric subspace we can replace any $a_{j\sigma}$ dependence with the following pseudospin operators. Note, for the A^Z operator we have three operations which produce the same result, and hence are equivalent in the pseudospin language:

$$A^+_j \equiv a^\dagger_{j\uparrow} a^\dagger_{j\downarrow}, \tag{15.9}$$

$$A^-_j \equiv a_{j\downarrow} a_{j\uparrow}, \tag{15.10}$$

$$\frac{1}{2} + A^Z_j \equiv \begin{cases} a^\dagger_{j\uparrow} a_{j\uparrow} a^\dagger_{j\downarrow} a_{j\downarrow}, \\ a^\dagger_{j\uparrow} a_{j\uparrow}, \\ a^\dagger_{j\downarrow} a_{j\downarrow}, \end{cases} \tag{15.11}$$

where the final equivalence is true as $a^\dagger_{j\sigma}$ only occurs in pairs in the symmetric space. Explicitly we can see this as

$$A^+_j |\uparrow_S\rangle \equiv a^\dagger_{j\uparrow} a^\dagger_{j\downarrow} a^\dagger_{j\uparrow} a^\dagger_{j\downarrow} |0\rangle = 0, \quad A^+_j |\downarrow_S\rangle \equiv a^\dagger_{j\uparrow} a^\dagger_{j\downarrow} |0\rangle \equiv |\uparrow_S\rangle\,, \tag{15.12}$$

$$A^-_j |\uparrow_S\rangle \equiv a_{j\downarrow} a_{j\uparrow} a^\dagger_{j\uparrow} a^\dagger_{j\downarrow} |0\rangle = |0\rangle \equiv |\downarrow_S\rangle\,, \quad A^-_j |\downarrow_S\rangle \equiv a_{j\downarrow} a_{j\uparrow} |0\rangle = |0\rangle \tag{15.13}$$

$$\left[\frac{1}{2}+A_j^Z\right]|\uparrow_S\rangle \equiv \left\{\begin{array}{c} a_{j\uparrow}^\dagger a_{j\uparrow} a_{j\downarrow}^\dagger a_{j\downarrow} a_{j\uparrow}^\dagger a_{j\downarrow}^\dagger |0\rangle \\ a_{j\uparrow}^\dagger a_{j\uparrow} a_{j\uparrow}^\dagger a_{j\downarrow}^\dagger |0\rangle \\ a_{j\downarrow}^\dagger a_{j\downarrow} a_{j\uparrow}^\dagger a_{j\downarrow}^\dagger |0\rangle \end{array}\right\} = a_{j\uparrow}^\dagger a_{j\downarrow}^\dagger |0\rangle \equiv \left[\frac{1}{2}+\frac{1}{2}\right]|\uparrow_S\rangle \tag{15.14}$$

$$\left[\frac{1}{2}+A_j^Z\right]|\downarrow_S\rangle \equiv \left\{\begin{array}{c} a_{j\uparrow}^\dagger a_{j\uparrow} a_{j\downarrow}^\dagger a_{j\downarrow} |0\rangle \\ a_{j\uparrow}^\dagger a_{j\uparrow} |0\rangle \\ a_{j\downarrow}^\dagger a_{j\downarrow} |0\rangle \end{array}\right\} = 0 \equiv \left[\frac{1}{2}-\frac{1}{2}\right]|\downarrow_S\rangle \tag{15.15}$$

Upon direct substitution we get

$$H_S = -2t\sum_{\langle ij\rangle\sigma} s_{i\sigma}^\dagger s_{j\sigma} + \frac{U}{2}\sum_j \Bigg[s_{j\uparrow}^\dagger s_{j\uparrow} s_{j\downarrow}^\dagger s_{j\downarrow} + s_{j\uparrow}^\dagger s_{j\downarrow}^\dagger A_j^- + s_{j\downarrow} s_{j\uparrow} A_j^+ + \left[1 + s_{j\uparrow}^\dagger s_{j\uparrow} + s_{j\downarrow}^\dagger s_{j\downarrow}\right]\left[\frac{1}{2}+A_j^Z\right]\Bigg]. \tag{15.16}$$

In this subsection we mapped the basis states and the Hamiltonian on to a pseudospin representation. The advantage of this is in the equivalence principles which will become clear in section 15.3. Now let's take a closer look at the Mott state.

15.2 The State at the Mott Point

At the Mott point, many physical phenomena occur such as spin glasses and anti-ferromagnetism. In our case the Mott point is not only physically relevant, but it also has properties which allow us to incorporate particle fluctuations. In this section we take a non-interacting Mott state and enforce our choice of symmetry upon it, and in doing so define a non-orthogonal operator.

The Mott point corresponds to half filling. A non-interacting state we could write at this point is given by

$$|\psi\rangle = \prod_{k\sigma}\left[u_k s_{k\sigma}^\dagger + i v_k a_{k\sigma}^\dagger\right]|0\rangle\,. \tag{15.17}$$

Subject to the condition (as we have two atoms per unit cell) that

$$\sum_{k\sigma}\left[s^\dagger_{k\sigma}s_{k\sigma}+a^\dagger_{k\sigma}a_{k\sigma}\right]|\psi\rangle=2. \tag{15.18}$$

Let's relabel our states via

$$g^\dagger_{k\sigma}=L_k s^\dagger_{k\sigma}, \tag{15.19}$$

where $L_k=u_k/v_k$. Note that this operator is not orthogonal so we define its dual as

$$\tilde{g}_{k\sigma}=R_k s_{k\sigma}, \tag{15.20}$$

such that $\{\tilde{g}_{k\sigma},g^\dagger_{k'\tau}\}=\delta_{kk'}\delta_{\sigma\tau}$. Though this is diagonal in momentum space, it is *not* diagonal in real space. We can transform from momentum to real space via a Bloch transformation. This does not need to be done explicitly as it is a linear transformation single creation operators map to single creation operators only. It is required that

$$|\psi\rangle\propto\prod_{j\sigma}\left[g^\dagger_{j\sigma}+ia^\dagger_{j\sigma}\right]|0\rangle \tag{15.21}$$

$$=\prod_{j}\left[g^\dagger_{j\uparrow}+ia^\dagger_{j\uparrow}\right]\left[g^\dagger_{j\downarrow}+ia^\dagger_{j\downarrow}\right]|0\rangle \tag{15.22}$$

$$=\prod_{j}\left[g^\dagger_{j\uparrow}g^\dagger_{j\downarrow}-a^\dagger_{j\uparrow}a^\dagger_{j\downarrow}+i\left[g^\dagger_{j\uparrow}a^\dagger_{j\downarrow}-g^\dagger_{j\downarrow}a^\dagger_{j\uparrow}\right]\right]|0\rangle\,. \tag{15.23}$$

Note the bracketed term, $g^\dagger_{j\uparrow}a^\dagger_{j\downarrow}-g^\dagger_{j\downarrow}a^\dagger_{j\uparrow}$, is anti-symmetric under the transformation $t_{i\sigma}\leftrightarrow b_{i\sigma}$; therefore, to ensure we maintain the symmetry of the chosen subspace, this is projected to zero. Rewriting this in terms of the pseudospin operators we get

$$|\psi\rangle=\prod_{j}\left[g^\dagger_{j\uparrow}g^\dagger_{j\downarrow}-A^+_j\right]|\downarrow\rangle\,. \tag{15.24}$$

This state is key in the analysis. Note, in the limit $U=\infty$ we *know* the state at the Mott

point is

$$|\psi\rangle_{U=\infty} = \prod_j \left[s^\dagger_{j\uparrow} s^\dagger_{j\downarrow} - a^\dagger_{j\uparrow} a^\dagger_{j\downarrow} \right] |0\rangle \,, \tag{15.25}$$

which corresponds to $g^\dagger_{i\sigma} = s^\dagger_{i\sigma}$. This gives $L_{k_{U=\infty}} = \delta_{k0}$, and we expect this to relax over different k points at finite U.

The Mott state has many properties which allow us to remove the pseudospin operators from the Hamiltonian and naturally incorporate particle fluctuations. This will be discussed in the next section.

15.3 The Method

The method in applying the technique is simple yet algebraically tedious. For that reason, in this section we will outline the process before taking a treacherous algebraic journey in the next section. The steps will be detailed later in this section but can be outlined as follows

1. Find any equivalence principles that hold true for the state being considered. This is where pseudospin operators can be replaced with non-orthogonal operators.

   These are very particular to the state being considered. If this step cannot be performed the method instantly fails.

2. Find any particle fluctuation properties the state being considered has. This is where two operator terms can be simplified. For the specific cases they occur we subtract the multiple operator term and add them back on after simplifying.

   This step is not necessary for the method, but if not taken produces terrible results when compared to the numerics.

3. Perform single particle paramagnetic averaging. This is simple but usually algebraically tedious.

15.3.1 Step 1 — Equivalence Principles

For our system we have the following equivalence principles for our chosen state

$$\left[\frac{1}{2}+A_j^z\right]|\psi\rangle \equiv \tilde{g}_{j\sigma}g_{j\sigma}^\dagger|\psi\rangle\,, \tag{15.26}$$

$$A_j^+|\psi\rangle \equiv g_{j\downarrow}^\dagger g_{j\uparrow}^\dagger|\psi\rangle\,, \tag{15.27}$$

$$A_j^-|\psi\rangle \equiv \tilde{g}_{j\uparrow}\tilde{g}_{j\downarrow}|\psi\rangle\,. \tag{15.28}$$

Demonstrating these explicitly we have

$$\left[\frac{1}{2}+A_{j'}^z\right]|\psi\rangle = \left[\frac{1}{2}+A_{j'}^z\right]\prod_j\left[g_{j\uparrow}^\dagger g_{j\downarrow}^\dagger - A_j^+\right]|\downarrow\rangle \tag{15.29}$$

$$= \left[\frac{1}{2}+A_{j'}^z\right]\left[g_{j'\uparrow}^\dagger g_{j'\downarrow}^\dagger - A_{j'}^+\right]\prod_{j\neq j'}\left[g_{j\uparrow}^\dagger g_{j\downarrow}^\dagger - A_j^+\right]|\downarrow\rangle \tag{15.30}$$

$$= -\left[\frac{1}{2}+A_{j'}^z\right]A_{j'}^+\prod_{j\neq j'}\left[g_{j\uparrow}^\dagger g_{j\downarrow}^\dagger - A_j^+\right]|\downarrow\rangle\,, \tag{15.31}$$

$$= -A_{j'}^+\prod_{j\neq j'}\left[g_{j\uparrow}^\dagger g_{j\downarrow}^\dagger - A_j^+\right]|\downarrow\rangle\,, \tag{15.32}$$

$$\tilde{g}_{j'\sigma}g_{j'\sigma}^\dagger|\psi\rangle = \tilde{g}_{j'\sigma}g_{j'\sigma}^\dagger\left[g_{j'\uparrow}^\dagger g_{j'\downarrow}^\dagger - A_{j'}^+\right]\prod_{j\neq j'}\left[g_{j\uparrow}^\dagger g_{j\downarrow}^\dagger - A_j^+\right]|\downarrow\rangle \tag{15.33}$$

$$= -A_{j'}^+\tilde{g}_{j'\sigma}g_{j'\sigma}^\dagger\prod_{j\neq j'}\left[g_{j\uparrow}^\dagger g_{j\downarrow}^\dagger - A_j^+\right]|\downarrow\rangle \tag{15.34}$$

$$= -A_{j'}^+\prod_{j\neq j'}\left[g_{j\uparrow}^\dagger g_{j\downarrow}^\dagger - A_j^+\right]|\downarrow\rangle\,, \tag{15.35}$$

and

$$A_{j'}^+|\psi\rangle = A_{j'}^+\left[g_{j'\uparrow}^\dagger g_{j'\downarrow}^\dagger - A_{j'}^+\right]\prod_{j\neq j'}\left[g_{j\uparrow}^\dagger g_{j\downarrow}^\dagger - A_j^+\right]|\downarrow\rangle \tag{15.36}$$

$$= A_{j'}^+ g_{j'\uparrow}^\dagger g_{j'\downarrow}^\dagger\prod_{j\neq j'}\left[g_{j\uparrow}^\dagger g_{j\downarrow}^\dagger - A_j^+\right]|\downarrow\rangle\,, \tag{15.37}$$

$$g^\dagger_{j'\downarrow} g^\dagger_{j'\uparrow} |\psi\rangle = g^\dagger_{j'\downarrow} g^\dagger_{j'\uparrow} \left[g^\dagger_{j'\uparrow} g^\dagger_{j'\downarrow} - A^+_{j'} \right] \prod_{j \neq j'} \left[g^\dagger_{j\uparrow} g^\dagger_{j\downarrow} - A^+_j \right] |\downarrow\rangle \tag{15.38}$$

$$= g^\dagger_{j'\uparrow} g^\dagger_{j'\downarrow} A^+_{j'} \prod_{j \neq j'} \left[g^\dagger_{j\uparrow} g^\dagger_{j\downarrow} - A^+_j \right] |\downarrow\rangle \,, \tag{15.39}$$

where in the last step we have swapped the creation operators and gained a Fermi minus sign, finally

$$A^-_{j'} |\psi\rangle = A^-_{j'} \left[g^\dagger_{j'\uparrow} g^\dagger_{j'\downarrow} - A^+_{j'} \right] \prod_{j \neq j'} \left[g^\dagger_{j\uparrow} g^\dagger_{j\downarrow} - A^+_j \right] |\downarrow\rangle \tag{15.40}$$

$$= -A^-_{j'} A^+_{j'} \prod_{j \neq j'} \left[g^\dagger_{j\uparrow} g^\dagger_{j\downarrow} - A^+_j \right] |\downarrow\rangle \tag{15.41}$$

$$= - \prod_{j \neq j'} \left[g^\dagger_{j\uparrow} g^\dagger_{j\downarrow} - A^+_j \right] |\downarrow\rangle \tag{15.42}$$

$$\tilde{g}_{j'\uparrow} \tilde{g}_{j'\downarrow} |\psi\rangle = \tilde{g}_{j'\uparrow} \tilde{g}_{j'\downarrow} \left[g^\dagger_{j'\uparrow} g^\dagger_{j'\downarrow} - A^+_{j'} \right] \prod_{j \neq j'} \left[g^\dagger_{j\uparrow} g^\dagger_{j\downarrow} - A^+_j \right] |\downarrow\rangle \tag{15.43}$$

$$= \tilde{g}_{j'\uparrow} \tilde{g}_{j'\downarrow} g^\dagger_{j'\uparrow} g^\dagger_{j'\downarrow} \prod_{j \neq j'} \left[g^\dagger_{j\uparrow} g^\dagger_{j\downarrow} - A^+_j \right] |\downarrow\rangle \tag{15.44}$$

$$= - \prod_{j \neq j'} \left[g^\dagger_{j\uparrow} g^\dagger_{j\downarrow} - A^+_j \right] |\downarrow\rangle \,, \tag{15.45}$$

where in the last step we swapped the annihilation operators and gained a Fermi minus sign.

These allow us to recast the Hamiltonian to one which is purely composed of $\tilde{g}_{j\sigma}$ operators. This is a special property of the state we're considering. If we can't do this the method instantly fails.

15.3.2 Step 2 — Particle Fluctuations

Particle fluctuations are usually difficult to incorporate in many averaging methods. It is these fluctuations that are clearly important in strongly correlated systems. To include

them in our model we note the following property

$$g^{\dagger}_{j\sigma}\tilde{g}_{j\bar{\sigma}}\left|\psi\right\rangle = 0. \tag{15.46}$$

Demonstrating this explicitly we have

$$g^{\dagger}_{j'\sigma}\tilde{g}_{j'\bar{\sigma}}\left|\psi\right\rangle = g^{\dagger}_{j'\sigma}\tilde{g}_{j'\bar{\sigma}}\left[g^{\dagger}_{j'\uparrow}g^{\dagger}_{j'\downarrow} - A^{+}_{j'}\right]\prod_{j\neq j'}\left[g^{\dagger}_{j\uparrow}g^{\dagger}_{j\downarrow} - A^{+}_{j}\right]\left|\downarrow\right\rangle = 0, \tag{15.47}$$

where the first term is zero from Pauli exclusion and the second term is zero from annihilating the vacuum.

Using this property is simple yet algebraically tedious. Wherever there are two or more operators of the form $g^{\dagger}_{j'\sigma}\tilde{g}_{j'\bar{\sigma}}$ acting on state $\left|\psi\right\rangle$ the fluctuation property should be enforced explicitly. This is in preparation of the third step as averaging only enforces fluctuations on average, and we are attempting to explicitly enforce this.

Things are more subtle than they initially seem as any $s^{\dagger}_{i\sigma}$ operators are linear superpositions of $g^{\dagger}_{i\sigma}$ operators. To see this, we require the real space transformation for $s_{j\sigma}$ to $\tilde{g}_{j\sigma}$ operators. Consider the Bloch transform of $s^{\dagger}_{j\sigma}$

$$s^{\dagger}_{j\sigma} = \frac{1}{\sqrt{N}}\sum_{k} e^{ijk}s^{\dagger}_{k\sigma}, \tag{15.48}$$

we then substitute the definition $s^{\dagger}_{k\sigma} = R_k g^{\dagger}_{k\sigma}$ followed by Bloch transforming $g^{\dagger}_{k\sigma}$

$$\begin{aligned} s^{\dagger}_{j\sigma} &= \frac{1}{\sqrt{N}}\sum_{k} e^{ijk}R_k\frac{1}{\sqrt{N}}\sum_{j'} e^{ij'k}g^{\dagger}_{j'\sigma} && (15.49)\\ &= \sum_{j'}\frac{1}{N}\sum_{k} e^{i(j-j')k}R_k g^{\dagger}_{j'\sigma} && (15.50)\\ &= \sum_{j'} R_{j-j'}g^{\dagger}_{j'\sigma}, && (15.51) \end{aligned}$$

where we have defined an anti-symmetric transform $R_l = \frac{1}{N}\sum_k e^{ilk}R_k$. This odd choice is done to help with calculations, as we do not need to worry about carrying factors of $\frac{1}{\sqrt{N}}$

when transforming and manipulating between orthogonal and non-orthogonal operators. Repeating this gives

$$s^\dagger_{j\sigma} = \sum_{j'} R_{j-j'} g^\dagger_{j'\sigma} \quad s_{j\sigma} = \sum_{j'} L_{j'-j} \tilde{g}_{j'\sigma}. \tag{15.52}$$

To use the fluctuation property (15.46), we take any combination of operators, transform into the $\tilde{g}_{j\sigma}$ representation, subtract any specific terms where the identity holds, and add it back but collapsed. For example

$$s^\dagger_{j\uparrow}\tilde{g}_{j\downarrow}g^\dagger_{j\downarrow}\left|\psi\right\rangle = \sum_{j'} R_{j-j'} g^\dagger_{j'\uparrow}\tilde{g}_{j\downarrow}g^\dagger_{j\downarrow}\left|\psi\right\rangle = \left[s^\dagger_{j\uparrow}\tilde{g}_{j\downarrow}g^\dagger_{j\downarrow} - R_0 g^\dagger_{j\uparrow}\tilde{g}_{j\downarrow}g^\dagger_{j\downarrow} + R_0 g^\dagger_{j\uparrow}\right]\left|\psi\right\rangle. \tag{15.53}$$

In doing so we have not changed the Hamiltonian, but once averaging occurs we will have modified H while incorporating particle fluctuations. Taking the previous example we have (after averaging)

$$s^\dagger_{j\uparrow}\langle\tilde{g}_{j\downarrow}g^\dagger_{j\downarrow}\rangle \quad \text{vs} \quad s^\dagger_{j\uparrow}\langle\tilde{g}_{j\downarrow}g^\dagger_{j\downarrow}\rangle - R_0 g^\dagger_{j\uparrow}\langle\tilde{g}_{j\downarrow}g^\dagger_{j\downarrow}\rangle + R_0 g^\dagger_{j\uparrow}, \tag{15.54}$$

where the additional terms are taking into account particle fluctuations.

15.3.3 Step 3 — Paramagnetic Averaging

The final step is to perform single particle paramagnetic averaging. For example

$$s^\dagger_{j\uparrow}s_{j\uparrow}s^\dagger_{j\downarrow}s_{j\downarrow} \to s^\dagger_{j\uparrow}s_{j\uparrow}\langle s^\dagger_{j\downarrow}s_{j\downarrow}\rangle + \langle s^\dagger_{j\uparrow}s_{j\uparrow}\rangle s^\dagger_{j\downarrow}s_{j\downarrow} - \langle s^\dagger_{j\uparrow}s_{j\uparrow}\rangle\langle s^\dagger_{j\downarrow}s_{j\downarrow}\rangle \tag{15.55}$$

15.3.4 Produce of the Theory

The method produces four things that can be measured: total energy E, particle dispersion ϵ_k, hole dispersion $\tilde{\epsilon}_k$, and occupation number n_k. These are defined via the following

equations and commutators, which are calculated at the start of the process.

$$H_S \left|\psi\right\rangle = E \left|\psi\right\rangle + \sum_{k\sigma} E_k \, g^\dagger_{k\sigma} \tilde{g}_{k\sigma} \left|\psi\right\rangle . \tag{15.56}$$

$$[H_S, s^\dagger_{k\sigma}] \left|\psi\right\rangle = \epsilon_k \, s^\dagger_{k\sigma} \left|\psi\right\rangle , \tag{15.57}$$

$$[s_{k\sigma}, H_S] \left|\psi\right\rangle = \tilde{\epsilon}_k \, s_{k\sigma} \left|\psi\right\rangle , \tag{15.58}$$

$$\frac{\left\langle\psi\right| \left\{ s_{k\sigma}, [H_S, s^\dagger_{k\sigma}] \right\} \left|\psi\right\rangle}{\left\langle\psi|\psi\right\rangle} = \epsilon_k \, (1 - n_k) + \tilde{\epsilon}_k \, n_k, \tag{15.59}$$

These are subtle assumptions at play with each of these equations. For equation 15.56 we are assuming that as there are equivalence principles between A and $g^\dagger$ that H is essentially a function of $g^\dagger$, therefore $\left|\psi\right\rangle$ can be represented as a sum of products of $g^\dagger_{k\sigma}$ states

$$\left|\psi\right\rangle = \sum_\mu c_\mu \prod_{k\sigma} g^\dagger_{k\sigma} \left|0\right\rangle , \tag{15.60}$$

and that, upon averaging, H_S can be represented as a single particle Hamiltonian such that there is a dispersion E_k upon application. A separate assumption that we make is that $\left|\psi\right\rangle$ is an eigenstate which sets $E_k = 0$. This defines R_k and its inverse L_k.

For equation 15.57 we assume that $s^\dagger_{k\sigma} \left|\psi\right\rangle$ is an eigenstate with eigenvalue $E + \epsilon_k$ such that

$$[H_S, s^\dagger_{k\sigma}] \left|\psi\right\rangle = [H_S s^\dagger_{k\sigma} - s^\dagger_{k\sigma} H_S] \left|\psi\right\rangle \approx [(E + \epsilon_k) s^\dagger_{k\sigma} - s^\dagger_{k\sigma} E] \left|\psi\right\rangle = \epsilon_k s^\dagger_{k\sigma} \left|\psi\right\rangle . \tag{15.61}$$

Similarly we have for equation 15.58

$$[s_{k\sigma}, H_S] \left|\psi\right\rangle = [s_{k\sigma} H_S - H_S s_{k\sigma}] \left|\psi\right\rangle \approx [s_{k\sigma} E - (E - \tilde{\epsilon}_k) s_{k\sigma}] \left|\psi\right\rangle = \tilde{\epsilon}_k s_{k\sigma} \left|\psi\right\rangle . \tag{15.62}$$

Finally, and most interestingly, we can use 15.59 to solve for the occupation factor.

Taking the Hermitian conjugate of 15.62 gives $\langle\psi|\,[H_S, s^\dagger_{k\sigma}] = \langle\psi|\, s^\dagger_{k\sigma}\tilde{\epsilon}_k$ such that

$$\langle\psi|\left\{s_{k\sigma}, [H_S, s^\dagger_{k\sigma}]\right\}|\psi\rangle = \langle\psi|\left(s_{k\sigma}[H_S, s^\dagger_{k\sigma}] - [H_S, s^\dagger_{k\sigma}]s_{k\sigma}\right)|\psi\rangle \tag{15.63}$$

$$= \langle\psi|\left(s_{k\sigma}\epsilon_k s^\dagger_{k\sigma} - s^\dagger_{k\sigma}\tilde{\epsilon}_k s_{k\sigma}\right)|\psi\rangle\,. \tag{15.64}$$

By defining

$$\frac{\langle\psi|\, s^\dagger_{k\sigma}s_{k\sigma}\,|\psi\rangle}{\langle\psi|\psi\rangle} = n_k, \tag{15.65}$$

where we have divided by the norm for normalisation purposes, we get

$$\frac{\langle\psi|\left\{s_{k\sigma}, [H_S, s^\dagger_{k\sigma}]\right\}|\psi\rangle}{\langle\psi|\psi\rangle} = \epsilon_k\,(1 - n_k) + \tilde{\epsilon}_k\, n_k. \tag{15.66}$$

This means we can examine the Fermi liquid discontinuity in the system.

In this section we outlined the method. We discovered a set of equivalence principles relating $\tilde{g}_{i\sigma}$ operators to our pseudospin operators and how to incorporate particle fluctuations. In the following section we implement this method.

15.4 The Calculation — An Exercise in Arduous Algebra

This section is, as the title says, arduous. We've streamlined the process to the best of our ability while still making it easy to follow. We begin by calculating the commutators, and using the equivalence principles to recast them. In each of the following subsections we incorporate particle fluctuations and average to attain the appropriate quantities.

The following commutators can be directly calculated in the pseudospin basis.

$$[H, s^\dagger_{l\sigma}] = -2t_1\sum_{\langle il\rangle} s^\dagger_{i\sigma} - t_0 s^\dagger_{l\sigma} + \frac{U}{2}\Big[s^\dagger_{l\sigma}s^\dagger_{l\bar{\sigma}}s_{l\bar{\sigma}} + s_{l\bar{\sigma}}A^+_l + (\frac{1}{2} + A^z_l)s^\dagger_{l\sigma}\Big], \tag{15.67}$$

$$[s_{l\sigma}, H] = -2t_1 \sum_{\langle il \rangle} s_{i\sigma} - t_0 s_{l\sigma} + \frac{U}{2}\Big[s^\dagger_{l\bar{\sigma}} s_{l\bar{\sigma}} s_{l\sigma} + s^\dagger_{l\bar{\sigma}} A^-_l + (\frac{1}{2} + A^z_l) s_{l\sigma}\Big], \tag{15.68}$$

$$\{s_{j'\sigma}, [H, s^\dagger_{l\sigma}]\} = -2t_1 \delta_{\langle j'l \rangle} - t_0 \delta_{j'l} + \frac{U}{2}\Big[s^\dagger_{l\bar{\sigma}} s_{l\bar{\sigma}} + (\frac{1}{2} + A^z_l)\Big]\delta_{j'l}, \tag{15.69}$$

these will be recast using equivalence principles and Bloch transformed to get the appropriate commutators.

We have the following equivalence principles

$$(\frac{1}{2} + A^z_j)\,|\psi\rangle = (\frac{1}{2} + A^z_j)(g^\dagger_{j\uparrow} g^\dagger_{j\downarrow} - A^+_j) \prod_{j' \neq j} (g^\dagger_{j'\uparrow} g^\dagger_{j'\downarrow} - A^+_{j'})\,|\downarrow\rangle \tag{15.70}$$

$$= -A^+_j \prod_{j' \neq j} (g^\dagger_{j'\uparrow} g^\dagger_{j'\downarrow} - A^+_{j'})\,|\downarrow\rangle \tag{15.71}$$

$$\equiv \tilde{g}_{j\uparrow} g^\dagger_{j\uparrow}\,|\psi\rangle \tag{15.72}$$

$$\equiv \tilde{g}_{j\downarrow} g^\dagger_{j\downarrow}\,|\psi\rangle\,, \tag{15.73}$$

$$A^+_j\,|\psi\rangle = g^\dagger_{j\uparrow} g^\dagger_{j\downarrow} A^+_j \prod_{j' \neq j} (g^\dagger_{j'\uparrow} g^\dagger_{j'\downarrow} - A^+_{j'})\,|\downarrow\rangle \tag{15.74}$$

$$\equiv -g^\dagger_{j\uparrow} g^\dagger_{j\downarrow}\,|\psi\rangle\,, \tag{15.75}$$

$$\tag{15.76}$$

$$A^-_j = -\prod_{j' \neq j} (g^\dagger_{j'\uparrow} g^\dagger_{j'\downarrow} - A^+_{j'})\,|\downarrow\rangle \tag{15.77}$$

$$\equiv -\tilde{g}_{j\downarrow} \tilde{g}_{j\uparrow}\,|\psi\rangle\,. \tag{15.78}$$

Whenever the pseudospin operators occur we will replace them with the appropriate $\tilde{g}_{j\sigma}$ operators.

Upon substitution the commutators and Hamiltonian become when acting on $|\psi\rangle$

$$[H, s^\dagger_{l\sigma}] = -2t_1 \sum_{\langle il \rangle} s^\dagger_{i\sigma} - t_0 s^\dagger_{l\sigma} + \frac{U}{2}\Big[s^\dagger_{l\sigma} s^\dagger_{l\bar{\sigma}} s_{l\bar{\sigma}} - s_{l\bar{\sigma}} \tilde{g}_{j\downarrow} \tilde{g}_{j\uparrow} + s^\dagger_{l\sigma} \tilde{g}_{j\bar{\sigma}} g^\dagger_{j\bar{\sigma}}\Big], \tag{15.79}$$

$$[s_{l\sigma}, H] = -2t_1 \sum_{\langle il \rangle} s_{i\sigma} - t_0 s_{l\sigma} + \frac{U}{2}\Big[s^\dagger_{l\bar{\sigma}} s_{l\bar{\sigma}} s_{l\sigma} - s^\dagger_{l\bar{\sigma}} \tilde{g}_{j\downarrow} \tilde{g}_{j\uparrow} + s_{l\sigma} \tilde{g}_{j\bar{\sigma}} g^\dagger_{j\bar{\sigma}}\Big], \tag{15.80}$$

$$\{s_{j'\sigma}, [H, s^\dagger_{l\sigma}]\} = -2t_1 \delta_{\langle j'l \rangle} - t_0 \delta_{j'l} + \frac{U}{2}\Big[s^\dagger_{l\bar{\sigma}} s_{l\bar{\sigma}} + \tilde{g}_{j\bar{\sigma}} g^\dagger_{j\bar{\sigma}}\Big]\delta_{j'l}, \tag{15.81}$$

$$H_S = -2t \sum_{\langle ij \rangle \sigma} s^\dagger_{i\sigma} s_{j\sigma} + \frac{U}{2} \sum_j \Bigg[s^\dagger_{j\uparrow} s_{j\uparrow} s^\dagger_{j\downarrow} s_{j\downarrow} - s^\dagger_{j\uparrow} s^\dagger_{j\downarrow} \tilde{g}_{j\downarrow} \tilde{g}_{j\uparrow} - s_{j\downarrow} s_{j\uparrow} g^\dagger_{j\downarrow} g^\dagger_{j\uparrow} + \frac{1}{2}(\tilde{g}_{j\uparrow} g^\dagger_{j\uparrow} + \tilde{g}_{j\downarrow} g^\dagger_{j\downarrow}) + s^\dagger_{j\uparrow} s_{j\uparrow} \tilde{g}_{j\downarrow} g^\dagger_{j\downarrow} + s^\dagger_{j\downarrow} s_{j\downarrow} \tilde{g}_{j\uparrow} g^\dagger_{j\uparrow} \Bigg]. \tag{15.82}$$

To deal with particle fluctuations we utilise

$$g^\dagger_{j\sigma} \tilde{g}_{j\bar{\sigma}} |\psi\rangle = 0, \tag{15.83}$$

$$\tilde{g}_{j\bar{\sigma}} g^\dagger_{j\sigma} \tilde{g}_{j\sigma} |\psi\rangle = \tilde{g}_{j\bar{\sigma}} |\psi\rangle . \tag{15.84}$$

Wherever there is an $s^\dagger_\sigma$ or s_σ we use the transformation

$$s^\dagger_{j\sigma} = \sum_{j'} R_{j-j'} g^\dagger_{j'\sigma} \quad s_{j\sigma} = \sum_{j'} L_{j'-j} \tilde{g}_{j'\sigma}, \tag{15.85}$$

which is simply a Bloch transformation of the definitions $s^\dagger_{k\sigma} = R_k g^\dagger_{k\sigma}$ and $s_{k\sigma} = L_k \tilde{g}_{k\sigma}$ where

$$R_{j-j'} = \frac{1}{N} \sum_k e^{ik(j-j')} R_k \quad L_{j'-j} = \frac{1}{N} \sum_k e^{ik(j'-j)} L_k. \tag{15.86}$$

We will use Bloch transformations

$$\tilde{g}_{j\sigma} = \frac{1}{\sqrt{N}} \sum_k e^{ikj} \tilde{g}_{k\sigma}, \quad g^\dagger_{j\sigma} = \frac{1}{\sqrt{N}} \sum_k e^{-ikj} g^\dagger_{k\sigma}, \tag{15.87}$$

and the inverse transformations

$$\tilde{g}_{k\sigma} = \frac{1}{\sqrt{N}} \sum_j e^{-ikj} \tilde{g}_{j\sigma}, \quad g^\dagger_{k\sigma} = \frac{1}{\sqrt{N}} \sum_j e^{ikj} g^\dagger_{j\sigma}. \tag{15.88}$$

These transformations allow us to calculate the required momentum space commutators from our real space commutators via

$$[s_{q\sigma}, H] = \frac{1}{\sqrt{N}} \sum_j e^{-iqj} [s_{j\sigma}, H], \quad [H, s^\dagger_{q\sigma}] = \frac{1}{\sqrt{N}} \sum_j e^{iqj} [H, s^\dagger_{j\sigma}]. \tag{15.89}$$

Now that we've detailed the process we move on to calculating the appropriate quantities beginning with n_k.

15.4.1 Calculating the Occupation factor n_k

This is the simplest calculation in this part. We have the definition and equivalence

$$n_k = \frac{\langle\psi|\, s^\dagger_{k\sigma} s_{k\sigma}\, |\psi\rangle}{\langle\psi|\psi\rangle} \equiv \frac{\langle\psi|\, g^\dagger_{k\sigma} \tilde{g}_{k\sigma}\, |\psi\rangle}{\langle\psi|\psi\rangle}. \tag{15.90}$$

The real space commutator is given by

$$\{s_{j'\sigma}, [H, s^\dagger_{l\sigma}]\} = -2t_1 \delta_{\langle j'l\rangle} - t_0 \delta_{j'l} + \frac{U}{2} \Big[s^\dagger_{l\bar{\sigma}} s_{l\bar{\sigma}} + (\frac{1}{2} + A^z_l) \Big] \delta_{j'l}, \tag{15.91}$$

which, upon substitution of the equivalence principles becomes

$$\{s_{j'\sigma}, [H, s^\dagger_{l\sigma}]\} = -2t_1 \delta_{\langle j'l\rangle} - t_0 \delta_{j'l} + \frac{U}{2} \Big[s^\dagger_{l\bar{\sigma}} s_{l\bar{\sigma}} + \tilde{g}_{j\bar{\sigma}} g^\dagger_{j\bar{\sigma}} \Big] \delta_{j'l}. \tag{15.92}$$

Upon Bloch transformation we get

$$\frac{\langle\psi| \left\{ s_{k\sigma}, [H_S, s^\dagger_{k\sigma}] \right\} |\psi\rangle}{\langle\psi|\psi\rangle} = -2t_1 Z \gamma_k + (\frac{U}{2} - t_0). \tag{15.93}$$

This result is equated to equation 15.59

$$\frac{\langle\psi| \left\{ s_{k\sigma}, [H_S, s^\dagger_{k\sigma}] \right\} |\psi\rangle}{\langle\psi|\psi\rangle} = \epsilon_k (1 - n_k) + \tilde{\epsilon}_k n_k, \tag{15.94}$$

$$= -2t_1 Z \gamma_k + (\frac{U}{2} - t_0), \tag{15.95}$$

which gives

$$n_k = \frac{-2t_1 Z\gamma_k - \epsilon_k - t_0 + \frac{U}{2}}{\tilde{\epsilon}_k - \epsilon_k}. \tag{15.96}$$

Note that this calculation solves for the occupation factor and is not set. We now calculate the particle dispersion.

15.4.2 Calculating the Particle Dispersion ϵ_k

In this subsection we repeat the previous procedure to calculate the particle dispersion. This time we will be required to consider particle fluctuations.

We are solving with the following definition

$$[H_S, s^\dagger_{k\sigma}]\,|\psi\rangle = \epsilon_k\, s^\dagger_{k\sigma}\,|\psi\rangle\,. \tag{15.97}$$

In real space the commutator is given by

$$[H, s^\dagger_{l\sigma}] = -2t_1 \sum_{\langle il\rangle} s^\dagger_{i\sigma} - t_0 s^\dagger_{l\sigma} + \frac{U}{2}\Big[s^\dagger_{l\sigma} s^\dagger_{l\bar{\sigma}} s_{l\bar{\sigma}} + s_{l\bar{\sigma}} A^+_l + (\frac{1}{2} + A^z_l) s^\dagger_{l\sigma}\Big], \tag{15.98}$$

which upon substitution of the equivalence principles becomes

$$[H, s^\dagger_{l\sigma}] = -2t_1 \sum_{\langle il\rangle} s^\dagger_{i\sigma} - t_0 s^\dagger_{l\sigma} + \frac{U}{2}\Big[s^\dagger_{l\sigma} s^\dagger_{l\bar{\sigma}} s_{l\bar{\sigma}} - s_{l\bar{\sigma}} \tilde{g}_{j\downarrow} \tilde{g}_{j\uparrow} + s^\dagger_{l\sigma} \tilde{g}_{j\bar{\sigma}} g^\dagger_{j\bar{\sigma}}\Big]. \tag{15.99}$$

At this point we are required to consider particle fluctuations. This is performed by following the procedure outlined in equation 15.53, subject to equation 15.84. As this is rather involved we take this term by term. Take $s^\dagger_{l\sigma} s^\dagger_{l\bar{\sigma}} s_{l\bar{\sigma}}$, after expanding and averaging we get

$$s^\dagger_{l\sigma} \langle s^\dagger_{l\bar{\sigma}} s_{l\bar{\sigma}}\rangle - \sum_{j_1} R_{j-j_1} L_{j_1-j} g^\dagger_{j_1\sigma} \langle s^\dagger_{j\bar{\sigma}} \tilde{g}_{j_1\bar{\sigma}}\rangle, \tag{15.100}$$

which upon Bloch transformation becomes

$$s^\dagger_{q\sigma}\frac{1}{N}\sum_{k_1}\Big[n_{k_1} - L_q\frac{1}{N}\sum_{k_2}R_{j_1}L_{k_2}[Rn]_{k_1-k_2+q}\Big]. \tag{15.101}$$

For $s_{l\bar{\sigma}}\tilde{g}_{j\downarrow}\tilde{g}_{j\uparrow}$

$$\langle s_{l\bar{\sigma}}g^\dagger_{l\bar{\sigma}}\rangle g^\dagger_{l\sigma} - L_0\langle\tilde{g}_{j\bar{\sigma}}g^\dagger_{j\bar{\sigma}}\rangle g^\dagger_{j\sigma} + L_0 g^\dagger_{j\sigma}, \tag{15.102}$$

$$\Rightarrow s^\dagger_{q\sigma}\frac{1}{N}\sum_{k_1}\Big[L_qL_{k_1}(1-n_{k_1}) - L_qL_0(1-n_{k_1}) + L_0L_q\Big]. \tag{15.103}$$

For $s^\dagger_{l\sigma}\tilde{g}_{j\bar{\sigma}}g^\dagger_{j\bar{\sigma}}$

$$s^\dagger_{j\sigma}\langle\tilde{g}_{j\bar{\sigma}}g^\dagger_{l\bar{\sigma}}\rangle - R_0 g^\dagger_{j\sigma}\langle\tilde{g}_{j\bar{\sigma}}g^\dagger_{j\bar{\sigma}}\rangle + R_0 g^\dagger_{j\sigma}, \tag{15.104}$$

$$\Rightarrow s^\dagger_{q\sigma}\frac{1}{N}\sum_{k_1}\Big[(1-n_{k_1}) - L_qR_0(1-n_{k_1}) + L_qR_0\Big]. \tag{15.105}$$

Putting everything together and equating to 15.97 gives

$$\epsilon_q = -2t_1Z\gamma_q - t_0 + \frac{U}{2}[1 - L_qB_q] \tag{15.106}$$

$$B_q = \frac{1}{N}\sum_{k_1}\Big[\frac{1}{N}\sum_{k_2}R_{k_1}L_{k_2}[Rn]_{k_1-k_2+q} - (L_0+R_0)n_{k_1} - L_{k_1}(1-n_{k_1})\Big] \tag{15.107}$$

15.4.3 Calculating the Hole Dispersion $\tilde{\epsilon}_k$

In this subsection we repeat this process for the hole dispersion defined by

$$[s_{k\sigma}, H_S]\,|\psi\rangle = \tilde{\epsilon}_k\, s_{k\sigma}\,|\psi\rangle\,. \tag{15.108}$$

In real space this commutator is given by

$$[s_{l\sigma}, H] = -2t_1\sum_{\langle il\rangle}s_{i\sigma} - t_0 s_{l\sigma} + \frac{U}{2}\Big[s^\dagger_{l\bar{\sigma}}s_{l\bar{\sigma}}s_{l\sigma} + s^\dagger_{l\bar{\sigma}}A^-_l + (\frac{1}{2}+A^z_l)s_{l\sigma}\Big], \tag{15.109}$$

which upon substitution of the equivalence principles becomes

$$[s_{l\sigma}, H] = -2t_1 \sum_{\langle il \rangle} s_{i\sigma} - t_0 s_{l\sigma} + \frac{U}{2}\Big[s^\dagger_{l\bar{\sigma}} s_{l\bar{\sigma}} s_{l\sigma} - s^\dagger_{l\bar{\sigma}} \tilde{g}_{j\downarrow} \tilde{g}_{j\uparrow} + s_{l\sigma} \tilde{g}_{j\bar{\sigma}} g^\dagger_{j\bar{\sigma}}\Big]. \tag{15.110}$$

Now we consider each term's particle fluctuations. For $s^\dagger_{l\bar{\sigma}} s_{l\bar{\sigma}} s_{l\sigma}$

$$\langle s^\dagger_{j\bar{\sigma}} s_{j\bar{\sigma}} \rangle s_{j\sigma} - \sum_{j_1} R_{j-j_1} L_{j_1-j} \langle g^\dagger_{j_1\bar{\sigma}} s_{j_\sigma} \rangle \tilde{g}_{j_1\sigma} + \sum_{j_1} R_{j-j_1} L_{j_1-j} L_{j_1-j} \tilde{g}_{j_1\sigma}, \tag{15.111}$$

$$\Rightarrow s_{q\sigma} \frac{1}{N} \sum_{k_1} \Big[n_{k_1} + R_{k_1} L_{k_2} [L(1-n)]_{q-k_1+k_2} R_q \Big]. \tag{15.112}$$

For $-s^\dagger_{l\bar{\sigma}} \tilde{g}_{j\downarrow} \tilde{g}_{j\uparrow}$

$$-\tilde{g}_{j\sigma} \langle s^\dagger_{j\bar{\sigma}} \tilde{g}_{j\bar{\sigma}} \rangle - R_0 \langle g^\dagger_{j\bar{\sigma}} \tilde{g}_{j\bar{\sigma}} \rangle \tilde{g}_{j\sigma} + R_0 \tilde{g}_{j\sigma}, \tag{15.113}$$

$$\Rightarrow s_{q\sigma} \frac{1}{N} \sum_{k_1} \Big[- R_q R_{k_1} n_{k_1} - R_q R_0 n_{k_1} + R_0 R_q \Big]. \tag{15.114}$$

For $s_{l\sigma} \tilde{g}_{j\bar{\sigma}} g^\dagger_{j\bar{\sigma}}$

$$s_{j\sigma} \langle \tilde{g}_{j\bar{\sigma}} g^\dagger_{j\bar{\sigma}} \rangle - L_0 \tilde{g}_{j\sigma} \langle \tilde{g}_{j\bar{\sigma}} g^\dagger_{j\bar{\sigma}} \rangle, \tag{15.115}$$

$$\Rightarrow s_{q\sigma} \frac{1}{N} \sum_{k_1} [(1 - n_{k_1}) - L_0 R_q (1 - n_{k_1})]. \tag{15.116}$$

Putting everything together and equating to 15.108 gives

$$\tilde{\epsilon}_q = -2t_1 Z \gamma_q - t_0 + \frac{U}{2}[1 + R_q \tilde{B}_q] \tag{15.117}$$

$$\tilde{B}_q = \frac{1}{N} \sum_{k_1} \Big[R_{k_1} L_{k_2} [L(1-n)]_{q-k_1+k_2} - R_{k_1} n_{k_1} - (L_0 + R_0)(1 - n_{k_1}) \Big] \tag{15.118}$$

15.4.4 Calculating E_k

In this subsection we calculate E_k by applying this process to the Hamiltonian given by

$$H_S = -2t\sum_{\langle ij\rangle\sigma} s^\dagger_{i\sigma}s_{j\sigma} + \frac{U}{2}\sum_j \Bigg[s^\dagger_{j\uparrow}s_{j\uparrow}s^\dagger_{j\downarrow}s_{j\downarrow} + s^\dagger_{j\uparrow}s^\dagger_{j\downarrow}A^-_j + s_{j\downarrow}s_{j\uparrow}A^+_j + \Big[1 + s^\dagger_{j\uparrow}s_{j\uparrow} + s^\dagger_{j\downarrow}s_{j\downarrow}\Big]\Big[\frac{1}{2} + A^Z_j\Big]\Bigg], \quad (15.119)$$

which upon substitution of the equivalence principles yields

$$H_S = -2t\sum_{\langle ij\rangle\sigma} s^\dagger_{i\sigma}s_{j\sigma} + \frac{U}{2}\sum_j \Bigg[s^\dagger_{j\uparrow}s_{j\uparrow}s^\dagger_{j\downarrow}s_{j\downarrow} - s^\dagger_{j\uparrow}s^\dagger_{j\downarrow}\tilde{g}_{j\downarrow}\tilde{g}_{j\uparrow} - s_{j\downarrow}s_{j\uparrow}g^\dagger_{j\downarrow}g^\dagger_{j\uparrow} + \frac{1}{2}(\tilde{g}_{j\uparrow}g^\dagger_{j\uparrow} + \tilde{g}_{j\downarrow}g^\dagger_{j\downarrow}) + s^\dagger_{j\uparrow}s_{j\uparrow}\tilde{g}_{j\downarrow}g^\dagger_{j\downarrow} + s^\dagger_{j\downarrow}s_{j\downarrow}\tilde{g}_{j\uparrow}g^\dagger_{j\uparrow}\Bigg]. \quad (15.120)$$

Now we apply the particle fluctuations to each term and average. For the $s^\dagger_{j\uparrow}s_{j\uparrow}s^\dagger_{j\downarrow}s_{j\downarrow}$

$$\begin{aligned}
&s^\dagger_{j\uparrow}s_{j\downarrow}\langle s^\dagger_{j\downarrow}s_{j\downarrow}\rangle + \langle s^\dagger_{j\uparrow}s_{j\downarrow}\rangle s^\dagger_{j\downarrow}s_{j\downarrow} - \langle s^\dagger_{j\uparrow}s_{j\downarrow}\rangle\langle s^\dagger_{j\downarrow}s_{j\downarrow}\rangle - \sum_{j_1} R_{j-j_1}L_{j_1-j}\langle g^\dagger_{j_1\uparrow}s_{j\uparrow}\rangle s^\dagger_{j\downarrow}\tilde{g}_{j_1\downarrow} \\
&-\sum_{j_1} R_{j-j_1}L_{j_1-j}g^\dagger_{j_1\uparrow}s_{j\uparrow}\langle s^\dagger_{j\downarrow}\tilde{g}_{j_1\downarrow}\rangle + \sum_{j_1} R_{j-j_1}L_{j_1-j}\langle g^\dagger_{j_1\uparrow}s_{j\uparrow}\rangle\langle s^\dagger_{j\downarrow}\tilde{g}_{j_1\downarrow}\rangle + \sum_{j_2} R_{j-j_2}L_{j_2-j}L_{j_2-j}s^\dagger_{j\uparrow}\tilde{g}_{j_2\uparrow} \\
&\quad - \sum_{j_1j_2j_3} R_{j-j_2}L_{j_2-j}s^\dagger_{j\uparrow}\tilde{g}_{j_2\uparrow}\langle g^\dagger_{j_2\downarrow}s_{j\downarrow}\rangle - \sum_{j_1j_2j_3} R_{j-j_2}L_{j_2-j}\langle s^\dagger_{j\uparrow}\tilde{g}_{j_2\uparrow}\rangle g^\dagger_{j_2\downarrow}s_{j\downarrow} \\
&\quad + \sum_{j_1j_2j_3} R_{j-j_2}L_{j_2-j}\langle s^\dagger_{j\uparrow}\tilde{g}_{j_2\uparrow}\rangle\langle g^\dagger_{j_2\downarrow}s_{j\downarrow}\rangle + \sum_{j_1j_2} R_{j-j_1}R_{j-j_2}L_{j_1-j}L_{j_2-j}\langle g^\dagger_{j_1\uparrow}\tilde{g}_{j_2\uparrow}\rangle g^\dagger_{j_2\downarrow}\tilde{g}_{j_1\downarrow} \\
&+\sum_{j_1j_2} R_{j-j_1}R_{j-j_2}L_{j_1-j}L_{j_2-j}g^\dagger_{j_1\uparrow}\tilde{g}_{j_2\uparrow}\langle g^\dagger_{j_2\downarrow}\tilde{g}_{j_1\downarrow}\rangle - \sum_{j_1j_2} R_{j-j_1}R_{j-j_2}L_{j_1-j}L_{j_2-j}\langle g^\dagger_{j_1\uparrow}\tilde{g}_{j_2\uparrow}\rangle\langle g^\dagger_{j_2\downarrow}\tilde{g}_{j_1\downarrow}\rangle \\
&+\sum_{j_1} R_{j-j_1}L_{j_1-j}L_{j_1-j}s^\dagger_{j\downarrow}\tilde{g}_{j_1\downarrow} - \frac{1}{2}\sum_{j_1j_2} R_{j-j_1}R_{j-j_1}L_{j_1-j}L_{j_1-j}(g^\dagger_{j_1\uparrow}\tilde{g}_{j_1\uparrow} + g^\dagger_{j_1\downarrow}\tilde{g}_{j_1\downarrow}), \quad (15.121)
\end{aligned}$$

$$\Rightarrow [g^\dagger_{q\uparrow}\tilde{g}_{q\uparrow}+g^\dagger_{q\downarrow}\tilde{g}_{q\downarrow}]\frac{1}{N}\sum_{k_1}\Big[n_{k_1}-\frac{1}{N}\sum_{k_2}R_{k_1}L_{k_2}[Rn]_{k_1-k_2+q}L_q+\frac{1}{N}\sum_{k_2}R_{k_1}L_{k_2}[L(1-n)]_{k_2-k_1+q}$$
$$+\frac{1}{N^2}\sum_{k_2k_3}R_{k_1}R_{k_2}L_{k_3}L_{k_1+k_2-k_3}[n_{k_1-k_3+q}-\frac{1}{2}]\Big]-\frac{1}{N^2}\sum_{k_1k_2}n_{k_1}n_{k_2}+\frac{1}{N^3}\sum_{k_2k_3}R_{k_1}L_{k_2}[Ln]_{k_3}[Rn]_{k_1-k_2+k_3}$$
$$+\frac{1}{N^3}\sum_{k_2k_3}R_{k_1}L_{k_2}[Ln]_{k_3}[Rn]_{k_1-k_2+k_3}+\frac{1}{N^3}\sum_{k_2k_3}R_{k_1}L_{k_2}n_{k_3}n_{k_1-k_2+k_3}. \quad (15.122)$$

For the $-s_{j\downarrow}s_{j\uparrow}\tilde{g}_{j\downarrow}\tilde{g}_{j\uparrow}$ term

$$s^\dagger_{j\uparrow}\tilde{g}_{j\uparrow}[-\langle s^\dagger_{j\downarrow}\tilde{g}_{j\downarrow}\rangle+R_0\langle g^\dagger_{j\uparrow}\tilde{g}_{j\downarrow}\rangle-R_0]+s^\dagger_{j\downarrow}\tilde{g}_{j\downarrow}[-\langle s^\dagger_{j\uparrow}\tilde{g}_{j\uparrow}\rangle+R_0\langle g^\dagger_{j\uparrow}\tilde{g}_{j\uparrow}\rangle-R_0]$$
$$+g^\dagger_{j\uparrow}\tilde{g}_{j\uparrow}[R_0\langle s^\dagger_{j\downarrow}\tilde{g}_{j\downarrow}\rangle-R_0^2\langle g^\dagger_{j\downarrow}\tilde{g}_{j\downarrow}\rangle+\frac{1}{2}R_0^2]+g^\dagger_{j\downarrow}\tilde{g}_{j\downarrow}[R_0\langle s^\dagger_{j\uparrow}\tilde{g}_{j\uparrow}\rangle-R_0^2\langle g^\dagger_{j\uparrow}\tilde{g}_{j\uparrow}\rangle+\frac{1}{2}R_0^2]$$
$$+\langle s^\dagger_{j\uparrow}\tilde{g}_{j\uparrow}\rangle\langle s^\dagger_{j\downarrow}\tilde{g}_{j\downarrow}\rangle-R_0\langle s^\dagger_{j\uparrow}\tilde{g}_{j\uparrow}\rangle\langle g^\dagger_{j\downarrow}\tilde{g}_{j\downarrow}\rangle-R_0\langle g^\dagger_{j\uparrow}\tilde{g}_{j\uparrow}\rangle\langle s^\dagger_{j\downarrow}\tilde{g}_{j\downarrow}\rangle+R_0^2\langle g^\dagger_{j\uparrow}\tilde{g}_{j\uparrow}\rangle\langle g^\dagger_{j\downarrow}\tilde{g}_{j\downarrow}\rangle, \quad (15.123)$$

$$\Rightarrow [s^\dagger_{j\uparrow}\tilde{g}_{j\uparrow}+s^\dagger_{j\downarrow}\tilde{g}_{j\downarrow}]\frac{1}{N}\sum_{k_1}[-R_{k_1}n_{k_1}-R_0(1-n_{k_1})]+[g^\dagger_{j\uparrow}\tilde{g}_{j\uparrow}+g^\dagger_{j\downarrow}\tilde{g}_{j\downarrow}]\frac{1}{N}\sum_{k_1}[R_0R_{k_1}n_{k_1}-R_0^2n_{k_1}+\frac{1}{2}R_0^2]$$
$$\frac{1}{N^2}\sum_{k_1k_2}[R_{k_1}n_{k_1}R_{k_2}n_{k_2}-R_{k_1}n_{k_1}R_0n_{k_1}-R_0n_{k_1}R_{k_1}n_{k_1}+R_0^2n_{k_1}n_{k_2}]. \quad (15.124)$$

For $-s_{j\downarrow}s_{j\uparrow}\tilde{g}_{j\downarrow}\tilde{g}_{j\uparrow}$ term

$$s_{j\downarrow}g^\dagger_{j\downarrow}[-\langle s_{j\uparrow}g^\dagger_{j\uparrow}\rangle+L_0\langle\tilde{g}_{j\uparrow}g^\dagger_{j\uparrow}\rangle-L_0]+s_{j\uparrow}g^\dagger_{j\uparrow}[-\langle s_{j\downarrow}g^\dagger_{j\downarrow}\rangle+L_0\langle\tilde{g}_{j\downarrow}g^\dagger_{j\downarrow}\rangle-L_0]$$
$$+\tilde{g}_{j\downarrow}g^\dagger_{j\downarrow}[L_0\langle s_{j\uparrow}g^\dagger_{j\uparrow}\rangle-L_0^2\langle\tilde{g}_{j\uparrow}g^\dagger_{j\uparrow}\rangle+\frac{1}{2}L_0^2]+\tilde{g}_{j\uparrow}g^\dagger_{j\uparrow}[L_0\langle s_{j\downarrow}g^\dagger_{j\downarrow}\rangle-L_0^2\langle\tilde{g}_{j\downarrow}g^\dagger_{j\downarrow}\rangle+\frac{1}{2}L_0^2]$$
$$+\langle s_{j\downarrow}g^\dagger_{j\downarrow}\rangle\langle s_{j\uparrow}g^\dagger_{j\uparrow}\rangle-L_0\langle\tilde{g}_{j\downarrow}g^\dagger_{j\downarrow}\rangle\langle s_{j\uparrow}g^\dagger_{j\uparrow}\rangle-L_0\langle s_{j\downarrow}g^\dagger_{j\downarrow}\rangle\langle\tilde{g}_{j\uparrow}g^\dagger_{j\uparrow}\rangle+L_0^2\langle\tilde{g}_{j\downarrow}g^\dagger_{j\downarrow}\rangle\langle\tilde{g}_{j\uparrow}g^\dagger_{j\uparrow}\rangle, \quad (15.125)$$

$$\Rightarrow [g^\dagger_{j\downarrow}s_{j\downarrow} + g^\dagger_{j\uparrow}s_{j\uparrow}]\frac{1}{N}\sum_{k_1}[L_{k_1}(1-n_{k_1}) + L_0 n_{k_1}]$$
$$+ [g^\dagger_{j\downarrow}\tilde{g}_{j\downarrow} + g^\dagger_{j\uparrow}\tilde{g}_{j\uparrow}]\frac{1}{N}\sum_{k_1}[L_0^2(1-n_{k_1}) - L_0 L_{k_1}(1-n_{k_1}) - \frac{1}{2}L_0^2]$$
$$\frac{1}{N^2}\sum_{k_1 k_2}\Big[L_{k_1}(1-n_{k_1})L_{k_2}(1-n_{k_2}) - L_0(1-n_{k_1})L_{k_2}(1-n_{k_2}) - L_{k_1}(1-n_{k_1})L_0(1-n_{k_2})$$
$$+ L_0^2(1-n_{k_1})(1-n_{k_2}) - L_{k_1}(1-n_{k_1}) - L_0 n_{k_1} + L_0 L_{k_1}(1-n_{k_1}) - L_0^2(1-n_{k_1}) + \frac{1}{2}L_0^2\Big]. \tag{15.126}$$

For the $\frac{1}{2}(\tilde{g}_{j\uparrow}g^\dagger_{j\uparrow} + \tilde{g}_{j\downarrow}g^\dagger_{j\downarrow})$ term

$$\Rightarrow -[\frac{1}{2}(g^\dagger_{j\uparrow}\tilde{g}_{j\uparrow} + g^\dagger_{j\downarrow}\tilde{g}_{j\downarrow})] + 1. \tag{15.127}$$

For the $s_{j\uparrow}\tilde{g}_{j\downarrow}g^\dagger_{j\downarrow}$ term

$$s^\dagger_{j\uparrow}s_{j\uparrow}\langle\tilde{g}_{j\downarrow}g^\dagger_{j\downarrow}\rangle - L_0 s^\dagger_{j\uparrow}\tilde{g}_{j\uparrow}\langle\tilde{g}_{j\downarrow}g^\dagger_{j\downarrow}\rangle + g^\dagger_{j\uparrow}s_{j\uparrow}[-R_0\langle\tilde{g}_{j\downarrow}g^\dagger_{j\downarrow}\rangle + R_0] + g^\dagger_{j\uparrow}\tilde{g}_{j\uparrow}[R_0 L_0\langle\tilde{g}_{j\downarrow}g^\dagger_{j\downarrow}\rangle - \frac{1}{2}R_0 L_0]$$
$$\tilde{g}_{j\downarrow}g^\dagger_{j\downarrow}[\langle s^\dagger_{j\uparrow}s_{j\uparrow}\rangle - L_0\langle s^\dagger_{j\uparrow}\tilde{g}_{j\uparrow}\rangle - R_0\langle g^\dagger_{j\uparrow}s_{j\uparrow}\rangle + R_0 L_0\langle g^\dagger_{j\uparrow}\tilde{g}_{j\uparrow}\rangle - \frac{1}{2}R_0 L_0 + R_0 L_0]$$
$$-\langle s^\dagger_{j\uparrow}s_{j\uparrow}\rangle\langle\tilde{g}_{j\downarrow}g^\dagger_{j\downarrow}\rangle + L_0\langle s^\dagger_{j\uparrow}\tilde{g}_{j\uparrow}\rangle\langle\tilde{g}_{j\downarrow}g^\dagger_{j\downarrow}\rangle + R_0\langle g^\dagger_{j\uparrow}s_{j\uparrow}\rangle\langle\tilde{g}_{j\downarrow}g^\dagger_{j\downarrow}\rangle - R_0 L_0\langle g^\dagger_{j\uparrow}\tilde{g}_{j\uparrow}\rangle\langle\tilde{g}_{j\downarrow}g^\dagger_{j\downarrow}\rangle - \frac{1}{2}R_0 L_0, \tag{15.128}$$

$$s^\dagger_{j\uparrow}s_{j\uparrow}\frac{1}{N}\sum_{k_1}[(1-n_{k_1})] + s^\dagger_{j\uparrow}\tilde{g}_{j\uparrow}\frac{1}{N}\sum_{k_1}[-L_0(1-n_{k_1})] + g^\dagger_{j\uparrow}s_{j\uparrow}\frac{1}{N}\sum_{k_1}[R_0 n_{k_1}]$$
$$g^\dagger_{j\uparrow}\tilde{g}_{j\uparrow}\frac{1}{N}\sum_{k_1}[R_0 L_0(1-n_{k_1}) - \frac{1}{2}R_0 L_0] + g^\dagger_{j\downarrow}\tilde{g}_{j\downarrow}\frac{1}{N}\sum_{k_1}[-n_{k_1} + L_0 R_{k_1} n_{k_1} - R_0 L_{k_1}(1-n_{k_1}) - R_0 L_0 n_{k_1}$$
$$+\frac{1}{2}R_0 L_0] + \frac{1}{N^2}\sum_{k_1 k_2}\Big[n_{k_1}(1-n_{k_2}) + L_0 R_{k_1} n_{k_1}(1-n_{k_2}) + R_0 L_{k_1} n_{k_1}(1-n_{k_2}) - R_0 L_0 n_{k_1}(1-n_{k_2})$$
$$- R_0 L_0 + n_{k_1} - L_0 R_{k_1} n_{k_1} + R_0 L_{k_1}(1-n_{k_1}) + R_0 L_0 n_{k_1}\Big]. \tag{15.129}$$

For the $s^\dagger_{j\downarrow}s_{j\downarrow}\tilde{g}_{j\uparrow}g^\dagger_{j\uparrow}$ term

$$s^\dagger_{j\downarrow}s_{j\downarrow}\langle\tilde{g}_{j\uparrow}g^\dagger_{j\uparrow}\rangle - L_0 s^\dagger_{j\downarrow}\tilde{g}_{j\downarrow}\langle\tilde{g}_{j\uparrow}g^\dagger_{j\uparrow}\rangle + g^\dagger_{j\downarrow}s_{j\downarrow}[-R_0\langle\tilde{g}_{j\uparrow}g^\dagger_{j\uparrow}\rangle + R_0] + g^\dagger_{j\downarrow}\tilde{g}_{j\downarrow}[R_0L_0\langle\tilde{g}_{j\uparrow}g^\dagger_{j\uparrow}\rangle - \frac{1}{2}R_0L_0]$$
$$\tilde{g}_{j\uparrow}g^\dagger_{j\uparrow}[\langle s^\dagger_{j\downarrow}s_{j\downarrow}\rangle - L_0\langle s^\dagger_{j\downarrow}\tilde{g}_{j\downarrow}\rangle - R_0\langle g^\dagger_{j\downarrow}s_{j\downarrow}\rangle + R_0L_0\langle g^\dagger_{j\downarrow}\tilde{g}_{j\downarrow}\rangle - \frac{1}{2}R_0L_0 + R_0L_0]$$
$$-\langle s^\dagger_{j\downarrow}s_{j\downarrow}\rangle\langle\tilde{g}_{j\uparrow}g^\dagger_{j\uparrow}\rangle + L_0\langle s^\dagger_{j\downarrow}\tilde{g}_{j\downarrow}\rangle\langle\tilde{g}_{j\uparrow}g^\dagger_{j\uparrow}\rangle + R_0\langle g^\dagger_{j\downarrow}s_{j\downarrow}\rangle\langle\tilde{g}_{j\uparrow}g^\dagger_{j\uparrow}\rangle - R_0L_0\langle g^\dagger_{j\downarrow}\tilde{g}_{j\downarrow}\rangle\langle\tilde{g}_{j\uparrow}g^\dagger_{j\uparrow}\rangle - \frac{1}{2}R_0L_0, \tag{15.130}$$

$$s^\dagger_{j\downarrow}s_{j\downarrow}\frac{1}{N}\sum_{k_1}[(1-n_{k_1})] + s^\dagger_{j\downarrow}\tilde{g}_{j\downarrow}\frac{1}{N}\sum_{k_1}[-L_0(1-n_{k_1})] + g^\dagger_{j\downarrow}s_{j\downarrow}\frac{1}{N}\sum_{k_1}[R_0n_{k_1}]$$
$$g^\dagger_{j\downarrow}\tilde{g}_{j\downarrow}\frac{1}{N}\sum_{k_1}[R_0L_0(1-n_{k_1}) - \frac{1}{2}R_0L_0] + g^\dagger_{j\uparrow}\tilde{g}_{j\uparrow}\frac{1}{N}\sum_{k_1}[-n_{k_1} + L_0R_{k_1}n_{k_1} - R_0L_{k_1}(1-n_{k_1}) - R_0L_0n_{k_1}$$
$$+\frac{1}{2}R_0L_0] + \frac{1}{N^2}\sum_{k_1k_2}\Big[n_{k_1}(1-n_{k_2}) + L_0R_{k_1}n_{k_1}(1-n_{k_2}) + R_0L_{k_1}n_{k_1}(1-n_{k_2}) - R_0L_0n_{k_1}(1-n_{k_2})$$
$$- R_0L_0 + n_{k_1} - L_0R_{k_1}n_{k_1} + R_0L_{k_1}(1-n_{k_1}) + R_0L_0n_{k_1}\Big]. \tag{15.131}$$

Putting it together we get

$$E_q = \frac{U}{2}[R_q\tilde{B}_q - L_qB_q - 2C_q]$$
$$2C_q = \frac{2}{U}\Big[2t_1Z\gamma_q + 2t_0\Big] + \frac{1}{N}\sum_{k_1}\Big[\big[[L_0+R_0]^2+1\big]\big[n_{k_1}-\frac{1}{2}\big]$$
$$+\big[L_0+R_0\big]\big[L_{k_1}(1-n_{k_1}) - R_{k_1}n_{k_1}\big] - \frac{1}{N^2}\sum_{k_2k_3}R_{k_1}R_{k_2}L_{k_3}L_{k_1+k_2-k_3}\big[n_{k_1-k_3+q}-\frac{1}{2}\big]\Big]$$

15.4.5 Calculating the Total Energy E

This is simple to calculate. We take the terms not contributing towards E_k and perform the summations.

$$E = -4t_1 Z \sum_k \gamma_k n_k + \frac{U}{2}\frac{1}{N^2}\sum_{k_1 k_2}\Bigg[1 + n_{k_1}\big[1-n_{k_2}\big]\big[1+[R_0+L_0]^2\big] - \big[R_0+L_0\big]\big[[1-n_{k_1}]R_{k_2}n_{k_2} + n_{k_1}L_{k_2}[1-n_{k_2}]\big] - \frac{B_{k_1}\tilde{B}_{k_1}}{\sqrt{C_{k_1}^2 + B_{k_1}\tilde{B}_{k_1}}} - \mathcal{R}_{k_1}\mathcal{L}_{k_1}\mathcal{N}_{k_1}\Bigg], \tag{15.132}$$

$$\mathcal{R}_k = \frac{1}{N}\frac{1}{2}\sum_{k_1} R_{k_1}[L_{k_1-k} + L_{k+k_1}] \tag{15.133}$$

$$\mathcal{L}_k = \frac{1}{N}\frac{1}{2}\sum_{k_1} L_{k_1}[R_{k_1-k} + R_{k+k_1}] \tag{15.134}$$

$$\mathcal{N}_k = \frac{1}{N}\frac{1}{2}\sum_{k_1}[1-n_{k_1}][n_{k_1-k} + n_{k+k_1}] \tag{15.135}$$

15.5 The Results

In this section we review the results and test them against exact diagonalisation. To recap the particle dispersion is given by

$$\epsilon_k = -2tZ\gamma_k + \frac{U}{2}\Big[1 + L_k B_k\Big], \tag{15.136}$$

and the hole dispersion is

$$\tilde{\epsilon}_k = -2tZ\gamma_k + \frac{U}{2}\Big[1 - R_k\tilde{B}_k\Big]. \tag{15.137}$$

The occupation factor is

$$n_k = \frac{-2t_1 Z\gamma_k - \epsilon_k - t_0 + \frac{U}{2}}{\tilde{\epsilon}_k - \epsilon_k}, \tag{15.138}$$

which can be rearranged using equations 15.136 and 15.137 to

$$n_k = \frac{L_k B_k}{L_k B_k + R_k \tilde{B}_k}, \tag{15.139}$$

which can be further simplified with $E_k = 0$ to

$$n_k = \frac{1}{2}\left[1 + \left[1 + \frac{B_k}{C_k}\frac{\tilde{B}_k}{C_k}\right]^{-\frac{1}{2}}\right]. \tag{15.140}$$

The total energy is

$$E = -4t_1 Z \sum_k \gamma_k n_k + \frac{U}{2}\frac{1}{N^2}\sum_{k_1 k_2}\Bigg[1 + n_{k_1}\big[1 - n_{k_2}\big]\big[1 + [R_0 + L_0]^2\big] \\ - \big[R_0 + L_0\big]\big[[1 - n_{k_1}]R_{k_2} n_{k_2} + n_{k_1} L_{k_2}[1 - n_{k_2}]\big] - \frac{B_{k_1}\tilde{B}_{k_1}}{\sqrt{C_{k_1}^2 + B_{k_1}\tilde{B}_{k_1}}} - \mathcal{R}_{k_1}\mathcal{L}_{k_1}\mathcal{N}_{k_1}\Bigg], \tag{15.141}$$

where

$$L_k = \frac{C_k}{B_k}\left[1 + \left[1 + \frac{B_k}{C_k}\frac{\tilde{B}_k}{C_k}\right]^{\frac{1}{2}}\right] \qquad R_k = \frac{1}{L_k}, \tag{15.142}$$

$$B_k = \frac{1}{N}\sum_{k_1}\left[[L_0 + R_0]\, n_{k_1} + [1 - n_{k_1}]\, L_{k_1} - \frac{1}{N}\sum_{k_2} R_{k_1} L_{k_2}[Rn]_{k-k_1+k_2}\right], \tag{15.143}$$

$$\tilde{B}_k = \frac{1}{N}\sum_{k_1}\left[[L_0 + R_0]\,[1 - n_{k_1}] + n_{k_1} R_{k_1} - \frac{1}{N}\sum_{k_2} R_{k_1} L_{k_2}[L[1 - n]]_{k+k_1-k_2}\right], \tag{15.144}$$

$$2C_k = \frac{4}{U} t Z \gamma_k - \frac{1}{N^3} \sum_{k_1 k_2 k_3} R_{k_1} L_{k_2} R_{k_3} L_{k_1 - k_2 + k_3} \left[n_{k_1 - k_2 - k} - \frac{1}{2} \right] + \left[[L_0 + R_0]^2 + 1 \right] \left[\frac{1}{N} \sum_k n_k - \frac{1}{2} \right] + [L_0 + R_0] \frac{1}{N} \sum_{k_1} \left[[1 - n_{k_1}] L_{k_1} - n_{k_1} R_{k_1} \right]. \tag{15.145}$$

$$\mathcal{R}_k = \frac{1}{N} \frac{1}{2} \sum_{k_1} R_{k_1} [L_{k_1 - k} + L_{k + k_1}] \tag{15.146}$$

$$\mathcal{L}_k = \frac{1}{N} \frac{1}{2} \sum_{k_1} L_{k_1} [R_{k_1 - k} + R_{k + k_1}] \tag{15.147}$$

$$\mathcal{N}_k = \frac{1}{N} \frac{1}{2} \sum_{k_1} [1 - n_{k_1}][n_{k_1 - k} + n_{k + k_1}] \tag{15.148}$$

So how do we see the fruits of our labour? This procedure is self consistent. We start with an ansatz of C_k, B_k, and $\tilde{B}_k$. These can be used to calculate n_k, L_k, and R_k which are then used to calculate C_k, B_k, and $\tilde{B}_k$. This cycle is repeated until convergence.

Figures 15.1 on page 160 and 15.2 on page 160 depict the particle and hole dispersion for varying U. The agreement to numerics is remarkable! The larger U is the better the agreement, but even down to approximately $U = 5$ has good agreement. Past this the convergence breaks down. The source of this breakdown is unknown.

Figure 15.3 on page 161 depicts the occupation factor for varying U. Again the agreement is remarkable. Analytically we expect the Fermi-Liquid discontinuity to be zero at the Mott point, and that is exactly what we see.

Table 15.1 depicts the total energy per site for varying system sizes and U. At the Mott point, the system finite size scales very well. For this reason the total energy fits rather well in this calculation.

Figure 15.1: Particle Dispersion at the Mott Point

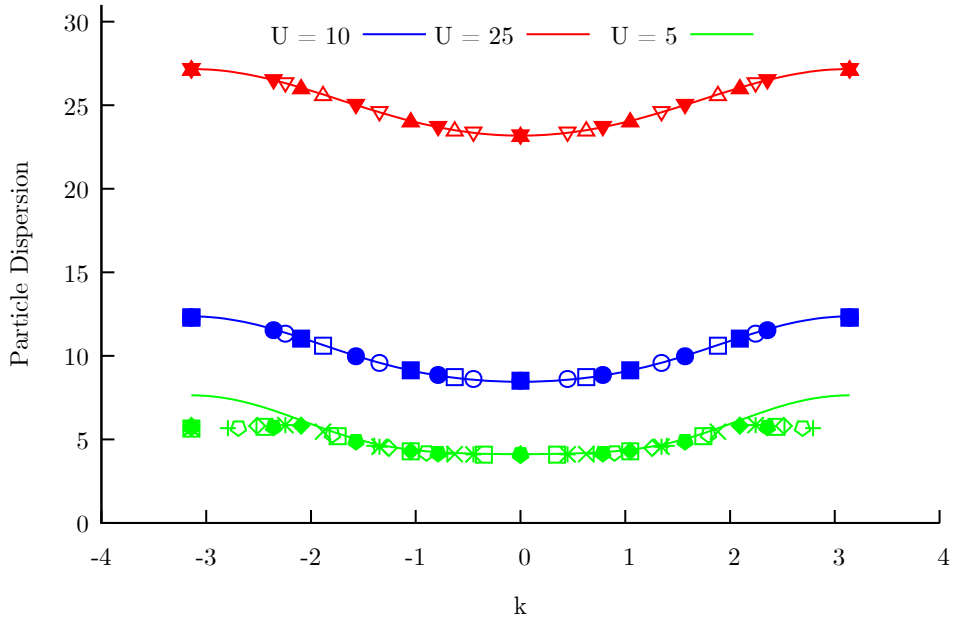

Plot of particle dispersion e_k against k for $U = 25$, $U = 10$ and $U = 5$. The points on the graph are finite size diagonalisation results for $n = 4, 5, 6, 7, 8, 9$ lattice sites.

Figure 15.2: Hole Dispersion at the Mott Point

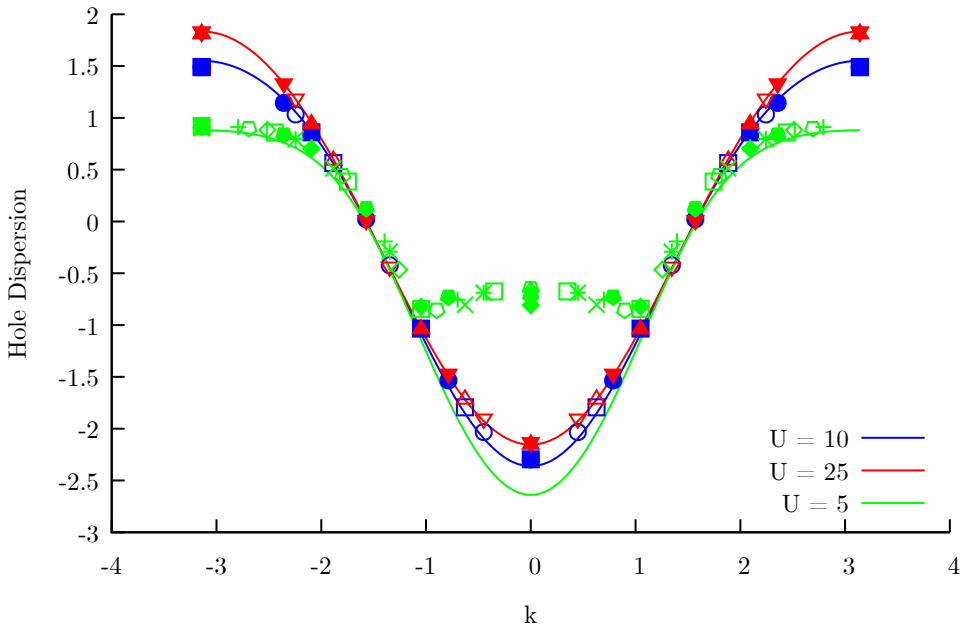

Plot of hole dispersion $\tilde{e}_k$ against k for $U = 25$, $U = 10$ and $U = 5$. The solid lines are the analytical results. The points on the graph are finite size diagonalisation results for $n = 4, 5, 6, 7, 8, 9$ lattice sites.

Figure 15.3: Occupation at the Mott Point

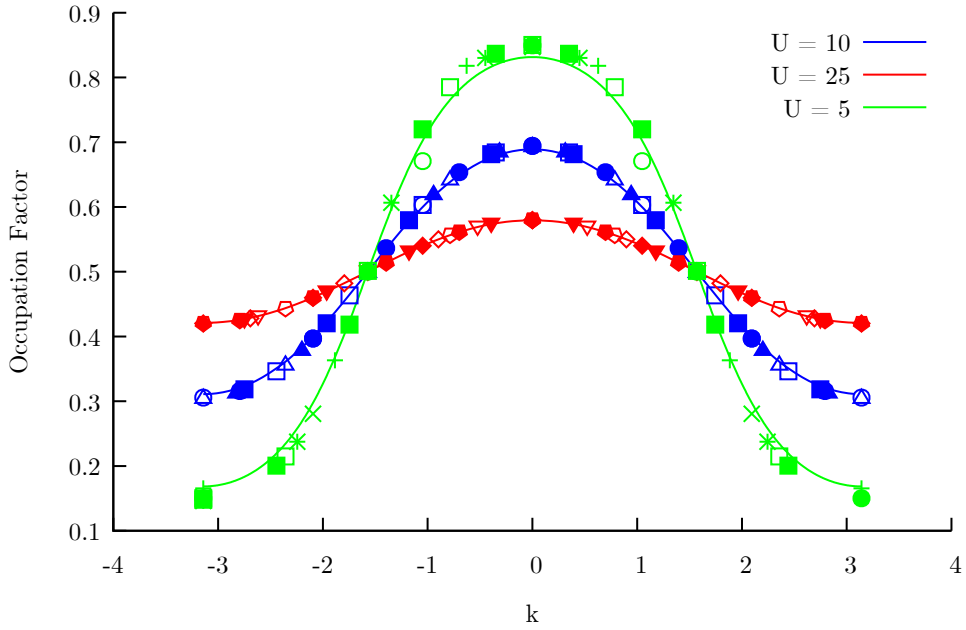

Plot of occupation factor n_k against k for $U = 25$, $U = 10$ and $U = 5$. The solid lines are the analytical results. The solid lines are the analytical results. The points on the graph are finite size diagonalisation results for $n = 4, 5, 6, 7, 8, 9$ lattice sites.

Table 15.1: Mott Point Total Energy

		$U = 10$	$U = 25$
Diagonalisation Energy System Size	4	-0.403186850861380	-0.160246118307604
	5	-0.398727682184652	-0.159985200325172
	6	-0.398814931982000	-0.159986038723485
	7	-0.398724733012764	-0.159985199309589
	8	-0.398727028565785	-0.159985202686994
	9	-0.398724721357989	-0.159985199311420
	10	-0.398724787565121	-0.159985199328586
Energy (Method)		-0.4016569360	-0.1600168947

Total energy per site for $U = 10$ and $U = 25$. Finite size diagonalisation compared to analytical result.

In this chapter we detailed and performed self-consistent distribution theory at the Mott point for our system. We were able to calculate the particle and hole dispersions, the occupation factor, and the total energy with remarkable accuracy. In the next chapter we extend this method away from the Mott point.

CHAPTER 16

BEYOND THE MOTT POINT — THE EFFECTS OF DOPING

This technique has shown remarkable success at the Mott point. However, if one were to pick a non-trivial point where a theory would be successful, it would be that point. Here the strong correlations are 'renormalised' into a simpler model, for example the Heisenberg model from the Hubbard model [74]. Away from this point things are more interesting and incredibly complicated, and usually very difficult to examine for example the $t - J$ model accurately. If our method extends to non-trivial doping and boasts the same success it could be of great use.

In this chapter we essentially repeat the work done in the previous chapter but at arbitrary doping. This is done by modifying the Mott state and reprocessing the calculations. The complications that arise are due to the equivalence principles. Namely, that they are only true at the Mott point. We deal with this via a set of commutators. After this the process is essentially identical except for more arduous algebra.

16.1 Modifications to the Method

In this section we modify the method to take into account doping. Essentially we require

$$H_S \left|K\right\rangle = E \left|K\right\rangle + \sum_{k\sigma} E_k \, g^\dagger_{k\sigma} \tilde{g}_{k\sigma} \left|K\right\rangle . \tag{16.1}$$

$$[H_S, s^\dagger_{k\sigma}] \left|K\right\rangle = \epsilon_k \, s^\dagger_{k\sigma} \left|K\right\rangle , \tag{16.2}$$

$$[s_{k\sigma}, H_S] \left|K\right\rangle = \tilde{\epsilon}_k \, s_{k\sigma} \left|K\right\rangle , \tag{16.3}$$

$$\frac{\left\langle K\right| \left\{ s_{k\sigma}, [H_S, s^\dagger_{k\sigma}] \right\} \left|K\right\rangle}{\left\langle K\right\rangle} = \epsilon_k \left(1 - n_k\right) + \tilde{\epsilon}_k \, n_k, \tag{16.4}$$

where

$$\left|K\right\rangle = \hat{K} \left|\psi\right\rangle \qquad \hat{K} = \prod_{k \in K\sigma} \tilde{g}_{k\sigma}. \tag{16.5}$$

the state $\left|K\right\rangle$ is simply hole doped away from the Mott state $\left|\psi\right\rangle$.

The issue with this is the equivalence principles

$$(\frac{1}{2} + A^z_j) \equiv \tilde{g}_{j\uparrow} g^\dagger_{j\uparrow} \equiv \tilde{g}_{j\downarrow} g^\dagger_{j\downarrow} \tag{16.6}$$

$$A^+_j \equiv g^\dagger_{j\downarrow} g^\dagger_{j\uparrow}, \tag{16.7}$$

$$A^-_j \equiv \tilde{g}_{j\uparrow} \tilde{g}_{j\downarrow}, \tag{16.8}$$

$$g^\dagger_{j\sigma} \tilde{g}_{j\bar{\sigma}} \left|\psi\right\rangle = 0, \tag{16.9}$$

$$\tilde{g}_{j\bar{\sigma}} g^\dagger_{j\sigma} \tilde{g}_{j\sigma} \left|\psi\right\rangle = \tilde{g}_{j\bar{\sigma}} \left|\psi\right\rangle . \tag{16.10}$$

are only true at the Mott point. We must therefore commute these operators through $\hat{K}$, apply the identity, and commute the result back. The commutators we require, and have been calculated, are

$$[\tilde{g}_{j_1\uparrow} g^\dagger_{j_2\uparrow}, \hat{K}] = \hat{K} \frac{1}{N} \sum_k e^{ik(j_1 - j_2)} \delta_{k \in K}, \quad [g^\dagger_{j_2\uparrow} \tilde{g}_{j_1\uparrow}, \hat{K}] = -\hat{K} \frac{1}{N} \sum_k e^{ik(j_1 - j_2)} \delta_{k \in K}, \tag{16.11}$$

$$[s_{j_1\uparrow}g^\dagger_{j_2\uparrow},\hat{K}] = \hat{K}\frac{1}{N}\sum_k e^{ik(j_1-j_2)}\delta_{k\in K}L_k, \quad [g^\dagger_{j_2\uparrow}s_{j_1\uparrow},\hat{K}] = -\hat{K}\frac{1}{N}\sum_k e^{ik(j_1-j_2)}\delta_{k\in K}L_k, \tag{16.12}$$

$$[\tilde{g}_{j_1\uparrow}s^\dagger_{j_2\uparrow},\hat{K}] = \hat{K}\frac{1}{N}\sum_k e^{ik(j_1-j_2)}\delta_{k\in K}R_k, \quad [s^\dagger_{j_2\uparrow}\tilde{g}_{j_1\uparrow},\hat{K}] = -\hat{K}\frac{1}{N}\sum_k e^{ik(j_1-j_2)}\delta_{k\in K}R_k. \tag{16.13}$$

We will use the following shorthand

$$\alpha = \frac{1}{N}\sum_k \delta_{k\in K}, \quad \tilde{L} = \frac{1}{N}\sum_k L_k\delta_{k\in K}, \quad \tilde{R} = \frac{1}{N}\sum_k R_k\delta_{k\in K}. \tag{16.14}$$

The rules of engagement are simple: If you have to commute a $\tilde{g}_{j\sigma}$ or $s_{j\sigma}$ we can do so without any worry. If we commute a $g^\dagger_{j\sigma}$ or $s^\dagger_{j\sigma}$ we must move the appropriate $g_{j\sigma}$ or $s_{j\sigma}$ with it. This is to ensure particle conservation.

In the following section we will repeat the calculation but away from the Mott point.

16.2 The Calculation — An Exercise in Arduous Algebra Part 2

In this section we will calculate E_k, this is a 'shortcut' to the all the key components. We will find that ϵ_k, $\tilde{\epsilon}_k$, n_k, L_k, and R_k are identical but B_k, $\tilde{B}_k$, and C_k are slightly augmented.

16.2.1 Calculating E_k

The Hamiltonian acting on $|K\rangle$ is given by

$$H_S = -2t\sum_{\langle ij\rangle\sigma} s^\dagger_{i\sigma}s_{j\sigma} - t_0\sum_{j\sigma}[s^\dagger_{j\sigma}s_{j\sigma} - \hat{K}\tilde{g}_{j\sigma}g^\dagger_{j\sigma}] + \frac{U}{2}\sum_j\Bigg[s^\dagger_{j\uparrow}s_{j\uparrow}s^\dagger_{j\downarrow}s_{j\downarrow}\hat{K} + s^\dagger_{j\uparrow}s^\dagger_{j\downarrow}\hat{K}\tilde{g}_{j\uparrow}\tilde{g}_{j\downarrow}$$
$$+ \hat{K}s_{j\downarrow}s_{j\uparrow}g^\dagger_{j\downarrow}g^\dagger_{j\uparrow} + \hat{K}\frac{1}{2}(\tilde{g}_{j\uparrow}g^\dagger_{j\uparrow} + \tilde{g}_{j\downarrow}g^\dagger_{j\downarrow}) + s^\dagger_{j\uparrow}s_{j\uparrow}\hat{K}\tilde{g}_{j\downarrow}g^\dagger_{j\downarrow} + s^\dagger_{j\downarrow}s_{j\downarrow}\hat{K}\tilde{g}_{j\uparrow}g^\dagger_{j\uparrow}\Bigg], \tag{16.15}$$

where application on $|\psi\rangle$ is implied. We consider each term, expand what would be the identity, commute through the terms and apply $g^\dagger_{j\sigma}\tilde{g}_{j\bar{\sigma}}|\psi\rangle = 0$, and commute back. For the $s^\dagger_{j\uparrow}s_{j\uparrow}s^\dagger_{j\downarrow}s_{j\downarrow}\hat{K}$ term

$$\begin{aligned}
s^\dagger_{j\uparrow}s_{j\uparrow}s^\dagger_{j\downarrow}s_{j\downarrow} \Rightarrow\ & s^\dagger_{j\uparrow}s_{j\uparrow}s^\dagger_{j\downarrow}s_{j\downarrow} - \sum_{j_1} R_{j-j_1}L_{j_1-j}g^\dagger_{j_1\uparrow}s_{j\uparrow}s^\dagger_{j\downarrow}\tilde{g}_{j_1\downarrow} + \sum_{j_1} R_{j-j_1}L_{j_1-j}g^\dagger_{j_1\uparrow}s_{j\uparrow}s^\dagger_{j\downarrow}\tilde{g}_{j_1\downarrow} \\
& - \sum_{j_2} R_{j-j_2}L_{j_2-j}s^\dagger_{j\uparrow}\tilde{g}_{j_2\uparrow}g^\dagger_{j_2\downarrow}s_{j\downarrow} + \sum_{j_1 j_2} R_{j-j_1}R_{j-j_2}L_{j_1-j}L_{j_2-j}g^\dagger_{j_1\uparrow}\tilde{g}_{j_2\uparrow}g^\dagger_{j_2\downarrow}\tilde{g}_{j_1\downarrow} \\
& + \sum_{j_2} R_{j-j_2}L_{j_2-j}s^\dagger_{j\uparrow}\tilde{g}_{j_2\uparrow}g^\dagger_{j_2\downarrow}s_{j\downarrow} - \sum_{j_1 j_2} R_{j-j_1}R_{j-j_2}L_{j_1-j}L_{j_2-j}g^\dagger_{j_1\uparrow}\tilde{g}_{j_2\uparrow}g^\dagger_{j_2\downarrow}\tilde{g}_{j_1\downarrow} \qquad (16.16)
\end{aligned}$$

The $\sum_{j_1 j_2} R_{j-j_1}R_{j-j_2}L_{j_1-j}L_{j_2-j}g^\dagger_{j_1\uparrow}\tilde{g}_{j_2\uparrow}g^\dagger_{j_2\downarrow}\tilde{g}_{j_1\downarrow}$ term is equal to (spin symmetry)

$$\begin{aligned}
& = \frac{1}{2}\Bigg[\sum_{j_1} R_{j-j_1}R_{j-j_1}L_{j_1-j}L_{j_1-j}g^\dagger_{j_1\downarrow}\tilde{g}_{j_1\downarrow} - \sum_{j_1 j_2} R_{j-j_1}R_{j-j_2}L_{j_1-j}L_{j_2-j}g^\dagger_{j_2\downarrow}\tilde{g}_{j_1\downarrow}\tilde{g}_{j_2\uparrow}g^\dagger_{j_1\uparrow} \\
& \sum_{j_1} R_{j-j_1}R_{j-j_1}L_{j_1-j}L_{j_1-j}g^\dagger_{j_1\uparrow}\tilde{g}_{j_1\uparrow} - \sum_{j_1 j_2} R_{j-j_1}R_{j-j_2}L_{j_1-j}L_{j_2-j}g^\dagger_{j_1\uparrow}\tilde{g}_{j_2\uparrow}\tilde{g}_{j_1\downarrow}g^\dagger_{j_2\downarrow}\Bigg]\hat{K} \qquad (16.17) \\
& = \frac{1}{2}\Bigg[\sum_{j_1} R_{j-j_1}R_{j-j_1}L_{j_1-j}L_{j_1-j}g^\dagger_{j_1\downarrow}\tilde{g}_{j_1\downarrow}\hat{K} + \sum_{j_1} R_{j-j_1}R_{j-j_1}L_{j_1-j}L_{j_1-j}g^\dagger_{j_1\uparrow}\tilde{g}_{j_1\uparrow}\hat{K} \\
& - \sum_{j_1 j_2} R_{j-j_1}R_{j-j_2}L_{j_1-j}L_{j_2-j}g^\dagger_{j_2\downarrow}\hat{K}\left(\tilde{g}_{j_2\uparrow}g^\dagger_{j_1\uparrow} + \frac{1}{N}\sum_k e^{ik(j_2-j_1)}\delta_{k\in K}\right)\tilde{g}_{j_1\downarrow} \\
& - \sum_{j_1 j_2} R_{j-j_1}R_{j-j_2}L_{j_1-j}L_{j_2-j}g^\dagger_{j_1\uparrow}\hat{K}\tilde{g}_{j_2\uparrow}\left(\tilde{g}_{j_1\downarrow}g^\dagger_{j_2\downarrow} + \frac{1}{N}\sum_k e^{ik(j_1-j_2)}\delta_{k\in K}\right)\Bigg] \qquad (16.18) \\
& = \frac{1}{2}\Bigg[\sum_{j_1} R_{j-j_1}R_{j-j_1}L_{j_1-j}L_{j_1-j}g^\dagger_{j_1\downarrow}\tilde{g}_{j_1\downarrow} + \sum_{j_1} R_{j-j_1}R_{j-j_1}L_{j_1-j}L_{j_1-j}g^\dagger_{j_1\uparrow}\tilde{g}_{j_1\uparrow} \\
& - \sum_{j_1 j_2} R_{j-j_1}R_{j-j_2}L_{j_1-j}L_{j_2-j}\frac{1}{N}\sum_k \delta_{k\in K}\left(e^{ik(j_2-j_1)}g^\dagger_{j_2\downarrow}\tilde{g}_{j_1\downarrow} + e^{ik(j_1-j_2)}g^\dagger_{j_1\uparrow}\tilde{g}_{j_2\uparrow}\right)\Bigg]\hat{K} \qquad (16.19)
\end{aligned}$$

The $\sum_{j_1} R_{j-j_1} L_{j_1-j} g^\dagger_{j_1\uparrow} s_{j\uparrow} s^\dagger_{j\downarrow} \tilde{g}_{j_1\downarrow} \hat{K}$ term is equal to

$$= \sum_{j_1} R_{j-j_1} L_{j_1-j} L_{j_1-j} s^\dagger_{j\downarrow} \tilde{g}_{j_1\downarrow} \hat{K} - \sum_{j_1} R_{j-j_1} L_{j_1-j} s^\dagger_{j\downarrow} s_{j\uparrow} g^\dagger_{j_1\uparrow} \tilde{g}_{j_1\downarrow} \hat{K} \tag{16.20}$$

$$= \sum_{j_1} R_{j-j_1} L_{j_1-j} L_{j_1-j} s^\dagger_{j\downarrow} \tilde{g}_{j_1\downarrow} \hat{K} - \sum_{j_1} R_{j-j_1} L_{j_1-j} s^\dagger_{j\downarrow} \hat{K} \left(s_{j\uparrow} g^\dagger_{j_1\uparrow} + \frac{1}{N} \sum_k e^{ik(j-j_1)} \delta_{k\in K} L_k \right) \tilde{g}_{j_1\downarrow} \tag{16.21}$$

$$= \sum_{j_1} R_{j-j_1} L_{j_1-j} L_{j_1-j} s^\dagger_{j\downarrow} \tilde{g}_{j_1\downarrow} \hat{K} - \sum_{j_1} R_{j-j_1} L_{j_1-j} s^\dagger_{j\downarrow} \hat{K} \frac{1}{N} \sum_k e^{ik(j-j_1)} \delta_{k\in K} L_k \tilde{g}_{j_1\downarrow} \tag{16.22}$$

The $\sum_{j_2} R_{j-j_2} L_{j_2-j} s^\dagger_{j\uparrow} \tilde{g}_{j_2\uparrow} g^\dagger_{j_2\downarrow} s_{j\downarrow} \hat{K}$ is equal to

$$= \sum_{j_2} R_{j-j_2} L_{j_2-j} L_{j_2-j} s^\dagger_{j\uparrow} \tilde{g}_{j_2\uparrow} \hat{K} - \sum_{j_2} R_{j-j_2} L_{j_2-j} s^\dagger_{j\uparrow} \tilde{g}_{j_2\uparrow} s_{j\downarrow} g^\dagger_{j_2\downarrow} \hat{K} \tag{16.23}$$

$$= \sum_{j_2} R_{j-j_2} L_{j_2-j} L_{j_2-j} s^\dagger_{j\uparrow} \tilde{g}_{j_2\uparrow} \hat{K} - \sum_{j_2} R_{j-j_2} L_{j_2-j} s^\dagger_{j\uparrow} \hat{K} \tilde{g}_{j_2\uparrow} \left(s_{j\downarrow} g^\dagger_{j_2\downarrow} + \frac{1}{N} \sum_k e^{ik(j-j_2)} \delta_{k\in K} L_k \right) \tag{16.24}$$

$$= \sum_{j_2} R_{j-j_2} L_{j_2-j} L_{j_2-j} s^\dagger_{j\uparrow} \tilde{g}_{j_2\uparrow} \hat{K} - \sum_{j_2} R_{j-j_2} L_{j_2-j} s^\dagger_{j\uparrow} \hat{K} \tilde{g}_{j_2\uparrow} \frac{1}{N} \sum_k e^{ik(j-j_2)} \delta_{k\in K} L_k \tag{16.25}$$

Putting all this together and averaging gives

$$
\begin{aligned}
&s^\dagger_{j\uparrow}s_{j\uparrow}\langle s^\dagger_{j\downarrow}s_{j\downarrow}\rangle + \langle s^\dagger_{j\uparrow}s_{j\uparrow}\rangle s^\dagger_{j\downarrow}s_{j\downarrow} - \langle s^\dagger_{j\uparrow}s_{j\uparrow}\rangle\langle s^\dagger_{j\downarrow}s_{j\downarrow}\rangle - \sum_{j_1} R_{j-j_1}L_{j_1-j}g^\dagger_{j_1\uparrow}s_{j\uparrow}\langle s^\dagger_{j\downarrow}\tilde{g}_{j_1\downarrow}\rangle \\
&-\sum_{j_1} R_{j-j_1}L_{j_1-j}\langle g^\dagger_{j_1\uparrow}s_{j\uparrow}\rangle s^\dagger_{j\downarrow}\tilde{g}_{j_1\downarrow} + \sum_{j_1} R_{j-j_1}L_{j_1-j}\langle g^\dagger_{j_1\uparrow}s_{j\uparrow}\rangle\langle s^\dagger_{j\downarrow}\tilde{g}_{j_1\downarrow}\rangle - \sum_{j_2} R_{j-j_2}L_{j_2-j}s^\dagger_{j\uparrow}\tilde{g}_{j_2\uparrow}\langle g^\dagger_{j_2\downarrow}s_{j\downarrow}\rangle \\
&\qquad - \sum_{j_2} R_{j-j_2}L_{j_2-j}\langle s^\dagger_{j\uparrow}\tilde{g}_{j_2\uparrow}\rangle g^\dagger_{j_2\downarrow}s_{j\downarrow} + \sum_{j_2} R_{j-j_2}L_{j_2-j}\langle s^\dagger_{j\uparrow}\tilde{g}_{j_2\uparrow}\rangle\langle g^\dagger_{j_2\downarrow}s_{j\downarrow}\rangle \\
&+ \sum_{j_1 j_2} R_{j-j_1}R_{j-j_2}L_{j_1-j}L_{j_2-j}g^\dagger_{j_1\uparrow}\tilde{g}_{j_2\uparrow}\langle g^\dagger_{j_2\downarrow}\tilde{g}_{j_1\downarrow}\rangle + \sum_{j_1 j_2} R_{j-j_1}R_{j-j_2}L_{j_1-j}L_{j_2-j}\langle g^\dagger_{j_1\uparrow}\tilde{g}_{j_2\uparrow}\rangle g^\dagger_{j_2\downarrow}\tilde{g}_{j_1\downarrow} \\
&\qquad - \sum_{j_1 j_2} R_{j-j_1}R_{j-j_2}L_{j_1-j}L_{j_2-j}\langle g^\dagger_{j_1\uparrow}\tilde{g}_{j_2\uparrow}\rangle\langle g^\dagger_{j_2\downarrow}\tilde{g}_{j_1\downarrow}\rangle + \sum_{j_1} R_{j-j_1}L_{j_1-j}L_{j_1-j}s^\dagger_{j\downarrow}\tilde{g}_{j_1\downarrow} \\
&\qquad - \sum_{j_1} R_{j-j_1}L_{j_1-j}\frac{1}{N}\sum_k e^{ik(j-j_1)}\delta_{k\in K}L_k s^\dagger_{j\downarrow}\tilde{g}_{j_1\downarrow} + \sum_{j_2} R_{j-j_2}L_{j_2-j}L_{j_2-j}s^\dagger_{j\uparrow}\tilde{g}_{j_2\uparrow} \\
&- \sum_{j_2} R_{j-j_2}L_{j_2-j}s^\dagger_{j\uparrow}\tilde{g}_{j_2\uparrow}\frac{1}{N}\sum_k e^{ik(j-j_2)}\delta_{k\in K}L_k - \frac{1}{2}\Bigg[\sum_{j_1} R_{j-j_1}R_{j-j_1}L_{j_1-j}L_{j_1-j}g^\dagger_{j_1\downarrow}\tilde{g}_{j_1\downarrow} \\
&\qquad + \sum_{j_1} R_{j-j_1}R_{j-j_1}L_{j_1-j}L_{j_1-j}g^\dagger_{j_1\uparrow}\tilde{g}_{j_1\uparrow} \\
&- \sum_{j_1 j_2} R_{j-j_1}R_{j-j_2}L_{j_1-j}L_{j_2-j}\frac{1}{N}\sum_k \delta_{k\in K}\left(e^{ik(j_2-j_1)}g^\dagger_{j_2\downarrow}\tilde{g}_{j_1\downarrow} + e^{ik(j_1-j_2)}g^\dagger_{j_1\uparrow}\tilde{g}_{j_2\uparrow}\right)\Bigg] \qquad (16.26)
\end{aligned}
$$

Bloch transforming this and putting it together gives

$$
\begin{aligned}
&\left[g^\dagger_{q\uparrow}\tilde{g}_{q\uparrow} + g^\dagger_{q\uparrow}\tilde{g}_{q\uparrow}\right]\frac{1}{N}\sum_{k_1}\Big[n_{k_1} - \frac{1}{N}\sum_{k_2} R_{k_1}L_{k_2}[Rn]_{k_1-k_2+q}L_q \\
&+\frac{1}{N}\sum_{k_2} R_{k_1}L_{k_2}[L(1-n-\delta_{\in K})]_{k_2-k_1+q}R_q\frac{1}{N^2}\sum_{k_2k_3} R_{k_1}R_{k_2}L_{k_3}L_{k_1+k_2-k_3}\big[[n+\frac{1}{2}\delta_{\in K}]_{k_1-k_3+q}-\frac{1}{2}\big]\Big] \\
&\qquad - \frac{1}{N^2}\sum_{k_1k_2} n_{k_1}n_{k_2} + \frac{1}{N^3}\sum_{k_1k_2k_3}\Big[2R_{k_1}L_{k_2}\big[[Ln][Rn] - [n][n]\big]_{k_3,k_1-k_2+k_3}\Big] \qquad (16.27)
\end{aligned}
$$

For the $s^\dagger_{j\uparrow}s^\dagger_{j\downarrow}\hat{K}\tilde{g}_{j\uparrow}\tilde{g}_{j\downarrow}$ term

$$
\begin{aligned}
&s^\dagger_{j\uparrow}s^\dagger_{j\downarrow}\hat{K}\tilde{g}_{j\uparrow}\tilde{g}_{j\downarrow} \Rightarrow s^\dagger_{j\uparrow}s^\dagger_{j\downarrow}\hat{K}\tilde{g}_{j\uparrow}\tilde{g}_{j\downarrow} - R_0 s^\dagger_{j\uparrow}g^\dagger_{j\downarrow}\hat{K}\tilde{g}_{j\uparrow}\tilde{g}_{j\downarrow} - R_0 g^\dagger_{j\uparrow}s^\dagger_{j\downarrow}\hat{K}\tilde{g}_{j\uparrow}\tilde{g}_{j\downarrow} \\
&\quad + R_0^2 g^\dagger_{j\uparrow}g^\dagger_{j\downarrow}\hat{K}\tilde{g}_{j\uparrow}\tilde{g}_{j\downarrow} + R_0 s^\dagger_{j\uparrow}g^\dagger_{j\downarrow}\hat{K}\tilde{g}_{j\uparrow}\tilde{g}_{j\downarrow} + R_0 g^\dagger_{j\uparrow}s^\dagger_{j\downarrow}\hat{K}\tilde{g}_{j\uparrow}\tilde{g}_{j\downarrow} - R_0^2 g^\dagger_{j\uparrow}g^\dagger_{j\downarrow}\hat{K}\tilde{g}_{j\uparrow}\tilde{g}_{j\downarrow} \qquad (16.28)
\end{aligned}
$$

Applying the identity gives

$$R_0 s^\dagger_{j\uparrow} g^\dagger_{j\downarrow} \hat{K} \tilde{g}_{j\uparrow} \tilde{g}_{j\downarrow} = -R_0 s^\dagger_{j\uparrow} g^\dagger_{j\downarrow} \tilde{g}_{j\downarrow} \hat{K} \tilde{g}_{j\uparrow} \tag{16.29}$$

$$= -R_0 s^\dagger_{j\uparrow} \hat{K} (g^\dagger_{j\downarrow} \tilde{g}_{j\downarrow} - \alpha) \tilde{g}_{j\uparrow} \tag{16.30}$$

$$= R_0(\alpha - 1) s^\dagger_{j\uparrow} \tilde{g}_{j\uparrow} \hat{K} \tag{16.31}$$

$$R_0 g^\dagger_{j\uparrow} s^\dagger_{j\downarrow} \hat{K} \tilde{g}_{j\uparrow} \tilde{g}_{j\downarrow} = R_0(\alpha - 1) s^\dagger_{j\downarrow} \tilde{g}_{j\downarrow} \hat{K} \tag{16.32}$$

Spin symmetry of this term requires averaging both spin-up and spin-down contributions

$$R_0^2 g^\dagger_{j\uparrow} g^\dagger_{j\downarrow} \hat{K} \tilde{g}_{j\uparrow} \tilde{g}_{j\downarrow} = -\frac{1}{2} R_0^2 (\alpha - 1)(g^\dagger_{j\uparrow} \tilde{g}_{j\uparrow} + g^\dagger_{j\downarrow} \tilde{g}_{j\downarrow}) \hat{K}. \tag{16.33}$$

Collecting these and averaging gives

$$\begin{aligned} &s^\dagger_{j\uparrow} \tilde{g}_{j\uparrow} [-\langle s^\dagger_{j\downarrow} \tilde{g}_{j\downarrow} \rangle + R_0 \langle g^\dagger_{j\downarrow} \tilde{g}_{j\downarrow} \rangle + R_0(\alpha - 1)] + s^\dagger_{j\downarrow} \tilde{g}_{j\downarrow} [-\langle s^\dagger_{j\uparrow} \tilde{g}_{j\uparrow} \rangle + R_0 \langle g^\dagger_{j\uparrow} \tilde{g}_{j\uparrow} \rangle + R_0(\alpha - 1)] \\ &+ g^\dagger_{j\uparrow} \tilde{g}_{j\uparrow} [R_0 \langle s^\dagger_{j\downarrow} \tilde{g}_{j\downarrow} \rangle - R_0^2 \langle g^\dagger_{j\downarrow} \tilde{g}_{j\downarrow} \rangle - \frac{1}{2} R_0^2 (\alpha - 1)] + g^\dagger_{j\downarrow} \tilde{g}_{j\downarrow} [R_0 \langle s^\dagger_{j\uparrow} \tilde{g}_{j\uparrow} \rangle - R_0^2 \langle g^\dagger_{j\uparrow} \tilde{g}_{j\uparrow} \rangle - \frac{1}{2} R_0^2 (\alpha - 1)] \\ &+ \langle s^\dagger_{j\uparrow} \tilde{g}_{j\uparrow} \rangle \langle s^\dagger_{j\downarrow} \tilde{g}_{j\downarrow} \rangle - R_0 \langle s^\dagger_{j\uparrow} \tilde{g}_{j\uparrow} \rangle \langle g^\dagger_{j\downarrow} \tilde{g}_{j\downarrow} \rangle - R_0 \langle g^\dagger_{j\uparrow} \tilde{g}_{j\uparrow} \rangle \langle s^\dagger_{j\downarrow} \tilde{g}_{j\downarrow} \rangle + R_0^2 \langle g^\dagger_{j\uparrow} \tilde{g}_{j\uparrow} \rangle \langle g^\dagger_{j\downarrow} \tilde{g}_{j\downarrow} \rangle. \end{aligned} \tag{16.34}$$

Bloch transforming this gives

$$\begin{aligned} [s^\dagger_{j\uparrow} \tilde{g}_{j\uparrow} + s^\dagger_{j\downarrow} \tilde{g}_{j\downarrow}] \frac{1}{N} \sum_{k_1} &[-R_{k_1} n_{k_1} - R_0(1 - n_{k_1} - \delta_{k_1 \in K})] \\ &+ [g^\dagger_{j\uparrow} \tilde{g}_{j\uparrow} + g^\dagger_{j\downarrow} \tilde{g}_{j\downarrow}] \frac{1}{N} \sum_{k_1} [R_0 R_{k_1} n_{k_1} - R_0^2 n_{k_1} + \frac{1}{2}(1 - \delta_{k_1 \in K})] \\ &\frac{1}{N^2} \sum_{k_1 k_2} [R_{k_1} n_{k_1} R_{k_2} n_{k_2} - R_{k_1} n_{k_1} R_0 n_{k_2} - R_0 n_{k_1} R_{k_2} n_{k_2} + R_0 n_{k_1} R_0 n_{k_2}] \end{aligned} \tag{16.35}$$

For the $\hat{K}s_{j\downarrow}s_{j\uparrow}g^\dagger_{j\downarrow}g^\dagger_{j\uparrow}$ term

$$\hat{K}s_{j\downarrow}s_{j\uparrow}g^\dagger_{j\downarrow}g^\dagger_{j\uparrow} \Rightarrow \hat{K}\Big[s_{j\downarrow}s_{j\uparrow}g^\dagger_{j\downarrow}g^\dagger_{j\uparrow} - L_0\tilde{g}_{j\downarrow}s_{j\uparrow}g^\dagger_{j\downarrow}g^\dagger_{j\uparrow} - L_0 s_{j\uparrow}g^\dagger_{j\uparrow} - L_0 s_{j\downarrow}\tilde{g}_{j\uparrow}g^\dagger_{j\downarrow}g^\dagger_{j\uparrow} - L_0 s_{j\downarrow}g^\dagger_{j\downarrow} + L_0^2\tilde{g}_{j\downarrow}\tilde{g}_{j\uparrow}g^\dagger_{j\downarrow}g^\dagger_{j\uparrow} + \frac{1}{2}(\tilde{g}_{j\uparrow}g^\dagger_{j\uparrow} + \tilde{g}_{j\downarrow}g^\dagger_{j\downarrow})\Big] \quad (16.36)$$

Commuting $\hat{K}$ through and averaging gives

$$\begin{aligned}
&- s_{j\downarrow}g^\dagger_{j\downarrow}\langle s_{j\uparrow}g^\dagger_{j\uparrow}\rangle - \langle s_{j\downarrow}g^\dagger_{j\downarrow}\rangle s_{j\uparrow}g^\dagger_{j\uparrow} + \langle s_{j\downarrow}g^\dagger_{j\downarrow}\rangle\langle s_{j\uparrow}g^\dagger_{j\uparrow}\rangle + L_0\tilde{g}_{j\downarrow}g^\dagger_{j\downarrow}\langle s_{j\uparrow}g^\dagger_{j\uparrow}\rangle + L_0\langle\tilde{g}_{j\downarrow}g^\dagger_{j\downarrow}\rangle s_{j\uparrow}g^\dagger_{j\uparrow}\\
&- L_0\langle\tilde{g}_{j\downarrow}g^\dagger_{j\downarrow}\rangle\langle s_{j\uparrow}g^\dagger_{j\uparrow}\rangle - L_0 s_{j\uparrow}g^\dagger_{j\uparrow} + L_0 s_{j\downarrow}g^\dagger_{j\downarrow}\langle\tilde{g}_{j\uparrow}g^\dagger_{j\uparrow}\rangle + L_0\langle s_{j\downarrow}g^\dagger_{j\downarrow}\rangle\tilde{g}_{j\uparrow}g^\dagger_{j\uparrow} - L_0\langle s_{j\downarrow}g^\dagger_{j\downarrow}\rangle\langle\tilde{g}_{j\uparrow}g^\dagger_{j\uparrow}\rangle\\
&- L_0 s_{j\downarrow}g^\dagger_{j\downarrow} - L_0^2\tilde{g}_{j\downarrow}g^\dagger_{j\downarrow}\langle\tilde{g}_{j\uparrow}g^\dagger_{j\uparrow}\rangle - L_0^2\langle\tilde{g}_{j\downarrow}g^\dagger_{j\downarrow}\rangle\tilde{g}_{j\uparrow}g^\dagger_{j\uparrow} + L_0^2\langle\tilde{g}_{j\downarrow}g^\dagger_{j\downarrow}\rangle\langle\tilde{g}_{j\uparrow}g^\dagger_{j\uparrow}\rangle + \frac{1}{2}L_0^2(\tilde{g}_{j\downarrow}g^\dagger_{j\downarrow} + \tilde{g}_{j\uparrow}g^\dagger_{j\uparrow})\\
&+ \tilde{L}(s_{j\downarrow}g^\dagger_{j\downarrow} + s_{j\uparrow}g^\dagger_{j\uparrow}) - \tilde{L}^2 - L_0\alpha s_{j\uparrow}g^\dagger_{j\uparrow} - L_0\tilde{L}\tilde{g}_{j\downarrow}g^\dagger_{j\downarrow} + \alpha L_0\tilde{L} + L_0\tilde{L} - L_0\alpha s_{j\downarrow}g^\dagger_{j\downarrow} - L_0\tilde{L}\tilde{g}_{j\uparrow}g^\dagger_{j\uparrow}\\
&+ L_0\alpha\tilde{L} + L_0\tilde{L} + L_0^2\alpha\tilde{g}_{j\uparrow}g^\dagger_{j\uparrow} + L_0^2\alpha\tilde{g}_{j\downarrow}g^\dagger_{j\downarrow} - L_0^2\alpha^2, \quad (16.37)
\end{aligned}$$

which upon Bloch transforming becomes

$$\begin{aligned}
&[s_{j\downarrow}g^\dagger_{j\downarrow} + s_{j\uparrow}g^\dagger_{j\uparrow}]\frac{1}{N}\sum_{k_1}[-L_{k_1}(1 - n_{k_1} - \delta_{k_1\in K}) - L_0(n_{k_1} + \delta_{k_1\in K})]\\
&\quad + [\tilde{g}_{j\downarrow}g^\dagger_{j\downarrow} + \tilde{g}_{j\uparrow}g^\dagger_{j\uparrow}]\frac{1}{N}\sum_{k_1}[L_0L_{k_1}(1 - n_{k_1} - \delta_{k_1\in K}) - L_0^2(1 - n_{k_1} - \delta_{k_1\in K}) + \frac{1}{2}L_0^2]\\
&\frac{1}{N^2}\sum_{k_1k_2}[L_{k_1}(1 - n_{k_1})L_{k_2}(1 - n_{k_2}) - L_{k_1}(1 - n_{k_1})L_0(1 - n_{k_2}) - L_0(1 - n_{k_1})L_{k_2}(1 - n_{k_2})\\
&\quad + L_0(1 - n_{k_1})L_0(1 - n_{k_2}) - \tilde{L}^2 - L_0^2\alpha^2 + 2\alpha L_0\tilde{L} + 2L_0\tilde{L}]. \quad (16.38)
\end{aligned}$$

For the $\hat{K}\frac{1}{2}(\tilde{g}_{j\uparrow}g^\dagger_{j\uparrow} + \tilde{g}_{j\downarrow}g^\dagger_{j\downarrow})$ we trivially get

$$\hat{K}\frac{1}{2}(\tilde{g}_{j\uparrow}g^\dagger_{j\uparrow} + \tilde{g}_{j\downarrow}g^\dagger_{j\downarrow}) = \frac{1}{2}(\tilde{g}_{j\uparrow}g^\dagger_{j\uparrow} + \tilde{g}_{j\downarrow}g^\dagger_{j\downarrow} - 2\alpha)\hat{K} \quad (16.39)$$

For the $s^\dagger_{j\uparrow}s_{j\uparrow}\hat{K}\tilde{g}_{j\downarrow}g^\dagger_{j\downarrow} + s^\dagger_{j\downarrow}s_{j\downarrow}\hat{K}\tilde{g}_{j\uparrow}g^\dagger_{j\uparrow}$ term we first consider $s^\dagger_{j\uparrow}s_{j\uparrow}\hat{K}\tilde{g}_{j\downarrow}g^\dagger_{j\downarrow}$ term and add the spin flipped result

$$\begin{aligned}s^\dagger_{j\uparrow}s_{j\uparrow}\hat{K}\tilde{g}_{j\downarrow}g^\dagger_{j\downarrow} \Rightarrow s^\dagger_{j\uparrow}s_{j\uparrow}\hat{K}\tilde{g}_{j\downarrow}g^\dagger_{j\downarrow} - L_0 s^\dagger_{j\uparrow}\tilde{g}_{j\uparrow}\hat{K}\tilde{g}_{j\downarrow}g^\dagger_{j\downarrow} - R_0 g^\dagger_{j\uparrow}s_{j\uparrow}\hat{K}\tilde{g}_{j\downarrow}g^\dagger_{j\downarrow} + R_0L_0 g^\dagger_{j\uparrow}\tilde{g}_{j\uparrow}\hat{K}\tilde{g}_{j\downarrow}g^\dagger_{j\downarrow}\\ + L_0 s^\dagger_{j\uparrow}\tilde{g}_{j\uparrow}\hat{K}\tilde{g}_{j\downarrow}g^\dagger_{j\downarrow} + R_0 g^\dagger_{j\uparrow}s_{j\uparrow}\hat{K}\tilde{g}_{j\downarrow}g^\dagger_{j\downarrow} - R_0L_0 g^\dagger_{j\uparrow}\tilde{g}_{j\uparrow}\hat{K}\tilde{g}_{j\downarrow}g^\dagger_{j\downarrow} \quad (16.40)\end{aligned}$$

Commuting through and averaging gives

$$\begin{aligned}&- \langle s^\dagger_{j\uparrow}s_{j\uparrow}\rangle\langle\tilde{g}_{j\downarrow}g^\dagger_{j\downarrow}\rangle + L_0\langle s^\dagger_{j\uparrow}\tilde{g}_{j\uparrow}\rangle\langle\tilde{g}_{j\downarrow}g^\dagger_{j\downarrow}\rangle + R_0\langle g^\dagger_{j\uparrow}s_{j\uparrow}\rangle\langle\tilde{g}_{j\downarrow}g^\dagger_{j\downarrow}\rangle - R_0L_0\langle g^\dagger_{j\uparrow}\tilde{g}_{j\uparrow}\rangle\langle\tilde{g}_{j\downarrow}g^\dagger_{j\downarrow}\rangle\\ &+ \langle s^\dagger_{j\uparrow}s_{j\uparrow}\rangle - L_0\langle s^\dagger_{j\uparrow}\tilde{g}_{j\uparrow}\rangle - R_0\langle g^\dagger_{j\uparrow}s_{j\uparrow}\rangle + R_0L_0\langle g^\dagger_{j\uparrow}\tilde{g}_{j\uparrow}\rangle - \frac{1}{2}R_0L_0(1-\alpha) - R_0\tilde{L} + R_0L_0\\ &- R_0L_0(1+\alpha) + R_0\tilde{L}(1+\alpha) - \frac{1}{2}R_0L_0(\alpha^2-1) + s^\dagger_{j\uparrow}\tilde{g}_{j\uparrow}[-L_0\langle\tilde{g}_{j\downarrow}g^\dagger_{j\downarrow}\rangle + L_0\alpha]\\ &+ g^\dagger_{j\uparrow}s_{j\uparrow}[-R_0\langle\tilde{g}_{j\downarrow}g^\dagger_{j\downarrow}\rangle + R_0(\alpha+1)] + g^\dagger_{j\uparrow}\tilde{g}_{j\uparrow}[R_0L_0\langle\tilde{g}_{j\downarrow}g^\dagger_{j\downarrow}\rangle - \frac{1}{2}R_0L_0 - R_0L_0\alpha]\\ &+ s^\dagger_{j\downarrow}\tilde{g}_{j\downarrow}[\langle s^\dagger_{j\uparrow}s_{j\uparrow}\rangle + L_0\langle s^\dagger_{j\uparrow}\tilde{g}_{j\uparrow}\rangle + R_0\langle g^\dagger_{j\uparrow}s_{j\uparrow}\rangle - R_0L_0\langle g^\dagger_{j\uparrow}\tilde{g}_{j\uparrow}\rangle\\ &\frac{1}{2}R_0L_0(1-\alpha) + R_0\tilde{L} - R_0L_0] + s^\dagger_{j\uparrow}s_{j\uparrow}[\langle g^\dagger_{j\downarrow}s_{j\downarrow}\rangle - \alpha]. \quad (16.41)\end{aligned}$$

Bloch transforming and adding the spin flipped component gives

$$\begin{aligned}&- [s^\dagger_{j\uparrow}\tilde{g}_{j\uparrow} + s^\dagger_{j\downarrow}\tilde{g}_{j\downarrow}]\frac{1}{N}\sum_{k_1}[L_0(1-n_{k_1}-\delta_{k_1\in K})] + [g^\dagger_{j\uparrow}\tilde{g}_{j\uparrow} + g^\dagger_{j\downarrow}\tilde{g}_{j\downarrow}]\frac{1}{N}\sum_{k_1}[R_0(n_{k_1}+\delta_{k_1\in K})]\\ &[s^\dagger_{j\uparrow}s_{j\uparrow} + s^\dagger_{j\downarrow}s_{j\downarrow}]\frac{1}{N}\sum_{k_1}[1-n_{k_1}-\delta_{k_1\in K}] + [g^\dagger_{j\uparrow}\tilde{g}_{j\uparrow} + g^\dagger_{j\downarrow}\tilde{g}_{j\downarrow}]\frac{1}{N}\sum_{k_1}[R_0(1-L_{k_1})(1-n_{k_1}-\delta_{k_1\in K})\\ &-R_0L_0n_{k_1} - \frac{1}{2}R_0L_0\delta_{k_1\in K} - n_{k_1} + L_0R_{k_1}n_{k_1}] + 2\frac{1}{N^2}\sum_{k_1k_2}[(1-n_{k_2})(-n_{k_1} + R_{k_1}n_{k_1}L_0 + R_0L_{k_1}n_{k_1}\\ &- R_0L_0n_{k_1}) + R_0L_{k_1}(1-nk_1-\delta_{k_1\in K}) + n_{k_1} - L_0R_{k_1}n_{k_1} + R_0L_0n_{k_1}\\ &R_0L_0(1+\delta_{k_1\in K}) + R_0L_{k_1}\delta_{k_1\in K}(1+\delta_{k_2\in K}) + \frac{1}{2}R_0L_0\delta_{k_1\in K}(1-\delta_{k_2\in K})] \quad (16.42)\end{aligned}$$

Combining everything and Bloch transforming we get

$$E_q = \frac{U}{2}[R_q\tilde{B}_q - L_qB_q - 2C_q] \quad (16.43)$$

$$B_k = \frac{1}{N}\sum_{k_1}\left[\left[L_0+R_0\right]\left[n_{k_1}+\delta_{k_1\in K}\right]+\left[1-n_{k_1}-\delta_{k_1\in K}\right]L_{k_1}-\frac{1}{N}\sum_{k_2}R_{k_1}L_{k_2}[Rn]_{k-k_1+k_2}\right], \tag{16.44}$$

$$\tilde{B}_k = \frac{1}{N}\sum_{k_1}\left[\left[L_0+R_0\right]\left[1-n_{k_1}-\delta_{k_1\in K}\right]+n_{k_1}R_{k_1}-\frac{1}{N}\sum_{k_2}R_{k_1}L_{k_2}[L[1-n-\delta_{\in K}]]_{k+k_1-k_2}\right], \tag{16.45}$$

$$2C_k = \frac{2}{U}[2tZ\gamma_k+2t_0]-\frac{1}{N^3}\sum_{k_1k_2k_3}R_{k_1}L_{k_2}R_{k_3}L_{k_1-k_2+k_3}\left[[n+\frac{1}{2}\delta_{\in K}]_{k_1-k_2-k}-\frac{1}{2}\right]+\frac{1}{2}R_0^2\delta_{k_1\in K}$$
$$+\left[\left[L_0+R_0\right]^2+1\right]\left[\frac{1}{N}\sum_k[n_k+\delta_{k_1\in K}]-\frac{1}{2}\right]+\left[L_0+R_0\right]\frac{1}{N}\sum_{k_1}\left[\left[1-n_{k_1}-\delta_{k_1\in K}\right]L_{k_1}-n_{k_1}R_{k_1}\right]. \tag{16.46}$$

This result is remarkably similar to the previous result, and in the limit $\delta \to 0$ we retrieve the Mott point solution. The rest of the results are calculated in a similar manner and are presented in the following section.

16.3 The Results

Upon application of the method we get the particle dispersion to be

$$\epsilon_k = -2tZ\gamma_k + \frac{U}{2}\Big[1 + L_k B_k\Big], \tag{16.47}$$

the hole dispersion to be

$$\tilde{\epsilon}_k = -2tZ\gamma_k + \frac{U}{2}\Big[1 - R_k \tilde{B}_k\Big], \tag{16.48}$$

the occupation factor to be

$$n_k = \frac{1}{2}\left[1 + \left[1 + \frac{B_k}{C_k}\frac{\tilde{B}_k}{C_k}\right]^{-\frac{1}{2}}\right], \tag{16.49}$$

and the total energy to be

$$\begin{aligned} E = \frac{1}{N^2}\sum_{k_1 k_2} -2t_0[2n_{k_1} + \delta_{k_1\in K} - 1] - 4t_1 Z\gamma_{k_1} n_{k_1} + \frac{U}{2}\Bigg[[1-\delta_{k_1\in K}][1-\delta_{k_2\in K}] \\ + [n_{k_1} + \delta k_1 \in K][1 - n_{k_2} - \delta k_2 \in K] + \big[1 - n_{k_1} - \delta_{k_1\in K}\big]\big[n_{k_2}[R_0 + L_0]^2 + \delta_{k_2\in K} L_0^2\big] \\ - 2\big[R_0 + L_0\big]\big[[1 - n_{k_1} - \delta_{k_1\in K}]R_{k_2} n_{k_2} + [n_{k_1} + \delta_{k_1\in K}]L_{k_2}[\delta_{k_2\in K} - n_{k_2}]\big] \\ - L_{k_1}[\delta_{k_1\in K} - n_{k_1}]L_{k_2}[\delta_{k_2\in K} - n_{k_2}] - R_{k_1} n_{k_1} R_{k_2} n_{k_2} + 2\mathcal{R}_{k_1}\mathcal{M}_{k_1} - \mathcal{R}_{k_1}\mathcal{L}_{k_1}\mathcal{N}_{k_1}\Bigg] \end{aligned} \tag{16.50}$$

where

$$\mathcal{R}_k = \frac{1}{N}\frac{1}{2}\sum_{k_1} R_{k_1}[L_{k_1-k} + L_{k+k_1}] \tag{16.51}$$

$$\mathcal{L}_k = \frac{1}{N}\frac{1}{2}\sum_{k_1} L_{k_1}[R_{k_1-k} + R_{k+k_1}] \tag{16.52}$$

$$\mathcal{N}_k = \frac{1}{N}\frac{1}{2}\sum_{k_1} [\delta_{k_1\in K} - n_{k_1}][n_{k_1-k} + n_{k+k_1}] \tag{16.53}$$

$$\mathcal{M}_k = \frac{1}{N}\frac{1}{2}\sum_{k_1} L_{k_1}[\delta_{k_1\in K} - n_{k_1}][n_{k_1-k} R_{k_1-k} + n_{k+k_1} R_{k+k_1}] \tag{16.54}$$

$$L_k = \frac{C_k}{B_k}\left[1+\left[1+\frac{B_k}{C_k}\frac{\tilde{B}_k}{C_k}\right]^{\frac{1}{2}}\right] \qquad R_k = \frac{1}{L_k}, \tag{16.55}$$

$$B_k = \frac{1}{N}\sum_{k_1}\left[\left[L_0+R_0\right]\left[n_{k_1}+\delta_{k_1\in K}\right]+\left[1-n_{k_1}-\delta_{k_1\in K}\right]L_{k_1}-\frac{1}{N}\sum_{k_2}R_{k_1}L_{k_2}[Rn]_{k-k_1+k_2}\right], \tag{16.56}$$

$$\tilde{B}_k = \frac{1}{N}\sum_{k_1}\left[\left[L_0+R_0\right]\left[1-n_{k_1}-\delta_{k_1\in K}\right]+n_{k_1}R_{k_1}-\frac{1}{N}\sum_{k_2}R_{k_1}L_{k_2}[L[1-n-\delta_{\in K}]]_{k+k_1-k_2}\right], \tag{16.57}$$

$$\begin{aligned}2C_k = \frac{2}{U}[2tZ\gamma_k+2t_0]-\frac{1}{N^3}\sum_{k_1k_2k_3}R_{k_1}L_{k_2}R_{k_3}L_{k_1-k_2+k_3}\left[[n+\frac{1}{2}\delta_{\in K}]_{k_1-k_2-k}-\frac{1}{2}\right]+\frac{1}{2}R_0^2\delta_{k_1\in K}\\ +\left[\left[L_0+R_0\right]^2+1\right]\left[\frac{1}{N}\sum_k[n_k+\delta_{k_1\in K}]-\frac{1}{2}\right]+\left[L_0+R_0\right]\frac{1}{N}\sum_{k_1}\left[\left[1-n_{k_1}-\delta_{k_1\in K}\right]L_{k_1}-n_{k_1}R_{k_1}\right].\end{aligned} \tag{16.58}$$

Figure 16.1: Total Energy Analytical vs Numeric

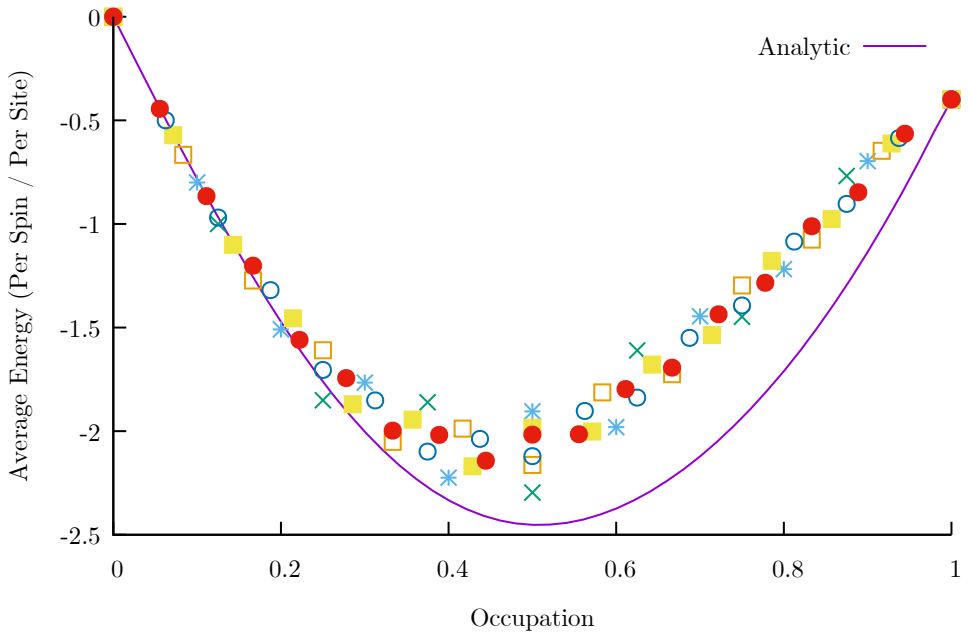

Total energy per spin per site, self consistent distribution theory vs exact diagonalisation. The points on the graph are finite size diagonalisation results for $n = 4, 5, 6, 7, 8, 9$ lattice sites. At the Mott point and at low occupation the agreement is rather good. However, at high occupation the analytical result overestimates the energy.

The one result that highlights the success and and failures of this theory is figure 16.1 on page 175. From this we can see that the theory overestimates the total energy at high doping. When we analyse the calculation we find that the U term is very sensitive. More specifically each component of the U term is large and cancels almost perfectly to give the answer. When the theory agrees well, i.e. at the Mott point and at low occupation, this cancellation occurs well. However, when there is a discrepancy, i.e. at higher occupation, this cancellation is off by $\approx 10\%$. This is not that large but when multiplied by the highest energy scale in the system makes a large difference. To improve this we imagine that there are effects that occur in the physical system that occur that have not been modelled in the theory.

In this section we extended the theory from the previous section. This was done by adding doping in order to examine the entire occupation range. In order to add doping

we manipulated the state considered in the theory; this required adapting the equivalence principles by commuting operators through the state manipulator. The result was a remarkably similar answer to the previous section with a few small amendments. The results, however, were not as successful: in certain areas of the phase diagram the total energy was off by $\approx 10\%$. To improve this calculation we would have to take into account other possible physical effects. In the next section we conclude this Part.

CHAPTER 17

SUMMARY

We have developed a new technique which can be used to calculate observables in a strongly correlated model with remarkable accuracy. We began with the same Hubbard model from part II. Symmetries were extracted in the same way as the previous part and attention was focused on the 'symmetric subspace', as this was the subspace which exhibited superconductivity in part II. Initial calculations were performed at the Mott point $|\psi\rangle$ as it was easiest to deal with. We defined a non-orthogonal operator $g^\dagger_{k\sigma}$ which was proportional one of the original basis operators $s^\dagger_{k\sigma}$, and in the limit $U = \infty$ the two were equal. Thanks to some equivalence principles we were able to recast the action of the Hamiltonian on $|\psi\rangle$ in terms of only $g^\dagger_{i\sigma}$ and its dual $\tilde{g}_{i\sigma}$. After making some assumptions about being able to represent $|\psi\rangle$ as a sum of products of $g^\dagger_{i\sigma}$, averaging to create a single particle Hamiltonian, and taking particle fluctuations into account we were able to examine the produce of the technique. Particle dispersion, hole dispersion, and the occupation factor were calculated and agreed remarkably with exact diagonalisation. Following this further calculations were performed away from the Mott point by modifying the state $|\psi\rangle$. This boasted similar results.

We are left asking whether this technique is generally useful or just a specific success story. The natural extension of superconductivity could not be examined trivially. This was due to the construction inherently assuming a single particle picture, whereas

superconductivity requires a two-particle description.

The next question to ask is whether we could apply this technique to another Hamiltonian. This best answer to this question is maybe. We require many things to be true to even begin attempting the technique. The most critical example of this is the state used. In our case the Mott state was closely related to a known state at $U = \infty$. Additionally, the state had equivalence principles which allowed us to remove any dependence on $a^{\dagger}_{i\sigma}$ operators. This is a pretty stringent set of conditions to attempt a technique.

Finally, we have not mentioned the relevance of 'Ward-Takahashi Identities' in this technique. These are quantum conservation laws, akin to Noether's theorem in classical mechanics, which are required to be imposed to ensure the success of a mean-field theory. In our case we have not considered them.

From this, it is clear what future work should be done. First, one should examine the importance of Ward-Takahashi identities in this technique, imposing them where necessary. Second, another Hamiltonian where this technique could be applied should be found. Third, this technique should be modified to be able to take into account superconductivity. If this technique is to be useful for others, these points must be examined.

Part IV

Conclusion & Appendices

CHAPTER 18

CONCLUSION

Three parts and 181 pages later, we come to the end of this thesis. The first thing we did was set the stage. We primarily covered superconductivity, both conventional and unconventional, and the core physical properties of both. Next we used physical chemistry to model both conventional and unconventional superconductors. We went through the argument Zhang and Rice presented when they argued the cuprates could be modelled by a Hubbard model.

At the heart of parts II and III was one particular Hubbard model

$$H = -t_1 \sum_{\langle ij\rangle\sigma} (t^\dagger_{i\sigma} + b^\dagger_{i\sigma})(t_{j\sigma} + b_{j\sigma}) - t_0 \sum_{i\sigma} (t^\dagger_{i\sigma} b_{i\sigma} + b^\dagger_{i\sigma} t_{i\sigma}) + U \sum_i (t^\dagger_{i\uparrow} t_{i\uparrow} t^\dagger_{i\downarrow} t_{i\downarrow} + b^\dagger_{i\uparrow} b_{i\uparrow} b^\dagger_{i\downarrow} b_{i\downarrow}).$$

Its collection of local symmetries were core to its many examinations. Extracting those symmetries created a much more manageable Hamiltonian for further analysis.

In part II we took the limit $U = \infty$ exactly, probed superconducting hole-pair formation, and used BCS mean field theory to examine superconductivity. We found that there was coexistence between ferromagnetism and superconductivity which could be tuned with t_0. Total energy, excess pairing, superconducting gap, and occupation factor were all examined and showed good agreement with exact diagonalisation. Finally, we extended the analysis to 2D and finite U perturbatively showing that superconductivity persisted

and anti-ferromagnetic phase manifested close to the Mott point.

In part III we created a new technique to deal with finite U more accurately. The central component of the technique was a non-orthogonal operator; one that was distributed over multiple sites. The purpose of this operator was to take into account n-th order 'perturbations' self consistently. This produced particle dispersions, hole dispersions, and the occupation factor which agreed remarkably well with exact diagonalisation.

The key takeaways from this work is that: symmetries are incredibly useful and are the reason any of this work could have been done; a repulsive Hubbard model can be rigorously shown to be superconducting; and non-orthogonal mean field theories might be useful in dealing with strongly correlated physics. The key lessons however are that: exact techniques aren't always useful when following them with approximate ones; manifesting the phase diagram of the cuprates does not mean that your model *is* the model of the cuprates; and the effectiveness of a technique does not mean it is by default a general approach. As hard as this thesis was to write, I hope it wasn't too hard to read.

APPENDIX A

SECOND QUANTISATION & FERMIONIC OPERATORS

The single particle picture is unwieldy when extended to a many body system. As most systems contain more than one particle we require an extension. Second quantisation is that extension and forms the foundation of quantum many particle systems.

In this appendix we will give an overview of the current methods used in quantum mechanics. We will then extend this to the far superior method that is second quantisation. Then we will present information on how to deal with many body states and Hamiltonians in this formalism.

A.1 First Quantisation

Quantum mechanics for a single particle is governed by the Schrödinger equation [77]

$$\hat{H}\Psi = E\Psi. \tag{A.1}$$

This elegant equation has its roots in Lagrangian mechanics [78] as the Hamiltonian is often represented as

$$\hat{H} = \hat{T} + \hat{V}, \tag{A.2}$$

where $\hat{T}$ is the kinetic energy operator, and $\hat{V}$ is the potential operator. From this point forward we will drop the operator-hat notation.

This picture is trivially extended to many particles via a Hamiltonian of the form

$$H = \sum_{i}^{n} H^{(1)}(\mathbf{r}_i) + \sum_{1 \leq i < j \leq n} V(\mathbf{r}_i, \mathbf{r}_j), \tag{A.3}$$

acting on the many body wavefunction

$$\Psi(\mathbf{r}_1, ..., \mathbf{r}_n). \tag{A.4}$$

Here $\mathbf{r}_i$ is the position of the i-th particle, $H^{(1)}(\mathbf{r}_i)$ is the generalised one body term for the i-th particle, and $V(\mathbf{r}_i, \mathbf{r}_j)$ is the two body term for interactions between the i-th and j-th particles. In general we assume the maximal number of particles involved in an interaction is two. Higher particle terms are usually only occur in high energy systems and are not of concern for most of condensed matter. For example, the Hamiltonian for n particles with mass m and charge e in a background potential $W(\mathbf{r})$ interacting via a Coulomb potential [79] is given by

$$H = \sum_{i}^{n} \left[-\frac{\hbar^2}{2m} \nabla_i^2 + W(\mathbf{r}_1) \right] + \sum_{1 \leq i < j \leq n} \frac{e^2}{|\mathbf{r}_i - \mathbf{r}_j|}. \tag{A.5}$$

A system like this is generally impossible to solve exactly. Even if it were, dealing with a n-particle wavefunction is not practical. The solution is to introduce second quantisation.

A.2 Second Quantisation

Second quantisation, or more accurately occupation number representation, is a refined way to deal with many particle states and Hamiltonians. Instead of writing an n-particle wavefunction we describe a many-body state by its occupation numbers [80]. We state

that there are n_{r_1} particles in state r_1, n_{r_2} particles in state r_2 and so on. Then we can use *creation operators* $a_r^\dagger$ and *annihilation operators* a_r which increase or decrease the occupation number of state r by one. This is the same picture as the ladder operators used when solving the simple harmonic oscillator [81].

In this section we will formulate second quantisation, beginning with many body states and moving on to many body Hamiltonians.

A.2.1 Many Body States

Before we deal with many body states, let us focus on the single particle level. In an ideal world we would like to describe the absence of a particle with a vacuum $|0\rangle$, and create a particle with wavefunction $\psi(\mathbf{r})$ via a creation operator $a^\dagger |0\rangle$. This state could then be annihilated using annihilation operator a, just as for the simple harmonic oscillator, to give back the vacuum. Mathematically this corresponds to

$$a |0\rangle = 0 \quad a a^\dagger |0\rangle = |0\rangle . \tag{A.6}$$

Unfortunately, this picture breaks down when we add more particles due to wavefunction overlap. Take a particle with wavefunction $\psi(\mathbf{r}_1)$ and $a_1^\dagger |0\rangle_1$, and another with wavefunction $\psi(\mathbf{r}_2)$ and $a_2^\dagger |0\rangle_2$. As there is *always* overlap between the two wavefunctions we will always have

$$a_1 a_2^\dagger |0\rangle_1 |0\rangle_2 = O_{12} |0\rangle_1 |0\rangle_2 . \tag{A.7}$$

This is a non-orthogonal setup and is incredibly difficult to deal with.

To fix this, we almost always use the Wannier basis [82] $c_i^\dagger |0\rangle$ corresponding to a particle with a Wannier wavefunction $\psi_W(\mathbf{r}_i)$ such that

$$c_1 c_2^\dagger |0\rangle_1 |0\rangle_2 = \delta_{12} |0\rangle_1 |0\rangle_2 , \tag{A.8}$$

and the $c_i^\dagger$ create 'independent' degrees of freedom. To connect this to the original wave-

function we use the fact that the Wannier wavefunctions form a complete basis and therefore by definition

$$\psi(\mathbf{r}) = \sum_i u_i \psi_W(\mathbf{r} - \mathbf{r}_i). \tag{A.9}$$

We can then use the operator

$$\hat{\psi}(\mathbf{r}) = \sum_i \psi_W(\mathbf{r} - \mathbf{r}_i) c_i, \tag{A.10}$$

to return the wavefunction.

Shorthand: Instead of writing the vacuum for each possible state when considering many body systems we frequently write a generic vacuum to denote the product over all vacuums. For example $|0\rangle = |0\rangle_1 |0\rangle_2 \cdots |0\rangle_n$.

Now comes the tricky bit: statistics. In an ideal world we would like to associate the application of $c_i^\dagger$ with the creation of a particle with wavefunction $\psi(\mathbf{r}_i)$ *independently* of whether there is another particle there or not. The issue is that not all types of particles are independent. Bosons and fermions obey different statistics. Namely, the wavefunction of a fermion is anti-symmetric under exchange of any two particles, whilst a bosonic wavefunction is symmetric under exchange. For bosons we require

$$b_1^\dagger b_2^\dagger |0\rangle \to \psi_1(\mathbf{r}_1)\psi_2(\mathbf{r}_2) + \psi_1(\mathbf{r}_2)\psi_2(\mathbf{r}_1), \tag{A.11}$$

with fermions we actually require

$$f_1^\dagger f_2^\dagger \to \psi_1(\mathbf{r}_1)\psi_2(\mathbf{r}_2) - \psi_1(\mathbf{r}_2)\psi_2(\mathbf{r}_1). \tag{A.12}$$

So how do we enforce this? We can rewrite this two fermion term (by adding and subtracting $f_2^\dagger f_1^\dagger$) as

$$f_1^\dagger f_2^\dagger |0\rangle = \frac{1}{2}\left[f_1^\dagger f_2^\dagger - f_2^\dagger f_1^\dagger\right]|0\rangle + \frac{1}{2}\left[f_1^\dagger f_2^\dagger + f_2^\dagger f_1^\dagger\right]|0\rangle . \tag{A.13}$$

If we were to demand that

$$f_1^\dagger f_2^\dagger + f_2^\dagger f_1^\dagger = 0, \tag{A.14}$$

the two particle fermion state would automatically obey Fermi statistics.

The method by which we incorporate statistics into this second quantised picture is by enforcing the commutators

$$[b_i^\dagger, b_{i'}^\dagger] = 0, \quad [b_i, b_{i'}] = 0, \quad [b_i, b_{i'}^\dagger] = \delta_{ii'}, \tag{A.15}$$

for bosons, and the *anti-commutators*

$$\{f_i^\dagger, f_{i'}^\dagger\} = 0, \quad \{f_i, f_{i'}\} = 0, \quad \{f_i, f_{i'}^\dagger\} = \delta_{ii'}, \tag{A.16}$$

for fermions. Note that for fermions the first two anti-commutators enforce Pauli exclusion when $i = i'$; there can only be up to one fermion in a given state.

And we're done! We've set up second quantisation for many particle states of both bosons and fermions. Now let's introduce some practical tips and notes on how to use second quantisation.

As stated at the start of this section, second quantisation is more accurately described as occupation number representation. The state

$$|\Psi\rangle = |0\rangle_1 |2\rangle_2 |2\rangle_3 |1\rangle_4 \equiv |0, 2, 2, 1\rangle , \tag{A.17}$$

has zero particles in state 1, two in state 2, two in state 3 and one in state 4. Clearly, as there are more than one particle in each state this is a system of bosons which could be rewritten as

$$|\Psi\rangle = b_2^\dagger b_2^\dagger b_3^\dagger b_3^\dagger b_4^\dagger |0\rangle . \tag{A.18}$$

It is important to be able to fluidly change from one representation to the other. Just as

in the single particle case if we annihilate a state with no particles in it zero is returned

$$b_1 |\Psi\rangle = b_1 |0\rangle_1 |2\rangle_2 |2\rangle_3 |1\rangle_4 = 0. \tag{A.19}$$

Funnily, as bosons commute, they are easier to handle but the physics that results is usually far more difficult.

As all of the work in this thesis is centred around fermions, let's add a few notes about handling them. The first thing to remember is the Fermi minus sign, namely

$$f_1^\dagger f_2^\dagger |0\rangle = -f_2^\dagger f_1^\dagger |0\rangle . \tag{A.20}$$

The order of states matters! For this reason, we usually denote an order of application to make handling these minus signs easier. Second, the fermions we deal with tend to have spin. This acts as a second quantum number and the operators anti-commute with respect to it, giving

$$\{f_{i,\sigma}, f_{i',\tau}^\dagger\} = \delta_{ii'}\delta_{\sigma\tau}. \tag{A.21}$$

Now that we have detailed second quantisation for many body operators lets move on to Hamiltonians.

A.2.2 Many Body Hamiltonians

We are now in a position to consider many body Hamiltonians in second quantised form. In essence this is just a change of basis. Our first quantised Hamiltonian is given by

$$H = \sum_i^n H^{(1)}(\mathbf{r}_i) + \sum_{1\leq i<j\leq n} V(\mathbf{r}_i, \mathbf{r}_j), \tag{A.22}$$

and we wish to convert this to a second quantised form

$$H = H_1 + H_2, \tag{A.23}$$

where $H^{(1)}(\mathbf{r}_i) \to H_1$, and $V(\mathbf{r}_i, \mathbf{r}_j) \to H_2$.

In the Wannier basis we have the wavefunction annihilation operator

$$\hat{\psi}(\mathbf{r}) = \sum_i \psi_W(\mathbf{r} - \mathbf{r}_i) c_i, \tag{A.24}$$

and

$$H_1 = \int \mathrm{d}^3\mathbf{r} \int \mathrm{d}^3\mathbf{r}' \hat{\psi}^\dagger(\mathbf{r}) H^{(1)}(\mathbf{r}, \mathbf{r}') \hat{\psi}(\mathbf{r}). \tag{A.25}$$

For the general case of a particle with mass m moving in a background potential $W(\mathbf{r})$ we have

$$H_1 = \int \mathrm{d}^3\mathbf{r} \int \mathrm{d}^3\mathbf{r}' \hat{\psi}^\dagger(\mathbf{r}) \delta(\mathbf{r} - \mathbf{r}') \left[-\frac{\hbar^2}{2m} \nabla^2_{\mathbf{r}'} + W(\mathbf{r}') \right] \hat{\psi}(\mathbf{r}) \tag{A.26}$$

$$= \sum_{ii'} H_{ii'} c_i^\dagger c_{i'}, \tag{A.27}$$

where

$$H_{ii'} = \int \mathrm{d}^3\mathbf{r} \psi_i^* (\mathbf{r} - \mathbf{r}_i) \left[-\frac{\hbar^2}{2m} \nabla^2 + U(\mathbf{r}) \right] \psi_{i'} (\mathbf{r} - \mathbf{r}_{i'}). \tag{A.28}$$

Similarly for the two particle interaction

$$V(\mathbf{r}_i, \mathbf{r}') = \frac{e^2}{|\mathbf{r} - \mathbf{r}'|}, \tag{A.29}$$

and then

$$H_2 = \frac{1}{2} \int \mathrm{d}^3\mathbf{r} \int \mathrm{d}^3\mathbf{r}' \hat{\psi}^\dagger(\mathbf{r}) \hat{\psi}^\dagger(\mathbf{r}') \frac{e^2}{|\mathbf{r} - \mathbf{r}'|} \hat{\psi}(\mathbf{r}') \hat{\psi}(\mathbf{r}) \tag{A.30}$$

$$= \frac{1}{2} \sum_{ii'} \sum_{jj'} I_{ii',jj'} c_i^\dagger c_{i'}^\dagger c_{j'} c_j, \tag{A.31}$$

where

$$I_{ii',jj'} = \int \mathrm{d}^3\mathbf{r} \int \mathrm{d}^3\mathbf{r}' \psi_i^* (\mathbf{r} - \mathbf{r}_i) \psi_{i'}^* (\mathbf{r} - \mathbf{r}_{i'}) \frac{e^2}{|\mathbf{r} - \mathbf{r}'|} \psi_{j'} (\mathbf{r}' - \mathbf{r}_{j'}) \psi_j (\mathbf{r} - \mathbf{r}_j). \tag{A.32}$$

Putting it all together gives the spinless fermion Hamiltonian in second quantised form, is given by

$$H = \sum_{ii'} H_{ii'} c_i^\dagger c_{i'} + \frac{1}{2} \sum_{ii'} \sum_{jj'} I_{ii',jj'} c_i^\dagger c_i^\dagger c_j c_j, \tag{A.33}$$

which is clearly more elegant and easier to deal with than the original Hamiltonian.

We can add spin in a similar way. The important change is that two particle interaction now sums over spin indices on each site. Note, we haven't considered physics, such as Hund's rules [83] , in generating this Hamiltonian. This gives the spin inclusive fermion Hamiltonian in second quantised form as

$$H = \sum_{\sigma ii'} H_{ii'} c_{i\sigma}^\dagger c_{i'\sigma} + \frac{1}{2} \sum_{\sigma\tau} \sum_{ii'} \sum_{jj'} I_{ii',jj'} c_{i\sigma}^\dagger c_{i'\tau}^\dagger c_{j'\tau} c_{j\sigma}. \tag{A.34}$$

Most of the work in this thesis is on a regular lattice. This means the electron wavefunctions are localised around sites $\mathbf{R}_i$. In this limit we expect the wavefunction overlap to become negligible if they are more than one site away. The on site same spin $I_{ii',jj'}$ is zero due to Pauli exclusion. By labelling $H_{ii} = \epsilon$, $H_{\langle ii'\rangle} = -t$ (where $\langle ii'\rangle$ denote i and i' are nearest neighbours), $I_{ii,ii} = U$, and summing over τ we get

$$H = \epsilon \sum_{i\sigma} c_{i\sigma}^\dagger c_{i\sigma} - t \sum_{\langle ii'\rangle\sigma} c_{i\sigma}^\dagger c_{i'\sigma} + U \sum_i c_{i\uparrow}^\dagger c_{i\downarrow}^\dagger c_{i\downarrow} c_{i\uparrow}. \tag{A.35}$$

This is the *Hubbard Model* [84], and is where most lattice models begin. A plethora of physics is encapsulated in this rather simple model: metals, insulators, ferromagnets, anti-ferromagnets, charge density waves, and (as will be shown in this thesis) superconductivity.

In this appendix we introduced second quantised operators and their relationship to many body states and Hamiltonians. Second quantisation is essentially an extension to the simple harmonic oscillator, but there are caveats such as Wannier states and statistics. We now have the foundations to understand the work that is presented in this thesis.

APPENDIX B

PHYSICAL CHEMISTRY CRASH COURSE — HOW TO THINK ABOUT MATERIALS

As much as theorists love to think about models in a vacuum, models are created to *model* physical systems. These are often generated upon examining materials from condensed matter systems. These materials are governed by a wide variety of physics. Broadly speaking, the two categories of materials are metals and insulators. Of course there are other systems, like magnets and superconductors, but at the lowest level of modelling many materials are either metals or insulators.

Physical chemistry is an entangled web of a subject. Many properties are contingent on one another, and it is often difficult to understand why a material does what it does. This appendix is written for a young scientist attempting to model a material. My aim is to cut through the web of physical chemistry and create a set of principles that can be followed. These principles will be at the end of this introduction to serve as a future reference.

The structure of this appendix is as follows: examine atoms in free space, consider atoms in a solid, modelling insulators, and modelling metals. We begin by investigating

atoms in free space, treating them as extensions to the Hydrogen atom. This will generate a physical picture of the periodic table. Electrons are also affected by one another and their angular momentum; these effects are encapsulated in screening and Hund's rules. In condensed matter systems however, atoms exist in the vicinity of other atoms. This crystal generates a field which distorts the free space behaviour, which is the last section that pertains to modelling. Finally, we are able to generate a model.

The following steps are the principles of physical chemistry modelling. They may not seem meaningful if this is the first time you're reading this document, but they should become clear as you learn.

1. Make a note of whether the material is a metal or insulator. It will affect your decision making.

2. Separate the atom into core and valence electrons.

3. Add electrons to the most electronegative atoms.

4. If the material is an insulator the number of electrons on each atom is defined, if the material is a metal it is not. What shell can the remaining electrons occupy?

5. What is the crystal structure of the compound? How will this affect the crystal field?

6. What is the dominant interaction, crystal field or Hund's rules? Hund's rules win for atoms on the left of Co and all lanthanides. How does this lift orbital degeneracy?

7. Lanthanides are dominantly 3+ cores except sometimes at the edges.

8. If the model is an insulator what are the low lying excitations doing? Consider super exchange.

9. If the model is a metal write the tight-binding model, diagonalise it, and compare to DFT calculations.

B.1 Atoms in Free Space — Extending the Hydrogen Atom

Atoms are the building blocks of solid state physics. Unfortunately, they also happen to be quite complicated to solve. We, like many before us, will simplify this complexity by assuming all atoms are just extensions to the hydrogen atom [85]. This gross simplification works rather well, and we only need to add a handful of caveats.

We will begin with a review of the solution to the hydrogen atom. This will provide the hydrogenic wavefunctions. Next, we will consider screening and its effects within an atom. Lastly, we will consider the effects of angular momentum which are governed by Hund's rules [83].

The Schrödinger equation for the hydrogen atom is given by

$$\left[\frac{|\mathbf{p}^2|}{2m} - \frac{e^2}{|\mathbf{r}|} - E\right]\Psi(\mathbf{r}) = 0, \tag{B.1}$$

subject to the commutation relations $[r_\alpha, p_\beta] = i\hbar\delta_{\alpha\beta}$. We must then employ spherical symmetry i.e. angular momentum commutes with the Hamiltonian. Using

$$\hat{\mathbf{p}} = -i\hbar\frac{\partial}{\partial\mathbf{r}} \quad \text{and} \quad \hat{\mathbf{L}} = \hat{\mathbf{r}} \wedge \hat{\mathbf{p}}, \tag{B.2}$$

$$\hat{\mathbf{p}}^2 = \frac{1}{r^2}\left[(\hat{\mathbf{r}}\cdot\hat{\mathbf{p}})^2 - i\hbar\hat{\mathbf{r}}\cdot\hat{\mathbf{p}} + \hat{\mathbf{L}}\cdot\hat{\mathbf{L}}\right]. \tag{B.3}$$

We wish to solve for the radial and spherical motion independently. This is done by separation of variables

$$\Psi(\mathbf{r}) = Y_{lm}(\theta,\phi)\psi(r). \tag{B.4}$$

First we solve the spherical motion to generate the spherical harmonics. This is done

by stating $Y_{lm}(\theta,\phi)$ is an eigenfunction of $\hat{\mathbf{L}}^2$ with eigenvalue equation

$$\hat{\mathbf{L}}^2 Y_{lm}(\theta,\phi) = \hbar^2 l(l+1) Y_{lm}(\theta,\phi). \tag{B.5}$$

The equation left to solve

$$\left[\frac{1}{\sin\theta}\frac{\partial}{\partial\theta}\sin\theta\frac{\partial}{\partial\theta} + \frac{1}{\sin^2\theta}\frac{\partial^2}{\partial\phi^2} + l(l+1)\right] Y_{lm}(\theta,\phi) = 0. \tag{B.6}$$

We can use separation of variables on Y_{lm}

$$Y_{lm}(\theta,\phi) = \frac{1}{\sqrt{2\pi}} e^{im\phi} P_{lm}(\theta), \tag{B.7}$$

where m must be an integer to ensure the single valued nature of Y_{lm}. The details of derivation are omitted as the result is more important. Instead we outline the key steps [85]. Use the more natural variable $u = \cos\theta$ and rewrite $P_{lm}(u) = [1-u^2]^{\frac{|m|}{2}} Q_{lm}(u)$, force the operator to be self-adjoint, use the ansatz $Q_{lm}(u) = N_{lm}(1-u^2)^{-m}\left(\frac{\partial}{\partial u}\right)^{l-m}(1-u^2)^l$, and consider the inner product $(Q_{l'm}, Q_{lm})$ to calculate $Q_{lm}(u)$. This gives

$$Y_{lm}(\theta,\phi) = \frac{1}{\sqrt{2\pi}} e^{im\phi}\left[\frac{2l+1}{2}\right]^{\frac{1}{2}}\left[\frac{(l+m)!}{(l-m)!}\right]^{\frac{1}{2}}\frac{1}{2^l l!}(1-u^2)^{-m}\left[\frac{\partial}{\partial u}\right]^{l-m}(1-u^2)^l. \tag{B.8}$$

The first few are given by [86]

$$Y_{00} = \frac{1}{\sqrt{4\pi}} \qquad Y_{20} = \frac{1}{\sqrt{4\pi}}\frac{\sqrt{5}}{2}(3\cos^2\theta - 1) \tag{B.9}$$

$$Y_{11} = \frac{e^{i\phi}}{\sqrt{4\pi}}\left(\frac{3}{2}\right)^{\frac{1}{2}}\sin\theta \qquad Y_{33} = \frac{e^{3i\phi}}{\sqrt{4\pi}}\frac{\sqrt{35}}{2}\sin^3\theta \tag{B.10}$$

$$Y_{10} = \frac{1}{\sqrt{4\pi}}(-1)\sqrt{3}\cos\theta \qquad Y_{32} = \frac{e^{2i\phi}}{\sqrt{4\pi}}(-1)\left(\frac{105}{8}\right)^{\frac{1}{2}}\sin^2\theta\cos\theta \tag{B.11}$$

$$Y_{22} = \frac{e^{2i\phi}}{\sqrt{4\pi}}\left(\frac{15}{8}\right)^{\frac{1}{2}}\sin^2\theta \qquad Y_{31} = \frac{e^{i\phi}}{\sqrt{4\pi}}\frac{\sqrt{21}}{4}(5\cos^2\theta - 1)\sin\theta \tag{B.12}$$

$$Y_{21} = \frac{e^{i\phi}}{\sqrt{4\pi}}(-1)\left(\frac{15}{2}\right)^{\frac{1}{2}}\sin\theta\cos\theta \qquad Y_{30} = \frac{1}{\sqrt{4\pi}}(-1)\frac{\sqrt{7}}{2}(5\cos^2\theta - 3)\cos\theta \tag{B.13}$$

These will form the basis of the cubic harmonics examined in the next section, and are therefore the key result from the spherical solution.

We now move on to finding the radial solution. In spherical polar coordinates $\mathbf{r}\cdot\hat{\mathbf{p}} = -i\hbar r\frac{\partial}{\partial r}$. Combining this with a rescaling of space by $r = \frac{\hbar^2}{me^2}x$ and energy by $E = \frac{me^4}{2\hbar^2}\epsilon$ gives the dimensional representation

$$\left[x\frac{\partial^2}{\partial x^2} + 2\frac{\partial}{\partial x} - \frac{l(l+1)}{x} + 2 + \epsilon x\right]\psi(x) = 0. \tag{B.14}$$

Just as before, the details of derivation are omitted as the result is more important. Instead, we outline the key steps. The general procedure is to extract out asymptotic behaviour at the origin and employ a contour ansatz. Assume the behaviour close to the origin is $\psi_l(x) = x^l\phi_l(x)$, represent this as a complex integral $\phi_l(x) = \int_C \mathrm{d}z e^{zx} f_l(z)$, integrate by parts to give an ODE for $f_l(z)$, parametrise $\epsilon = -\frac{1}{n^2}$ and integrate directly, as we're considering bound states we need to find the residues at $z \to -\frac{1}{n}$. This leads to restrictions on the principle quantum number $n > l$, and using the Liebnitz differentiation theorem provides the radial wavefunctions

$$\psi_{nl}(x) \propto x^l e^{-\frac{x}{n}} \sum_{r=0}^{n-l-1} \frac{(n-l-1)!}{(n-l-1-r)!r!}\left[-\frac{2}{n}\right]^{r+2l+1}\frac{(n+l)!}{(r+2l+1)!}x^r, \tag{B.15}$$

where the normalisation can be found. By definition the radial probability is given by

$$P_{nl}(x) = x^2|\psi_{nl}(x)|^2. \tag{B.16}$$

The ground state has energy $\epsilon = -1$ and its wavefunction is given by

$$\psi_{10}(x) = 2e^{-x}, \tag{B.17}$$

the first excitations have energy $\epsilon = -\frac{1}{4}$ and their wavefunctions are given by

$$\psi_{20}(x) = \frac{1}{2\sqrt{2}}(2-x)e^{-\frac{x}{2}}, \qquad \psi_{21}(x) = \frac{1}{\sqrt{6}}xe^{-\frac{x}{2}}, \tag{B.18}$$

and the second excitations have energy $\epsilon = -\frac{1}{9}$ and their wavefunctions are given by

$$\psi_{30}(x) = \frac{2}{81\sqrt{3}}(27-18x+2x^2)e^{-\frac{x}{3}}, \quad \psi_{31}(x) = \frac{2\sqrt{2}}{81\sqrt{3}}(6-x)xe^{-\frac{x}{3}}, \quad \psi_{32}(x) = \frac{2\sqrt{2}}{81\sqrt{15}}x^2e^{-\frac{x}{3}}. \tag{B.19}$$

These wavefunctions and their radial probabilities are depicted in figures B.1 on page 197 and B.2 on page 197. At this point we should make note of a few things:

- Wavefunctions with the same principle quantum number have the same decay rate $e^{-\frac{x}{n}}$, so have similar extent.
- The higher angular momentum wavefunctions are slightly more localised because that they have fewer electrons to 'statistically' avoid.
- Wavefunctions with different principle quantum numbers have very different innate radii.

Nomenclature: Angular momentum quantum numbers are frequently labelled with letters: $l = 0 \equiv s$, $l = 1 \equiv p$, $l = 2 \equiv d$, $l = 3 \equiv f$. For example $3d$ is equivalent to principle quantum number $n = 3$ and angular momentum quantum number $l = 2$. These are often called 'shells'.

This elementary picture provides a consistent sketch for the periodic table but the order of the states is not quite as expected. We should expect the ordering to be

$$1s \quad 2s \quad 2p \quad 3s \quad 3p \quad 3d \quad 4s \quad 4p \quad 4d \quad 4f, \tag{B.20}$$

but in reality the order is

$$1s \quad 2s \quad 2p \quad 3s \quad 3p \quad 4s \quad 3d \quad 4p \quad 5s \quad 4d \quad 5p \quad 6s \quad 4f \quad 5d. \tag{B.21}$$

Figure B.1: Hydrogenic Radial Wavefunctions

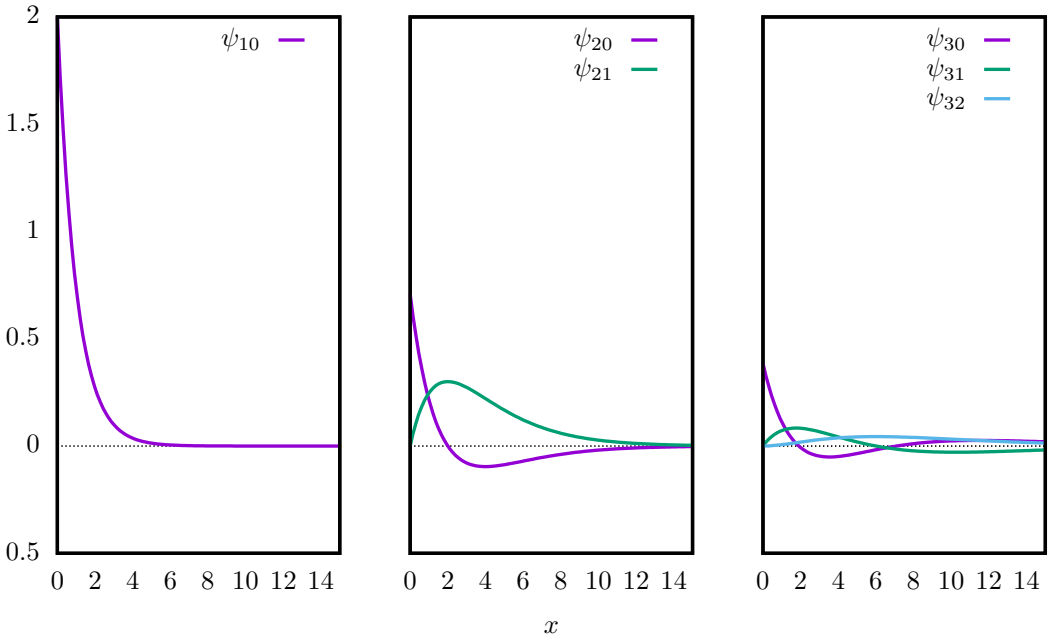

Wavefunctions for the lowest three energy states. Higher angular momentum wavefunctions are slightly more localised.

Figure B.2: Hydrogenic Radial Probabilities

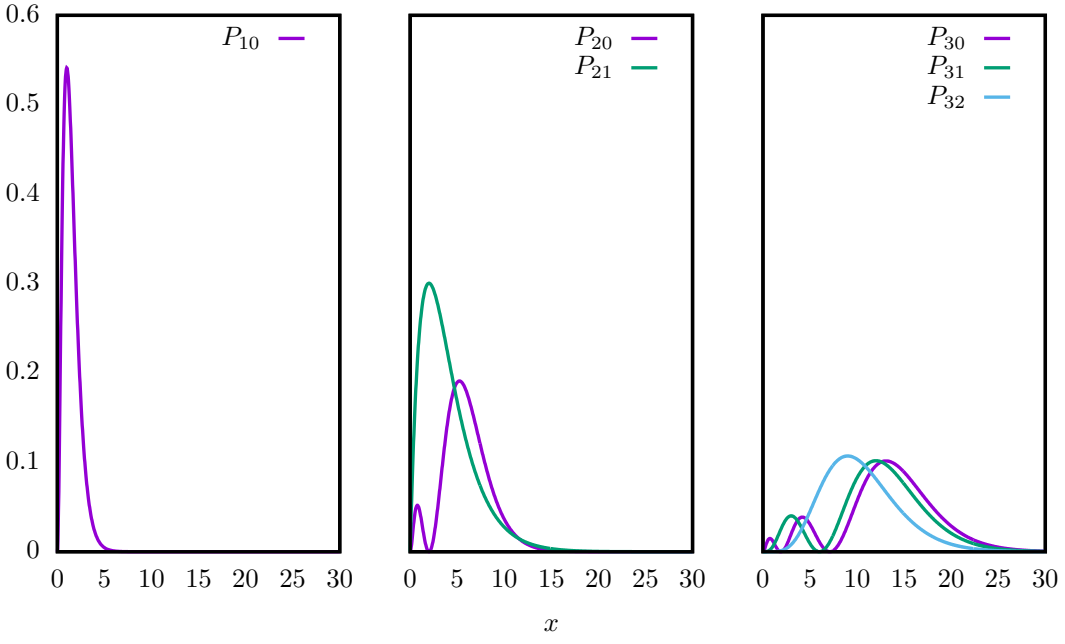

Probabilities of the lowest three hydrogenic wavefunctions. Wavefunctions with different principle quantum numbers have very different innate radii.

So why do higher principle quantum numbers arrive before completing the previous quantum number? The answer is relativity! The two energies to compare are

$$E_{non-relativistic} = mc^2 + \frac{p^2}{2m}, \quad \text{and} \quad E_{relativistic} = \left[p^2c^2 + m^2c^4\right]^{\frac{1}{2}}. \tag{B.22}$$

From this we can see that if something is relativistic then it has a higher momentum for the same energy.

The lowest shells have the highest energies and are the most relativistic. This means they have higher momentum and are therefore more localised (from the uncertainty principle). This causes higher lying electrons of the same type to drop down to also lower their energy.

The last thing to understand for the periodic table is electron counting. The degeneracy of a state with angular momentum l is $2l + 1$. Taking into account spin this means the s shell can occupy 2 electrons, p can occupy 6, d can occupy 10, and f can occupy 14. This is equally split between spin up and down electrons.

When considering the electrons in an atom (also known as its 'electron configuration') in a compound we split the electrons into core and valence [85]. The 'core' is labelled by the heaviest noble gas that is lighter than the atom, denoted by square brackets. All other electrons are 'valence'. They are labelled by a principle quantum number, a letter for the angular momentum, and a superscript number which counts the number of electrons that occupy that shell. For example iron's (Fe) electron configuration is $[\mathrm{Ar}]3\mathrm{d}^6 4\mathrm{s}^2$. This means it has an argon (Ar) core and is also occupied by 6 electrons in the $n = 3$, $l = 2$ shell, and 2 electrons in the $n = 4$, $l = 0$ shell.

At this point we have an elementary physical picture of the periodic table. However, things are slightly more complicated. The source of this complication is electron-electron interactions within atoms; this is detailed in the next section.

B.2 Hartree and Screening

So far we've tried to explain the periodic table using the hydrogen atom. When we consider other atoms there are modifications from electron-electron interactions. The basic picture will be the same but the details are completely different. The basic picture one should think of is as follows: electrons are much closer to the nucleus than the 6s electrons. To a first approximation the 1s electron can be thought of as part of the nucleus, essentially reducing its charge. The electrons within the current radius of the reference electron are said to 'screen' the charge of the nucleus. We will be using the Hartree approximation [87] (the electrons are assumed to be independent of one other) and ignore Fermi statistics for simplicity. The role of the other electrons is to provide an electrostatic potential applied to the current electron. We find this potential with the use of a Green's function.

In general we can solve an equation of the following form with a Green's function [88]

$$\int \mathrm{d}^3\mathbf{s}\hat{O}(\mathbf{r},\mathbf{s})A(\mathbf{s}) = a(\mathbf{r}), \tag{B.23}$$

where $a(\mathbf{r})$ is a given forcing term, $\hat{O}(\mathbf{r},\mathbf{s})$ is an operator, and $A(\mathbf{s})$ is an unknown to be found. The Green's function is the analogue of the inverse of $\hat{O}$ and is constructed to satisfy

$$\int \mathrm{d}^3\mathbf{s}\hat{O}(\mathbf{r},\mathbf{s})G(\mathbf{s},\mathbf{r}) = \delta^3(\mathbf{r}-\mathbf{r}'). \tag{B.24}$$

The solution of the posed problem, verified by direct substitution, is then just

$$A(\mathbf{r}) = \int \mathrm{d}^3\mathbf{s}G(\mathbf{s},\mathbf{r})a(\mathbf{s}). \tag{B.25}$$

The Hartree problem is exactly of this type! We have a static charge distribution arising from the other electrons. From Maxwell's equations [79] we have

$$\nabla \wedge \mathbf{E} = \mathbf{0} \quad \Rightarrow \quad \mathbf{E} = -\nabla\phi(\mathbf{r}), \tag{B.26}$$

$$\nabla \cdot \mathbf{E} = 4\pi e^2 \rho(\mathbf{r}) \quad \Rightarrow \quad \nabla^2 \phi(\mathbf{r}) = -4\pi^2 \rho(\mathbf{r}), \tag{B.27}$$

where $\phi(\mathbf{r})$ is the electrostatic potential and $\rho(\mathbf{r})$ is the density profile of electrons. The final equation is known as Poisson's equation [88], and it is the form required to apply the theory of Green's functions. Again, as the result is more important than the derivation we will sketch the key steps. The operator in question is $\hat{O}(\mathbf{r}, \mathbf{s}) = \delta(\mathbf{r} - \mathbf{s})\nabla^2_{\mathbf{s}}$, hence we are required to solve $\nabla^2_{\mathbf{r}} G(\mathbf{r}, \mathbf{s}) = \delta(\mathbf{r} - \mathbf{s})$. We will solve this using spherical polar co-ordinates as the delta function is spherically symmetric and only non-zero at the origin. This is solved by $G(x) = a + \frac{b}{x}$. By demanding $\int_V \mathrm{d}^3\mathbf{x} \nabla^2 G(\mathbf{x}) = 1$ and use of the divergence theorem we get $G(\mathbf{x}) = -\frac{1}{4\pi|\mathbf{x}|}$. The associated potential is consequently $\phi(\mathbf{r}) = \int \mathrm{d}\mathbf{s} \frac{e^2 \rho(\mathbf{r})}{|\mathbf{r}-\mathbf{s}|}$. We simplify the problem by assuming the charge distribution is spherically symmetric, this is true for closed shell configurations. This gives the radially depended effective charge as [79]

$$Z(r) = Z_e - \int_r^\infty \mathrm{d}s(s - r)s4\pi\rho(s), \tag{B.28}$$

where Z_e is the total electric charge.

As $r \to 0$ the integral tends to Z_e, and so $Z(r)$ vanishes and the nuclear charge is unscreened. As $r \to \infty$ the integral vanishes and the nucleus is screened by all other electrons.

Each principle quantum number has the same effective range and therefore this extra potential should *not* change the physics *within* each principle quantum number. It is natural to think of the inner electrons as a 'screen' of the nuclear charge for outer electrons. This is the source of the statement that 'all atoms are about the same size'. More directly the 'outer most electrons' only 'see' a singular positive charge. Electrostatics therefore dictate the radius of the atom. This, of course, is not exact and the radius of atoms is only the same order of magnitude; which results in interesting structural properties of many compounds.

B.3 Hund's Rules

The final thing to understand about spherically symmetric isolated atoms is Hund's rules [83]. There are three rules that govern the behaviour of **S**, **L**, and **J**.

The largest relevant atomic physics energy scale is that of exchange. Fermionic wavefunctions must be anti-symmetric due to their statistics. As electrons are fermions their wavefunction must be anti-symmetric. The electron wavefunction is composed of a spin and spatial component. If two electrons have parallel spins their spin wavefunction is symmetric; therefore, to ensure the overall wavefunction is anti-symmetric their spatial component must be anti-symmetric. Conversely if the spins are anti-parallel the spatial wavefunction must therefore be symmetric. Mathematically this corresponds to

$$\psi_{\uparrow\uparrow}(\mathbf{r}_1, \mathbf{r}_2) \propto [\psi_1(\mathbf{r}_1)\psi_2(\mathbf{r}_2) - \psi_1(\mathbf{r}_2)\psi_2(\mathbf{r}_1)] \left|\uparrow\right\rangle_1 \left|\uparrow\right\rangle_2, \tag{B.29}$$

$$\psi_{\uparrow\downarrow}(\mathbf{r}_1, \mathbf{r}_2) \propto \psi_1(\mathbf{r}_1)\psi_2(\mathbf{r}_2) \left[\left|\uparrow\right\rangle_1 \left|\downarrow\right\rangle_2 - \left|\downarrow\right\rangle_1 \left|\uparrow\right\rangle_2\right] \tag{B.30}$$

The electron-electron interaction, also known as the Coulomb penalty, takes the form

$$\int \mathrm{d}^3\mathbf{r}_1 \int \mathrm{d}^3\mathbf{r}_2 |\psi(\mathbf{r}_1, \mathbf{r}_2)|^2 \frac{e^2}{|\mathbf{r}_1 - \mathbf{r}_2|}. \tag{B.31}$$

Note that the integrand of this function is maximal when $\mathbf{r}_1 = \mathbf{r}_2$ but this is *precisely* where the wavefunction for the parallel spins vanishes. We can mitigate the Coulomb penalty by using a parallel spin wavefunction. Hence, it is energetically favourable for two spins to be parallel. Hund's Rule 1 (H1): The total spin of an open shell is maximal. Simply put maximise **S**.

The next most important scale controls the choice of orbitals and directly competes with the crystal field (discussed in the following sections). Hund's Rule 2 (H2): The orbital angular momentum is maximised subject to the restriction of Fermi statistics. Simply put maximise **L**.

The third rule originates from relativity and is usually small. The terminology is spin

orbit coupling and the result is optimising **J**. Care should be taken as for the first half $j = |l - s|$ and for the second half $j = l + s$. Hund's Rule 3 (H3): Maximise $\mathbf{J} = \mathbf{L} + \mathbf{J}$. For the first half of the shell **S** and **J** are anti-parallel, for the second half they are parallel. Simply put optimise **J**

Applying Hund's rules is simple. We apply them in the order they were presented. Handily, this is also the the order of their energy scales. The origin of H1 is Coulomb and therefore depends on the *extent* of the shell. For example, if the shell is localised its energy is higher. This gives the 3d shell an energy scale of approximately 1-2eV and 2-10eV for the 4f shell. H2 is approximately the same order of H1 but a fraction of it. H3 is smaller still, being approximately 0.25eV for Ce and 1eV for Yb.

At this point we have a good physical picture of the periodic table, which is that of isolated atoms. However, in condensed matter systems we care about solids. The next two sections we focus on the caveats that pertain to the physics of atoms in solids.

B.4 Bonding — How Atoms Form a Solid

The physics of solids is all about bonding verses Coulomb repulsion and statistics. When atoms come together they 'stick' because, to a good approximation, electrons can make use of each other's nuclei's potentials while avoiding each other. This process is chemical bonding and effects the energies of different orbitals.

Let's take a look at the first failure of the gaseous picture of atoms in a solid. Consider the 4s and 3d shell. The 3d shell is more localised as $e^{-\frac{x}{3}}$ decays faster than $e^{-\frac{x}{4}}$. As the 4s electrons have a larger extent we would predict they will bond first, and only when the 3d wavefunctions begin to overlap will they bond. This prediction is incorrect.

Figure B.3 on page 203 depicts the hydrogenic probabilities for the 4s and 3d orbitals. We see that the 3d orbital will only overlap when the neighbouring atom is in the middle of of where the 4s electron would be! In practice the 3d electrons do bond and so the 4s electrons are in trouble. The 4s electrons experience strong Pauli exclusion from the 3d

Figure B.3: 4s vs 3d Radial Probabilities

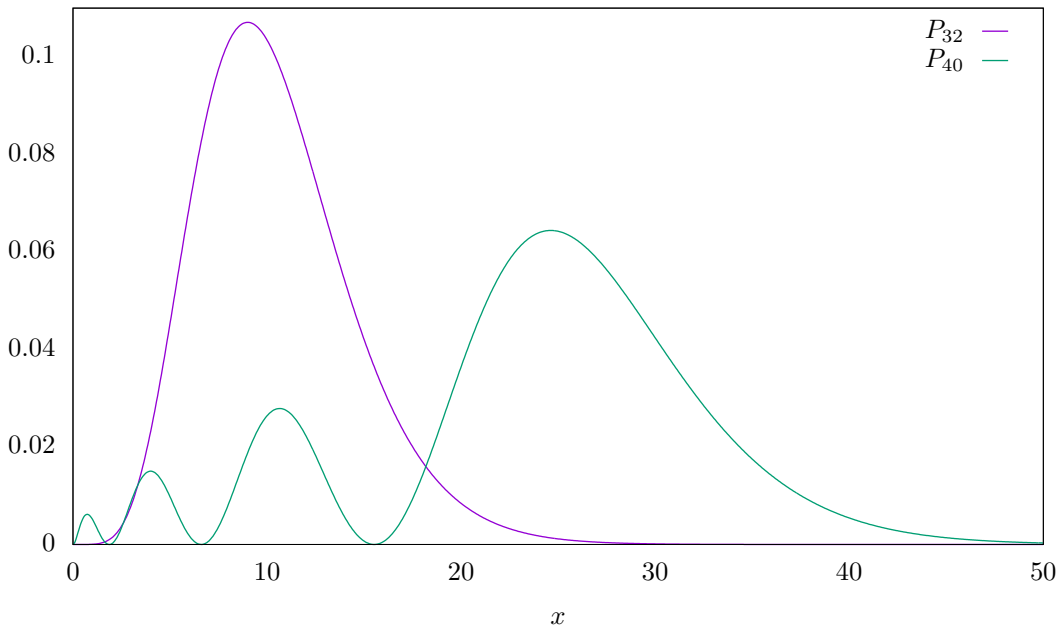

The 3d state is maximal where there is a large probability in the 4s shell. This will cause a large Pauli exclusion penality.

electrons. We can view the 4s electrons as being forced into the 'hole' where the atom sits causing a rise in their energy.

The physical picture of bonding in the transition metals is that of a balance between the 3d electrons (which are strongly chemically bonded) and the 4s or 4p electrons (which are under high pressure): the 3d electrons form the 'glue' which is compressing the 4s electronic subsystem. In practice, there are usually very few 4s electrons i.e $\frac{1}{2}$ an electron per manganese in γ-Mn [89]. For oxides this is even worse as the highly negative oxygen atoms usually force the 4s electrons out of accessibility and all that remains is the '3d core'. A similar 'anomaly' occurs in the 4f shell which occurs at the same time as the 6s shell. However, the f-electrons are so localised that they never directly bond, and instead must hybridise via other electrons to gain energy. This is the so called 'Hill limit' [90].

Note that both of these situations are exacerbated by the nature of screening. Comparing 3d to 4s again, we see that the 4s electrons are screened by the more localised 3d electrons. This means the 4s electrons are even more weakly bound than expected!

At this point we have taken our elementary gaseous picture of the periodic table and begun to see the effects of forming a solid. Namely, solids form due to bonding: the energetic gain from using neighbouring atom's potentials. This has radical consequences on the order of occupation for shells due to pauli exclusion. Next we will see the effects due to the lack of spherical symmetry.

B.5 Cubic Harmonics and The Crystal Field

So far we have a spherical representation of orbitals. This is acceptable in free space where there is spherical symmetry but in real systems there are other atoms which are charged. This set of surrounding atoms is called the *crystal field*. These atoms have electrons which will need to be Pauli avoided but also provide an opportunity for chemical bonding. This potential will also lift the spherical symmetry. In general we do not know the crystal field potential but we do know one thing: *the potential will respect the local point group of the atom.*

This key concept in this section, is that of the *irreducible representation* [91]. The group we have in mind is *the point group* where the elements are *spatial reflections and rotations*. This group acts on a vector space which is composed of *linear combinations of spherical harmonics*. It should be clear that upon application of a group element a spherical harmonic is mapped onto a linear combination of other spherical harmonics. For example under a 90° rotation about the y-axis

$$Y_{10}(\hat{\mathbf{r}}) \to \frac{1}{\sqrt{2}}\left[Y_{11}(\hat{\mathbf{r}}) + Y_{1\bar{1}}(\hat{\mathbf{r}})\right]. \tag{B.32}$$

The mapping of a vector space onto itself is described by a matrix and the collection of matrices which correspond to the group are known as a representation of the point group. Any representation of a group must have the same multiplicative properties as the

underlying group, in other words

$$g_1 g_2 = g_3 \quad \Rightarrow \quad R(g_1)R(g_2) = R(g_3), \tag{B.33}$$

where g_i is a group element and $R(g_i)$ is a representation.

The basic idea is to *choose linear combinations of spherical harmonics* which behave in the *simplest* possible way under the *action* of the *appropriate point group*. A vector space which is acted on by a group can be split into *irreducible subspaces* which are closed under the action of a group. Simply put, *they map onto themselves*.

The choice of basis of an invariant subspace provides an irreducible representation of the group acting on that basis. This gives a collection of $n \times n$ matrices which correspond to the action of the group on the chosen basis. We will apply these ideas to the cubic point group which has 48 elements and present the results [91].

Obviously the s orbital ($l = 0$) is irreducible as it is one dimensional. This is depicted in figure B.4 on page 206 and is given by

$$s = \frac{1}{\sqrt{4\pi}}. \tag{B.34}$$

The p orbitals ($l = 1$) are best represented in three dimensions. They are depicted in figure B.5 on page 206 and are given by

$$p_x = \sqrt{\frac{3}{4\pi}}\frac{x}{r}, \quad p_y = \sqrt{\frac{3}{4\pi}}\frac{y}{r}, \quad p_z = \sqrt{\frac{3}{4\pi}}\frac{z}{r}. \tag{B.35}$$

The d orbitals ($l = 2$) are split into two subspaces: a three dimensional t_{2g} (yes it's poorly named) and a two dimensional e_g. They are depicted in figures B.6 on page 207

Figure B.4: The s orbital

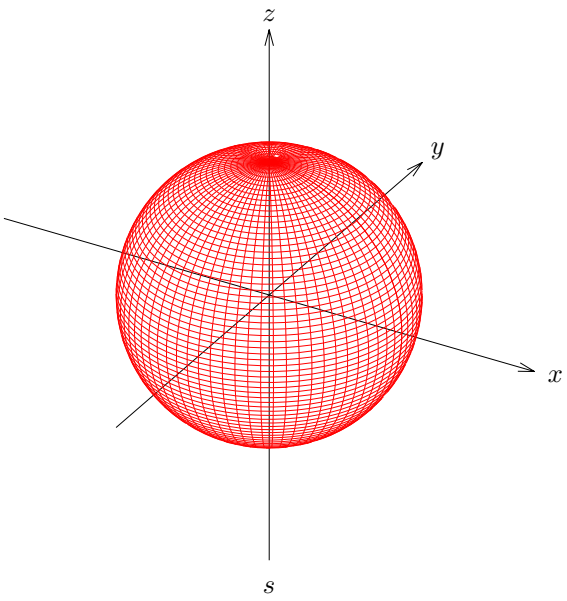

The s orbital is spherically symmetric and has a uniform positive (red) phase in each direction.

Figure B.5: The Three p Orbitals

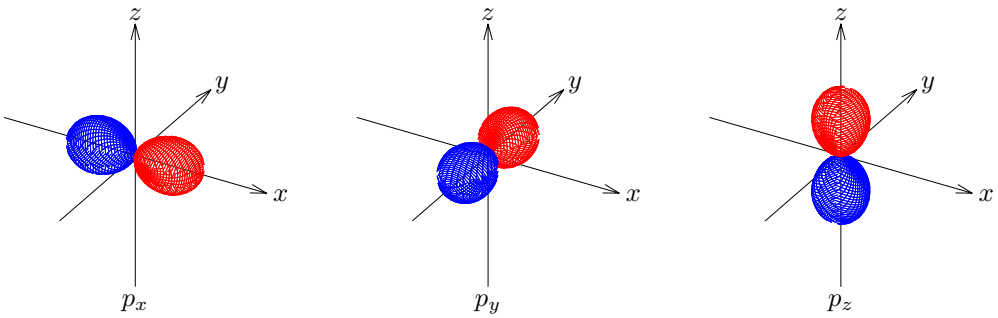

The three p orbitals lie along the Cartesian axes. Their phase is positive (red) in one half and negative(blue) in the other.

Figure B.6: The Three t_{2g} Orbitals

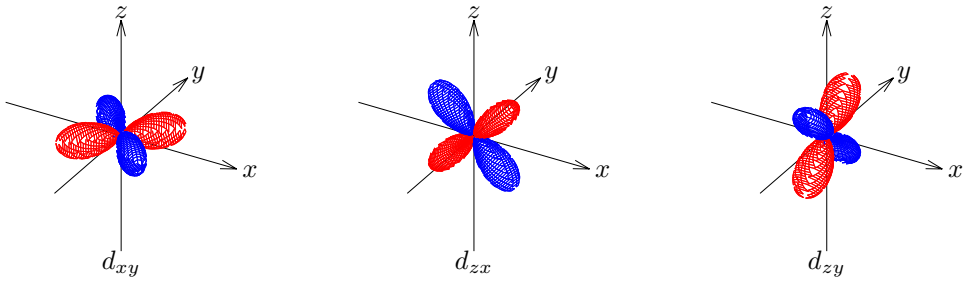

The three t_{2g} orbitals lie along the Cartesian planes. Their phase is positive (red) in opposite quarters and negative (blue) in the other.

and B.7 on page 208 respectively. The t_{2g} are given by

$$d_{yz} = \sqrt{\frac{15}{4\pi}}\frac{yz}{r^2}, \quad d_{xz} = \sqrt{\frac{15}{4\pi}}\frac{xz}{r^2}, \quad d_{xy} = \sqrt{\frac{15}{4\pi}}\frac{xy}{r^2}, \tag{B.36}$$

and the e_g subspace is given by

$$d_{x^2-y^2} = \sqrt{\frac{15}{16\pi}}\frac{x^2-y^2}{r^2}, \quad d_{3z^2-r^2} = \sqrt{\frac{5}{16\pi}}\frac{3z^2-r^2}{r^2}. \tag{B.37}$$

The f orbitals are split into 3 irreducible subspaces and are not named anything special. We have picked the most symmetric representation, in other documents you may see them represented another way. These are not depicted as the f electrons are dominated by Hund's rules and their crystal field are often irrelevant. The first set are given by

$$f_{x^2-r^2} = \sqrt{\frac{7}{16\pi}}\frac{x}{r}\frac{5x^2-3r^2}{r^2}, \quad f_{y^2-r^2} = \sqrt{\frac{7}{16\pi}}\frac{y}{r}\frac{5y^2-3r^2}{r^2}, \quad f_{z^2-r^2} = \sqrt{\frac{7}{16\pi}}\frac{z}{r}\frac{5z^2-3r^2}{r^2}, \tag{B.38}$$

Figure B.7: The Two e_g Orbitals

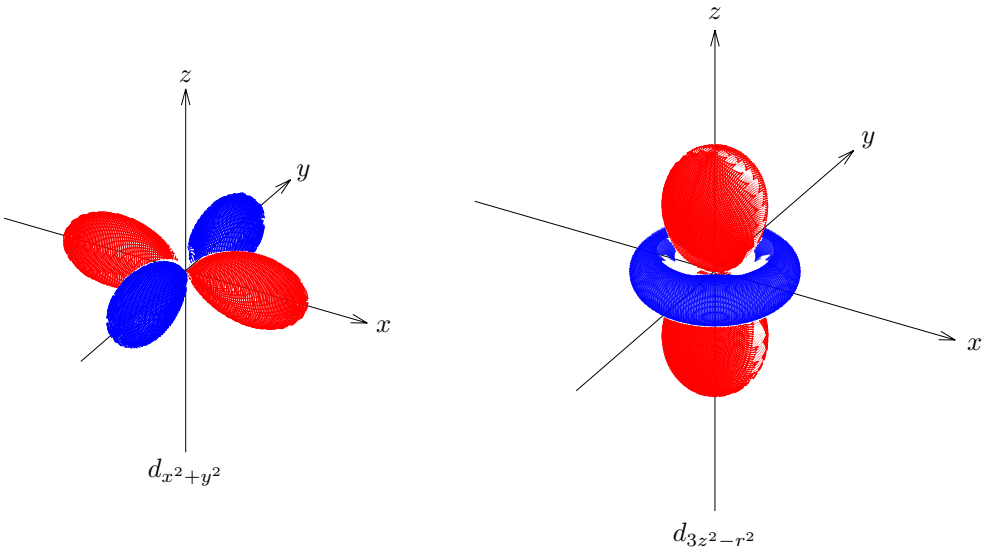

The two e_g orbitals lie along the Cartesian axis. The phase for the $d_{x^2-y^2}$ orbital is positive (red) along the x axis and negative (blue) along the y axis. The phase for the $d_{3z^2-y^2}$ orbital is positive along the z axis and negative in the 'ring' around the xy plane.

the second set are given by

$$f_{y^2-z^2} = \sqrt{\frac{105}{16\pi}}\frac{x}{r}\frac{y^2-z^2}{r^2}, \quad f_{z^2-x^2} = \sqrt{\frac{105}{16\pi}}\frac{y}{r}\frac{z^2-x^2}{r^2}, \quad f_{x^2-y^2} = \sqrt{\frac{105}{16\pi}}\frac{z}{r}\frac{x^2-y^2}{r^2}, \tag{B.39}$$

and the final one is given by

$$f_{xyz} = \sqrt{\frac{105}{4\pi}}\frac{xyz}{r^3}. \tag{B.40}$$

The application of these ideas is simple. There exist degeneracies in condensed matter systems. It is our job to discover how they are lifted. Including the *crystal field breaks spherical symmetry* hence different irreducible representations have different energies. The magnitude and sign of this change is unknown and must be solved for. For example, if an electron is in the $d_{x^2-y^2}$ orbital its wavefunction is maximal along the axis directions. If there are negatively charged ions in those directions, Coulomb repulsion would state it is unfavourable. Therefore both this and $d_{3z^2-r^2}$ (the other orbital in its irreducible

Figure B.8: Example Crystal Field Penality of $d_{x^2-y^2}$

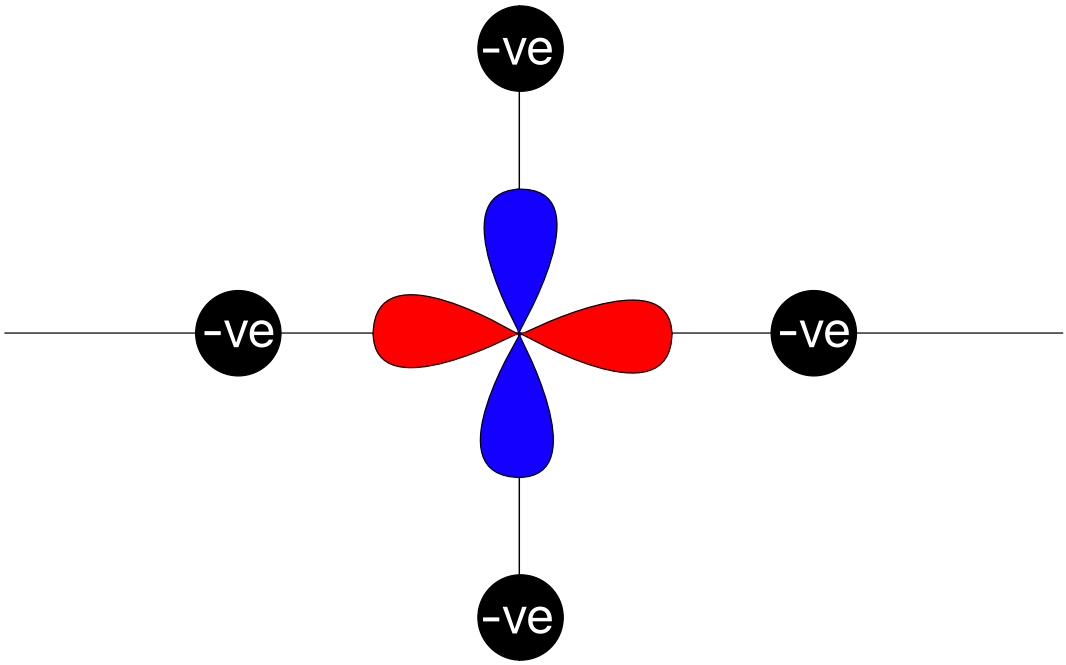

An electron is negatively charged and therefore pays a large Coulomb penality when its wavefunction overlaps with another electron. This figure depicts the view of a $d_{x^2-y^2}$ orbital and four surrounding negative charges. The angular wavefunction is maximal along the axis directions where the charges are placed. Therefore, this orbital will pay a high Coulomb penality.

representation e_g) are a higher energy than the three orbitals in t_{2g}. This is depicted in figure B.8 on page 209.

Crystal field and Hund's rules directly compete. In the first row transition metals there is competition between these energies *centred around Co.* H1 win for atoms to the left of Co and crystal field wins on the right. H2 is never relevant in this row unless the orbitals can be combined to gain more energy, for example $d_{xy} + id_{yz}$. *The Lanthanide series are dominated by Hund's rules [85].* Note, in general all Lanthanides form 3+ except at the edges where Ce can form Ce^{4+} and Yb can form Yb^{2+}. Both the Lanthanides and Actinides are tricky to deal with as the the size of f and d shells are comparable and they compete.

The rules of engagement are rather simple. If the Hund's rules win on the atom in question then just apply the appropriate rules in order. If the crystal field wins, determine which of the irreducible representations is lower in energy and fill the levels from the

bottom up. In either case the 'loser' between Hund's rules and crystal field acts to lift any residual degeneracy that may remain.

After all this work we have a physical picture of how atoms behave in solid state physics. The following sections will give two examples: modelling an insulating material and modelling a metal.

B.6 Example: MnO, An Antiferromagnetic Insulator

We will work through the list highlighted at the introduction of this chapter.

Step 1: This material is an insulator, we will keep this in mind while modelling this system.

Step 2: Let's separate this system into its core and valence electrons. To do this we begin with the electron configuration of both of the compounds atoms. Mn's electron configuration is $[Ar]3d^5 4s^2$ and O's is $[He]2s^2 2p^4$.

Step 3: Oxygen is incredibly electronegative. It is very rare in solid state to observe system where oxygen does not have a closed shell. In this material oxygen atoms will gain electrons to act as O^{2-}. As this is a full shell, the oxygen atoms do little but act as a field for the remaining electrons.

Step 4: If we recall from step 1, this material is an insulator. Therefore the number of electrons on each atom is defined. If the oxygen atom has gained two electrons, they must have come from the manganese atom. In this material manganese is said to 'donate' its electrons and will act as Mn^{2+}. From manganese's electron configuration we know that these electrons could come from either the 4s or 3d shell. Recalling that in solids the 4s shell feels a strong Pauli repulsion and are energetically unfavourable, we expect the electrons to be donated from the 4s shell. This leaves five electrons in the 3d shell.

Step 5: The structure of this compound is FCC [92]; this is usually very easy to find online. Now we consider the crystal field. The local environment of a Mn atom is depicted in figure B.9 on page 211. Electrons are negative and so are the oxygen sites which form

Figure B.9: Manganese's Octahedral Oxygen Cage

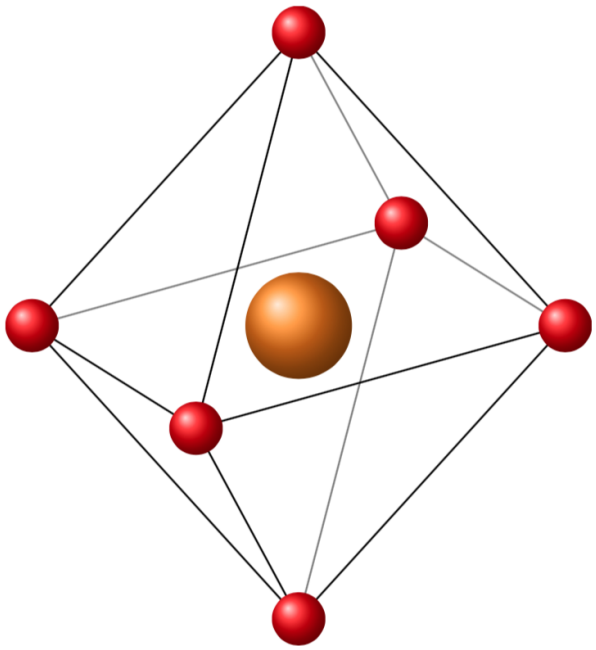

Each manganese atom (orange) is surrounded by six oxygen atoms (red). This forms an octahedral cage.

the 'cage' for the manganese atom. Therefore, the electrons do *not* want to be near each other. Of the t_{2g} and e_g orbitals it can be seen that the e_g orbitals violently overlap with the O^{2-} sites, therefore will be a higher energy.

Step 6: As Mn is on the left side of Co we know that Hund's rules will dominate over crystal field. From Hund's first rule we are told to maximise **S**. This results in the parallel alignment of all the electrons in each d orbital. This is depicted in figure B.10 on page 212. We are left with a Heisenberg model of the spin $\frac{5}{2}$ state on the manganese atoms.

Step 7: This does not apply for us.

Step 8: Superexchange is the coupling between two next-nearest neighbouring atoms through a non-magnetic atom. In our case the two atoms are Mn and the non magnetic atom is O. Electrons virtually hop from the Mn atom onto the O atom, and then (if they can) on to a further Mn atom. This is only facilitated if next-nearest neighbouring atoms are anti-ferromagnetically coupled. This is due to pauli exclusion prohibiting double

Figure B.10: Crystal Field Levels of MnO

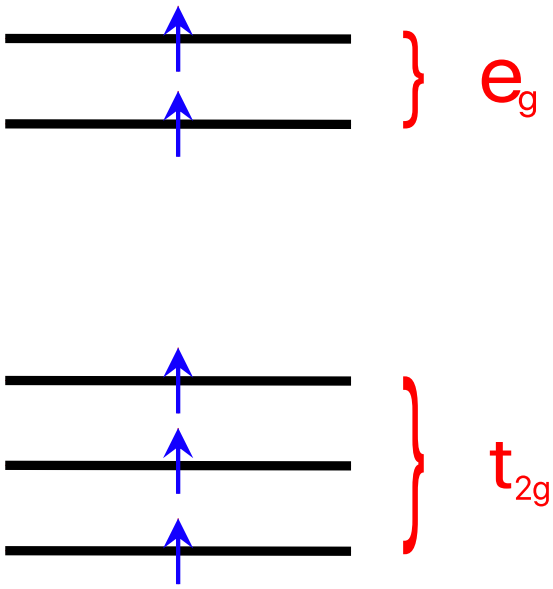

The crystal field lifts the d degeneracy, such that the t_{2g} band is a lower energy the e_g band. However, in this material Hund's rules dominate and spin must be maximised.

occupation from the hop if their spins were aligned. This is depicted in figure B.11 on page 213. We are left with an *anti-ferromagnetic Heisenberg model to solve.*

Step 9: This does not apply to us.

B.7 Example: Bulk Copper, a Metal

Step 1: This material is a metal.

Step 2: Copper's electron configuration is $[Ar]3d^{10}4s^1$.

Step 3: This step does not apply.

Step 4: For the case of copper, the d shell is full. This means that the only electron that can bond is the $4s^1$ electron.

Step 5: The structure of this metal is FCC [85]. As there is only one electron in the 4s shell the crystal field has no effect.

Step 6: Copper is to the right of Co and hence crystal field effects dominate over Hund's

Figure B.11: Depiction of Superexchange

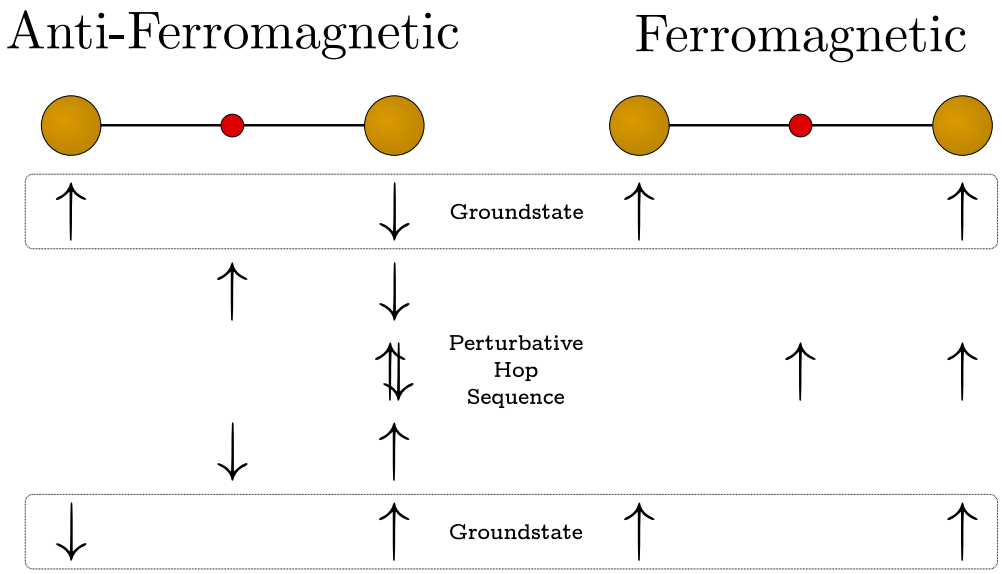

Visual representation explaining the source of antiferromagnetism. The large orange sites are manganese and small red sites are oxygen. Antiferromagnetic order allows for virtual hopping onto neighbouring states, ferromagnetism does not.

rules. However, there are no degeneracies to lift in this case.

Step 7: This step does not apply.

Step 8: This step does not apply.

Step 9: This metal has one electron in the 4s shell that forms a tight binding model. As the 4s shell is spherically symmetric we are left with a trivial tight binding model given by

$$H = -t \sum_{\langle ij \rangle \sigma} c^\dagger_{i\sigma} c_{j\sigma} + \epsilon \sum_{i\sigma} c^\dagger_{i\sigma} c_{j\sigma}, \tag{B.41}$$

with an FCC structure. This is trivially solved with a Bloch transformation giving

$$H = \sum_{\mathbf{k}\sigma} (\epsilon - Zt\gamma_{1,\mathbf{k}}) c^\dagger_{k\sigma} c_{k\sigma}, \tag{B.42}$$

where Z is the co-ordination number (12 in this case) and $\gamma_{1,\mathbf{k}}$ is the nearest neighbour structure factor. For an FCC lattice this is given by $\gamma_{\mathbf{k}} = \frac{1}{3}[\cos k_y \cos k_z + \cos k_z \cos k_x +$

$\cos k_x \cos k_y$]. If this is unfamiliar, it is explained in detail in the following section. This can be used to generate a band structure which can be compared to DFT (Density Functional Theory) or experiment.

This model is very basic, and in reality the 4s and even some 4p electrons hybridise with the 3d electrons. For a full picture this interaction must be taken into account.

B.8 Efficiently Solving the Tight Binding Model

In this final section we will go over, in detail, how to solve the many tight binding models that could occur in your analysis of materials. We will build complexity, beginning with s wave hopping on a linear chain, moving to a three dimensional system with one atom per unit cell, extending to a system with more than one atom per unit cell, and finally extending to a system with different electron shells.

The tight binding model is an elementary Hamiltonian that describes bonding between atoms. Though it begins as a simple model, it very quickly can become convoluted and messy. Implicit in every tight binding model is the structure that it acts on. The exact same Hamiltonian on a different structure can provide radically different results. Let's consider an ordinary nearest neighbour tight binding model with s-wave hopping on the linear chain. The Hamiltonian for which is

$$H = \epsilon \sum_{i\sigma} c^\dagger_{i\sigma} c_{i\sigma} - t \sum_{\langle ij \rangle \sigma} c^\dagger_{i\sigma} c_{j\sigma}, \tag{B.43}$$

where ϵ is the occupation energy and can be set to zero without loss of generality. Due to translational invariance, this is solved with a Bloch transform [93]

$$c^\dagger_{i\sigma} = \frac{1}{\sqrt{N}} \sum_{\mathbf{k}} e^{i\mathbf{k}\cdot\mathbf{R}_i} c^\dagger_{\mathbf{k}\sigma}, \quad c_{i\sigma} = \frac{1}{\sqrt{N}} \sum_{\mathbf{k}} e^{-i\mathbf{k}\cdot\mathbf{R}_i} c_{\mathbf{k}\sigma}, \tag{B.44}$$

which upon substitution yields

$$H = -t \sum_{\langle ij \rangle \sigma} \frac{1}{N} \sum_{\mathbf{k}\mathbf{k}'} e^{i\mathbf{k}\cdot\mathbf{R}_i} e^{-i\mathbf{k}'\cdot\mathbf{R}_j} c^\dagger_{\mathbf{k}\sigma} c_{\mathbf{k}'\sigma}. \tag{B.45}$$

We can define the nearest neighbours by writing $\mathbf{R}_j = \mathbf{R}_i + \mathbf{a}$, where $\mathbf{a}$ is a vector that takes to our nearest neighbours. This substitution gives

$$H = -t \sum_{i\sigma} \sum_{\mathbf{a}} \frac{1}{N} \sum_{\mathbf{k}\mathbf{k}'} e^{i[\mathbf{k}-\mathbf{k}']\cdot\mathbf{R}_i} e^{-i\mathbf{k}'\cdot\mathbf{a}} c^\dagger_{\mathbf{k}\sigma} c_{\mathbf{k}'\sigma}. \tag{B.46}$$

Bloch's theorem states that $\frac{1}{N}\sum_i e^{i[\mathbf{k}-\mathbf{k}']\cdot\mathbf{R}_i} = \delta_{\mathbf{k}\mathbf{k}'}$, combining this with a sum over $\mathbf{k}'$ and defining $Z\gamma_{1,\mathbf{k}} = \sum_{\mathbf{a}} e^{-i\mathbf{k}\cdot\mathbf{a}}$ gives

$$H = -Zt \sum_{\mathbf{k}\sigma} \gamma_{1,\mathbf{k}} c^\dagger_{\mathbf{k}\sigma} c_{\mathbf{k}\sigma}, \tag{B.47}$$

where Z is the co-ordination number: the number of nearest-neighbour atoms. We have diagonalised the Hamiltonian and hence solved the problem. Note that all the physics of the problem is encapsulated in $Z\gamma_{1,\mathbf{k}}$, known as the structure factor. For the 1D chain the set of neighbours is $\{-\hat{\mathbf{x}}, \hat{\mathbf{x}}\}$, where we have normalised the set the distance between neighbours to 1 without loss of generality. This gives $\gamma_{1,\mathbf{k}} = \cos(k_x)$.

It is the structure factor that changes when we consider different, more complex systems. When there is only one atom per unit cell the calculation is rather trivial, regardless of dimension. For example the structure factor for: the square lattice is

$$\gamma_{\mathbf{k}} = \frac{1}{2}[\cos k_x + \cos k_y], \tag{B.48}$$

the triangular lattice is

$$\gamma_{\mathbf{k}} = \frac{1}{3}\left[\cos k_x + \cos\left(\frac{k_x + \sqrt{3}k_y}{2}\right) + \cos\left(\frac{k_x - \sqrt{3}k_y}{2}\right)\right], \tag{B.49}$$

the cubic lattice is

$$\gamma_{\mathbf{k}} = \frac{1}{3}[\cos k_x + \cos k_y + \cos k_z], \tag{B.50}$$

the body centred cubic lattice is

$$\gamma_{\mathbf{k}} = \cos k_x \cos k_y \cos k_z, \tag{B.51}$$

the face centred cubic lattice is

$$\gamma_{\mathbf{k}} = \frac{1}{3}[\cos k_y \cos k_z + \cos k_z \cos k_x + \cos k_x \cos k_y]. \tag{B.52}$$

Things get more complicated when there are more than one atom per unit cell. In this case our elementary Hamiltonian gains some complexity and becomes

$$H = -\sum_{\langle ij\rangle\sigma} \left[t_{cc} c^\dagger_{i\sigma} c_{j\sigma} + t_{cf} \left(c^\dagger_{i\sigma} f_{j\sigma} + f^\dagger_{i\sigma} c_{j\sigma} \right) + t_{ff} f^\dagger_{i\sigma} f_{j\sigma} \right], \tag{B.53}$$

where we have labelled one site with c_σ operators and the second with f_σ, and $t_{\alpha\beta}$ are the hopping elements between sites α and β. Though this may look complex at first glance we can drastically simplify this by representing it as a matrix equation. This gives

$$H = \sum_{\langle ij\rangle\sigma} \begin{bmatrix} c^\dagger_{i\sigma}, & f^\dagger_{i\sigma} \end{bmatrix} \begin{bmatrix} -t_{cc} & -t_{cf} \\ -t_{cf} & -t_{ff} \end{bmatrix} \begin{bmatrix} c_{j\sigma} \\ f_{j\sigma} \end{bmatrix}, \tag{B.54}$$

which is just a matrix tight binding model. We can diagonalise this using a Bloch transform as before which yields

$$H = \sum_{\mathbf{k}\sigma} \begin{bmatrix} c^\dagger_{k\sigma}, & f^\dagger_{k\sigma} \end{bmatrix} \begin{bmatrix} -t_{cc} Z_{cc} \gamma_{cc,\mathbf{k}} & -t_{cf} Z_{cf} \gamma_{cf,\mathbf{k}} \\ -t_{cf} Z_{cf} \gamma_{cf,\mathbf{k}} & -t_{ff} Z_{ff} \gamma_{ff,\mathbf{k}} \end{bmatrix} \begin{bmatrix} c_{k\sigma} \\ f_{k\sigma} \end{bmatrix}, \tag{B.55}$$

where $Z_{\alpha\beta}$ is the number of β neighbours of site α, and $\gamma_{\alpha\beta,\mathbf{k}}$ is the structure factor of β neighbours of α. This matrix is the controlling object in tight binding analysis, which

when diagonalised produces the band structure.

We can simplify this analysis by introducing the following shorthand, often called the floating phase. We are interested in the sum

$$Z\gamma_{\mathbf{k}} = \sum_{\alpha} e^{i\mathbf{k}\cdot\mathbf{R}_\alpha}. \tag{B.56}$$

Upon substitution of $\mathbf{R}_\alpha = \alpha_x\hat{\mathbf{x}} + \alpha_y\hat{\mathbf{y}} + \alpha_z\hat{\mathbf{z}}$, we get

$$Z\gamma_{\mathbf{k}} = \sum_{\alpha} e^{i(\alpha_x k_x + \alpha_y k_y + \alpha_z k_z)}, \tag{B.57}$$

which can be decomposed into

$$Z\gamma_{\mathbf{k}} = \sum_{\alpha} e^{i\alpha_x k_x} e^{i\alpha_y k_y} e^{i\alpha_z k_z}. \tag{B.58}$$

By writing $x = e^{ik_x}$ etc. this becomes

$$Z\gamma_{\mathbf{k}} = \sum_{\alpha} x^{\alpha_x} y^{\alpha_y} z^{\alpha_z}. \tag{B.59}$$

Using this we can simply look at a geometry and read off the structure factor. We just count how many unit vectors each neighbour is away from the original atom and add the appropriate power of x, y or z. For example let's consider the cubic lattice. There neighbours are at $\hat{\mathbf{x}}$, $-\hat{\mathbf{x}}$, $\hat{\mathbf{y}}$, $-\hat{\mathbf{y}}$, $\hat{\mathbf{z}}$, and $-\hat{\mathbf{z}}$. Which give x, $\frac{1}{x}$, y, $\frac{1}{y}$, z and $\frac{1}{z}$ respectively. Putting these into the sum gives

$$Z\gamma_{\mathbf{k}} = x + \frac{1}{x} + y + \frac{1}{y} + z + \frac{1}{z} \tag{B.60}$$

$$= 2\cos k_x + 2\cos k_y + 2\cos k_z, \tag{B.61}$$

as required.

Let's use this simplification, and consider a system with two atoms per unit cell: the

diamond lattice. This is a FCC structure with two atoms per unit cell. We will consider nearest neighbours only, and hence only couple atom one with atom two. This is depicted in figure B.12 on page 219. From this we can simply read off the hoping matrix as

$$-t\begin{bmatrix} 0 & xyz+\frac{x}{yz}+\frac{y}{xz}+\frac{z}{xy} \\ \frac{1}{xyz}++\frac{yz}{x}+\frac{zx}{y}+\frac{xy}{z} & \end{bmatrix}, \tag{B.62}$$

which is trivially diagonalised to give the band structure

$$\epsilon_{\mathbf{k}} = \left[1+y^2z^2+z^2x^2+x^2y^2\right]\left[1+\frac{1}{y^2z^2}+\frac{1}{z^2x^2}+\frac{1}{x^2y^2}\right], \tag{B.63}$$

which upon direct substitution of the FCC structure factor $\gamma_{\mathbf{k}}^{FCC}$ gives

$$\epsilon_{\mathbf{k}} = \pm\left[4+12\gamma_{\mathbf{k}}^{FCC}\right]. \tag{B.64}$$

This highlights how much this simplifies the process of calculating the band structure.

The final thing to consider is the effect different orbitals have on this picture. So far we have only considered s-wave hopping which is spherically symmetric. In real systems electrons occupy other shells such as p, d and f. The occupation energy of these shells varies from one system to another, and we cannot simply set them to zero as before. These additional 'flavours' of electrons merely expand the hopping matrix, and now electrons can from any one site or shell to another. Unfortunately, as these shells are not spherically symmetric the phase difference is not always symmetric. This is highlighted in figure B.13 on page 219. Here the phase difference is positive for the s electron hopping right onto p_x but negative when hopping to the left onto p_x. This term would therefore look like $-t_{sp}(x-\frac{1}{x})$.

There is one final complication when considering different orbitals: symmetry. If there exists a plane that passes through the sites for which one orbital is symmetric under inversion and the other is anti-symmetric under inversion, the strength of that hop is zero. This is depicted in figure B.14 on page 220. In this diagram the xz plane passes through

Figure B.12: The Diamond Lattice

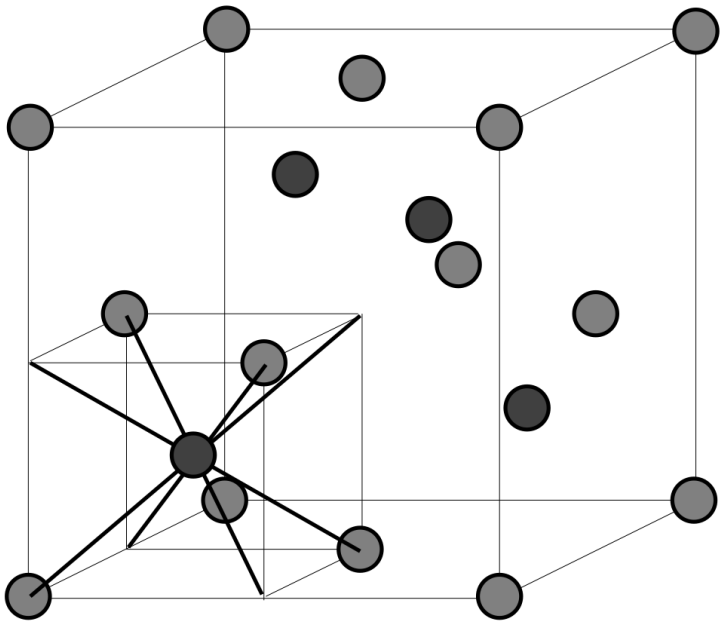

The diamond lattice is formed of two atoms per unit cell (grey and black), with an underlying FCC lattice for the unit cell.

Figure B.13: Hopping Asymmetry

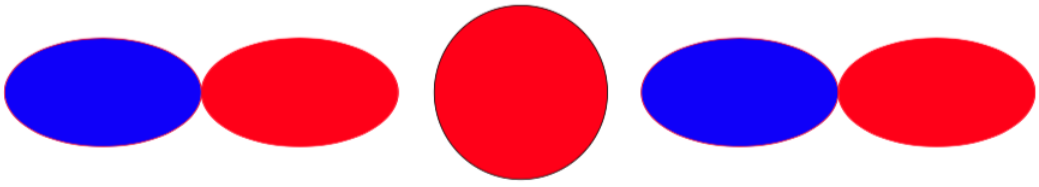

The asymmetry of the p_x orbital under inversion of x causes a phase asymmetry between hopping along the x axis between an s and p_x orbital.

Figure B.14: Orbital Symmetry Causing Vanishing Hopping

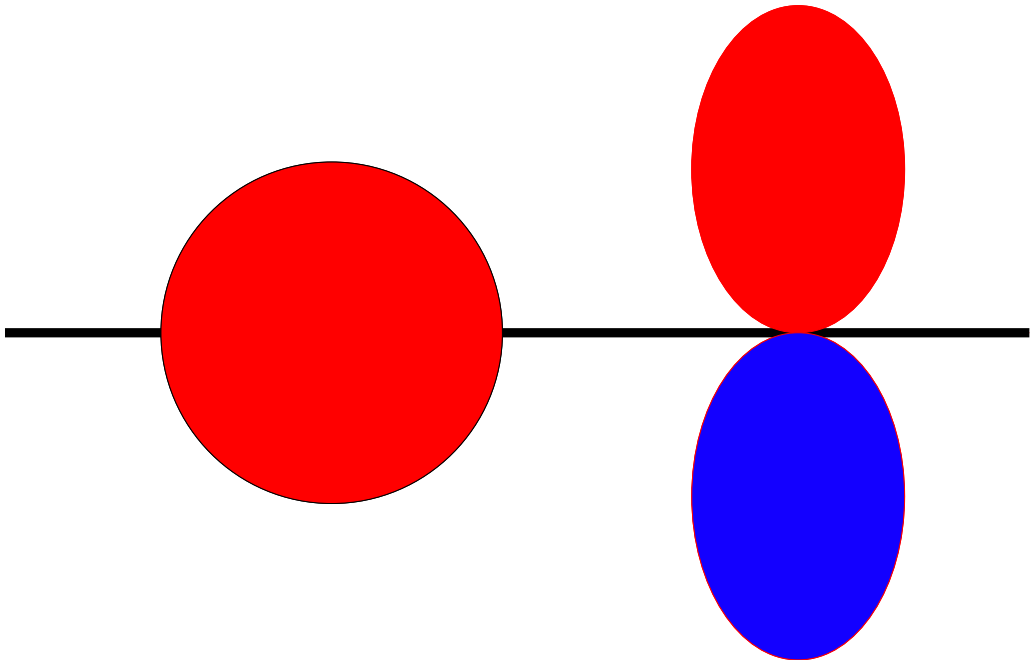

There is asymmetry of the p_y orbital under inversion of y and symmetry of s under the same transformation. This causes a phase cancellation when hopping along the x axis, resulting in this hop vanishing.

both sites. The s orbital is symmetric under inversion, but the p_y orbital is anti-symmetric under inversion. Hence this hop vanishes.

At this point we are able to solve any metallic tight binding model. We can extend this analysis to magnetic systems rather simply. If the system has antiferromagnetic order the unit cell will increase in size which needs to be taken into account. Adding magnetic order is as simple as changing the Hamiltonian to

$$H = -t \sum_{\langle ij \rangle \sigma} c^\dagger_{i\sigma} c_{i\sigma} + \Delta \sum_i \left[c^\dagger_{i\downarrow} c_{i\downarrow} - c^\dagger_{i\uparrow} c_{i\uparrow} \right], \tag{B.65}$$

where Δ is the magnetic penality (gain) for the incorrect (correct) alignment of a spin on a site.

With this we reach the end of this section and so too the appendix. The periodic table was modelled by extending the hydrogen atom. We then extended this to solid

state systems where affects such as bonding and crystal field were introduced. Finally, we thoroughly solved the tight binding model. With this you should be able to model many materials and in some cases even solve them.

APPENDIX C

THE LANCZOS ALGORITHM — EXACT DIAGONALISATION OF FINITE SYSTEMS

C.1 Introduction

Many body quantum mechanics is a difficult endeavour, where exact solutions are either for contrived models or are out of reach. As a result, we rely on sophisticated techniques with subtle approximation schemes. After all the hard work we are frequently left contemplating the decisions we made and the accuracy of the result. Thankfully there is a complementary technique we can use to compare our results against: exact diagonalisation.

Quantum mechanics is a linear algebra problem [80], hence we can represent any system of interest with a matrix. Subsequent diagonalisation of this matrix gives us access to the energy eigenvalues and eigenvectors, from which we can calculate any correlation we please. So why don't we deal with all quantum problems this way? It's simple: for an infinite system the matrix is infinite, which is notoriously difficult to write down, let alone diagonalise. Therefore, when discussing exact diagonalisation of quantum systems

we are strictly considering finite systems, but the perils are not yet done. For a system composed of objects with d degrees of freedom and n sites, the state space is of size d^n, and its matrix representation contains d^{2n} elements. This means that our state space grows exponentially with system size, and hence we are limited to rather small systems. To give a sense of scale, a computer with 8Gb of RAM can store 1×10^9 numbers, but this is only a state space of 31,622 which is equivalent to 7 sites of a spin-half fermion system. This scaling is so poor that doubling our RAM to 16Gb is still not enough to reach 8 sites.

All hope is not yet lost. Through the application of the Lanczos algorithm, extraction of symmetries, and some clever optimisations we are able to extend the number of sites to 17! With this increase techniques such as finite size scaling have a far higher success rate, and we are able to compare our results to analytics, hopefully corroborating the results.

This appendix will serve as a reference document for all future students who aspire to do exact diagonalisation. The technique will not only be explained with nuance but results will be given to compare against. We assume a competence in programming, so will not go into these details. We begin by detailing how to construct the matrix of a quantum system, namely the Heisenberg model. This is followed by an explanation of the Lanczos algorithm — the largest gain of memory in the process. Next we discuss the technical construction of the algorithm along with optimisations that can be made. Finally we extract symmetries of the Hamiltonian — the next largest gain of memory in the process. As an addendum to the appendix we include a section of particular results which will be invaluable to any student when they inevitably encounter errors in the process.

C.2 The Heisenberg Model

What follows is a quick overview of the Heisenberg model [74], the archetypal model for quantum magnets. A more detailed discussion on how to construct this Hamiltonian

computationally is given in section C.4.

Its Hamiltonian is

$$H = -J \sum_{\langle ij \rangle} \mathbf{S}_i \cdot \mathbf{S}_j, \tag{C.1}$$

where $\langle ij \rangle$ denotes that sites i and j are nearest neighbours, and J is the magnetic interaction strength, which is negative for a ferromagnetic system and positive for an anti-ferromagnetic system. Upon substitution of the vector spin operator $\mathbf{S} = S^x\hat{\mathbf{x}} + S^y\hat{\mathbf{y}} + S^z\hat{\mathbf{z}}$ we get

$$H = -J \sum_{\langle ij \rangle} \left(S_i^x S_j^x + S_i^y S_j^y + S_i^z S_j^z \right). \tag{C.2}$$

By choosing the z direction as special we can define the following spin raising and lowering operators

$$S^{\pm} = \left(S^x + iS^y \right), \tag{C.3}$$

such that upon substitution the Hamiltonian becomes

$$H = -J \sum_{\langle ij \rangle} \left(S_i^z S_j^z + \frac{1}{2} \left(S_i^+ S_j^- + S_i^- S_j^+ \right) \right). \tag{C.4}$$

Note that for a quantum mechanical state with spin l and z-projection m, denoted by $|l, m\rangle$, the spin operators [80] behave as

$$S^z |l, m\rangle = m |l, m\rangle, \tag{C.5}$$

$$S^{\pm} |l, m\rangle = \sqrt{l(l+1) - m(m \pm 1)}\, |l, m \pm 1\rangle. \tag{C.6}$$

We will be working with a spin-half system and as such will use the short hand $|\frac{1}{2}, \frac{1}{2}\rangle = |\uparrow\rangle$ and $|\frac{1}{2}, -\frac{1}{2}\rangle = |\downarrow\rangle$. The spin operators therefore result in

$$S^z |\uparrow\rangle = \frac{1}{2} |\uparrow\rangle, \quad S^z |\downarrow\rangle = -\frac{1}{2} |\downarrow\rangle, \tag{C.7}$$

$$S^+ |\uparrow\rangle = 0, \quad S^+ |\downarrow\rangle = |\uparrow\rangle, \quad S^- |\uparrow\rangle = |\downarrow\rangle, \quad S^- |\downarrow\rangle = 0. \tag{C.8}$$

We are now in a position to construct the Hamiltonian. The first thing to note is that the H can be written as a sum over local Hamiltonians that only act on two sites $H = -J\sum_{\langle ij\rangle} H_{ij}$. This means that when we 'apply' the Hamiltonian to a state we need only decompose the state into nearest neighbour pairs and apply the local change. Lets see what this corresponds to for a 4 site system with open boundaries $|\sigma_1\sigma_2\sigma_3\sigma_4\rangle$, where σ_i denotes the spin on site i.

$$H\,|\sigma_1\sigma_2\sigma_3\sigma_4\rangle \to \boxed{H_{12}}\,|\sigma_1\sigma_2\sigma_3\sigma_4\rangle + |\sigma_1\boxed{\sigma_2\sigma_3}\sigma_4\rangle + |\sigma_1\sigma_2\boxed{\sigma_3\sigma_4}\rangle$$

From the diagram above it becomes obvious that we need only see how the Hamiltonian affects two neighbouring spins. The effect of H_{ij} is

$$|\uparrow\uparrow\rangle \Rightarrow \frac{1}{4}\,|\uparrow\uparrow\rangle\,, \quad |\downarrow\downarrow\rangle \Rightarrow \frac{1}{4}\,|\downarrow\downarrow\rangle\,. \tag{C.9}$$

$$|\uparrow\downarrow\rangle \Rightarrow -\frac{1}{4}\,|\uparrow\downarrow\rangle + \frac{1}{2}\,|\downarrow\uparrow\rangle\,, \quad |\downarrow\uparrow\rangle \Rightarrow -\frac{1}{4}\,|\downarrow\uparrow\rangle + \frac{1}{2}\,|\uparrow\downarrow\rangle\,. \tag{C.10}$$

This may be written as a matrix in the basis $[|\uparrow\uparrow\rangle\,, |\uparrow\downarrow\rangle\,, |\downarrow\uparrow\rangle\,, |\downarrow\downarrow\rangle]$

$$H_{i,j} = \frac{1}{4}\begin{bmatrix} 1 & 0 & 0 & 0 \\ 0 & -1 & 2 & 0 \\ 0 & 2 & -1 & 0 \\ 0 & 0 & 0 & 1 \end{bmatrix}. \tag{C.11}$$

This is *not* the matrix representation of H. This is the local Hamiltonian, which is used to calculate the full H. The full Hamiltonian can be calculated by taking the tensor product of this with the identity as follows:

$$H = -J\sum_{\langle ij\rangle} \mathbb{1}_{1,2} \otimes \mathbb{1}_{2,3} \otimes \ldots H_{i,j} \ldots \mathbb{1}_{n-1,n}, \tag{C.12}$$

and an example is given at section C.9.

Figure C.1: Periodic vs Anti-periodic Boundary Conditions

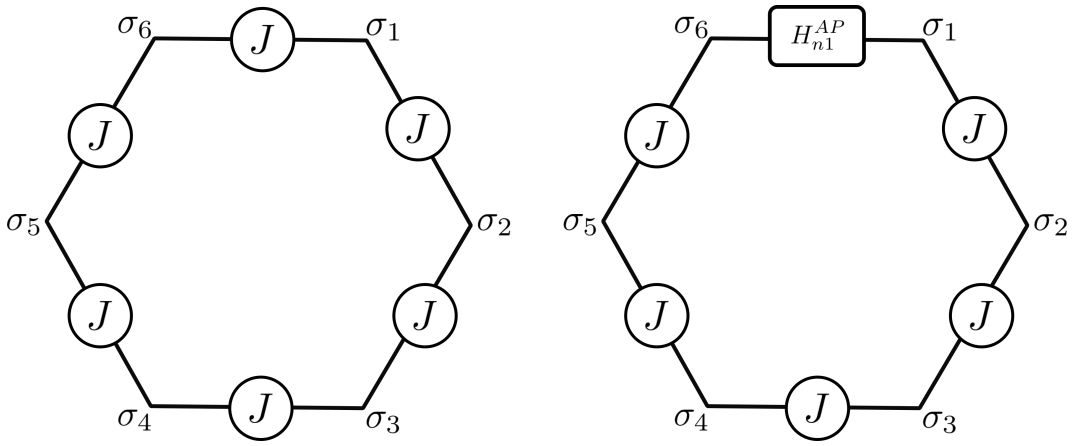

Pictorial representation of boundary conditions, periodic (left) and anti-periodic (right). In either case a 'ring' is formed of lattice sites, with a bond connecting the first and final site. For periodic boundary conditions this bond is the same as every other bond, whereas for anti-periodic boundary conditions this bond has a different Hamiltonian.

A note on boundary conditions. There are three natural types of boundary conditions: open, periodic and anti-periodic. Open boundary conditions have been discussed up to now, they describe a system with edges that are special as they only have one bond as opposed to two. Periodic and anti-periodic boundary conditions are an effective way to simulate an infinite system, in which there are no special sites. To implement these we add another bond between sites n and 1. For periodic boundary conditions this bond is the same strength as all other bonds, while for anti-periodic boundary conditions it is not as simple. This is explained in detail in section C.8, but for now it is enough to know that the Hamiltonian *on that bond* is changed to:

$$H_{n1}^{AP} = -J\left(S_n^z S_1^z - S_n^x S_1^x - S_n^y S_1^y\right), \tag{C.13}$$

where the sign of both the S^z and S^y term has switched. This is depicted in the figure C.1 on page 227.

C.3 The Lanczos Algorithm

The Lanczos algorithm [60] is an iterative tri-diagonalisation routine. It takes any Hermitian matrix and returns another with elements on the diagonal and nearest off-diagonals. If this was the only thing we did it would still be useful, resulting in a large saving of memory as we would go from N^2 matrix elements to $3N$ non-zero matrix elements. As it happens the routine has one added benefit: the lowest eigenvalues of the Lanczos matrix exponentially converge to those of the original matrix. This is what makes the Lanczos algorithm so powerful, it not only drastically reduces memory usage but it finds the lowest lying eigenvalues exponentially quickly. We will now derive the algorithm, discuss exponential convergence, and explain how to reconstruct the ground-state vector.

The aim is to generate a routine which converts the Hamiltonian from our basis to the Lanczos basis. Underlying the technique we are using $\{H^n\phi_0\}$ as a basis, where ϕ_0 is the initial vector, and performing Gram-Schmitt orthogonalisation [94]. The resulting iterative routine will generate the Lanczos basis $\{|n\rangle\}$, where $|1\rangle = \phi_0$ the initial vector.

Applying H to $|1\rangle$ gives

$$H|1\rangle = a_1|1\rangle + b_1|2\rangle . \tag{C.14}$$

We calculate a_1 then b_1 then $|2\rangle$ by

$$a_1 = \langle 1|H|1\rangle , \tag{C.15}$$

$$b_1 = \sqrt{\|(H-a_1)|1\rangle\|}, \tag{C.16}$$

$$|2\rangle = \frac{1}{b_1}(H-a_1)|1\rangle . \tag{C.17}$$

Now we apply the Hamiltonian to $|2\rangle$

$$H|2\rangle = c_2|1\rangle + a_2|2\rangle + b_2|3\rangle . \tag{C.18}$$

Taking the inner product with $|1\rangle$, and using the hermiticity of H we find that $c_2 = b_1$,

from which we find a_2 and b_2 in the same way as before

$$c_2 = \langle 1| H |2\rangle = \langle 2| H |1\rangle = b_1 * \tag{C.19}$$

$$a_2 = \langle 2| H |2\rangle \tag{C.20}$$

$$b_2 = \sqrt{\|(H - a_2) |2\rangle - b_1 |1\rangle\|}, \tag{C.21}$$

$$|2\rangle = \frac{1}{b_2}(H - a_2) |2\rangle - b_1 |1\rangle . \tag{C.22}$$

We apply the Hamiltonian one final time to $|3\rangle$

$$H |3\rangle = d_3 |1\rangle + c_3 |2\rangle + a_3 |3\rangle + b_3 |4\rangle . \tag{C.23}$$

By taking the inner product with $|1\rangle$ it is trivial to see (using Hermiticity) that $d_3 = 0$, and from here on in the process is repeated. To summarise

1. Apply the Hamiltonian to state $|n\rangle$ which will give

$$H |n\rangle = b_{n-1} |n-1\rangle + a_n |n\rangle + b_n |n+1\rangle ,$$

   where we have defined $b_0 = 0$.

2. Find a_n from $\langle n| H |n\rangle$ as $|n\rangle$ is known.

3. Find b_n from

$$\|H |n\rangle - b_{n-1} |n-1\rangle - a_n |n\rangle\| = b_n^2,$$

   as a_n, b_n and $|n-1\rangle$ are known.

4. Find $|n+1\rangle$ from

$$|n+1\rangle = \frac{1}{b_n}\Big(H |n\rangle - b_{n-1} |n-1\rangle - a_n |n\rangle \Big),$$

   as all entities on the right hand side are known quantities.

5. Store all values of a_n and b_n as they form the tri-diagonal matrix. Store states $|n-1\rangle, |n\rangle$ and $|n+1\rangle$ as they are required for the next iteration.

6. Repeat process, increasing n until the required eigenvalues of the tri-diagonal matrix converge to those of the Hamiltonian.

The iteration algorithm and tridiagonal matrix can be written as

$$\begin{bmatrix} H|1\rangle, & H|2\rangle, & ... \end{bmatrix} = \begin{bmatrix} |1\rangle, & |2\rangle, & ... \end{bmatrix} \begin{bmatrix} a_1 & b_1 & & \\ b_1 & a_2 & b_2 & \\ & b_2 & a_3 & \ddots \\ & & \ddots & \ddots \end{bmatrix} \tag{C.24}$$

Note that when beginning this process the original vector must have some overlap with the ground state, else it will not find it. This is most easily ensured by starting with a random vector.

C.3.1 Eigenvalue Convergence

If we were interested in the entire energy spectrum of H the Lanczos algorithm would only be useful as a means to save memory. In reality we usually only care about the ground state eigenvalue, and sometimes the first excitation to examine the gap. In this case the Lanczos algorithm reigns supreme, as the lowest lying eigenvalues of the Lanczos matrix converge onto those of the Hamiltonian exponentially quickly. To see why consider the following, where $|R\rangle$ is a random vector, μ is a shift that defines the zero of the problem, and E_0 is the lowest eigenvalue

$$\left(\frac{H-\mu}{E_0-\mu}\right)^N |R\rangle = \left(\frac{H-\mu}{E_0-\mu}\right)^N \sum_\lambda a_\lambda |\lambda\rangle \tag{C.25}$$

$$= \sum_\lambda \left(\frac{H-\mu}{E_0-\mu}\right)^N a_\lambda |\lambda\rangle . \tag{C.26}$$

In the case $\lambda = 0$ this returns one, but if $\lambda \neq 0$ as $E_0 < E_\lambda$ this operation returns a fraction less than one. This exponentially tends to zero. The Lanczos algorithm actually performs better than this as it is not simply repeated application of the Hamiltonian, it is simultaneously orthogonalising. For example $(0.3)^{30} = 2 \times 10^{-16}$, so the ground state eigenvalue can converge from a 30 by 30 matrix in the Lanczos basis.

There is a caveat however; the number of steps until convergence is heavily dependent on the energy gap. If there is a large degeneracy and the energies are very close together then convergence can take thousands of steps. Consider $(0.99)^{30} \approx 0.74$, to get the same convergence as before approximately 3500 steps must be taken as $(0.99)^{3500} \approx 5\text{x}10^{-16}$.

C.3.2 Reconstructing the Ground State Vector

In physics we are not only interested in the energetics but frequently care about correlations. These tell us to what degree two sites are affected by one another, and hence indicate the order that exists within the system. Reconstructing the ground state vector is mathematically trivial, it is just a conversion of basis

$$|GS\rangle = \sum_n v_n |n\rangle , \tag{C.27}$$

where $|GS\rangle$ is the ground state, $|n\rangle$ are the Lanczos basis vectors and v_n are elements of the tri-diagonal matrix's eigenvector. To calculate this a second run of Lanczos must be done, calculating the ground state vector on the go.

C.4 Technical Construction

There is little use in knowing the mathematical formalism of an algorithm; it must be implemented. That is the purpose of this section. There are many components that come together to set this up computationally: representing states, applying the Hamiltonian, and computing eigenvalues. Each will be discussed and by the end, the reader should be

able to program an elementary Lanczos algorithm.

At this point it is good to mention a little practical advice. Firstly, always make the most simple program you can to begin with. Complexity can be added in the future. To that end, invest in version control, GitHub is a great example. Secondly, check your code for small systems by hand. To aid with this point I have produced section C.9, which can act as a reference to check against.

C.4.1 Representing the State

When studying quantum mechanical systems it can often feel intuitive to apply operators to states. It is only when one tries to generate an algorithm for this action do they realise how awkward it really is. In this section we will learn how to represent quantum mechanical states numerically, in order for us to apply a Hamiltonian in the next section.

This may be a strange starting point, but lets take the binary representation of 5 and replace the digits 0 and 1 via the rules $0 \equiv \uparrow$ and $1 \equiv \downarrow$

$$5 \equiv 0101 \rightarrow \uparrow\downarrow\uparrow\downarrow \, . \tag{C.28}$$

Interestingly, we are returned a particular quantum mechanical state composed of four sites. It is not a giant leap to recognise that this could be done with any integer, subsequently generating another state. We also know that this procedure produces unique states as there is a unique binary representation of every integer. We can then use this to represent every state in our system.

Consider a four site Heisenberg spin chain. As there are two degrees of freedom on each site and four sites, we know that there are $2^4 = 16$ states in our Hilbert space. From our previous analysis we know that each integer from $[0, 15]$ will map to a state in our

Hilbert space. More directly we have

$$\begin{array}{cccccccccc} 0 & & 0000 & & \uparrow\uparrow\uparrow\uparrow & & 8 & & 1000 & & \downarrow\uparrow\uparrow\uparrow \\ 1 & & 0001 & & \uparrow\uparrow\uparrow\downarrow & & 9 & & 1001 & & \downarrow\uparrow\uparrow\downarrow \\ 2 & & 0010 & & \uparrow\uparrow\downarrow\uparrow & & 10 & & 1010 & & \downarrow\uparrow\downarrow\uparrow \\ 3 & \equiv & 0011 & \rightarrow & \uparrow\uparrow\downarrow\downarrow & & 11 & \equiv & 1011 & \rightarrow & \downarrow\uparrow\downarrow\downarrow \\ 4 & & 0100 & & \uparrow\downarrow\uparrow\uparrow & & 12 & & 1100 & & \downarrow\downarrow\uparrow\uparrow \\ 5 & & 0101 & & \uparrow\downarrow\uparrow\downarrow & & 13 & & 1101 & & \downarrow\downarrow\uparrow\downarrow \\ 6 & & 0110 & & \uparrow\downarrow\downarrow\uparrow & & 14 & & 1110 & & \downarrow\downarrow\downarrow\uparrow \\ 7 & & 0111 & & \uparrow\downarrow\downarrow\downarrow & & 15 & & 1111 & & \downarrow\downarrow\downarrow\downarrow \end{array} \tag{C.29}$$

Therefore, we can represent our entire Hilbert space with an array of size b^n, where b is the degrees of freedom on each site and n is the number of sites. The index of this array represents a unique state in our Hilbert space, and each state is accounted for.

In section C.2 we learned how to apply our Hamiltonian. The result was applying a sequence of local Hamiltonians. We therefore need a system to convert our array indices into binary. Application of a local Hamiltonian will produce a state in our Hilbert space, we therefore also require a method to convert a binary representation into an array index. Fortunately, both of these things are rather trivial.

Converting a number m to base b for an n site system requires integer division of m by b, n times. At each division store the resulting remainder. Reading this set of remainders backwards is the base b representation of m. For example, finding the base 2 representation of 5 for a 4 site system is as follows

$$\begin{array}{l} 5 \div 2 = 2 \quad \text{rem } 1 \\ 2 \div 2 = 1 \quad \text{rem } 0 \\ 1 \div 2 = 0 \quad \text{rem } 1 \\ 0 \div 2 = 0 \quad \text{rem } 0 \end{array} . \tag{C.30}$$

Reading the remainders backwards give 0101 as required.

Converting a base b number i_b into a base 10 number i_{10} consists of multiplying the digits of i_b by increasing powers of b (right to left) and summing them. For example, finding the base 10 representation of 0101 from base 2 is as follows

$$\begin{aligned} & 1 \times 2^0 + 0 \times 2^1 + 1 \times 2^2 + 0 \times 2^3 \\ & = 1 + 0 + 4 + 0 \\ & = 5 \end{aligned} \tag{C.31}$$

C.4.2 Applying the Hamiltonian

Now that we know how to represent the states of our Hilbert space with a vector, the next logical step is to apply the Hamiltonian to this state. The first thing to note is that we *never* calculate the full matrix, simply because it is too large. Instead when we 'apply' the Hamiltonian we recalculate its affects. At this point it is convenient to recall our local Hamiltonians H_{ij} from equation C.11, and remember that this is applied to each pair of neighbours. This is incredibly useful as it is easy to program H_{ij} with a series of if statements.

The following series of steps describe how to apply the Hamiltonian:

1. Create a second vector (the same size as the original) to store the application result.
2. Loop over each element of the original vector.
3. Save the value of the element P_x as this represents the probability amplitude of this state.
4. Convert the element index x to base b.
5. Loop over each digit of x_b.
6. Apply H_{ij} using a series of if statements. This will produce another state y_b.
7. Convert y_b to y_{10} (y in base 10).

8. Access the element y_{10} of the second vector and add to it the corresponding coefficient i.e. $J * P_x$

9. If considering closed boundary conditions ensure the correct Hamiltonian H_{1n} over the connecting bond.

Remember the process begins with a normalised random vector to ensure overlap with the ground state.

C.4.3 Calculating Eigenvalues and Truncation

At this point you should be able to generate a tri-diagonal matrix. The only thing left is to find the eigenvalues of this matrix. To do this, I recommend using a diagonalisation routine, many exist for every programming language [95].

The final thing left to understand is when to truncate the tri-diagonal matrix. We know that the lowest lying eigenvalues of these converge exponentially quickly to the those of the original, but when do we stop the routine? There are two ways to do this.

1. Compare the current lowest eigenvalue to the previous one, when the difference is almost zero it has converged.

2. Look at the last value of the tri-diagonal eigenvector associated with the lowest eigenvalues, when its almost zero it has converged.

Point 1 is faster but not as accurate, while point 2 is slower but more accurate. The speed is associated with the algorithm cost of each. Finding the eigenvalues of a matrix scales as N^3 while finding the eigenvectors scales as N^4 where N is the size of the matrix. So if a particular system has a high degeneracy, and hence requires many thousands of iterations, point 2 will be much slower. Great care should be taken in choosing one of these methods.

At this point I will mention the effects of numerical accuracy when doing this routine. The biggest issue is that of orthogonality. We have mathematically defined the set $|n\rangle$

Figure C.2: Convergence of Lanczos Eigenvalues

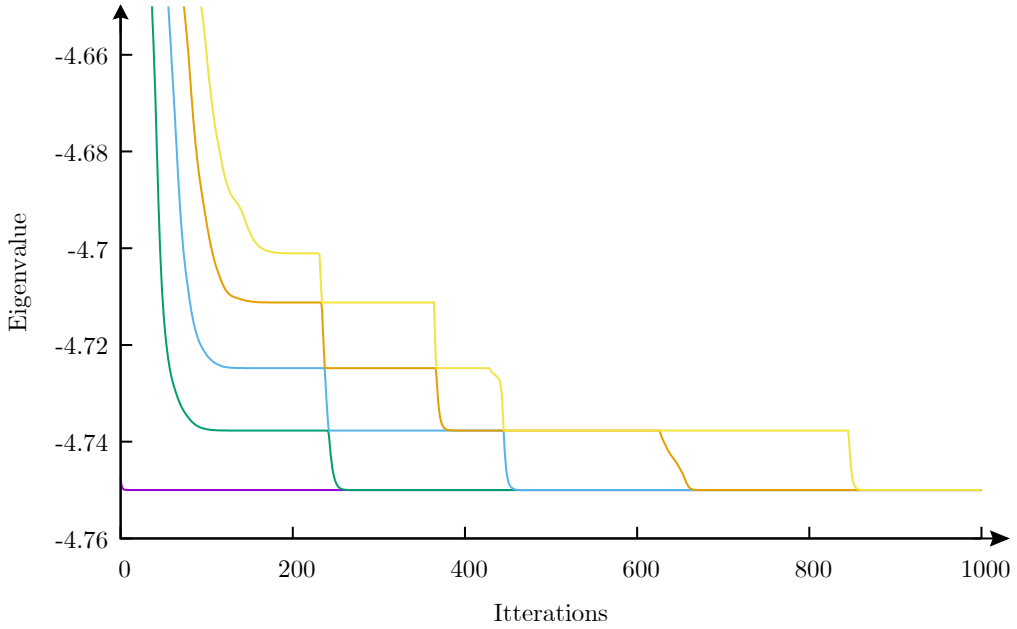

Lowest lying eigenvalues vs iteration number. Each eigenvalue plateaus and at a random point loses orthogonality due to numerical accuracy. At this point it begins to converge to the eigenvalue beneath it.

to form an orthonormal basis, but in reality this is only true up to numerical accuracy. When the deviations between these states becomes smaller than the accuracy available to us, orthonormality is broken and states begin to reconverge. This is complicated further by the fact that this happens at differing points for each eigenvalue. In figure C.2 on page 236 we see that after certain point eigenvalues begin to converge to the ones below. For this reason we can only automate truncation to a certain degree and caution must be taken.

You should now have all the knowledge required to write a Lanczos routine for the Heisenberg model. However this is just the beginning, the next sections will introduce optimisations and teach how to extract symmetries. With this the system sizes that are accessible to you will drastically increase.

C.5 Optimisations

In all the work up to now, we have been rather care free with our use of memory. That is somewhat foolish as the entire game of exact diagonalisation is to do with memory optimisation. In this section we will introduce two techniques that will save us memory; one is simple and the other sophisticated. The first optimisation is concerned with finding eigenvalues, where we will reduce the number of vectors required from three to two. The second optimisation is concerned with the eigenvectors, where we will reduce the number of vectors required from four to two.

C.5.1 Eigenvalues

This rather trivial optimisation will reduce the number of vectors required from three to two. This gives a saving of two thirds in memory, which could be enough to get an extra site or two. Let $\mathbf{A}$ and $\mathbf{B}$ represent the two vectors one uses in the computation. The stages these vectors go through are:

$$\begin{array}{lll} \mathbf{A} = |n\rangle & \mathbf{B} = |n-1\rangle & \\ \mathbf{A} = |n\rangle & \mathbf{B} = H\mathbf{A} - b_{n-1}\mathbf{B} \quad \Rightarrow & a_n = \mathbf{A}\cdot\mathbf{B} \\ \mathbf{A} = |n\rangle & \mathbf{B} = \mathbf{B} - a_n\mathbf{A} \quad \Rightarrow & b_n = |\mathbf{B}| \\ \mathbf{A} = |n\rangle & \mathbf{B} = \frac{\mathbf{B}}{b_n} \equiv |n+1\rangle & \\ \mathbf{A} = |n+1\rangle & \mathbf{B} = |n\rangle & \end{array} \tag{C.32}$$

Initially, we were required to store three vectors $|n-1\rangle, |n\rangle, |n+1\rangle$ in order to run the Lanczos routine. Thanks to this, we need only store $\mathbf{A}$ and $\mathbf{B}$ provided we follow the advised procedure.

C.5.2 Eigenvectors

Using the optimisation discussed in the former section we instantly reduce the number of vectors required to calculate the ground state by one. Though this is true, we can be

more cunning using mathematics and get this down to two. The trick is to generate the Lanczos algorithm where the basis automatically generates the ground state.

The three term recursion relationship developed in section C.3 was $H|n\rangle = b_{n-1}|n-1\rangle + a_n|n\rangle + b_n|n+1\rangle$. The aim is to find a similar relationship

$$H\psi_N = \delta\psi_{N-1} + \beta\psi_N + \gamma\psi_{N+1}. \tag{C.33}$$

Where

$$\psi_N = \sum_{n=0}^{N} v_n |n\rangle , \tag{C.34}$$

such that when $N = T$, where T is the size of the set v_n, $\psi_T = |GS\rangle$.

First we apply the Hamiltonian to ψ_N substituting in the definition and expanding the sums.

$$H\psi_N = H\sum_{n=0}^{N} v_n |n\rangle = \sum_{n=0}^{N} v_n \left(b_{n-1}|n-1\rangle + a_n|n\rangle + b_n|n+1\rangle\right) \tag{C.35}$$

As we have defined $b_{-1} = 0$ we can start the first summation from $n = 0$ and add a $n = 0$ term to the final sum without loss of generality, giving

$$H\psi_N = \sum_{n=0}^{N-1} v_{n+1}b_n|n\rangle + \sum_{n=0}^{N} a_n v_n|n\rangle + \sum_{n=0}^{N+1} v_{n-1}b_{n-1}|n\rangle . \tag{C.36}$$

We know

$$b_{n-1}v_{n-1} + a_n v_n + b_n v_{n+1} = \epsilon v_n, \tag{C.37}$$

where ϵ is the eigenvalue calculated. Substituting this into the above and adding extra

terms to complete the sum yields

$$H\psi_N = \epsilon\psi_N - v_{n+1}b_N |N\rangle + b_N v_N |N+1\rangle \tag{C.38}$$

$$= \epsilon\psi_N - \frac{v_{N+1}}{v_N}b_N(\psi_N - \psi_{N-1}) + b_N\frac{v_N}{v_{N+1}}(\psi_{N+1} - \psi_N) \tag{C.39}$$

$$= (\epsilon - b_N(\frac{v_{N+1}}{v_N} + \frac{v_N}{v_{N+1}}))\psi_N + \frac{v_{N+1}}{v_N}b_N\psi_{N-1} + b_N\frac{v_N}{v_{N+1}}\psi_{N+1} \tag{C.40}$$

We have arrived at our target and can simply read off that

$$\delta = \frac{v_{N+1}}{v_N}b_N, \tag{C.41}$$

$$\beta = \epsilon - b_N(\frac{v_{N+1}}{v_N} + \frac{v_N}{v_{N+1}}), \tag{C.42}$$

$$\gamma = b_N\frac{v_N}{v_{N+1}}. \tag{C.43}$$

As one can store the values of ϵ, a_n, b_n and the Lanczos basis eigenvector elements v_n, the coefficients δ, β and γ can be calculated. This along with the three term recursion relationship allows us to calculate the ground state using only two vectors, resulting in a 50% saving of memory.

C.6 Extracting Symmetries

Symmetries are staggeringly useful in physics; they drastically simplify problems. From a numerical standpoint we will use them to reduce the Hilbert space of the problem. In doing so we save memory and can therefore examine larger systems. In this section we will go over two symmetries: z-spin S_z and translation invariance. We will generate look-up tables as a means of saving memory.

Frequently, symmetries are simpler to calculate and diagonalise than the Hamiltonian. In this case we can use the vectors that diagonalise the symmetry to block diagonalise the Hamiltonian. We then run Lanczos in these blocks, which is quicker and more memory efficient than before. If S is a symmetry of the Hamiltonian H then S, by definition,

commutes with H $[H, S] = 0$. Lets pick the set of vectors $\{|v_1\rangle\}$ that diagonalise S with eigenvalue s_1

$$S\,|v_1\rangle = s_1\,|v_1\rangle\,. \tag{C.44}$$

We can left and right multiply the commutator with $|v_1\rangle$ and $\langle v_2|$ respectively

$$\begin{aligned} \langle v_2|\,[H, S]\,|v_1\rangle &= 0, \\ (s_1 - s_2)\,\langle v_2|\,H\,|v_1\rangle &= 0, \end{aligned} \tag{C.45}$$

and as $(s_1 - s_2)$ is non-zero by definition we are left with $\langle v_2|\,H\,|v_1\rangle = 0$ which is the definition of a block diagonal matrix.

$$[H, S] = 0 \quad \Rightarrow \quad H = \begin{bmatrix} \begin{bmatrix} & & \\ & \text{“}s_1\text{”} & \\ & & \end{bmatrix} & & & \\ & \begin{bmatrix} & & \\ & \text{“}s_2\text{”} & \\ & & \end{bmatrix} & & \\ & & \begin{bmatrix} \ddots \end{bmatrix} & \\ & & & \end{bmatrix}, \tag{C.46}$$

where the block matrices labelled with “s_n” are the corresponding matrices for states with eigenvalue s_n for operator S.

The process is simple.

1. We apply our symmetry to each state in our Hilbert space and extract the corresponding eigenvalue s.

2. Create a lookup table for the s you wish to examine.

3. Run your Lanczos routine for an initial vector the size of the shorter lookup table. Use the lookup table to reference to the original states.

This process is detailed below for the symmetry S_z.

C.6.1 Extracting S_z — Creating Lookup Tables

This symmetry is trivial to extract which makes it our first target. We have

$$S_z = \sum_i S_z^i, \tag{C.47}$$

where $S_z^i |\uparrow\rangle = \frac{1}{2}$ and $S_z^i |\downarrow\rangle = -\frac{1}{2}$. For each state in our Hilbert space we can easily calculate and identify states with the same S_z. If we are considering all states with $S_z = s$, then we should be using a Lanczos vector that only contains these states. However generating states that have $S_z = s$ from our array indices would be challenging to do in general. Instead we create look-up tables. These are a pair of arrays that point to each other's indices. A 'Long' array (size of full Hilbert space) is used to point to the indices of the 'Short' array (size of states with $S_z = s$). The 'Short' array is a reference to the original basis; it points to the indices of 'Long'. This way we can perform Lanczos with a vector with the size of 'Short'. An example of these two vectors for 4 sites, with $S_z = 0$ is shown below where we have reduced the size of the space from 16 to 6.

$$\text{Long} = \begin{bmatrix} - \\ - \\ - \\ 0 \\ - \\ 1 \\ 2 \\ - \\ - \\ 3 \\ 4 \\ - \\ 5 \\ - \\ - \\ - \end{bmatrix} \begin{matrix} \\ \\ \\ (\uparrow\uparrow\downarrow\downarrow) \\ \\ (\uparrow\downarrow\uparrow\downarrow) \\ (\uparrow\downarrow\downarrow\uparrow) \\ \\ \\ (\downarrow\uparrow\uparrow\downarrow) \\ (\downarrow\uparrow\downarrow\uparrow) \\ \\ (\downarrow\downarrow\uparrow\uparrow) \\ \\ \\ \end{matrix} \qquad \text{Short} = \begin{bmatrix} 3 \\ 5 \\ 6 \\ 9 \\ 10 \\ 12 \end{bmatrix} \tag{C.48}$$

Exercise: Show the ground state eigenvalue always exists in the $S_z = 0$ subspace.

C.6.2 Using S_z Conservation to Shorten the Look Up Tables

Though extracting S_z has proven useful, the cost of storing a vector of size 2^n is still a hefty cost of memory. In this section I will highlight how to be more artful while conserving S_z. This will allow one to use two arrays of length $2^{\frac{n}{2}}$ as look-up tables instead of one 2^n array, making a massive saving in memory.

This trick relies on understanding the nature of number ordering and S_z conservation in separate fractions of states. Let's first describe the goal and then spell out how to achieve it. The process is as follows

1. Take the state that is being referenced and cut it into two states half the size each. If the state has an odd number of sites make the left half state the size of the smaller odd number.

2. Take the left and right half state and convert them, individually, into a base 10 number.

3. Look up the value corresponding to the element of the left half state number in the left look up table and the same for the right side.

4. Add these two numbers together and they should reference the index of the short look up table.

As this is not trivial I will highlight it with an example of 8 sites for all possible values of S_z. The states on the left are the binary decompositions of numbers, as a reference. The vectors on the right are the look up tables, grouped in sets of two, named 'Left' and 'Right' for what side they are on. The 'Long' lookup table has been omitted as it is 256 in length, but the 'Short' lookup table for $S_z = 4$ and $S_z = 0$ is given. The look up tables are given by:

$$\text{Short}_{S_z=4} = \begin{bmatrix} 0 \end{bmatrix} \tag{C.49}$$

$$\text{Short}_{S_z=0} = \begin{bmatrix} 15 \\ 23 \\ 27 \\ 29 \\ 30 \\ 39 \\ 43 \\ 45 \end{bmatrix} \begin{bmatrix} 46 \\ 51 \\ 53 \\ 54 \\ 57 \\ 58 \\ 60 \\ 71 \end{bmatrix} \begin{bmatrix} 75 \\ 77 \\ 78 \\ 83 \\ 85 \\ 86 \\ 89 \\ 90 \end{bmatrix} \begin{bmatrix} 92 \\ 99 \\ 101 \\ 102 \\ 105 \\ 106 \\ 108 \\ 113 \end{bmatrix} \begin{bmatrix} 114 \\ 116 \\ 120 \\ 135 \\ 139 \\ 141 \\ 142 \\ 147 \end{bmatrix} \begin{bmatrix} 149 \\ 150 \\ 153 \\ 154 \\ 156 \\ 163 \\ 165 \\ 166 \end{bmatrix} \begin{bmatrix} 169 \\ 170 \\ 172 \\ 177 \\ 178 \\ 180 \\ 184 \\ 195 \end{bmatrix} \begin{bmatrix} 197 \\ 198 \\ 201 \\ 202 \\ 204 \\ 209 \\ 210 \\ 212 \end{bmatrix} \begin{bmatrix} 216 \\ 225 \\ 226 \\ 228 \\ 232 \\ 240 \end{bmatrix} \tag{C.50}$$

$0-\uparrow\uparrow\uparrow\uparrow$	0	0		0	1		0	2		0	3		0	0	
$1-\uparrow\uparrow\uparrow\downarrow$	–	–		4	0		6	1		4	2		1	0	
$2-\uparrow\uparrow\downarrow\uparrow$	–	–		5	0		10	1		10	2		5	1	
$3-\uparrow\uparrow\downarrow\downarrow$	–	–		–	–		14	0		16	1		9	0	
$4-\uparrow\downarrow\uparrow\uparrow$	–	–		6	0		15	1		20	2		15	2	
$5-\uparrow\downarrow\uparrow\downarrow$	–	–		–	–		19	0		26	1		19	1	
$6-\uparrow\downarrow\downarrow\uparrow$	–	–		–	–		20	0		30	1		25	2	
$7-\uparrow\downarrow\downarrow\downarrow$	–	–		–	–		–	–		34	0		31	0	
$8-\downarrow\uparrow\uparrow\uparrow$	–	–	,	7	0	,	21	1	,	35	2	,	35	3	
$9-\downarrow\uparrow\uparrow\downarrow$	–	–		–	–		25	0		41	1		39	3	
$10-\downarrow\uparrow\downarrow\uparrow$	–	–		–	–		26	0		45	1		45	4	
$11-\downarrow\uparrow\downarrow\downarrow$	–	–		–	–		–	–		49	0		51	1	
$12-\downarrow\downarrow\uparrow\uparrow$	–	–		–	–		27	0		50	1		55	5	
$13-\downarrow\downarrow\uparrow\downarrow$	–	–		–	–		–	–		54	0		61	2	
$14-\downarrow\downarrow\downarrow\uparrow$	–	–		–	–		–	–		55	0		65	3	
$15-\downarrow\downarrow\downarrow\downarrow$	–	–		–	–		–	–		–	–		69	0	
	$S_z=4$			$S_z=3$			$S_z=2$			$S_z=1$			$S_z=0$		

Lets begin with a trivial example. Consider the $S_z = 4$ state $\phi =\uparrow\uparrow\uparrow\uparrow\uparrow\uparrow\uparrow\uparrow$ where $\uparrow\uparrow\uparrow\uparrow\uparrow\uparrow\uparrow\uparrow\rightarrow 0$ in base 10. We then split the state in two and get $\phi_{\mathrm{L}} =\uparrow\uparrow\uparrow\uparrow$ and $\phi_{\mathrm{R}} =\uparrow\uparrow\uparrow\uparrow$. Converting these into base 10 (using the reference table on the left) we get $\uparrow\uparrow\uparrow\uparrow\rightarrow 0$. Then we look up these numbers in the left and right lookup tables for the appropriate S_z. This gives $\mathrm{Left}_{Sz=4}(0) = 0$ and $\mathrm{Right}_{Sz=4}(0) = 0$. If this method works then $Short(Left(\phi_{\mathrm{L}}) + Right(\phi_{\mathrm{R}}))$ should equal ϕ in base 10. Sure enough $\mathrm{Left}_{Sz=4}(0) + \mathrm{Right}_{Sz=4}(0) = 0 + 0 = 0$, and $\mathrm{Short}_{Sz=4}(0) = 0$ which is equivalent to ϕ in base 10.

Now lets move on to a more complicated example. Consider the $S_z = 0$ state $\phi =\downarrow\uparrow\uparrow\downarrow\uparrow\downarrow\downarrow\uparrow\rightarrow 150$. Splitting this in two give $\phi_L =\downarrow\uparrow\uparrow\downarrow\rightarrow 9$ and $\phi_R =\uparrow\downarrow\downarrow\uparrow\rightarrow 6$. Sure enough $\mathrm{Left}_{Sz=0}(9) + \mathrm{Right}_{Sz=0}(6) = 39 + 2 = 41$, and $\mathrm{Short}_{Sz=0}(41) = 150$ which is

equivalent to ϕ in base 10. This procedure has converted a lookup table of length 256 to two tables of length 16. This is a monumental saving in memory.

In order to create these look up tables first we must appreciate what S_z conservation means to each state. As we are in the subspace of a given $S_z = s$ each state must have $S_z = s$, though this may sound obvious the reason this trick works is that if we know the S_z value of the left half of the state we automatically know the S_z value of the right half of the state. This allows the information to split up. The second thing to appreciate is that numbers always appear in the same order, this is what controls the values of $\text{Long}_{\text{Left}}$.

In order to create the look up tables, we do the following procedure:

1. Loop through all the integers from 0 to 2^n checking if their corresponding states have the desired S_z, if so adding that number to 'Short'.

2. Loop through 'Short', converting the numbers to base b and split them into two. Convert the left half to base 10 and if it is the first time this number appears reference the original (long) number into $\text{Long}_{\text{Left}}$, where the index is the left half number.

3. Loop through all possible S_z which can occur for the right look-up table while running through $\text{Long}_{\text{Right}}$, converting each index into base b. When a state in the right look up table has the correct S_z $\text{Long}_{\text{Right}}$ of that state becomes its numerical position order for all the states with the same S_z.

As the final step is complex, I've highlighted the details in the example below for $S_z = 0$

Index	*State*	n_{up}	*Order*	*Combined*
0	↑↑↑↑	4	– – – – 0	0
1	↑↑↑↓	3	– – – 0 –	0
2	↑↑↓↑	3	– – – 1 –	1
3	↑↑↓↓	2	– – 0 – –	0
4	↑↓↑↑	3	– – – 2 –	2
5	↑↓↑↓	2	– – 1 – –	1
6	↑↓↓↑	2	– – 2 – –	2
7	↑↓↓↓	1	– – – – –	0
8	↓↑↑↑	3	– – – 3 –	3
9	↓↑↑↓	2	– – 3 – –	3
10	↓↑↓↑	2	– – 4 – –	4
11	↓↑↓↓	1	– 1 – – –	1
12	↓↓↑↑	2	– – 5 – –	5
13	↓↓↑↓	1	– 2 – – –	2
14	↓↓↓↑	1	– 3 – – –	3
15	↓↓↓↓	0	0 – – – –	0

Though it is possible to keep doing this splitting, the improvements are negligible as the controller of memory now becomes the 'Short' look-up table and the state vectors. One must focus on optimising memory usage for them instead, which leads us to the symmetry that is translational invariance.

C.6.3 Translational Invariance

Translational invariance is a symmetry that is much more difficult to extract, however it is well worth it. Upon extraction the Hilbert space goes from b^n to $\approx \frac{b^n}{n}$. This symmetry

Figure C.3: Translational Invariance of Two States

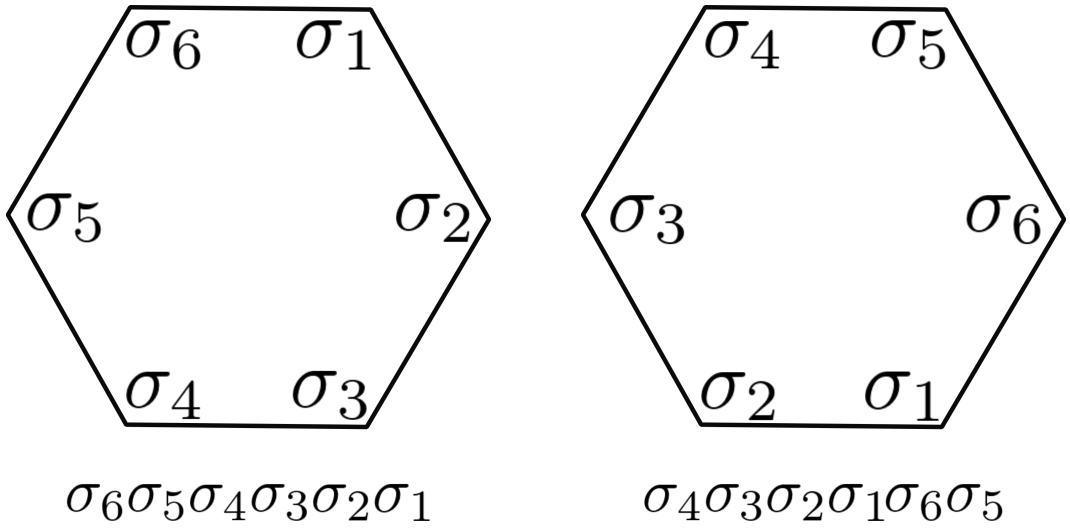

A visual comparison of two states which are identical under translation. When we represent them however they seem distinct. An appropriate linear superposition of the set of identical states under translation would however respect the symmetry.

only exists in systems with closed boundary conditions. Consider the two systems in figure C.3 on page 247. It is apparent that they are equivalent just rotated by two lattice sites, but our linear representation causes them to be distinct. In this section we will formulate translational invariance, applying the Hamiltonian to transitionally invariant states and changing the Lanczos routine to adjust for this.

Consider the translation operator $\hat{T}$ which, when acted on state $|\uparrow\uparrow\uparrow\downarrow\rangle$, does

$$\hat{T}\,|\uparrow\uparrow\uparrow\downarrow\rangle = w\,|\downarrow\uparrow\uparrow\uparrow\rangle\,. \tag{C.51}$$

As we have periodic boundary conditions upon four iterations we return back to the original state, in general this condition becomes

$$\hat{T}^n\,|\Psi_n\rangle = |\Psi_n\rangle = w^n\,|\Psi_n\rangle\,, \tag{C.52}$$

where n is the number of sites in the state Ψ_n. From this we can define w as the root of

unity obeying

$$w^n = 1. \tag{C.53}$$

There are n solutions to this equation obtained by

$$w^n = \mathrm{e}^{2\pi i m}, \tag{C.54}$$

where m is an integer, giving

$$w = \mathrm{e}^{\frac{2\pi i m}{n}}. \tag{C.55}$$

To utilise translational invariance one must group together states that are translated copies of one another. These are put together into a normalised state that is invariant under translation. In the case of four sites the states are given by

$$\begin{aligned}
|0\rangle &= |\uparrow\uparrow\uparrow\uparrow\rangle\,, \\
|1\rangle &= \tfrac{1}{2}\left(|\uparrow\uparrow\uparrow\downarrow\rangle + w\,|\downarrow\uparrow\uparrow\uparrow\rangle + w^2\,|\uparrow\downarrow\uparrow\uparrow\rangle + w^3\,|\uparrow\uparrow\downarrow\uparrow\rangle\right), \\
|2\rangle &= \tfrac{1}{2}\left(|\uparrow\uparrow\downarrow\downarrow\rangle + w\,|\downarrow\uparrow\uparrow\downarrow\rangle + w^2\,|\downarrow\downarrow\uparrow\uparrow\rangle + w^3\,|\uparrow\downarrow\downarrow\uparrow\rangle\right) \\
|3\rangle &= \tfrac{1+w^2}{2}\tfrac{1}{\sqrt{2}}\left(|\uparrow\downarrow\uparrow\downarrow\rangle + w\,|\downarrow\uparrow\downarrow\uparrow\rangle\right), \\
|4\rangle &= \tfrac{1}{2}\left(|\downarrow\downarrow\downarrow\uparrow\rangle + w\,|\uparrow\downarrow\downarrow\downarrow\rangle + w^2\,|\downarrow\uparrow\downarrow\downarrow\rangle + w^3\,|\downarrow\downarrow\uparrow\downarrow\rangle\right), \\
|5\rangle &= |\downarrow\downarrow\downarrow\downarrow\rangle\,.
\end{aligned} \tag{C.56}$$

Note that due to the additional translational symmetry of state $|3\rangle$ it has the added property that for $w^2 = -1$ $|3\rangle = 0$. When performing the numerics the existence of these vanishing states must be checked. Upon application of the Hamiltonian we get

$$\begin{aligned}
H\,|0\rangle &= |0\rangle\,, \\
H\,|1\rangle &= \tfrac{1}{2}(w + w^{-1})\,|1\rangle\,, \\
H\,|2\rangle &= \tfrac{1+w+w^2+w^3}{4}\sqrt{2}\,|3\rangle\,, \\
H\,|3\rangle &= -\,|3\rangle + \tfrac{(1+w^2)(1+w)}{4}\sqrt{2}\,|2\rangle\,, \\
H\,|4\rangle &= \tfrac{1}{2}(w + w^{-1})\,|4\rangle\,, \\
H\,|5\rangle &= |5\rangle\,.
\end{aligned} \tag{C.57}$$

These can be trivially diagonalised and give the following eigenvalues for $w = 1, i, -1, -i$

$$0 : \epsilon = 1 \tag{C.58}$$

$$1 : \epsilon = 1, 0, 0, -1 \tag{C.59}$$

$$2, 3 : \epsilon = 1, 0, 0, 0, -1, -2 \tag{C.60}$$

$$4 : \epsilon = 1, 0, 0, -1 \tag{C.61}$$

$$5 : \epsilon = 1 \tag{C.62}$$

The aim is create a general set of rules such that we only 'apply' the Hamiltonian to the first referenced state, and have it as if we applied it to the entire state. The rules generated in the case of the Heisenberg model is:

1. Check if the state that the Hamiltonian is being applied to exists, if it does not then skip to the next state.

2. Apply the Hamiltonian as normal.

3. Use the look up table and find the resulting state to find degeneracy, number of translations from original state, and reference state.

4. Check if the resulting state exists, if not then skip to the next state.

5. The matrix element references the reference state and its coefficient is

$$\frac{1}{2}\sqrt{\frac{D_I}{D_F}}w^{N-T}, \tag{C.63}$$

   where D_I is the number of states in the original reference state, D_F is the number of states in the final reference state, and T is the number of translations it takes to get from the initial state to the resultant state.

Checking whether a state exists or not requires an appreciation of how many applications of $\hat{T}$ are required to return the original state. If there are N states or 1 state in an

invariant state then it must exist. However, if there are a fraction of N states then it is more complicated. Take for example, the state $|3\rangle$, when creating it we would translate the state $|\uparrow\downarrow\uparrow\downarrow\rangle$ four times giving

$$(1 + w^2)\left(|\uparrow\downarrow\uparrow\downarrow\rangle + w\,|\downarrow\uparrow\downarrow\uparrow\rangle\right). \tag{C.64}$$

In the case $w = \pm 1$ this state exists, and it does not otherwise, therefore this check must be performed whenever referencing $|3\rangle$.

One may think as we are using complex numbers that the Lanczos matrix must also be complex, this however is not the case. Firstly, as the Hamiltonian is hermitian its diagonal components must be real. Transforming to the Lanczos basis conserves this therefore all a_n are real. Secondly, referring back to when the algorithm was being derived we had a choice of gauge when performing the modulus, this freedom is still available and we can choose the gauge where all b_n are also real without loss of generality.

C.7 2D Systems

This technique is not restricted to just one dimensional systems. We can extend to two or even three but the result is rather limited. This is due to system scaling with dimension. Say we can examine a 36 site linear chain, this corresponds to a 6×6 2D square lattice and a $3 \times 3 \times 4$ 3D cubic system. We are drastically limited by system size in higher dimensions hence our results are of less use. Nevertheless, we carry on as some results are better than none.

There are two ways we can extend into two dimensions. The obvious way to do it is to just create a square lattice with closed boundary conditions in both Cartesian directions. Doing this allows us to extract translational invariance for each axis, resulting in a moderately large saving in memory. Unfortunately, there are issues with this approach. Firstly, extracting translational invariance for each direction frequently comes at the cost of a dense matrix. The denser a matrix the more time an algorithm takes, sometimes

Figure C.4: Helical Boundary Conditions on a Cylinder

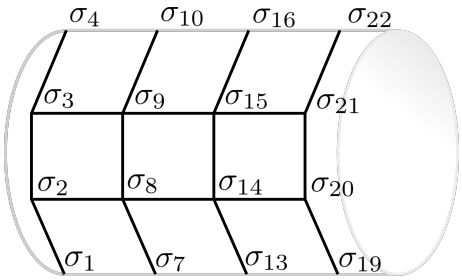

A geometric representation of helical boundary conditions. Each site is connected to the ones next to it but also the ones m away, where in this diagram $m = 6$.

to a point where it becomes the limiting factor. Secondly, as we are limited to rather small systems we introduce unwanted frustrated geometries into the system. Take a 3×3 square lattice depicted in figure C.5 on page 252, we are introducing triangles into our examination, notorious for generating frustrated systems.

Instead, I recommend using helical boundary conditions [96] which are depicted in figures C.5 on page 252 and C.4 on page 251. This is where we examine a one dimensional system but introduce long range bonds. These can be thought of connecting different sites across a helix. In the thermodynamic limit this system would exhibit a 1D to 2D crossover. Though we can only extract translational invariance in one direction, this approach is less susceptible to small system frustration and can finite size scale better. Mathematically we write the helical boundary condition Hamiltonian as

$$H_{helix} = -J \sum_i \mathbf{S}_i \cdot \mathbf{S}_{i\pm1} + \mathbf{S}_i \cdot \mathbf{S}_{i\pm m}, \tag{C.65}$$

where m characterises the diameter of the helix. The number of sites in the system is given by $n = 1 + m^2$, as this ensures square symmetry.

At this point we have reached the limit of our examination of the Heisenberg model. We know how to represent states numerically, apply a Hamiltonian, calculate the lowest lying eigenvalues and eigenvectors, optimise to use only two vectors, extract S_z^{tot} and translational invariance, and examine two dimensional systems. There is one thing yet to

Figure C.5: Helical and 2D Square Boundary Conditions

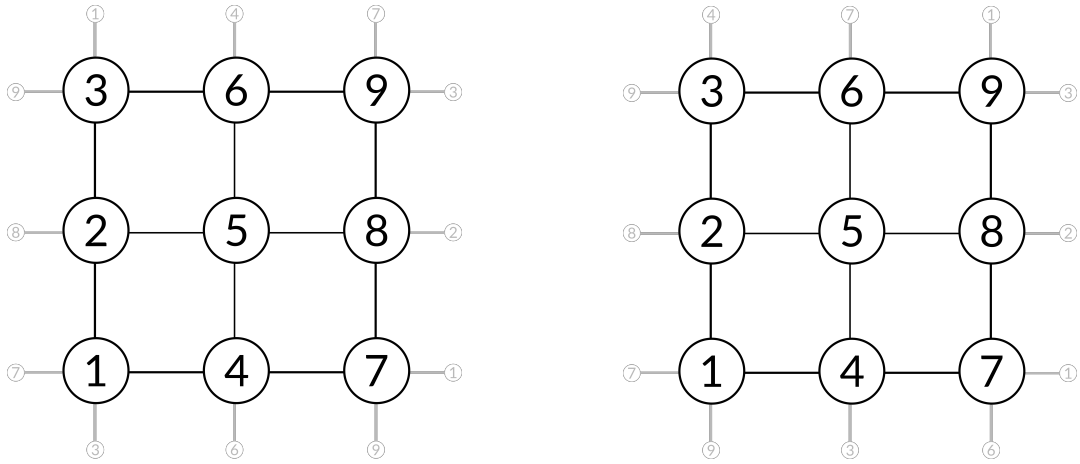

2D periodic boundary conditions, square (left) and helical (right). In each system there are only nine sites but the way they are connected is different. A square lattice is a series of connected rings of size three. Helical boundary conditions are a 1D chain with m neighbour interactions, in this case $m = 3$.

learn: how to apply everything we know to more general fermionic systems.

C.8 More General Fermionic Systems

There is more to life than quantum magnets, there are also metals! The archetypal model for metallic systems is the Hubbard model [84]. It treats chemical bonding and the screened Coulomb repulsion in an elementary yet elegant way. In this section we will briefly introduce the Hubbard model, explain the new issues that arise, and introduce another symmetry that can be extracted. The model is given by

$$H = -t \sum_{\langle ij \rangle \sigma} c^\dagger_{i\sigma} c_{j\sigma} + U \sum_i c^\dagger_{i\uparrow} c_{i\uparrow} c^\dagger_{i\downarrow} c_{i\downarrow}, \tag{C.66}$$

where t is the strength of chemical bonding, and U is the on-site screened Coulomb repulsion. The operators $c_{j\sigma}$ are second quantised fermionic operators that characterise electrons. If these are unfamiliar, they are explained in appendix A.

This model brings with it increased degrees of freedom and non-trivial commutation

relations. The four states that appear are

$$|0\rangle_i\,, \quad c^\dagger_{i\uparrow}|0\rangle_i\,, \quad c^\dagger_{i\downarrow}|0\rangle_i\,, \quad c^\dagger_{i\uparrow}c^\dagger_{i\downarrow}|0\rangle_i\,, \tag{C.67}$$

where $|0\rangle_i$ is the vacuum on site i. This is a great annoyance as it exponentially increases our Hilbert space, but there is nothing we can do. Along with this comes non-trivial commutation relations. Fermions anti-commute which results in $c^\dagger_{i\sigma}c^\dagger_{\bar{\sigma}} = -c^\dagger_{i\bar{\sigma}}c^\dagger_{i\sigma}$. This means we have to be cautious when applying operators to our states. We must also pick a system by which to order our fermions. The one I choose is ordered by site, and if there are multiple electrons on a site the $\uparrow$ electron is ordered before the $\downarrow$. An example state for a 6 site system with vacancies on the third and sixth site is

$$c^\dagger_{1\uparrow}c^\dagger_{2\uparrow}c^\dagger_{4\downarrow}c^\dagger_{5\uparrow}c^\dagger_{5\downarrow}|0\rangle\,.$$

Note that H is composed of local operators, just like the Heisenberg model. We can write $H = \sum_{\langle ij\rangle} H_{ij}$ where H_{ij} is a 16×16 matrix too large for this document.

Conveniently there is another symmetry we can extract for fermionic systems: particle number N. It is given by

$$N = \sum_{i\sigma} c^\dagger_{i\sigma}c_{i\sigma}. \tag{C.68}$$

This is extracted in just the way S_z was before.

C.8.1 Anti-Periodic Boundary Conditions

Closed boundary conditions are about gaining a phase when carriers travel around the system. For anti-periodic boundary conditions this phase is tuned such that n hops gains a phase of -1. This can be simply implemented in fermionic systems by changing the sign of t on the H_{1n} bond.

This is why things weren't as simple for the Heisenberg model. Closed boundary conditions are to do with the motion of carriers. The underlying motion within the Heisenberg

Figure C.6: Anti-Periodic Boundary Conditions — Translational Invariance

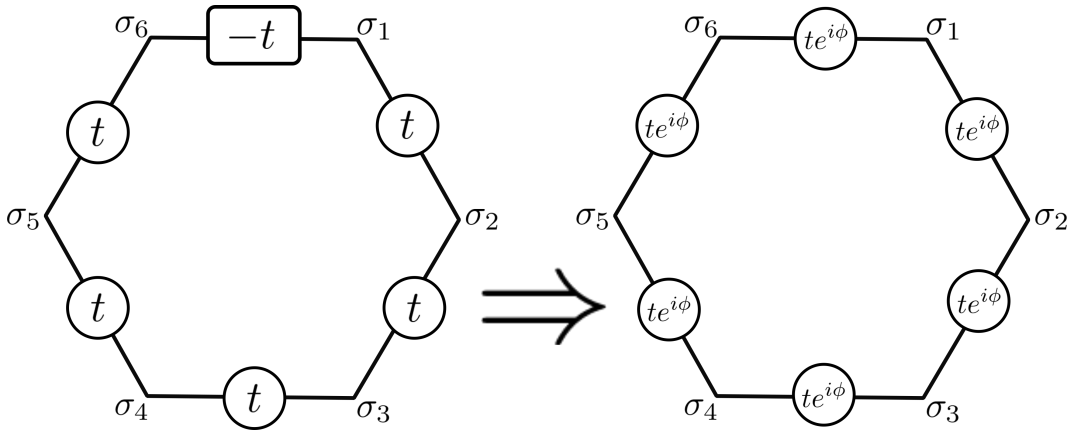

Two ways to represent anti-periodic boundary conditions. On the left is a trivial implementation but is not translationally invariant, while the right is for an appropriate choice of phase ϕ. If $\phi = \frac{2\pi}{6}$ the system would be both anti-periodic and translationally invariant.

model is only seen after performing the Holstein-Primakoff transformation [97]. Simply changing the sign of the final bond would not work, as it is not an commutator conserving transformation. Attaining equation C.13 is left as an exercise for an enthusiastic reader.

We can also consider anti-periodic boundary conditions with translational invariance, but not in their current state. We must transmute the original boundary conditions as is depicted in figure C.6 on page 254. The phase shift must be smeared across the lattice. This means $t \to te^{i\pi/n}$ for forward operators and $t \to te^{-i\pi/n}$ for backward operators. More accurately

$$H = -t \sum_{i\sigma} e^{i\pi/n} c^\dagger_{i\sigma} c_{i+1,\sigma} + e^{-i\pi/n} c^\dagger_{i+1,\sigma} c_{i\sigma}. \tag{C.69}$$

Now we have reached the end of what there is to learn for the Lanczos algorithm. In principle there may be other symmetries in the systems you choose to examine. The techniques you have learned from this document should help you extract them and examine larger systems still.

C.9 Results

In this section we give some results that can be used as reference to compare against. They are accurate to 16 decimal places.

Table C.1: Lowest eigenvalue Heisenberg model for $J = 1$, varying boundary conditions and system sizes

n	Open	Periodic
10	-4.258035207282886	-4.515446354492047
11	-4.632093302359579	-4.718936362524425
12	-5.142090632840548	-5.387390917445213
13	-5.525322097083683	-5.629584329744325
14	-6.026724661862179	-6.263549533547023

Table C.2: Lowest eigenvalue Heisenberg model for $J = -1$, varying boundary conditions and system sizes

n	Open	Periodic
10	-2.250000000000008	-2.500000000000008
11	-2.500000000000001	-2.74999999999999
12	-2.749999999999988	-3.000000000000004
13	-2.999999999999997	-3.250000000000007
14	-3.249999999999934	-3.500000000000009

Table C.3: $J = 1, n = 4$ Heisenberg model, all eigenvalues

Open	Periodic
-1.616025403784439	-2
-0.9571067811865481	-1
-0.9571067811865465	-1
-0.9571067811865465	-0.9999999999999999
-0.25	0
-0.2499999999999998	0
-0.2499999999999998	0
0.1160254037844387	0
0.4571067811865476	1.211175157689102e-17
0.4571067811865476	1.211175157689102e-17
0.4571067811865476	5.548233325764073e-17
0.7499999999999998	0.9999999999999992
0.7499999999999998	0.9999999999999992
0.75	1
0.75	1
0.7500000000000002	1.000000000000001

Table C.4: $J = -1, n = 4$ Heisenberg model, all eigenvalues

Open $J = -1$	Periodic $J = -1$
-0.7500000000000002	-1.000000000000001
-0.75	-1
-0.75	-1
-0.7499999999999998	-1
-0.7499999999999998	-1
-0.4571067811865476	-5.548233325764073e-17
-0.4571067811865476	0
-0.4571067811865476	0
-0.1160254037844387	0
0.2499999999999998	0
0.2499999999999998	1.211175157689102e-17
0.25	1.211175157689102e-17
0.9571067811865465	0.9999999999999992
0.9571067811865465	0.9999999999999992
0.9571067811865481	0.9999999999999999
1.616025403784439	2

APPENDIX D

MEAN-FIELD THEORY — SOLVING MODELS WHEN INTERACTIONS ARE MODERATE

Noteworthy physical problems are rarely solved trivially. In many cases exact solutions don't exist and hence approximate solutions must be used. In this appendix we will discuss one such technique: Hartree Fock mean field theory [67]. This is the process of creating an effective single particle theory from a many body Hamiltonian. In principle a particle will feel an effective field from the others in the system. This field affects the behaviour of that particle which in turn affects the behaviour of the field. This is a self consistent problem. Hartree Fock mean field theory is a variational solution to the problem and hence provides the *best* single particle solution which is an underestimate for the solution [67]. Nevertheless, when a problem is weakly correlated it is a remarkably effective tool.

The process is rather simple: calculate the average energy, create an effective Hamiltonian, and self consistently solve for the parameters. These steps are detailed in the

following sections, which is followed by two examples one paramagnetic and the other magnetic.

D.1 Calculating the Average Energy — Slater Determinants

The first step in Hartree Fock mean field theory is to calculate the average energy. This is done using Slater determinants [68]: a technique by which to calculate many particle correlations in terms of single particle correlations. Mean field theory comes in many 'flavours' based on assumptions one puts in. For example we can assume the system is paramagnetic and hence there is no spin dependence, or the system is transnationally invariant and there is no site dependence. Mathematically paramagnetism corresponds to

$$\langle c^\dagger_{i\uparrow} c_{i\uparrow}\rangle = \langle c^\dagger_{i\downarrow} c_{i\downarrow}\rangle \tag{D.1}$$

$$\langle c^\dagger_{i\uparrow} c_{j\uparrow}\rangle = \langle c^\dagger_{j\downarrow} c_{i\downarrow}\rangle \tag{D.2}$$

$$\langle c^\dagger_{i\uparrow} c_{j\downarrow}\rangle = \langle c^\dagger_{i\downarrow} c_{j\uparrow}\rangle = 0 \tag{D.3}$$

and translational invariance corresponds to

$$\langle c^\dagger_{i\sigma} c_{j\tau}\rangle = \langle c^\dagger_{i+n\sigma} c_{j+n\tau}\rangle. \tag{D.4}$$

These are defined before the calculation. Different assumptions lead to different physics.

The Slater determinant is defined as

$$\langle \prod_{n=1}^{n=N} c^\dagger_n \prod_{m=N+1}^{m=2N} c_m\rangle = \det A, \tag{D.5}$$

where $A_{ij} = \langle c^\dagger_i c_{2N-(j-1)}\rangle$. As an explicit example the following three particle term is

represented as

$$\langle c_1^\dagger c_2^\dagger c_3^\dagger c_4 c_5 c_6\rangle = \begin{vmatrix} \langle c_1^\dagger c_6\rangle & \langle c_2^\dagger c_6\rangle & \langle c_3^\dagger c_6\rangle \\ \langle c_1^\dagger c_5\rangle & \langle c_2^\dagger c_5\rangle & \langle c_3^\dagger c_5\rangle \\ \langle c_1^\dagger c_4\rangle & \langle c_2^\dagger c_4\rangle & \langle c_3^\dagger c_4\rangle \end{vmatrix}. \tag{D.6}$$

If, for example, the only permitted correlations are $\alpha = \langle c_1^\dagger c_4\rangle$, $\beta = \langle c_2^\dagger c_6\rangle$ and $\gamma = \langle c_3^\dagger c_4\rangle$ then the previous equation simplifies to

$$\langle c_1^\dagger c_2^\dagger c_3^\dagger c_4 c_5 c_6\rangle = \begin{vmatrix} \alpha & 0 & 0 \\ 0 & \beta & 0 \\ 0 & 0 & \gamma \end{vmatrix} = \alpha\beta\gamma. \tag{D.7}$$

If and when many particle correlations occur within the Hamiltonian, the Slater determinant is used to calculate them in terms of single particle correlations.

Our Hamiltonian is defined by second quantized operators, the average of which defines the average energy

$$E(\{\rho\}) = \langle H\rangle, \tag{D.8}$$

where $\{\rho\}$ denotes the set of correlations ρ allowed in our system.

Derivation of Slater Determinant (Not Necessary for Understanding)

Consider a single particle Hamiltonian which has been diagonalised

$$H = \sum_{jj'} H_{jj'} f_j^\dagger f_{j'} = \sum_n \epsilon_n d_n^\dagger d_n, \tag{D.9}$$

where H has been diagonalised using unitary operators defined as

$$\sum_n U_{jn} d_n = f_j \qquad \sum_n d^\dagger U_{nj} = f_j^\dagger. \tag{D.10}$$

Consider the following two particle correlation

$$\langle f_{j_1}^\dagger f_{j_2}^\dagger f_{j_3} f_{j_4} \rangle \sum_{n_1,n_2,n_3,n_4} U_{j_1 n_1} U_{j_2 n_2} \langle d_{n_1}^\dagger d_{n_2}^\dagger d_{n_3} d_{n_4} \rangle U_{j_3 n_3}^\dagger U_{j_4 n_4}^\dagger, \tag{D.11}$$

where we have diagonalised the operators. There is a state to take the average with respect to, and in general any state can be written as

$$|State\rangle = \sum_\alpha a_\alpha |\alpha\rangle, \tag{D.12}$$

where the set of states $\{|\alpha\rangle\}$ are the eigenstates. For $\langle d_{n_1}^\dagger d_{n_2}^\dagger d_{n_3} d_{n_4} \rangle$ to be non-zero we must be left with the same state after acting our operators on it. This only occurs when $n_1 = n_4$ & $n_2 = n_3$ or $n_1 = n_3$ & $n_2 = n_4$, where the latter picks up a Fermi minus sign. Therefore $\langle d_{n_1}^\dagger d_{n_2}^\dagger d_{n_3} d_{n_4} \rangle = \delta_{n_1 n_4} \delta_{n_2 n_3} - \delta_{n_1 n_3} \delta_{n_2 n_4}$ which upon substitution and converting back to the original operators gives

$$\langle f_{j_1}^\dagger f_{j_2}^\dagger f_{j_3} f_{j_4} \rangle = \langle f_{j_1}^\dagger f_{j_4} \rangle \langle f_{j_2}^\dagger f_{j_3} \rangle - \langle f_{j_1}^\dagger f_{j_3} \rangle \langle f_{j_2}^\dagger f_{j_4} \rangle \tag{D.13}$$

$$\equiv \begin{vmatrix} \langle f_{j_1}^\dagger f_{j_4} \rangle & \langle f_{j_2}^\dagger f_{j_4} \rangle \\ \langle f_{j_1}^\dagger f_{j_3} \rangle & \langle f_{j_2}^\dagger f_{j_3} \rangle \end{vmatrix}. \tag{D.14}$$

This is easily generalised to a $n \times n$ matrix for an n particle correlation.

D.2 Creating an Effective Hamiltonian — Wicks Theorem

The next step is to calculate an effective single particle Hamiltonian. We do this using the average energy and Wicks theorem [69]. This is the prescription

$$H^{EFF} = \sum_{\{\rho\}} \hat{\rho} \frac{\partial E}{\partial \rho} + E - \rho \frac{\partial E}{\partial \rho}, \tag{D.15}$$

where $\hat{\rho}$ is the single particle operator that generates ρ. For example if $\rho = \langle c_1^\dagger c_2 \rangle$ then $\hat{\rho} = c_1^\dagger c_2$. This resulting Hamiltonian should then be diagonalised. This will be used to solve for the self consistent parameters.

D.3 Solving for Self Consistent Parameters

At this point we have an average energy in terms of single particle correlations and a Hamiltonian in terms of diagonal operators. However, these correlations are only defined and must be solved for. This process is simple, we represent our correlations in terms of the diagonal operators and use

$$\langle c_l^\dagger c_{l'} \rangle = \int_C \frac{\mathrm{d}\epsilon}{2\pi i} f(\epsilon - \mu) G_{l'l}(\epsilon), \tag{D.16}$$

where $f(\epsilon - \mu)$ is the Fermi function and μ is the chemical potential and

$$G(\epsilon) = [\epsilon - H^{EFF}]^{-1}, \tag{D.17}$$

is the resolvent.

The result is often a self consistent sum or integral equation. Sometimes these can integrated directly to produce a result, but often it must be solved for numerically via an

iterative routine. Mathematically this would correspond to

$$x = \int \mathrm{d}k F(k, x), \tag{D.18}$$

numerically this corresponds to

$$x_n = \int \mathrm{d}k F(k, x_{n-1}), \tag{D.19}$$

which x_n exponentially converges to the solution as $n \to \infty$. We simply provide an initial guess x_0 and iterate this until numerical convergence.

Now that we have formulated Hartree Fock mean field theory we present two examples.

D.4 Example: Paramagnetic and Magnetic Mean Field Theory

In this section we will implement Hartree Fock mean field theory on a strange Hamiltonian. We will do both paramagnetic and magnetic field theory comparing the results. The Hamiltonian in question is

$$H = -t \sum_{\langle ij \rangle \sigma} c^\dagger_{i\sigma} c_{j\sigma} - \Delta \sum_{\langle ij \rangle} c^\dagger_{i\uparrow} c_{i\uparrow} c^\dagger_{j\uparrow} c_{j\uparrow}. \tag{D.20}$$

D.4.1 Paramagnetic Mean Field Theory

In this subsection we do something ridiculous for the sake of an easy calculation: calculate a paramagnetic mean field theory for a Hamiltonian that is clearly susceptible to magnetism. For a paramagnetic mean field theory we assume the result is independent of spin. We will also assume translational invariance. For this reason we state the correlations that exist are $n_0 = \langle c^\dagger_{i\sigma} c_{i\sigma} \rangle$, $n_1 = \langle c^\dagger_{i\sigma} c_{j\sigma} \rangle$, and that each spin species occur in equal quantities.

The first step is to calculate the average energy. This is given by

$$E = \langle H \rangle = -t \sum_{\langle ij \rangle \sigma} \langle c^\dagger_{i\sigma} c_{j\sigma} \rangle - \Delta \sum_{\langle ij \rangle} \langle c^\dagger_{i\uparrow} c_{i\uparrow} c^\dagger_{j\uparrow} c_{j\uparrow} \rangle. \tag{D.21}$$

For the second term we are required to use a Slater determinant where

$$\langle c^\dagger_{i\uparrow} c_{i\uparrow} c^\dagger_{j\uparrow} c_{j\uparrow} \rangle = \langle c^\dagger_{j\uparrow} c^\dagger_{i\uparrow} c_{i\uparrow} c_{j\uparrow} \rangle \tag{D.22}$$

$$= \begin{vmatrix} \langle c^\dagger_{j\uparrow} c_{j\uparrow} \rangle & \langle c^\dagger_{i\uparrow} c_{j\uparrow} \rangle \\ \langle c^\dagger_{j\uparrow} c_{i\uparrow} \rangle & \langle c^\dagger_{i\uparrow} c_{i\uparrow} \rangle \end{vmatrix} \tag{D.23}$$

$$= \begin{vmatrix} \frac{n_0}{2} & \frac{n_1}{2} \\ \frac{n_1}{2} & \frac{n_0}{2} \end{vmatrix} \tag{D.24}$$

$$= \frac{n_0^2}{4} - \frac{n_1^2}{4}. \tag{D.25}$$

This gives the average energy as

$$E = -t \sum_{\langle ij \rangle \sigma} n_1 - \Delta \sum_{\langle ij \rangle} \left[\frac{n_0^2}{4} - \frac{n_1^2}{4} \right] \tag{D.26}$$

$$= -2Ztn_1 - Z\frac{\Delta}{4}[n_0^2 - n_1^2], \tag{D.27}$$

where sum over neighbours gives Z the coordination number (the number of nearest neighbours) and the sum over spin gives a factor of two.

The next step is to calculate the effective Hamiltonian using Wick's theorem. The term $n_1 \to c^\dagger_{i\sigma} c_{j\sigma}$, $n_0^2 \to 2n_0 c^\dagger_{i\sigma} c_{i\sigma} + n_0^2$, and $n_1^2 \to 2n_1 c^\dagger_{i\sigma} c_{j\sigma} + n_1^2$ which gives

$$E = -t \sum_{\langle ij \rangle \sigma} n_1 - \Delta \sum_{\langle ij \rangle} \left[\frac{n_0^2}{4} - \frac{n_1^2}{4} \right] \tag{D.28}$$

$$\to H^{EFF} = -t \sum_{\langle ij \rangle \sigma} c^\dagger_{i\sigma} c_{j\sigma} - \frac{\Delta}{4} \sum_{\langle ij \rangle} \left[2n_0 c^\dagger_{i\sigma} c_{i\sigma} + n_0^2 - 2n_1 c^\dagger_{i\sigma} c_{j\sigma} - n_1^2 \right] \tag{D.29}$$

$$= -[t + \frac{\Delta}{4} n_1] \sum_{\langle ij \rangle \sigma} c^\dagger_{i\sigma} c_{j\sigma} - Zn_0 \frac{\Delta}{4} \sum_{i\sigma} c^\dagger_{i\sigma} c_{i\sigma} - Z\frac{\Delta}{4}[n_0^2 - n_1^2] \tag{D.30}$$

This is diagonalised with a Bloch transformation [93] (see Appendix B.8 if this is unfamiliar) giving

$$H^{EFF} = \sum_{\mathbf{k}\sigma}(-[t - \frac{\Delta}{4}n_1]Z\gamma_{1,\mathbf{k}} - Z\frac{\Delta}{4}n_0)c^\dagger_{\mathbf{k}\sigma}c_{\mathbf{k}\sigma} - Z\frac{\Delta}{4}[n_0^2 - n_1^2], \tag{D.31}$$

where $\gamma_{1,\mathbf{k}}$ is the nearest neighbour structure factor.

The final step is to calculate the parameters n_0 and n_1. For this we require the resolvent $G(\epsilon) = [\epsilon - H^{EFF}]^{-1}$, which in our case gives

$$G(\epsilon) = \frac{\delta_{\mathbf{k}\mathbf{k}'}}{\epsilon + [t - \frac{\Delta}{4}n_1]Z\gamma_{1,\mathbf{k}} + Z\frac{\Delta}{4}n_0)}. \tag{D.32}$$

In terms of diagonal operators, n_0 is

$$n_0 = \langle c^\dagger_{i\sigma}c_{i\sigma}\rangle = \sum_{\mathbf{k}}\langle c^\dagger_{\mathbf{k}\sigma}c_{\mathbf{k}\sigma}\rangle, \tag{D.33}$$

and by using equation D.16 this is

$$n_0 = \sum_{\mathbf{k}}\int_C \frac{\mathrm{d}\epsilon}{2\pi i}f(\epsilon - \mu)\frac{1}{\epsilon + [t - \frac{\Delta}{4}n_1]Z\gamma_{1,\mathbf{k}} + Z\frac{\Delta}{4}n_0)}, \tag{D.34}$$

and by use of the Cauchy residue theorem [98] this is

$$n_0 = \sum_{\mathbf{k}} f(-[t - \frac{\Delta}{4}n_1]Z\gamma_{1,\mathbf{k}} - Z\frac{\Delta}{4}n_0 - \mu), \tag{D.35}$$

which can be summed over or integrated in the continuum limit [99] where

$$n_0 = \int \frac{\mathrm{d}^d\mathbf{k}}{(2\pi)^d}f\left(-[t - \frac{\Delta}{4}n_1]Z\gamma_{1,\mathbf{k}} - Z\frac{\Delta}{4}n_0 - \mu\right). \tag{D.36}$$

Repeating the process for n_1 we have

$$n_1 = \int \frac{\mathrm{d}^d\mathbf{k}}{(2\pi)^d}f\left(-[t - \frac{\Delta}{4}n_1]Z\gamma_{1,\mathbf{k}} - Z\frac{\Delta}{4}n_0 - \mu\right)\gamma_{1,\mathbf{k}}. \tag{D.37}$$

These self consistent integral equations can be solved numerically, and the resulting energy is depicted in figure D.1 on page 269.

D.4.2 Magnetic Mean Field Theory

From the Hamiltonian we can see that the system favours neighbouring spins to be parallel. For this reason we examine a magnetic mean field theory. The only difference is the distinguishing between spin occupation, namely $n_\alpha^\sigma = \langle c_{i\sigma}^\dagger c_{i+\alpha,\sigma}\rangle$. This gives the average energy as

$$E = -Zt(n_1^\uparrow + n_1^\downarrow) - Z\Delta\left[n_0^{\uparrow 2} - n_1^{\uparrow 2}\right], \tag{D.38}$$

for which the effective Hamiltonian is

$$H^{EFF} = \sum_{\langle ij\rangle}(-[t - 2\Delta n_1^\uparrow]c_{i\uparrow}^\dagger c_{j\uparrow} - tc_{i\downarrow}^\dagger c_{j\downarrow}) - 2n_0^\uparrow Z\Delta\sum_i c_{i\uparrow}^\dagger c_{i\uparrow} - Z\Delta\left[n_0^{\uparrow 2} - n_1^{\uparrow 2}\right] \tag{D.39}$$

which when Bloch transformed gives

$$H^{EFF} = \sum_{\mathbf{k}}(-[t - 2\Delta n_1^\uparrow]Z\gamma_{1,\mathbf{k}} - 2n_0^\uparrow Z\Delta)c_{\mathbf{k}\uparrow}^\dagger c_{\mathbf{k}\uparrow} - tZ\gamma_{1,\mathbf{k}}c_{\mathbf{k}\downarrow}^\dagger c_{\mathbf{k}\downarrow} - Z\Delta\left[n_0^{\uparrow 2} - n_1^{\uparrow 2}\right] \tag{D.40}$$

where γ_{1k} is the nearest neighbour structure factor. We can represent this with a 2×2 matrix equation

$$H^{EFF} = \sum_k \begin{bmatrix} c_{k\uparrow}^\dagger, & c_{k\downarrow}^\dagger \end{bmatrix} \begin{bmatrix} -[t - 2\Delta n_1^\uparrow]Z\gamma_{1,\mathbf{k}} - 2n_0^\uparrow Z\Delta & 0 \\ 0 & -tZ\gamma_{1k} \end{bmatrix} \begin{bmatrix} c_{k\uparrow} \\ c_{k\downarrow} \end{bmatrix} - Z\Delta\left[n_0^{\uparrow 2} - n_1^{\uparrow 2}\right]. \tag{D.41}$$

This matrix is subtracted from ϵ and inverted to give the resolvent

$$G(\epsilon) = \begin{bmatrix} \frac{1}{(\epsilon + (t - 2\Delta n_1^\uparrow)Z\gamma_{1k} + 2n_0^\uparrow Z\Delta)} & 0 \\ 0 & \frac{1}{(\epsilon + tZ\gamma_{1k})} \end{bmatrix}. \tag{D.42}$$

We can then use this to calculate the correlations

$$n_0^{\uparrow} = \langle c_{i\uparrow}^{\dagger} c_{i\uparrow} \rangle = \sum_k \langle c_{k\uparrow}^{\dagger} c_{k\uparrow} \rangle \tag{D.43}$$

$$= \sum_k \int_C \frac{\mathrm{d}\epsilon}{2\pi i} f(\epsilon - \mu) G_{\uparrow\uparrow}(\epsilon) \tag{D.44}$$

$$= \sum_k \int_C \frac{\mathrm{d}\epsilon}{2\pi i} f(\epsilon - \mu) \frac{1}{(\epsilon + (t - 2\Delta n_1^{\uparrow}) Z\gamma_{1k} + 2n_0^{\uparrow} Z\Delta)} \tag{D.45}$$

$$= \sum_k f\left(- \left[t - 2\Delta n_1^{\uparrow} \right] Z\gamma_{1k} - 2n_0^{\uparrow} Z\Delta - \mu \right) \tag{D.46}$$

$$= \int_{-\pi}^{\pi} \frac{\mathrm{d}^d \mathbf{k}}{(2\pi)^d} f\left(- \left[t - 2\Delta n_1^{\uparrow} \right] Z\gamma_{1k} - 2n_0^{\uparrow} Z\Delta - \mu \right), \tag{D.47}$$

where $f(x)$ is the Fermi function. This is a self consistent integral equation for $n_0^{\uparrow}$ which must be solved for numerically. Repeating this process gives

$$n_0^{\downarrow} = \int_{-\pi}^{\pi} \frac{\mathrm{d}^d \mathbf{k}}{(2\pi)^d} f\left(-tZ\gamma_{1k} - \mu \right), \tag{D.48}$$

$$n_1^{\uparrow} = \int_{-\pi}^{\pi} \frac{\mathrm{d}^d \mathbf{k}}{(2\pi)^d} f\left(- \left[t - 2\Delta n_1^{\uparrow} \right] Z\gamma_{1,\mathbf{k}} - 2n_0^{\uparrow} Z\Delta - \mu \right) \gamma_{1,\mathbf{k}}, \tag{D.49}$$

$$n_1^{\downarrow} = \int_{-\pi}^{\pi} \frac{\mathrm{d}^d \mathbf{k}}{(2\pi)^d} f\left(-tZ\gamma_{1,\mathbf{k}} - \mu \right) \gamma_{1,\mathbf{k}}, \tag{D.50}$$

we numerically solve these self consistent integral equations by iteration and varying the controlling parameter μ. The result of which is depicted in figure D.1 on page 269.

In this appendix we outlined the simple three step process to perform Hartree-Fock mean field theory. This was then detailed with a two part example where the importance of correctly picking assumptions was highlighted.

Figure D.1: Paramagnetic and Magnetic Energy of Example Hamiltonian

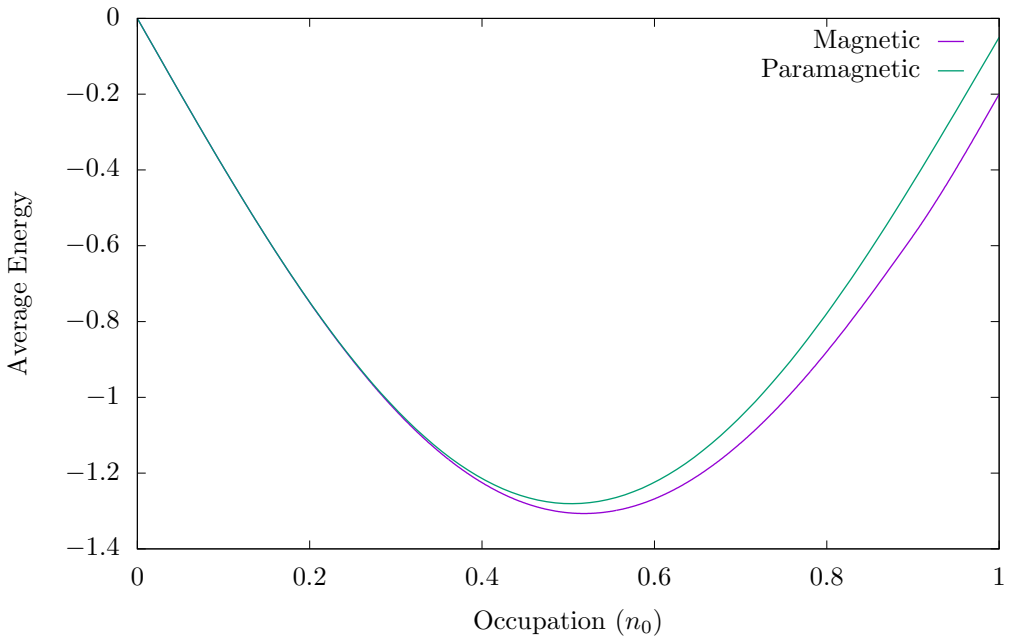

The average total energy per spin per site of the example Hamiltonian. At low occupancy there is little difference between the energies. As occupancy increases the system prefers magnetism in order to gain more of the Δ energy. In this calculation $\frac{\Delta}{t} = 0.2$.

APPENDIX E

IMPURITY THEORY — EXACT SOLUTIONS TO PARTICULAR MODELS

In noteworthy physical problems the Hamiltonian is rarely solved trivially. In this chapter we present a powerful mathematical technique which can give access to exact results [66]. If a problem can be split into an exactly solvable component and an 'impurity' component that only affects a finite number of elements, it can be solved exactly. This impurity distorts the exact solution in a way that can be analytically dealt with. We will begin by formulating the mathematics and follow this up with an example.

E.1 Theory

Before we begin let's sketch the theory. The key object in this analysis is the resolvent. If the Hamiltonian can be split into an exactly solvable component and an 'impurity', then we can split the resolvent in a similar manner. This can then be used to provide an eigenvalue equation which can subsequently be solved for a binding energy. Now let's detail the theory.

This method relies on understanding and dealing with the *resolvent*

$$G(\epsilon) = [\epsilon - H]^{-1}, \tag{E.1}$$

in which ϵ is a variable and H the Hamiltonian of the system. In its diagonal basis the resolvent can be written as

$$G(\epsilon)_{nn'} = \frac{\delta_{nn'}}{\epsilon - E_n}, \tag{E.2}$$

where E_n are the energy eigenvalues of H. From this it is clear to see that the poles of $G(\epsilon)$ are the energy eigenvalues of H.

Let's see how the resolvent relates to the eigenfunctions of H. Consider the states $|\psi_n\rangle_i$ where $\sum_{i'} H_{ii'} |\psi_{i'}^{(n)}\rangle = E_n |\psi_n\rangle_i$. These can be used as a unitary transformation as they diagonalise the Hamiltonian. Using this we get the spectral representation of the resolvent

$$G(\epsilon)_{ii'} = \sum_{nn'} |\psi_i^{(n)}\rangle\, G(\epsilon)_{nn'}\, \langle\psi_{i'}^{(n')}| = \sum_n \frac{|\psi_i^{(n)}\rangle\, \langle\psi_{i'}^{(n)}|}{\epsilon - E_n}. \tag{E.3}$$

The resolvent has poles at the energy eigenvalues of H whose residues are the wavefunction.

In the following subsections we explicitly formulate how to calculate the ground state energy and its wavefunction.

E.1.1 Energy Eigenvalues

This technique relies on having a Hamiltonian that can be split in the following manner

$$H = H_E + H_I, \tag{E.4}$$

where H is the full Hamiltonian, H_E is the exactly solvable Hamiltonian, and H_I is the 'impurity' which only has a finite number of non-zero eigenvalues. This number is directly related to the dimension of the final eigenvalue problem and thus must be small for the tractability of the solution.

The next step is to manipulate the resolvent to 'split' it in a similar manner to the Hamiltonian where all the 'information' for the exact solution is in one component and the impurity in the other. We begin by substituting H into $G(\epsilon)$

$$G(\epsilon) = [\epsilon - H_E - H_I]^{-1}, \tag{E.5}$$

we then factorise $G_E(\epsilon) = [\epsilon - H_E]^{-1}$

$$G(\epsilon) = G_E(\epsilon)[1 - H_I G_E(\epsilon)]^{-1}, \tag{E.6}$$

which is manipulated in the following manner

$$\begin{aligned} G(\epsilon) &= \left(1 + G_E(\epsilon)H_I + G_E(\epsilon)H_I G_E(\epsilon)H_I + \ldots\right) G_E(\epsilon) && \text{(E.7)} \\ &= G_E(\epsilon) + G_E(\epsilon)\left(H_I + H_I G_E(\epsilon)H_I + \ldots\right) G_E(\epsilon) && \text{(E.8)} \\ &= G_E(\epsilon) + G_E(\epsilon)\Sigma(\epsilon)G_E(\epsilon). && \text{(E.9)} \end{aligned}$$

From this we can see there are two sources of poles of $G(\epsilon)$, $G_E(\epsilon)$ and $\Sigma(\epsilon)$. The poles of $G_E(\epsilon)$ are simply the eigenvalues of H_E, but we are interested in the poles due to the addition of H_I. Therefore we must calculate the poles of

$$\Sigma(\epsilon) = \left[H_I^{-1} - G_E(\epsilon)\right]^{-1}, \tag{E.10}$$

where we have projected onto the non-zero eigenbasis of H_I to ensure an inverse. This is equivalent to solving the eigenvalue equation

$$\Sigma(\epsilon)^{-1}\left|\phi\right\rangle = \left[H_I^{-1} - G_E(\epsilon)\right]\left|\phi\right\rangle = 0, \tag{E.11}$$

which upon substitution of $\left|\Phi\right\rangle = H_I\left|\phi\right\rangle$ yields

$$\left|\Phi\right\rangle = G_E(\epsilon)H_I\left|\Phi\right\rangle. \tag{E.12}$$

This calculation involves a finite dimensional inverse, controlled by the number of states affected by H_E, and is tractable for small matrices.

At this point we have two independent methods to calculate $G_E(\epsilon)$, the sum (E.3) and the eigenvalue equation (E.12), which we can equate to solve for ϵ. If this energy is lower than the ground state energy of H_E then there is a bound state. In the next section we formulate how to calculate the wavefunctions of the bound states.

E.1.2 Wavefunctions of Bound States

In this section we will calculate the wavefunction of the bound state $E_{n'}$. We begin with the spectral representation of the resolvent

$$G(\epsilon)_{ii'} = \sum_n \frac{|\psi_i^{(n)}\rangle \langle\psi_{i'}^{(n)}|}{\epsilon - E_n}, \tag{E.13}$$

and split the sum to pick out the $E_{n'}$ term

$$G(\epsilon)_{ii'} = \sum_{n\neq n'} \frac{|\psi_i^{(n)}\rangle \langle\psi_{i'}^{(n)}|}{\epsilon - E_n} + \frac{|\psi_i^{(n')}\rangle \langle\psi_{i'}^{(n')}|}{\epsilon - E_{n'}}. \tag{E.14}$$

However we also have

$$G(\epsilon)_{ii'} = G_E(\epsilon) + G_E(\epsilon)\Sigma(\epsilon)G_E(\epsilon), \tag{E.15}$$

and therefore

$$\sum_{n\neq n'} \frac{|\psi_i^{(n)}\rangle \langle\psi_{i'}^{(n)}|}{\epsilon - E_n} + \frac{|\psi_i^{(n')}\rangle \langle\psi_{i'}^{(n')}|}{\epsilon - E_{n'}} = G_E(\epsilon) + G_E(\epsilon)\Sigma(\epsilon)G_E(\epsilon). \tag{E.16}$$

By calculating the residue of $G(\epsilon)$ at $\epsilon = E_{n'}$, from equation (E.16) we get

$$|\psi_i^{(n')}\rangle \langle\psi_{i'}^{(n')}| = G_E(E_{n'})\sigma(E_{n'})G_E(E_{n'}), \tag{E.17}$$

Figure E.1: Linear Chain With a Funny Atom

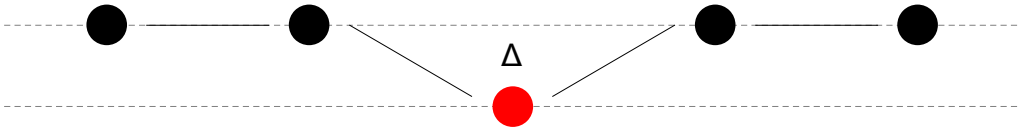

Tight binding chain with a funny atom highlighted in red. Gray lines correspond to available hops from one atom to the next. If an electron is situated on the red atom it gains energy Δ.

where $\sigma(E_{n'})$ is the residue of $\Sigma(\epsilon)$ at $\epsilon = E_{n'}$. By representing $\sigma(E_{n'}) = |\varphi^{(n')}\rangle \langle\varphi^{(n')}|$ we can see the wavefunction of the bound state $E_{n'}$ is given by

$$|\psi_i^{(n')}\rangle = G_E(E_{n'}) |\varphi^{(n')}\rangle . \tag{E.18}$$

In this section we formulated the mathematics to exactly calculate the bound state eigenvalue and eigenvector of systems with $H = H_E + H_I$. In the following section we implement this technique with an example.

E.2 Implementation

Like many mathematical techniques this is best explained with an example. We consider a linear chain with a 'funny' atom and examine whether this atom creates a bound state. The system is depicted in figure E.1 on page 275. First we will calculate the bound state energy and then its associated wavefunction.

E.2.1 Bound State Energy

The problem is a simple tight binding Hamiltonian with one site gaining extra energy, the Hamiltonian for this problem is given by

$$H = -t \sum_{\langle ij \rangle} c_i^\dagger c_j - \Delta c_0^\dagger c_0. \tag{E.19}$$

Note how this Hamiltonian can be split into an exactly solvable component H_E and an impurity component H_I where

$$H_E = -t \sum_{\langle ij \rangle} c_i^\dagger c_j \qquad\qquad H_I = -\Delta c_0^\dagger c_0, \tag{E.20}$$

such that $H = H_E + H_I$.

First we consider the 'sum definition' of $G(\epsilon)$. In our example H_E is exactly solved by a Bloch transformation giving rise to the energy dispersion $E_k = -2t\cos(k)$. This gives our spectral definition of $G_E(\epsilon)$ as

$$G_E(\epsilon) = \frac{1}{N} \sum_k \frac{1}{\epsilon + 2t\cos(k)}. \tag{E.21}$$

We can take the continuum limit [99] which gives us the integral

$$G_E(\epsilon) = \int_{-\pi}^{\pi} \frac{\mathrm{d}k}{2\pi} \frac{1}{\epsilon + 2t\cos(k)}. \tag{E.22}$$

Performing this integral requires complex analysis [98] and, as the details are irrelevant for the broad analysis, is left as an exercise for an enthusiastic reader. Provided $\epsilon < -2t$, the result is

$$G_E(\epsilon) = -\frac{1}{\sqrt{\epsilon^2 - 4t^2}}. \tag{E.23}$$

Next we solve the eigenvalue equation $|\Phi\rangle = G_E(\epsilon) H_I |\Phi\rangle$ for $G^0(\epsilon)$. As the non-zero eigenbasis of H_I is a 1×1 matrix all we are required to solve is $1 = -\Delta G_E(\epsilon)$ which gives

$$G_E(\epsilon) = -\frac{1}{\Delta}. \tag{E.24}$$

The final step is to equate equations E.23 and E.24

$$-\frac{1}{\sqrt{\epsilon^2 - 4t^2}} = -\frac{1}{\Delta}, \tag{E.25}$$

which is rearranged to give

$$\epsilon = -\sqrt{\Delta^2 + 4t^2}. \tag{E.26}$$

As the ground state energy for H_E is $-2t$ and $\epsilon < -2t$ for all $\Delta > 0$ the particle is always bound to the funny atom.

As there is a bound state, we calculate the wavefunction of the bound state in the following section.

E.2.2 Wavefunction of the Bound State

To find the wavefunction of the impurity we are required to calculate $\sigma(E_{n'})$. This is simply the non-zero states of H_I, therefore

$$\sigma(E_{n'}) = |0\rangle \langle 0| . \tag{E.27}$$

Similarly from the spectral representation of G_E we have

$$G(E_{n'})_{ii'} = \sum_n \frac{|\psi_i^{(n)}\rangle \langle \psi_{i'}^{(n)}|}{E_{n'} - E_n}. \tag{E.28}$$

Upon substitution of the bound state energy $E_{n'} = -\sqrt{\Delta^2 + 4t^2}$ into equation E.18, we find the wavefunction is given by

$$|\psi_i^{(n')}\rangle = \sum_n \frac{|\psi_i^{(n)}\rangle}{-\sqrt{\Delta^2 + 4t^2} - E_n}. \tag{E.29}$$

This example highlighted how to perform impurity theory. In this section we calculated the bound state energy and its wavefunction for the linear chain with a funny atom.

Note in general the 'impurity' is not one dimensional and matrix algebra will be required. This is tractable if the size of the non-zero eigenbasis set is small. Impurity theory is a powerful technique by which to calculate exact quantities for non-trivial problems.

APPENDIX F

PERTURBATION THEORY — FROM HUBBARD TO HEISENBERG

In this chapter we detail how to perform second order perturbation theory on the infinite U Hubbard model and attain the Heisenberg model. We will begin by discussing the Hubbard model at half occupation and understanding the Mott point. This is followed by a second order perturbation theory [100] on an large U Hubbard model at the Mott point. Finally, we transform the resulting Hamiltonian and see that it maps on to the Heisenberg Model.

F.1 The Hubbard Model at the Mott Point

The Hubbard model is given by

$$H = -t \sum_{\langle ij \rangle \sigma} c^{\dagger}_{i\sigma} c_{j\sigma} + U \sum_{i} c^{\dagger}_{i\uparrow} c_{i\uparrow} c^{\dagger}_{i\downarrow} c_{i\downarrow}, \tag{F.1}$$

where $\langle ij \rangle$ denotes nearest neighbours. Let's consider the model at half filling. In the limit $U = 0$ this becomes the tight binding model and is trivially solved, with the solution

being a metal. However, in the limit $U = \infty$ something more interesting occurs. The on site interaction is divergent and hence double occupation in real space is prohibited. This is the so called Mott insulator [76]: a system where every electron is localised due to the Coulomb interaction.

Interestingly, the system has 2^N spin degeneracy at $U = \infty$ which we expect to be lifted as we decrease U. Note that this also will cause a metal to insulator transition [101] at a certain value of $\frac{U}{t}$ due to the differing physics in each limiting case.

F.2 Perturbation in the Large U Limit

Consider the Hubbard model at half filling with a large but not infinite U. In this limit the electrons are localised to a first approximation. For this reason we will begin with the solution for infinite U and perform perturbation theory with hopping matrix t. This means before and after our perturbation we must be left with a state that is a solution to the infinite U Hubbard model: one particle on each site. As one hop will cause double occupation we require perturbation with two hops and hence second order perturbation theory.

Hopping must occur between opposite spins. This is because Pauli exclusion [102] prohibits double occupation of the same particle. Hopping occurs between neighbours. Either the left particle hops on to the right or vice versa. At this point either the original particle hops back or the other particle does. This is depicted in figure F.1 on page 281

From second order perturbation theory we know

$$\Delta H = \sum_k \frac{\hat{V}_{0k}\hat{V}_{k0}}{E_0 - E_k}, \tag{F.2}$$

where $\hat{V}_{k0}$ is a perturbation hop that takes a particle from the groundstate to an excited state, $\hat{V}_{0k}$ does the opposite, E_0 is the ground state energy, and E_k is the excited state energy. The energy terms are simple. As $E_k = E_0 + U$ this gives $E_0 - E_k = -U$. The perturbation operators are a little more complicated. Let's label the two neighbouring

Figure F.1: Second Order Perturbation Hops in the Hubbard Model

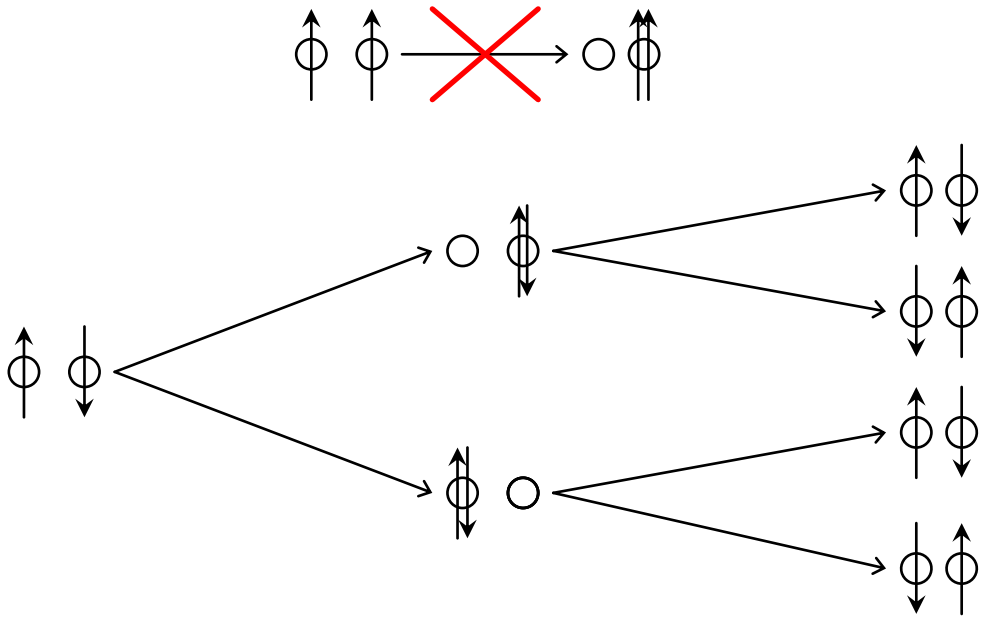

Schematic for accessible hops in the large U perturbative calculation. The top hop is forbidden due to Pauli exclusion. The bottom four are able to occur. Either particle can hop on to its neighbour. Then either the original particle can hop back or the other particle can hop back.

sites under consideration 1σ and $2\bar{\sigma}$ for the left and right sites with opposite spins respectively. The two operators for $\hat{V}_{k0}$ are $\hat{V}^{(1)}_{k0} = -tc^{\dagger}_{1\bar{\sigma}}c_{2\bar{\sigma}}$ and $\hat{V}^{(2)}_{k0} = -tc^{\dagger}_{2\sigma}c_{1\sigma}$. For each $\hat{V}_{k0}$ there are two $\hat{V}_{0k}$ operators that bring the state back to a ground state. For $\hat{V}^{(1)}_{k0}$ we have $\hat{V}^{(1,1)}_{0k} = -tc^{\dagger}_{2\sigma}c_{1\sigma}$ and $\hat{V}^{(1,2)}_{0k} = -tc^{\dagger}_{2\bar{\sigma}}c_{1\bar{\sigma}}$, whilst for $\hat{V}^{(2)}_{k0}$ we have $\hat{V}^{(2,1)}_{0k} = -tc^{\dagger}_{1\sigma}c_{2\sigma}$ and $\hat{V}^{(2,2)}_{0k} = -tc^{\dagger}_{1\bar{\sigma}}c_{2\bar{\sigma}}$.

The Hamiltonian that results from second order perturbation theory is therefore

$$H^{Mott} = -\frac{2t^2}{U}\sum_{\langle ij\rangle\sigma} c^{\dagger}_{i\sigma}c_{i\sigma}c^{\dagger}_{j\bar{\sigma}}c_{j\bar{\sigma}} - c^{\dagger}_{i\bar{\sigma}}c_{i\sigma}c^{\dagger}_{j\sigma}c_{j\bar{\sigma}} + c^{\dagger}_{i\bar{\sigma}}c_{i\sigma}. \tag{F.3}$$

As there is a particle on each site the $c^{\dagger}_{i\bar{\sigma}}c_{i\sigma}$ term is just a constant energy shift and therefore can (and will) be neglected for the rest of the calculation.

F.3 Second Quantized Operators to Spin Operators

In this section we transform the resulting Hamiltonian from the previous section to the Heisenberg model. This is an exact transformation [80] that acts on a Hilbert space where there is one electron per site. The transformation is given by

$$S_i^z = \frac{1}{2}\left[c_{i\uparrow}^\dagger c_{i\uparrow} - c_{i\downarrow}^\dagger c_{i\downarrow}\right], \quad S_i^+ = c_{i\uparrow}^\dagger c_{i\downarrow}, \quad S_i^- = c_{i\downarrow}^\dagger c_{i\uparrow}. \tag{F.4}$$

To invert S_i^z we are required to understand projection. Note $S_i^z c_{i\uparrow}^\dagger |0\rangle = \frac{1}{2} c_{i\uparrow}^\dagger |0\rangle$ and $S_i^z c_{i\downarrow}^\dagger |0\rangle = -\frac{1}{2} c_{i\downarrow}^\dagger |0\rangle$. Rearranging these gives $\left(S_i^z - \frac{1}{2}\right) c_{i\uparrow}^\dagger |0\rangle = 0$, and $\left(S_i^z + \frac{1}{2}\right) c_{i\downarrow}^\dagger |0\rangle = 0$. These are the on site spin half projectors and clearly define

$$\left(S_i^z + \frac{1}{2}\right) = c_{i\uparrow}^\dagger c_{i\uparrow} \quad \left(S_i^z - \frac{1}{2}\right) = c_{i\downarrow}^\dagger c_{i\downarrow}. \tag{F.5}$$

We substitute these into the Hamiltonian giving

$$H^{Mott} = -\frac{2t^2}{U} \sum_{\langle ij \rangle} c_{i\uparrow}^\dagger c_{i\uparrow} c_{j\downarrow}^\dagger c_{j\downarrow} + c_{i\downarrow}^\dagger c_{i\downarrow} c_{j\uparrow}^\dagger c_{j\uparrow} + c_{i\downarrow}^\dagger c_{i\uparrow} c_{j\uparrow}^\dagger c_{j\downarrow} + c_{i\uparrow}^\dagger c_{i\downarrow} c_{j\downarrow}^\dagger c_{j\uparrow} \tag{F.6}$$

$$= -\frac{2t^2}{U} \sum_{\langle ij \rangle} \left(S_i^z + \frac{1}{2}\right)\left(S_j^z - \frac{1}{2}\right) + \left(S_i^z - \frac{1}{2}\right)\left(S_j^z + \frac{1}{2}\right) + S_i^- S_j^+ + S_i^+ S_j^- \tag{F.7}$$

$$= -\frac{4t^2}{U} \sum_{\langle ij \rangle} S_i^z S_j^z + \frac{1}{2}\left(S_i^- S_j^+ + S_i^+ S_j^-\right). \tag{F.8}$$

Next we directly substitute the definitions $S^+ = S^x + iS^y$ and $S^- = S^x - iS^y$ into the Hamiltonian, which gives

$$H^{Mott} = -J \sum_{\langle ij \rangle} \mathbf{S}_i \cdot \mathbf{S}_j, \tag{F.9}$$

where $J = \frac{4t^2}{U}$. This is the Heisenberg model [74].

We have detailed how to perform second order perturbation theory on the large U Hubbard model at the Mott point. This process can be repeated for any large U Hubbard model but the hopping details will be model dependent.

APPENDIX G

MAXWELL CONSTRUCTION

Free energy curves cannot be concave [103]. This simple fact means that when two phases compete to be the lowest energy the system will compensate by gaining from both phases. This occurs in the form of a phase separated mixture where there is one region of space per phase.

So that explains the physics but what about the energy curve? Well this is where the Maxwell construction [104] comes in. All we are required to do is connect the minima with a straight line. This schematic is depicted in figure G.1 on page 284.

G.1 More Detail

Mathematically we can flesh this out further. Historically, the source of Maxwell constructions is liquid-to-vapour phase transitions [105]. Consider the Gibbs free energy of two coexisting phases

$$G = g_1 M_1 + g_2 M_2, \tag{G.1}$$

where g_1, g_2 are the Gibbs free energy and M_1, M_2 are the masses in states 1 and 2 respectively. We are also enforcing mass conservation, which is mathematically given by

$$dM_1 = -dM_2. \tag{G.2}$$

Figure G.1: Typical Maxwell Construction

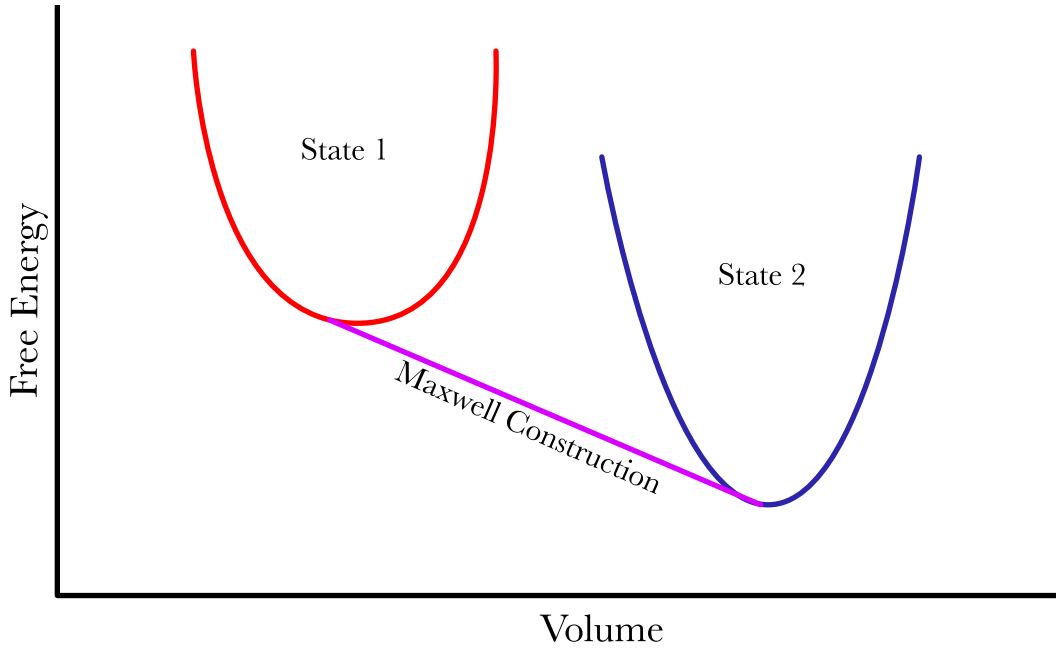

Schematic of a Maxwell construction between states 1 and 2.

If we minimise G at equilibrium we get

$$dG = g_1 dM_1 + g_2 dM_2 = 0, \tag{G.3}$$

which directly yields

$$g_1 = g_2. \tag{G.4}$$

Specific Gibbs free energies are equal for coexisting phases! If $g_1 > g_2$ the second law of thermodynamics allows for transfer of material from state $1 \rightarrow 2$. There are three variables: pressure P, volume V, and temperature T, along with two constraints: the equation of state, and $g_1 = g_1$. Therefore, phase coexistence is a line in pressure and temperature.

What can we say about this line? Let's consider a system in equilibrium at constant

T and V and minimise the Helmholtz free energy $F = U - TS$

$$dF = PdV - SdT = 0, \tag{G.5}$$

subject to the constraint

$$V = v_1 + v_2, \tag{G.6}$$

where v_1 and v_2 are the individual volumes for states 1 and 2. F is minimised by a mixture of phases, where the slope of the common tangent is the coexistence pressure

$$\left(\frac{\partial F}{\partial V}\right)_T = P. \tag{G.7}$$

This is the Maxwell construction.

BIBLIOGRAPHY

[1] W. Meissner and R. Ochsenfeld. Ein neuer effekt bei eintritt der supraleitfähigkeit. *Naturwissenschaften*, 21(44):787–788, 1933.

[2] K. H. Bennemann and John B. Ketterson, editors. *Superconductivity*. Springer Berlin Heidelberg, 2008.

[3] Pegor Aynajian. *Electron-Phonon Interaction in Conventional and Unconventional Superconductors*. 01 2011.

[4] J. Bardeen, L. N. Cooper, and J. R. Schrieffer. Theory of superconductivity. *Phys. Rev.*, 108:1175–1204, Dec 1957.

[5] F. Steglich, J. Aarts, C. D. Bredl, W. Lieke, D. Meschede, W. Franz, and H. Schäfer. Superconductivity in the presence of strong pauli paramagnetism: $Cecu_2si_2$. *Phys. Rev. Lett.*, 43:1892–1896, Dec 1979.

[6] G. R. Stewart. Heavy-fermion systems. *Rev. Mod. Phys.*, 56:755–787, Oct 1984.

[7] J. G. Bednorz and K. A. Müller. Possible hightc superconductivity in the ba la cu o system. *Zeitschrift für Physik B Condensed Matter*, 64(2):189–193, 1986.

[8] Mingpu Qin, Chia-Min Chung, Hao Shi, Ettore Vitali, Claudius Hubig, Ulrich Schollwöck, Steven White, and Shiwei Zhang. Absence of superconductivity in the pure two-dimensional hubbard model. 10 2019.

[9] Heike Kamerlingh Onnes. Further experiments with liquid helium d - on the change of the electrical resistance of pure metals at very low temperatures, etc v the disappearance of the resistance of mercury. *Proceedings of the koninklijke akademie van wetenschappen te amsterdam*, 14:113 – 115, 1911.

[10] Roland Hott, Reinhold Kleiner, Thomas Wolf, and Gertrud Zwicknagl. Review on superconducting materials. 2013.

[11] Ch. Buchal, F. Pobell, R. M. Mueller, M. Kubota, and J. R. Owers-Bradley. Superconductivity of rhodium at ultralow temperatures. *Phys. Rev. Lett.*, 50:64–67, Jan 1983.

[12] B. T. Matthias, T. H. Geballe, and V. B. Compton. Superconductivity. *Rev. Mod. Phys.*, 35:1–22, Jan 1963.

[13] M. Tinkham. Introduction to superconductivity. 2004.

[14] J. N. Rjabinin and L. W. Shubnikow. Magnetic properties and critical currents of supra-conducting alloys. *Nature*, 135(3415):581–582, 1935.

[15] C. Kittel. *Introduction to Solid State Physics*. Wiley, 2004.

[16] Adrian Crisan. *Vortices and Nanostructured Superconductors*, volume 261. 01 2017.

[17] F. London, H. London, and Frederick Alexander Lindemann. The electromagnetic equations of the supraconductor. *Proceedings of the Royal Society of London. Series A - Mathematical and Physical Sciences*, 149(866):71–88, 1935.

[18] M Cyrot. Ginzburg-landau theory for superconductors. *Reports on Progress in Physics*, 36(2):103–158, feb 1973.

[19] Gin-ichiro Oya and E. J. Saur. Preparation of nb3ge films by chemical transport reaction and their critical properties. *Journal of Low Temperature Physics*, 34(5):569–583, 1979.

[20] G. R. Stewart. Unconventional superconductivity. *Advances in Physics*, 66(2):75–196, 2017.

[21] C. W. Chu. Superconductivity at higher temperatures in the hg-ba-ca-cu-o compound system. *Journal of Superconductivity*, 7(1):1–7, 1994.

[22] Patrick A. Lee, Naoto Nagaosa, and Xiao-Gang Wen. Doping a mott insulator: Physics of high-temperature superconductivity. *Rev. Mod. Phys.*, 78:17–85, Jan 2006.

[23] Richard L. Greene, Pampa R. Mandal, Nicholas R. Poniatowski, and Tarapada Sarkar. The strange metal state of the electron-doped cuprates, 2019.

[24] A Kobayashi, A Tsuruta, T Matsuura, and Y Kuroda. Origins of electron–hole asymmetry in cuprate superconductors. *Journal of Magnetism and Magnetic Materials*, 272-276:E187 – E188, 2004. Proceedings of the International Conference on Magnetism (ICM 2003).

[25] Cuprate phase diagram accessed at https://commons.wikimedia.org/wiki/file:cuprates_phasedigagram_en.svg on 14th march, 2019.

[26] Charu Kapoor and S.P. Tewari. Superconductivity in a heavy fermion system: Cecu2si2. *Physica C: Superconductivity and its Applications*, 528:9 – 11, 2016.

[27] K. H. Bennemann and J. B. Ketterson, editors. *The Physics of Superconductors*. Springer Berlin Heidelberg, 2003.

[28] Elbio Dagotto and T. M. Rice. Surprises on the way from one- to two-dimensional quantum magnets: The ladder materials. *Science*, 271(5249):618, Feb 02 1996. Copyright - Copyright American Association for the Advancement of Science Feb 2, 1996; Last updated - 2017-10-31; CODEN - SCIEAS.

[29] R. S. Eccleston, T. Barnes, J. Brody, and J. W. Johnson. Inelastic neutron scattering from the spin ladder compound $(VO)_2p_2o_7$. *Phys. Rev. Lett.*, 73:2626–2629, Nov 1994.

[30] Y Kitaoka, K Asayama, M Azuma, Z Hiroi, Kenji Ishida, Yoshio Kitaoka, Kunisuke Asayama, Masaki Azuma, Zenji Hiroi, and Mikio Takano. Spin gap behavior in ladder-type of quasi-one-dimensional spin (s=1/2) system srcu2o3. *Journal of the Physical Society of Japan*, 63(9):3222–3225, 1994.

[31] M. Azuma, Z. Hiroi, M. Takano, K. Ishida, and Y. Kitaoka. Observation of a spin gap in $srcu_2o_3$ comprising spin-1/2 quasi-1d two-leg ladders. *Phys. Rev. Lett.*, 73:3463–3466, Dec 1994.

[32] Masatomo Uehara, Takashi Nagata, Jun Akimitsu, Hiroki Takahashi, Nobuo Môri, and Kyoichi Kinoshita. Superconductivity in the ladder material sr0.4ca13.6cu24o41.84. *Journal of the Physical Society of Japan*, 65(9):2764–2767, 1996.

[33] D. Mohan Radheep, R. Thiyagarjan, S. Esakkimuthu, Guochu Deng, E. Pomjakushina, C. L. Prajapat, G. Ravikumar, K. Conder, G. Baskaran, and S. Arumugam. A spin ladder compound doubles its superconducting tc under a gentle uniaxial pressure, 2013.

[34] Neil W. Ashcroft Russell J. Hemley. The revealing role of pressure in the condensed matter sciences. *Physics Today*, 51(8):26, 1998.

[35] Herbert Fröhlich. On the theory of superconductivity: the one-dimensional case. *Proceedings of the Royal Society of London. Series A. Mathematical and Physical Sciences*, 223(1154):296–305, 1954.

[36] J. F and J.F. Annett. *Oxford Master Series in Physics*. Superconductivity, Superfluids and Condensates. OUP Oxford, 2004.

[37] J.W. Garland. *The Isotope Effect in Superconductivity*. University of Chicago, Department of Physics., 1966.

[38] P. M. Tedrow, R. Meservey, and B. B. Schwartz. Experimental evidence for a first-order magnetic transition in thin superconducting aluminum films. *Phys. Rev. Lett.*, 24:1004–1007, May 1970.

[39] Leon N. Cooper. Bound electron pairs in a degenerate fermi gas. *Phys. Rev.*, 104:1189–1190, Nov 1956.

[40] J. G. Valatin. Comments on the theory of superconductivity. *Il Nuovo Cimento (1955-1965)*, 7(6):843–857, Mar 1958.

[41] F. C. Zhang and T. M. Rice. Effective hamiltonian for the superconducting cu oxides. *Phys. Rev. B*, 37:3759–3761, Mar 1988.

[42] P. W. Anderson. The resonating valence bond state in la2cuo4 and superconductivity. *Science*, 235(4793):1196–1198, 1987.

[43] P. W. Anderson. Localized magnetic states in metals. *Phys. Rev.*, 124:41–53, Oct 1961.

[44] M.-H. Julien. Magnetic order and superconductivity in la2xsrxcuo4: a review. *Physica B: Condensed Matter*, 329-333:693 – 696, 2003. Proceedings of the 23rd International Conference on Low Temperature Physics.

[45] C Chaillout, S W Cheong, Z Fisk, M S Lehmann, M Marezio, B Morosin, and J E Schirber. The crystal structure of superconducting la2cuo4.032 by neutron diffraction. *Physica Scripta*, T29:97–99, jan 1989.

[46] P. W. Anderson. Antiferromagnetism. theory of superexchange interaction. *Phys. Rev.*, 79:350–356, Jul 1950.

[47] A. Fujimori, E. Takayama-Muromachi, Y. Uchida, and B. Okai. Spectroscopic evidence for strongly correlated electronic states in la-sr-cu and y-ba-cu oxides. *Phys. Rev. B*, 35:8814–8817, Jun 1987.

[48] M.A. Dixon. The normal state electronic structure of cuprate superconductors: a covalent picture. *Physica C: Superconductivity*, 174(1):117 – 125, 1991.

[49] V. J. Emery and G. Reiter. Mechanism for high-temperature superconductivity. *Phys. Rev. B*, 38:4547–4556, Sep 1988.

[50] Louis Taillefer. Scattering and pairing in cuprate superconductors. *Annual Review of Condensed Matter Physics*, 1, 03 2010.

[51] Yang He, Yi Yin, M. Zech, Anjan Soumyanarayanan, Michael M. Yee, Tess Williams, M. C. Boyer, Kamalesh Chatterjee, W. D. Wise, I. Zeljkovic, Takeshi Kondo, T. Takeuchi, H. Ikuta, Peter Mistark, Robert S. Markiewicz, Arun Bansil, Subir Sachdev, E. W. Hudson, and J. E. Hoffman. Fermi surface and pseudogap evolution in a cuprate superconductor. *Science*, 344(6184):608–611, 2014.

[52] Yosuke Nagaoka. Ferromagnetism in a narrow, almost half-filled s band. *Phys. Rev.*, 147:392–405, Jul 1966.

[53] K. Andres, J. E. Graebner, and H. R. Ott. $4f$-virtual-bound-state formation in $ceal_3$ at low temperatures. *Phys. Rev. Lett.*, 35:1779–1782, Dec 1975.

[54] Karl F. Herzfeld, Emanuel Maxwell, and Russell B. Scott. Isotope effect and lattice properties in superconductivity. *Phys. Rev.*, 79:911–911, Sep 1950.

[55] C. A. Reynolds, B. Serin, W. H. Wright, and L. B. Nesbitt. Superconductivity of isotopes of mercury. *Phys. Rev.*, 78:487–487, May 1950.

[56] Y. J. Uemura, G. M. Luke, B. J. Sternlieb, J. H. Brewer, J. F. Carolan, W. N. Hardy, R. Kadono, J. R. Kempton, R. F. Kiefl, S. R. Kreitzman, P. Mulhern, T. M. Riseman, D. Ll. Williams, B. X. Yang, S. Uchida, H. Takagi, J. Gopalakrishnan, A. W. Sleight, M. A. Subramanian, C. L. Chien, M. Z. Cieplak, Gang Xiao, V. Y. Lee, B. W. Statt, C. E. Stronach, W. J. Kossler, and X. H. Yu. Universal correlations between T_c and $\frac{n_s}{m^*}$ (carrier density over effective mass) in high-T_c cuprate superconductors. *Phys. Rev. Lett.*, 62:2317–2320, May 1989.

[57] Deepak Singh, Joel Barker, Arumugam Thamizhavel, Adrian Hillier, D Mck, Don Paul, and Ravi Singh. Superconducting properties and mu-sr study of the noncentrosymmetric superconductor nb 0.5 os 0.5. *Journal of Physics Condensed Matter*, 30:075601, 01 2018.

[58] N. D. Mermin and H. Wagner. Absence of ferromagnetism or antiferromagnetism in one- or two-dimensional isotropic heisenberg models. *Phys. Rev. Lett.*, 17:1133–1136, Nov 1966.

[59] J M F Gunn and M W Long. Correlations near the atomic limit of the anderson lattice. *Journal of Physics C: Solid State Physics*, 21(25):4567, 1988.

[60] R. L. Causey and R. T. Gregory. On lanczos' algorithm for tridiagonalizing matrices. *SIAM Review*, 3(4):322–328, 1961.

[61] Ivar Fredholm. Sur une classe d'équations fonctionnelles. *Acta Mathematica*, 27(1):365–390, Dec 1903.

[62] H. Bethe. Zur theorie der metalle. *Zeitschrift für Physik*, 71(3):205–226, 1931.

[63] D. Baeriswyl, D.K. Campbell, J.M.P. Carmelo, F. Guinea, and E. Louis. *The Hubbard Model: Its Physics and Mathematical Physics*. Nato Science Series B:. Springer US, 2013.

[64] P B Ramos and M J Martins. Algebraic bethe ansatz approach for the one-dimensional hubbard model. *Journal of Physics A: Mathematical and General*, 30(7):L195–L202, apr 1997.

[65] Kazuhiko Kuroki and Hideo Aoki. Realization of negative-u superconductivity in a class of purely repulsive systems: Interacting carrier and insulating bands. *Phys. Rev. Lett.*, 69:3820–3823, Dec 1992.

[66] Ivar Fredholm. Sur une classe d'équations fonctionnelles. *Acta Mathematica*, 27(1):365–390, Dec 1903.

[67] Charlotte Froese Fischer. General hartree-fock program. *Computer Physics Communications*, 43(3):355 – 365, 1987.

[68] J. C. Slater. A simplification of the hartree-fock method. *Phys. Rev.*, 81:385–390, Feb 1951.

[69] G. C. Wick. The evaluation of the collision matrix. *Phys. Rev.*, 80:268–272, Oct 1950.

[70] C J Hamer. Finite-size scaling in the transverse ising model on a square lattice. *Journal of Physics A: Mathematical and General*, 33(38):6683–6698, sep 2000.

[71] Gohil S. Thakur, G. Fuchs, K. Nenkov, Zeba Haque, L. C. Gupta, and A. K. Ganguli. Coexistence of superconductivity and ferromagnetism in sr(0.5)ce(0.5)fbis(2-x)se(x) (x = 0.5 and 1.0), a non-u material with t(c) ¡ t(fm). *Sci Rep*, 6:37527–37527, Nov 2016. 27892482[pmid].

[72] Theodore Reber, S. Parham, Nicholas Plumb, Yue Cao, Haoxiang Li, Zijie Sun, Qiang Wang, Hideaki Iwasawa, Masahiko Arita, J. Wen, Z. Xu, G. Gu, Yoshihito Yoshida, H. Eisaki, G. Arnold, and Dan Dessau. Pairing, pair-breaking, and their roles in setting the tc of cuprate high temperature superconductors. 08 2015.

[73] L. F. Feiner, J. H. Jefferson, and R. Raimondi. Effective single-band models for the high-t_c cuprates. i. coulomb interactions. *Phys. Rev. B*, 53:8751–8773, Apr 1996.

[74] Assa Auerbach. *Interacting Electrons and Quantum Magnetism*. Springer New York, 1994.

[75] John Christiana (cover), Alejandro L. Garcia, Bruce Kenselaar (cover), Alison Reeves, and Paul F. Corey. *Numerical Methods for Physics (2nd Edition)*. Prentice-Hall, Inc., USA, 2nd edition, 1999.

[76] Sindhunil Barman Roy. *Mott Insulators*. 2053-2563. IOP Publishing, 2019.

[77] L.D. Landau and E.M. Lifshitz. *Chapter III - Schrödinger's Equation*. Pergamon, third edition edition, 1977.

[78] A.J. Brizard. *An Introduction to Lagrangian Mechanics*. World Scientific, 2008.

[79] I.S. Grant and W.R. Phillips. *Electromagnetism*. Manchester Physics Series. Wiley, 2013.

[80] M.E. Peskin and D.V. Schroeder. *An Introduction to Quantum Field Theory*. Advanced book classics. Avalon Publishing, 1995.

[81] F.J. Dyson and D. Derbes. *Advanced Quantum Mechanics*. Fisica y astronomia. World Scientific Publishing Company, 2011.

[82] Gregory H. Wannier. The structure of electronic excitation levels in insulating crystals. *Phys. Rev.*, 52:191–197, Aug 1937.

[83] G. Herzberg and J.W.T. Spinks. *Atomic Spectra and Atomic Structure*. A Dover paperback. Dover publications, 1944.

[84] A. Altland, P.T.C.M.P.A. Altland, and B. Simons. *Condensed Matter Field Theory*. Cambridge University Press, 2006.

[85] P. Atkins and J. de Paula. *The Elements of Physical Chemistry*. W. H. Freeman, 2005.

[86] C. Müller. *Spherical Harmonics*. Lecture Notes in Mathematics. Springer Berlin Heidelberg, 2006.

[87] Yehuda B. Band and Yshai Avishai. *10 - Electronic Structure of Multielectron Systems*. Academic Press, Amsterdam, 2013.

[88] Richard Bellman and George Adomian. *Partial Differential Equations*. Springer Netherlands, 1985.

[89] N A Cade. A self-consistent bandstructure calculation for antiferromagnetic γ manganese. *Journal of Physics F: Metal Physics*, 10(7):L187–L191, jul 1980.

[90] H.H. Hill. Early actinides: The periodic system's f electron transition metal series. *Nucl. Met., Met. Soc. AIME 17: 2-19(1970).*

[91] Zhong-Qi Ma. Group theory for physicists. 2007.

[92] C. G. Shull, W. A. Strauser, and E. O. Wollan. Neutron diffraction by paramagnetic and antiferromagnetic substances. *Phys. Rev.*, 83:333–345, Jul 1951.

[93] Felix Bloch. Über die quantenmechanik der elektronen in kristallgittern. *Zeitschrift für Physik*, 52(7):555–600, 1929.

[94] G. Strang. *Introduction to linear algebra*. Wellesley-Cambridge Press, 1993.

[95] Y. Saad. *Numerical methods for large eigenvalue problems*. Algorithms and architectures for advanced scientific computing. Manchester University Press, 1992.

[96] PM. E. J. Newman and G. T. Barkema. *Monte Carlo Methods in Statistical Physics*, volume 0 of *0*. Oxford University Press, Great Clarendon Street, Oxford OX2 6DP, 3 edition, 2 1999.

[97] Jerryman Gyamfi. *An Introduction to the Holstein-Primakoff Transformation, with Applications in Magnetic Resonance*. 06 2019.

[98] J. Bak and D.J. Newman. *Complex Analysis*. Undergraduate Texts in Mathematics. Springer New York, 2011.

[99] I. Montvay and G. Münster. *Quantum Fields on a Lattice*. Cambridge Monographs on Mathematical Physics. Cambridge University Press, 1997.

[100] L.D. Landau and E.M. Lifshitz. *Chapter VI - Perturbation Theory*. Pergamon, third edition edition, 1977.

[101] N. F. Mott. Metal-insulator transition. *Rev. Mod. Phys.*, 40:677–683, Oct 1968.

[102] M. Massimi, M. Massimi, and Cambridge University Press. *Pauli's Exclusion Principle: The Origin and Validation of a Scientific Principle*. Cambridge University Press, 2005.

[103] H.C. Van Ness. *Understanding thermodynamics*. McGraw-Hill, 1969.

[104] R. I. Rivers. Effective potential convexity and finite-temperature phase transitions. *Zeitschrift für Physik C Particles and Fields*, 22(2):137–142, Jun 1984.

[105] Carl W. David. Avoiding the cubic equation in finding the van der waals fluid's vapor pressures. *Chemistry Education Materials*, 96, 2017.